Nemaline myopathy: pathophysiology and therapeutic targets

de Winter, J.M.

2017

NEMALINE MYOPATHY

Pathophysiology & therapeutic targets

Josine Marieke de Winter

The work presented in this thesis was performed at the department of Physiology, Institute for Cardiovascular Research of the VU University Medical Center, Amsterdam, The Netherlands.

ISBN	978-94-91602-79-5
Print	Printservice Ede
Lay-out	Anne Leijdekkers
Cover design	Pleuni Hooijman & Josine de Winter

VRIJE UNIVERSITEIT

Nemaline myopathy: pathophysiology and therapeutic targets

ACADEMISCH PROEFSCHRIFT

ter verkrijging van de graad Doctor aan
de Vrije Universiteit Amsterdam,
op gezag van de rector magnificus
prof.dr. V. Subramaniam,
in het openbaar te verdedigen
ten overstaan van de promotiecommissie
van de Faculteit der Geneeskunde
op vrijdag 27 januari 2017 om 13.45 uur
in de aula van de universiteit,
De Boelelaan 1105

door

Josine Marieke de Winter
geboren te Naaldwijk

promotoren: prof.dr. C.A.C. Ottenheijm

prof.dr. G.J.M. Stienen

CONTENTS

CHAPTER 1

INTRODUCTION

Background on nemaline myopathy

Nemaline myopathy is among the most common non-dystrophic congenital myopathies (incidence 1: 50.000) (Wallgren-Pettersson and Laing, 2000). Hallmark features of nemaline myopathy are muscle weakness and the presence of the so-called 'nemaline bodies' in the patient's muscle (Figure 1). In 1963, clinicians discovered that when zooming in on these electron-dense entities, they are threadlike structures. Hence they are named after the Greek word for thread (νήμα = nèma) (Conen et al., 1963; Shy et al., 1963). Since then, patients that have muscle weakness and exhibit these typical nemaline bodies in their muscles are diagnosed with nemaline myopathy.

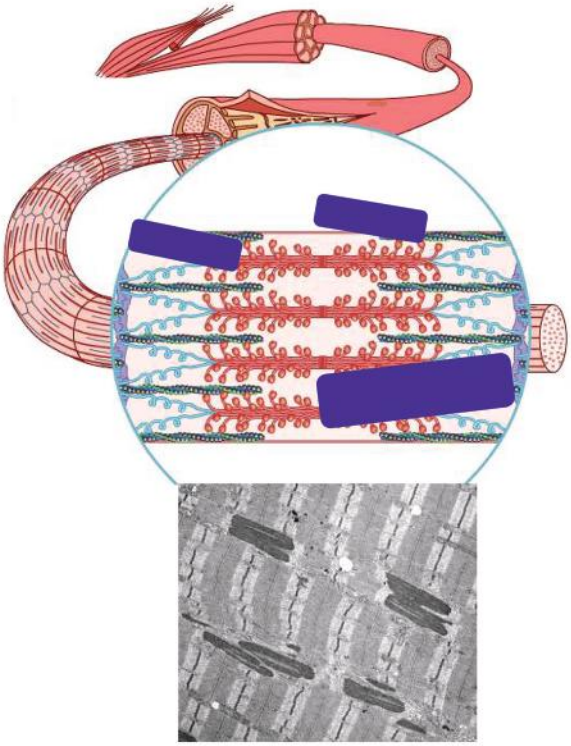

Figure 1 Schematic of nemaline bodies in skeletal muscle

Nemaline bodies are the hallmark feature of nemaline myopathy. They appear as rounded dense structures in electron microscopy images. Nemaline bodies are located in the muscle fiber. It is hypothesized that nemaline bodies contain sarcomeric proteins that are accumulating in the muscle fiber. Thus far, no clear correlation between the number of nemaline bodies and clinical severity of the disease has been observed. Thus, it is still unclear to what extent nemaline bodies interfere with sarcomeric function.

The clinical phenotype of patients with nemaline myopathy is quite diverse, ranging from neonatal death to normal lifespan with almost normal motor function (Sanoudou and Beggs, 2001). As the respiratory muscles also get involved in the disease, severely affected patients are ventilator-dependent (North et al., 1997). Nemaline myopathy is a progressive muscle disorder of which the mechanisms underlying weakness are poorly understood. Therefore, no therapeutic treatment is available yet.

The discovery of specific genes that are implicated in nemaline myopathy was an impetus for unraveling the pathophysiology of muscle weakness in this debilitating disease. In 1995, it was discovered that a mutation in the gene encoding alpha-tropomyosin – a contractile protein in skeletal muscle - resulted in nemaline myopathy (Laing et al., 1995). From thereon, more and more genes have been implicated in the disease. Currently, eleven genes have been identified. Strikingly, ten genes encode proteins that are either components of the skeletal muscle thin filament (Figure 2), including nebulin (*NEB*), skeletal muscle alpha-actin1 (*ACTA1*), beta-tropomyosin 2 (*TPM2*), alpha-tropomyosin 3 (*TPM3*), troponin T type 1 (*TNNT1*), cofilin-2 (*CFL2*), and leiomodin-3 (*LMOD3*), or are thought to contribute to stability or turnover of thin filament proteins, such as kelch repeat and BTB (POZ) Domain Containing 13 (*KBTBD13*), kelch-like family members 40 (*KLHL40*) and -41 (*KLHL41*) (Gupta et al., 2013; Ravenscroft et al., 2013; Sambuughin et al., 2010; Sanoudou and Beggs, 2001; Yuen et al., 2014). As the thin filament is an essential structure for muscle contraction, mutations in genes that code for proteins that are associated with the thin filament can result in muscle weakness.

Muscle contraction: a molecular dance between the thin and thick filament

Muscle contraction involves a cascade of events, starting in the central nervous system that commands the muscle to contract. In nemaline myopathy, the central nervous system is intact, hence commands travel along the nerve and arrive at the muscle as in healthy people. Once arrived at the muscle, the command depolarizes the membrane of the muscle fiber, which triggers the release of calcium from the sarcoplasmic reticulum towards the contractile machinery. Once calcium activates the contractile proteins, muscle contraction takes place (Figure 3). It is at this level of contraction

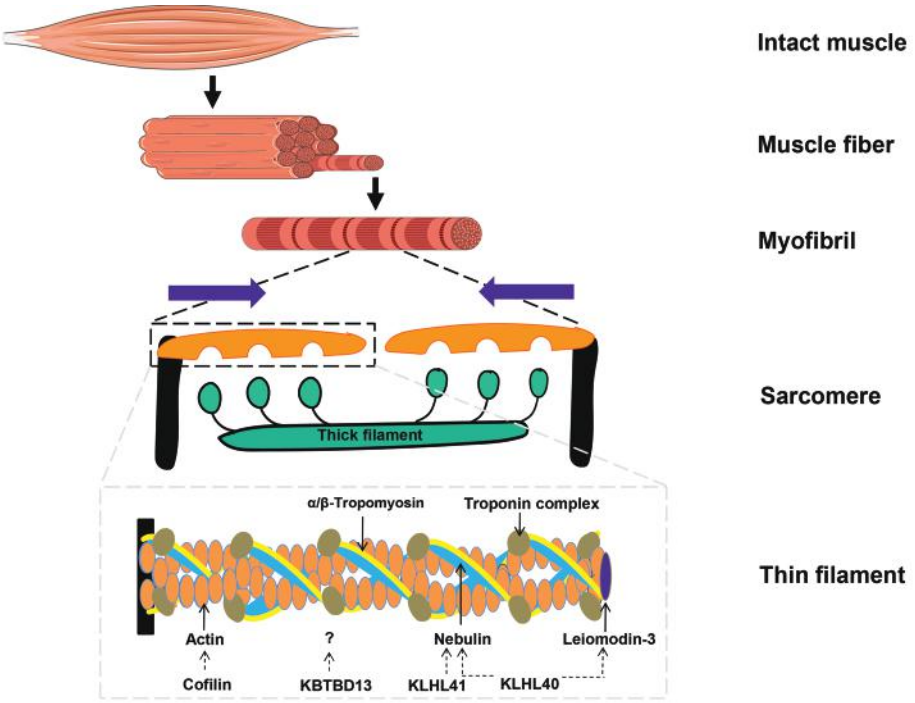

Figure 2 From intact muscle to the skeletal muscle thin filament
The thin filament is an essential structure in the sarcomere. Tropomyosin and the troponin complex are important players in thin filament activation. Actin, nebulin and leiomodin-3 are involved in both specifying the length of the thin filament as well as the regulation of acto-myosin interaction. Cofilin-2 and the kelch proteins –KBTBD13, KLHL40 and KHL41 – are associated with thin filament proteins: cofilin-2 by regulating actin dynamics, KLHL40 and KLHL41 by interacting with nebulin and KLHL40 by stabilizing leiomodin-3 and nebulin. The role of KBTBD13 has not been elucidated yet.

– function of the contractile proteins in muscle – where muscle weakness originates in patients with nemaline myopathy.

The skeletal muscle thin filament – the structure that is affected in nemaline myopathy - is important for force generation, as it is an essential structure of the sarcomere – the smallest contractile unit in muscle (Figure 2). The sarcomere is named after the Greek words ‘sarco’ = flesh and ‘meros’ = part: a sarcomere is a part of flesh. The sarcomere has four main components: the Z-disks, the thick filament, the thin filament and titin, a molecular spring that connects all components. In between Z-disks, the boarders, are the thick and the thin filament: the thin filaments are composed of actin monomers that possess binding sites for the thick filament, which is composed of

myosin molecules. Myosin, a molecular motor, has a high affinity to actin and wants to bind to actin, i.e. form a cross-bridge. Myosin heads can pull on the thin filament, moving the Z-disks towards each other, hereby shortening the muscle. However, interaction between the thin and thick filament does not take place spontaneously, but is strictly regulated by various players, starting with tropomyosin. This molecule spans 7 actin monomers, and these form a regulatory unit together with the troponin complex. Tropomyosin can move along the axis of the actin backbone, thereby controlling the availability of myosin binding sites on the actin filament. Three states of tropomyosin are described, corresponding to the position of tropomyosin along the thin filament. In the blocked state no calcium is present and tropomyosin sterically blocks myosin heads to bind to actin. In the closed state calcium binds to the troponin complex, and as a consequence tropomyosin unlocks and thereby partially unblocks the binding of myosin to actin. In the open state, tropomyosin shifts further away through initial binding of myosin hence exposing adjacent binding sites on actin to enable cross-bridge formation. That way, the thin filament is cooperatively activated by cross-bridge-induced cross-bridge (Gordon et al., 2000; McKillop and Geeves, 1993).

Commando: contraction

The state of tropomyosin and thus the likelihood of cross-bridge formation depends on upstream commands: at rest, no depolarization of the muscle's membrane takes place and troponin keeps tropomyosin in the blocked state. However, when we command our muscle to contract, the membrane of the muscle depolarizes, which results in the release of calcium from the sarcoplasmic reticulum. Calcium translocates to the troponin complex, which changes its conformation. As troponin and tropomyosin are tightly coupled, this conformational change of the troponin complex results in a shift of tropomyosin, enabling acto-myosin interaction, i.e. cross-bridge formation. Once a cross-bridge is formed, a power stroke takes place when phosphate is released from the acto-myosin complex. After the power stroke, ADP is released from the acto-myosin complex so that ATP can bind. Binding of ATP to the acto-myosin complex induces dissociation of myosin from actin. Next, ATP hydrolyses into ADP and phosphate, so that myosin is ready for the next cross-bridge cycle. To induce muscle relaxation, calcium is pumped back into the sarcoplasmic reticulum by SERCA, which requires ATP (Gordon et al., 2000) (Figure 3). When calcium dissociates from the troponin complex,

tropomyosin moves back to the blocked state and no acto-myosin interaction can take place anymore. In conclusion, contractile proteins are crucial for force generation. Therefore, mutations in genes encoding contractile proteins can have a dramatic impact on muscle strength.

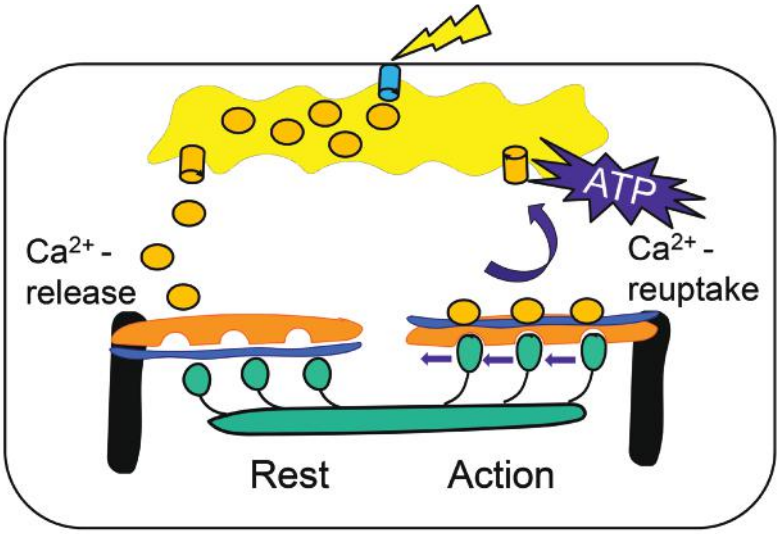

Figure 3 Schematic of the regulation of sarcomere contraction
At rest, interaction between actin (in orange) and myosin (in green) is hindered by the presence of tropomyosin (in blue). Sarcomeric contraction is induced by depolarization of the muscle fiber membrane, which triggers the release of calcium from the sarcoplasmic reticulum (in yellow). Calcium translocates to the troponin complex on actin, which results in a conformational change of the troponin complex. This change induces a shift in tropomyosin, enabling interaction of actin and myosin, i.e. sarcomere contraction. Relaxation is induced by removal of calcium form the troponin complex and reuptake of calcium by the sarcoplasmic reticulum.

Genes implicated in nemaline myopathy

Figure 4 provides an overview of genes that are implicated in nemaline myopathy. As mentioned before, ten of the eleven implicated genes code for thin filament proteins or for proteins that are thought to contribute to the stability of thin filament proteins. Roughly, the function(s) of these proteins are thin filament length regulation and/or the regulation of acto-myosin interaction. The most frequently affected gene is *NEB*, encoding nebulin. This thesis largely focuses on the pathogenesis of muscle weakness in nemaline myopathy patients with nebulin mutations. The second focus is the relatively new class of proteins involved in nemaline myopathy, proteins from the kelch family. Therefore, here I highlight nebulin's role in healthy muscle and describe the function of kelch proteins.

Nebulin

The multifunctional protein nebulin was discovered in 1982 (Wang, 1982). It has been challenging to study nebulin's function due to its enormous size – with 800 kDa one of the largest proteins in muscle. However, thanks to specialized techniques and the generation of nebulin-deficient mice it has been shown that nebulin is indispensable for muscle contraction (Bang et al., 2006; Li et al., 2015; Ottenheijm et al., 2013; Witt et al., 2006). It possesses various roles in thin filament function, which involve both specifying the length of the thin filament and the regulation of acto-myosin interaction. The protein runs along the entire thin filament, with its C-terminus anchoring in the Z-disk and the N-terminus close to the thin filament capping proteins tropomodulin and leiomodin (Castillo et al., 2009; Ottenheijm et al., 2009). Nebulin has a highly modular structure that is organized in a C-terminal domain, super-repeats and an N-terminal domain. The super-repeats consist of 7 repeats and span 43 nanometer. Typically, with its 43 nanometer, one super-repeat spans one regulatory unit: seven actin monomers, one tropomyosin molecule and one troponin complex (Jin and Wang, 1991; Ogut et al., 2003). Hence, nebulin's structure suggests a close interaction with these thin filament proteins and their function.

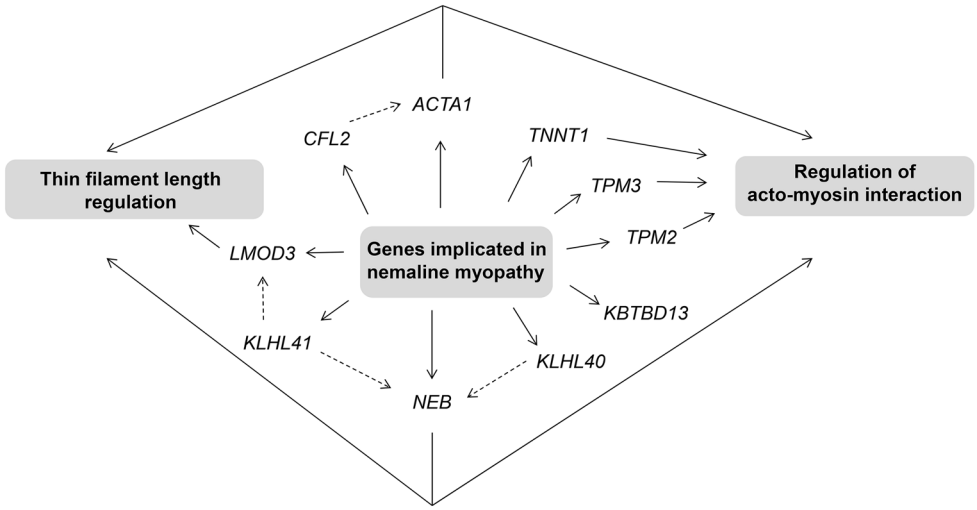

Figure 4 Genes implicated in nemaline myopathy

Currently, eleven genes have been implicated in nemaline myopathy: ten encode proteins that are either components of the skeletal muscle thin filament or are thought to contribute to stability or turnover of thin filament proteins. These proteins are involved in specifying the length of the thin filament and/or in the regulation of acto-myosin interaction. Dashed lines indicate that the specific gene interacts with the target gene.

Most nebulin mutations that have been studied thus far reveal muscle weakness at the intact muscle and myofilament level. Studies on muscle fibers isolated from patients with nebulin mutations (Ottenheijm et al., 2009), nebulin-free mouse models (Bang et al., 2006; Li et al., 2015; Ottenheijm et al., 2013; Witt et al., 2006) and cell culture (Pappas et al., 2010) revealed that muscle that lack nebulin have shorter thin filament lengths. In addition, muscle fibers from patients with nebulin mutations have a lower maximal active tension, slower cross-bridge cycling kinetics (Lawlor et al., 2011; Ottenheijm et al., 2010), and a lower calcium-sensitivity of force generation (Ottenheijm et al., 2010). Finally, nebulin plays an important role in the integrity of muscle: it augments lateral force transmission through its anchoring and interactions in the Z-disk. Muscle that lacks nebulin displays Z-disk streaming, which weakens the tight alignment that the Z-line is supposed to possess (Tonino et al., 2010).

Kelch proteins

Recently, a new class of genes was discovered to be implicated in nemaline myopathy: genes from the kelch family - a through evolution strongly conserved superfamily. These genes encode kelch proteins and first studies reveal that they interact with thin filament proteins (Garg et al., 2014; Gupta et al., 2013). In 2010, the first publication was released that linked a kelch gene – *KBTBD13* - to nemaline myopathy (Olivé et al., 2010; Sambuughin et al., 2010). To date, little is known about the function of KBTBD13 in muscle function. However, there is evidence that KBTBD13 interacts with the Cullin E3 ubiquitin-ligase, a core component of the ubiquitin-proteasome pathway (Sambuughin et al., 2012). This pathway is involved in the regulation of protein turnover. It is hypothesized that KBTBD13 functions as a substrate adaptor for specific proteins to form a functional complex with the Cullin E3 ubiquitin-ligase. Only when a protein is ligated by Cullin E3, it can be recognized by the proteasome and be degraded. Hence, proper function of Cullin E3 – as crucial player in the ubiquitin-proteasome system- is of significant importance of protein homeostasis, i.e. in controlling the quality of proteins. For KBTBD13, the specific target proteins for Cullin E3 interaction are not known yet, but it is presumed to be a thin filament protein as nemaline myopathy is a thin filament disease.

In 2014, two novel kelch genes were discovered: *KLHL40* and *KLHL41*

(Gupta et al., 2013; Ravenscroft et al., 2013). For KLHL40 it has been shown that it binds to the thin filament proteins nebulin and leiomodin-3 and to Cullin E3. That way, KLHL40 stabilizes the presence of nebulin and leiomodin-3 (Garg et al., 2014). In addition, KLHL41 interacts with nebulin and Cullin E3 (Gupta et al., 2013). Although not proven yet, it is presumed that also KLHL40 plays a role in stabilizing nebulin by forming a functional ubiquitin-complex through interaction with Cullin E3.

Hence, the first data on these recently implicated genes suggest that kelch proteins act as stabilizers for specific thin filament proteins. Thus, the discovery of kelch genes involved in nemaline myopathy is the start of a new journey in the pathophysiology of this disease.

What is the cause of muscle weakness in nemaline myopathy?

Now that the players that are involved in nemaline myopathy are known (i.e. implicated genes and proteins), we are trying to understand why muscles are weak. This is an ongoing adventure: unraveling the physiology and pathophysiology of muscle function. First, gene mutations can result in altered gene and protein levels, which leads to changes in protein function. These changes in protein function can directly influence the supposed task of the specific protein: i.e., the regulation of thin filament length and/or the regulation of acto-myosin interaction. In addition, altered thin filament function can lead to secondary changes in the muscle's ultrastructure that further contribute to muscle weakness. First, changes in contractile function of muscle fibers from patients with nemaline myopathy are described, and next changes in the ultrastructure of nemaline myopathic muscle are discussed.

Contractile performance of muscle fibers from patients with nemaline myopathy

To test contractile performance of muscle fibers, techniques have been developed to isolate single muscle fibers from frozen patient biopsies and activate these fibers using experimental solutions (Ottenheijm et al., 2009). In brief, a small piece is cut from of a frozen muscle biopsy (at -80 degrees) and slowly thawed to -20 degrees in relaxation solution containing glycerol to prevent damage. At the day of experiment, individual muscle fibers are isolated from this glycerinated piece of biopsy. Next, individual muscle fibers are permeabilized using a relaxation solution containing a detergent. This

detergent permeabilizes the lipid membrane of the muscle fibers. After washing the individual muscle fibers thoroughly with relaxation solution, they are mounted using aluminum T-clips between a length motor and a force transducer in a single fiber set-up. As the membranous structures in the muscle fibers are now permeable, the muscle fibers can be activated with experimental solutions containing exogenous calcium. That way, also compounds can be added to the experimental solutions, to investigate their effect at contractile function. Studies on permeabilized muscle fibers revealed that even when force of muscle fibers of nemaline myopathy patients is normalized to their cross-sectional area - typically force scales with the diameter of the muscle fiber -, these fibers are still weaker than muscle fibers from healthy control subjects. Hence, nemaline myopathy muscle fibers display intrinsic muscle weakness: the mutations in sarcomeric genes result in muscle weakness at the level of the sarcomere. Permeabilized muscle fiber studies taught us *that* myofilament function is lower in muscle fibers from nemaline myopathy patients and provided insight into which mechanisms implicated in force generation are compromised.

Calcium-sensitivity of force generation

As mentioned before, calcium is needed to initiate movement of muscle. By exposing the muscle fibers to graded calcium solutions, the response of the muscle fibers to various calcium levels – that reflect levels of activity – can be investigated. That way, the force generation at submaximal activity levels can be investigated. Note that these levels typically reflect physiological activity levels. These studies taught us that the calcium-sensitivity of force generation can be affected in nemaline myopathy patients. Hence, at submaximal calcium levels, less force is generated compared to healthy muscle fibers (Ottenheijm et al., 2010).

Cross-bridge cycling kinetics

At a maximal calcium concentration – which reflects maximal muscle performance – still weakness is observed in muscle fibers isolated from nemaline myopathy patient's muscles. Here, the calcium-sensitivity of force generation does not play a role anymore, as a saturating calcium concentration results in fully occupied troponin complexes: all tropomyosins are switched away, maximally enabling cross-bridge formation. Studies revealed that the cross-bridge cycling kinetics – i.e. the rate with which myosin is attached to

and released from actin – are severely altered in nemaline myopathy (Lawlor et al., 2011; Ottenheijm et al., 2010, 2011). The rate of attachment and detachment determines the period that a cross-bridge is formed and a power stroke can take place. In nemaline myopathy patients that period is shorter, as a result from slower myosin attachment and/or faster detachment. This majorly hampers force generation as the number of strongly bound cross-bridges determines the amount of force that can be generated.

Thin filament length regulation

Besides intrinsic muscle weakness caused by impaired regulation of muscle contraction, also changes in the structure of the thin filament hampers force generation. As stated above, cross-bridge formation is the basis of muscle contraction. Structurally, the number of cross-bridges is determined by the amount of overlap between the thin and the thick filament. The length of the thick filament is evolutionally conserved through species and muscle types: 1.6 um. The length of the thin filament varies between 1.1 – 1.3 um, and is tightly regulated by various proteins of which nebulin, tropomodulins and leiomodins are important players (Littlefield and Fowler, 2002). As mentioned above, genes that are implicated in nemaline myopathy are typically associated with the thin filament. Hence, when one of these thin filament length regulator genes is mutated, this can affect the length of the thin filament. Shorter than normal thin filament lengths are reported in nemaline myopathy (Ottenheijm et al., 2009; Yuen et al., 2014), and result in less overlap between the thin and the thick filament, i.e. a lower number of cross-bridges. Therefore, another factor that contributes to muscle weakness in nemaline myopathy is reduced cross-bridge formation as a result of shorter thin filaments.

Ultrastructure of muscle from patients with nemaline myopathy

The hallmark feature of nemaline myopathy is the presence of nemaline bodies in the sarcomere. Mechanisms underlying the origin of nemaline bodies and whether the presence of nemaline bodies correlates with the degree of muscle weakness are not clearly understood yet, (Ryan et al., 2003). A phenomenon that is linked to the presence of nemaline bodies is streaming of the Z-disk (Figure 1). Comparing the ultrastructure of the Z-disk of nemaline myopathy patients to healthy controls reveals that Z-disks in nemaline myopathy lose integrity. In general, in nemaline myopathy the Z-disk is wider and less structured, and nemaline bodies can emerge from

here (Tonino et al., 2010). It is postulated that a more compliant Z-disk negatively influences force generation in muscle.

In healthy muscle, the order of myofibrils is highly structured and nicely aligned from neighbor to neighbor. Nemaline myopathic muscle reveals an abnormal myofibrillar organization: myofibrils point in multiple directions and contacts with adjacent myofibrils are reduced. This hampers force transmission both laterally as well as in the direction of contraction. Hence, force generation is highly compromised.

Another pathological feature studying electron microscopy images from nemaline myopathy patients is abnormal mitochondrial organization (Malfatti et al., 2014). Mitochondria are of major importance for muscle, as they are the number one energy supplier: mitochondria produce ATP. In healthy muscle the mitochondria are oval-shaped and form a tight network below the muscle's sarcolemma and along the triads next to the Z-disk and the sarcoplasmic reticulum. Here, they provide the muscle of energy for muscle contraction (to dissociate myosin from actin in the cross-bridge cycle and to fuel SERCA to pump calcium back in the sarcoplasmic reticulum), for cell homeostasis and for other ATP requiring processes. In nemaline myopathy, various abnormalities in mitochondrial shape and organization are observed, however no clear causal relation with the disease has been determined yet.

The last morphological feature that is typical for muscle fibers from nemaline myopathy patients is that the diameter of their muscle fibers is smaller than that of healthy muscle fibers, i.e. muscle fibers are atrophic. As the number of sarcomeres in parallel is related to the amount of force that can be generated, smaller fibers generate less force. Hence, the smaller fiber diameter in muscle from nemaline myopathy patients contributes to muscle weakness.

In conclusion, the origin of muscle weakness in nemaline myopathy is a gene mutation. This gene mutation results in altered levels of the specific gene and protein or in a malfunctioning protein. Next, altered protein levels influence normal protein function and interaction with other proteins. In nemaline myopathy, thin filament protein function is affected either by changes in thin filament length regulation or the regulation of acto-myosin interaction. In

addition, altered thin filament function and structure can result in changes in the muscle's ultrastructure and atrophy. All factors can contribute to muscle weakness observed in muscle fibers of nemaline myopathy patients (see Figure 4). However, when a nemaline myopathy patient enters the clinic, we have no clue which specific mechanisms causes the muscle weakness that this patients experiences. Hence, to be able to develop targeted therapies, it is crucial to gain more insight in the pathophysiology of nemaline myopathy across all implicated genes and to investigate genotype-functional phenotype correlations. Next, therapeutic mechanisms to augment muscle strength are lacking in nemaline myopathy. Thus, novel therapeutic interventions need to be tested to be able to direct the development of targeted therapeutic therapy.

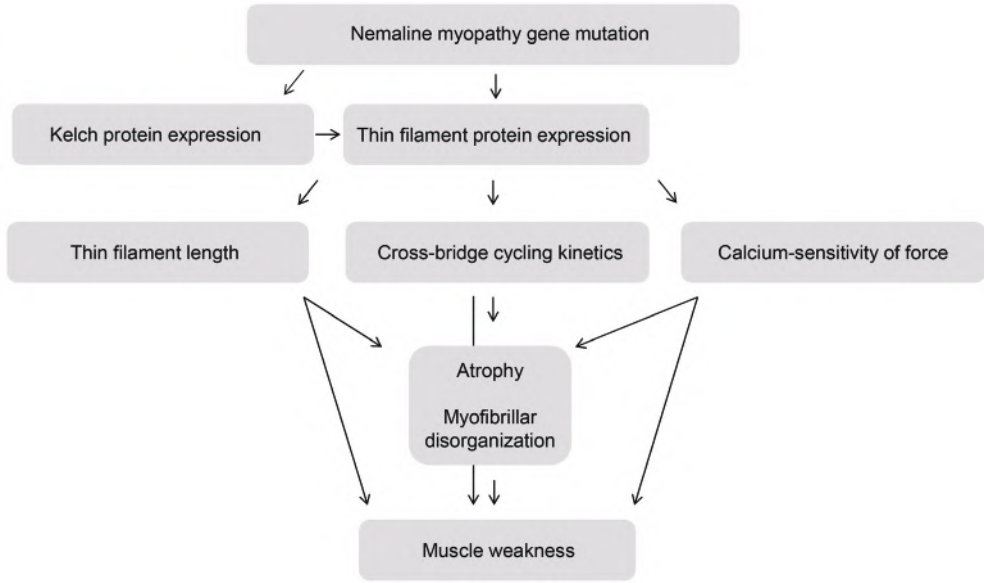

Figure 5 Mechanisms underlying muscle weakness in nemaline myopathy
Sarcomere gene mutations result in altered gene expression and protein levels, which can directly compromise sarcomere function by altering thin filament length, cross-bridge cycling kinetics and the calcium-sensitivity of force generation. Sarcomere dysfunction on its turn can lead to secondary changes in the muscle's ultrastructure that further contribute to muscle weakness: e.g. muscle fiber atrophy and myofibrillar disorganization.

Aim of the thesis

Currently no treatment exists for nemaline myopathy patients, as the mechanisms underlying muscle weakness are only partly understood. The aim of this thesis is to gain more insight into the pathophysiology of muscle weakness in nemaline myopathy, to investigate the presence of genotype-functional phenotype correlations, and to test potential therapeutic targets to restore muscle strength. This thesis is divided into two parts: (1) Pathophysiology of nemaline myopathy (chapter 1-4) and (2) Therapeutic targets for nemaline myopathy (chapter 5-7).

Pathophysiology of nemaline myopathy (Chapter 2-5)

The first four chapters elucidate mechanisms that contribute to muscle weakness in nemaline myopathy. We collected a large number of muscle biopsies covering the majority of genes implicated in nemaline myopathy to further investigate genotype-functional phenotype correlations in the disease. In Chapter 2 we investigated whether thin filament dysregulation contributed to muscle weakness across muscle fibers isolated from fifty-one biopsies of patients with nemaline myopathy harboring mutations in 8 genes. The large number of affected genes that are implicated in this study provides us the possibility to investigate whether genotype-functional phenotype correlations exists regarding the contribution of thin filament dysregulation to muscle weakness. In Chapter 3 we combined ultrastructural studies with functional studies on muscle fibers from nemaline myopathy patients with mutation in the nebulin gene. That way, we investigated whether the muscle's ultrastructure and the presence and localization of nemaline bodies are correlated to muscle weakness in these fibers. In Chapter 4 we characterized the in vivo and in vitro contractile performance of heterozygous nebulin-knockout mice, and investigated whether changes in sarcomeric gene and protein levels were correlated to the contractile phenotype. In Chapter 5 we investigated the role of KBTBD13 in the pathogenesis of muscle weakness. We collected muscle biopsies from patients with mutations in the *KBTBD13* gene and generated a *Kbtbd13*-KO mouse model to characterize the contractile performance of KBTBD13-deficient muscle at the intact muscle level and at the myofilament level.

Therapeutic targets for nemaline myopathy (Chapter 6-8)

The second part of this thesis focuses on potential therapeutic targets to restore muscle strength in nemaline myopathy. Troponin activation is a mechanism to augment muscle force at submaximal calcium levels: it slows the dissociation of calcium from the troponin complex, thereby stabilizing the open conformation of the troponin/tropomyosin complex to enhance cross-bridge formation at a given calcium concentration (Russell et al., 2012). Chapter 6 describes the effect of a slow-troponin activator - Levosimendan, which exerts its effect through slow troponin C - on muscle fibers from nemaline myopathy patients with mutations in the nebulin gene. In Chapter 7 and 8 the effect of a fast troponin activation on augmenting muscle force in nebulin-deficient muscle is investigated. Chapter 7 describes the effect of the fast troponin activator CK-2066260 on nebulin-deficient mouse tissue, and Chapter 8 describes the effect of CK-2066260 on muscle fibers from nemaline myopathy patients with mutations in the nebulin gene.

REFERENCES

Bang M-L, Li X, Littlefield R, Bremner S, Thor A, Knowlton KU, et al. Nebulin-deficient mice exhibit shorter thin filament lengths and reduced contractile function in skeletal muscle. J. Cell. Biol. 2006; 173: 905–916.

Castillo A, Nowak R, Littlefield KP, Fowler VM, Littlefield RS. A nebulin ruler does not dictate thin filament lengths. Biophys. J. 2009; 96: 1856–1865.

Conen PE, Murphy EG, Donohue WL. Light and electron microscopic studies of 'myogranules' in a child with hypotonia and muscle weakness. Can. Med. Assoc. J. 1963; 89: 983–6.

Garg A, O'Rourke J, Long C, Doering J, Ravenscroft G, Bezprozvannaya S, et al. KLHL40 deficiency destabilizes thin filament proteins and promotes nemaline myopathy. J. Clin. Invest. 2014; 124: 3529–3539.

Gordon AM, Homsher E, Regnier M. Regulation of Contraction in Striated Muscle. Physiol Rev 2000; 80: 853–924.

Gupta VA, Ravenscroft G, Shaheen R, Todd EJ, Swanson LC, Shiina M, et al. Identification of KLHL41 Mutations Implicates BTB-Kelch-Mediated Ubiquitination as an Alternate Pathway to Myofibrillar Disruption in Nemaline Myopathy. Am. J. Hum. Genet. 2013; 93: 1108–17.

Jin J-P, Wang K. Nebulin as a giant actin-binding template protein in skeletal muscle sarcomere Interaction of actin and cloned human nebulin fragments. FEBS Lett. 1991; 281: 93–96..

Laing NG, Wilton SD, Akkari PA, Dorosz S, Boundy K, Kneebone C, et al. A mutation in the alpha tropomyosin gene TPM3 associated with autosomal dominant nemaline myopathy. Nat. Genet. 1995; 9: 75–9.

Lawlor MW, Ottenheijm CA, Lehtokari V-L, Cho K, Pelin K, Wallgren-Pettersson C, et al. Novel mutations in NEB cause abnormal nebulin expression and markedly impaired muscle force generation in severe nemaline myopathy. Skelet. Muscle. 2011; 1: 23.

Li F, Buck D, De Winter J, Kolb J, Meng H, Birch C, et al. Nebulin deficiency in adult muscle causes sarcomere defects and muscle-type dependent changes in trophicity--novel insights in nemaline myopathy. Hum. Mol. Genet. 2015

Littlefield R, Fowler VM. Measurement of thin filament lengths by distributed deconvolution analysis of fluorescence images. Biophys. J. 2002; 82: 2548–64.

Malfatti E, Lehtokari V-L, Böhm J, De Winter JM, Schäffer U, Estournet B, et al. Muscle histopathology in nebulin-related nemaline myopathy: ultrastructural findings correlated to disease severity and genotype. Acta Neuropathol. Commun. 2014; 2: 44.

McKillop DF, Geeves MA. Regulation of the interaction between actin and myosin subfragment 1: evidence for three states of the thin filament. Biophys. J. 1993; 65: 693–701.

North KN, Laing NG, Consortium I. Nemaline myopathy: current concepts. The ENMC International Consortium and Nemaline Myopathy. J. Med. Genet. 1997; 34: 705–713.

Ogut O, Hossain MM, Jin J-P. Interactions between nebulin-like motifs and thin filament regulatory proteins. J. Biol. Chem. 2003; 278: 3089–3097.

Olivé M, Goldfarb LG, Lee H-S, Odgerel Z, Blokhin A, Gonzalez-Mera L, et al. Nemaline myopathy type 6: clinical and myopathological features. Muscle Nerve 2010; 42: 901–7.

Ottenheijm CAC, Buck D, de Winter JM, Ferrara C, Piroddi N, Tesi C, et al. Deleting exon 55 from the nebulin gene induces severe muscle weakness in a mouse model for nemaline myopathy. Brain 2013; 136: 1718–31.

Ottenheijm CAC, Hooijman P, DeChene ET, Stienen GJ, Beggs AH, Granzier H. Altered myofilament function depresses force generation in patients with nebulin-based nemaline myopathy (NEM2). J. Struct. Biol. 2010; 170: 334–343.

Ottenheijm CAC, Lawlor MW, Stienen GJM, Granzier H, Beggs AH. Changes in cross-bridge cycling underlie muscle weakness in patients with tropomyosin 3-based myopathy. Hum. Mol. Genet. 2011; 20: 2015–2025.

Ottenheijm CAC, Witt CC, Stienen GJ, Labeit S, Beggs AH, Granzier H. Thin filament length dysregulation contributes to muscle weakness in nemaline myopathy patients with nebulin deficiency. Hum. Mol. Genet. 2009; 18: 2359–2369.

Pappas CT, Krieg PA, Gregorio CC. Nebulin regulates actin filament lengths by a stabilization mechanism. J. Cell. Biol. 2010; 189: 859–870.

Ravenscroft G, Miyatake S, Lehtokari V-L, Todd EJ, Vornanen P, Yau KS, et al. Mutations in KLHL40 Are a Frequent Cause of Severe Autosomal-Recessive Nemaline Myopathy. Am. J. Hum. Genet. 2013; 93: 6–18.

Russell AJ, Hartman JJ, Hinken AC, Muci AR, Kawas R, Driscoll L, et al. Activation of fast skeletal muscle troponin as a potential therapeutic approach for treating neuromuscular diseases. Nat. Med. 2012; 18: 452–455.

Ryan MM, Ilkovski B, Strickland CD, Schnell C, Sanoudou D, Midgett C, et al. Clinical course correlates poorly with muscle pathology in nemaline myopathy. Neurology 2003; 60: 665–673.

Sambuughin N, Swietnicki W, Techtmann S, Matrosova V, Wallace T, Goldfarb L, et al. KBTBD13 interacts with Cullin 3 to form a functional ubiquitin ligase. Biochem. Biophys. Res. Commun. 2012; 421: 743–9.

Sambuughin N, Yau KS, Olivé M, Duff RM, Bayarsaikhan M, Lu S, et al. Dominant mutations in KBTBD13, a member of the BTB/Kelch family, cause nemaline myopathy with cores. Am. J. Hum. Genet. 2010; 87: 842–847.

Sanoudou D, Beggs AH. Clinical and genetic heterogeneity in nemaline myopathy-a disease of skeletal muscle thin filaments. Trends Mol. Med. 2001; 7: 362–368.

Shy GM, Engel WK, Somers JE, Wanko T. Nemaline Myopathy. Brain 1963; 86: 793–810.

Tonino P, Pappas CT, Hudson BD, Labeit S, Gregorio CC, Granzier H. Reduced myofibrillar connectivity and increased Z-disk width in nebulin-deficient skeletal muscle. J. Cell Sci. 2010; 123: 384–91.

Wallgren-Pettersson C, Laing NG. Report of the 70th ENMC International Workshop: Nemaline myopathy, 11-13 June 1999, Naarden, The Netherlands. Neuromuscul. Disord. 2000; 10: 299–306.

Wang K. Structural and Contractile Proteins Part B: The Contractile Apparatus and the Cytoskeleton. Elsevier; 1982.

Witt CC, Burkart C, Labeit D, McNabb M, Wu Y, Granzier H, et al. Nebulin regulates thin filament length, contractility, and Z-disk structure in vivo. EMBO J. 2006; 25: 3843–3855.

Yuen M, Sandaradura SA, Dowling JJ, Kostyukova AS, Moroz N, Quinlan KG, et al. Leiomodin-3 dysfunction results in thin filament disorganization and nemaline myopathy. J. Clin. Invest. 2014; 124

CHAPTER 2

MUTATION-SPECIFIC EFFECTS ON THIN FILAMENT LENGTH IN THIN FILAMENT MYOPATHY

Josine M. de Winter, B. Joureau, E.J. Lee, B. Kiss, M. Yuen, V.A. Gupta, C.T. Pappas C.C. Gregorio, G.J.M. Stienen, S. Edvardson, C. Wallgren-Pettersson, V.L. Lehtokari, K. Pelin, E. Malfatti, N.B. Romero, B.G. van Engelen, N.C. Voermans, S. Donkervoort, C.G. Bönnemann, N.F. Clarke, A.H. Beggs, H. Granzier, and C.A.C. Ottenheijm

Annals of Neurology, 2016

ABSTRACT

Background | Thin filament myopathies are among the most common non-dystrophic congenital muscular disorders, and are caused by mutations in genes encoding proteins that are associated with the skeletal muscle thin filament. Mechanisms underlying muscle weakness are poorly understood, but might involve the length of the thin filament, an important determinant of force generation.

Methods | We investigated the sarcomere length-dependence of force, a functional assay that provides insights into the contractile strength of muscle fibers as well as the length of the thin filaments, in muscle fibers from fifty-one patients with thin filament myopathy caused by mutations in *NEB, ACTA1, TPM2, TPM3, TNNT1, KBTBD13, KLHL40 and KLHL41*.

Results | Lower force generation was observed in muscle fibers from patients of all genotypes. In a subset of patients that harbor mutations in *NEB* and *ACTA1*, the lower force was associated with downward shifted force-sarcomere length relations, indicative of shorter thin filaments. Confocal microscopy confirmed shorter thin filaments in muscle fibers of these patients. A conditional Neb knock-out mouse model, which recapitulates thin filament myopathy, revealed a compensatory mechanism: the lower force generation that was associated with shorter thin filaments was compensated by increasing the number of sarcomeres in series. This allowed muscle fibers to operate at a shorter sarcomere length and maintain optimal thin-thick filament overlap.

Interpretation | These findings might provide a novel direction for the development of therapeutic strategies for thin filament myopathy patients with shortened thin filament lengths.

INTRODUCTION

Nemaline myopathy and congenital fiber type disproportion are among the most common non-dystrophic congenital muscular disorders (Colombo et al., 2015). Genes that are implicated in these myopathies encode proteins that are either components of the skeletal muscle thin filament, including nebulin (*NEB*), skeletal muscle alpha-actin1 (*ACTA1*), beta-tropomyosin 2 (*TPM2*), alpha-tropomyosin 3 (*TPM3*), troponin T type 1 (*TNNT1*), cofilin-2 (*CFL2*), and leiomodin-3 (*LMOD3*), or are thought to contribute to stability or turnover of thin filament proteins, such as kelch repeat and BTB (POZ) Domain Containing 13 (*KBTBD13*), kelch-like family members 40 (*KLHL40*) and -41 (*KLHL41*) (Gupta et al., 2013; Ravenscroft et al., 2013; Sambuughin et al., 2010; Sanoudou and Beggs, 2001; Yuen et al., 2014). Hence, muscle diseases caused by mutations in these genes are here referred to as thin filament myopathies. For a schematic of the thin filament and its associated proteins, see figure 1). Patients with thin filament myopathy suffer from muscle weakness, but the underlying mechanisms are poorly understood.
The thin filament is a major constituent of the sarcomere, the smallest contractile unit in muscle, and is essential for force generation: its length determines the overlap between the thin and thick filament, and thereby the number of force-generating interactions that can be formed between actin and myosin. In healthy human muscle, the length of the thick filament is 1.6 μm and that of the thin filament is regulated at 1.1-1.3 μm (Littlefield and Fowler, 2002). Accordingly, force depends on sarcomere length, with increasing force as the overlap between thick and thin filaments increases (up to a sarcomere length of ~2.6 μm, i.e. the ascending limb of the force-sarcomere length relation), and decreasing force at longer sarcomere lengths as the overlap between thick and thin filaments decreases (i.e., the descending limb) (Fig 2A; (Gordon et al., 1966; Granzier et al., 1991)). Hence, appropriate length of the thin filament is important for muscle fiber strength - a shorter length causes lower force generation by shifting the descending limb of the force-sarcomere length relation downward.

Whether mutations in genes implicated in thin filament myopathy contribute to force loss by affecting thin filament length is unclear. Mouse models with mutations in *Neb* exhibit a shorter thin filament length associated with lower force generation that becomes more prominent as sarcomere length increases

(Bang et al., 2006; Ottenheijm et al., 2013; Witt et al., 2006). Preliminary studies on a small number of human biopsies were largely in agreement with this observation (Ochala et al., 2011; Ottenheijm et al., 2009). Whether these findings translate to a large group of patients, and whether shorter thin filament length is a general mechanism underlying force loss in thin filament myopathies with a variety of different gene defects, is unknown.

Therefore, we studied muscle fibers from fifty-one patients with thin filament myopathy caused by mutations in *NEB, ACTA1, TPM2, TPM3, TNNT1, KBTBD13, KLHL40* and *KLHL41*. In these fibers we determined the sarcomere length-dependence of force, a functional assay that provides insight into the contractile strength of muscle fibers as well as the length of the thin filaments. In a novel, conditional *Neb* knock-out mouse model that recapitulates thin filament myopathy - including shorter thin filament length - we studied whether muscle possesses mechanisms that compensate for shorter thin filament length, and we specifically focused on the addition of sarcomeres in series.

METHODS

Muscle biopsies

Ethical approval for the use of muscle specimens – remaining from diagnostic procedures or obtained during clinically indicated surgical procedures - was obtained from the Human Research Ethics Committees of the Boston Children's Hospital Institutional Review Board (03-08-128R) (*NEB-1 – NEB-3; ACTA1-1 – ACTA1-4; KLHL40-1; KLHL41-1*), the Children's Hospital at Westmead (10/CHW/45) (*ACTA1-5 – ACTA1-13; TPM3-1 – TPM3-10; TPM2-1 – TPM2-3; CTRL 1-8*), National Institutes of Health, Neuromuscular and Neurogenetic Disorders of Childhood Section, Bethesda (*TPM3-11 - 12*), Groupe Hospitalier Pitié-Salpêtrière in Paris (DC-2012-1693) (*NEB-4 – NEB-7, NEB-9 and ACTA1-14*), the Radboud University Medical Centre in Nijmegen (*KBTBD13-1 – KBTBD13-10*), the Children's Hospital of the University of Helsinki (6/E7/2005) (*NEB-8*) and the Hadassah Medical Center in Jerusalem (0421-14-HMO) (*TNNT1-1*). Supplemental Table 1 shows the clinical and genetic data of the subjects that were biopsied. From all participants, written informed consent was obtained for genetic testing and biobanking of muscle.

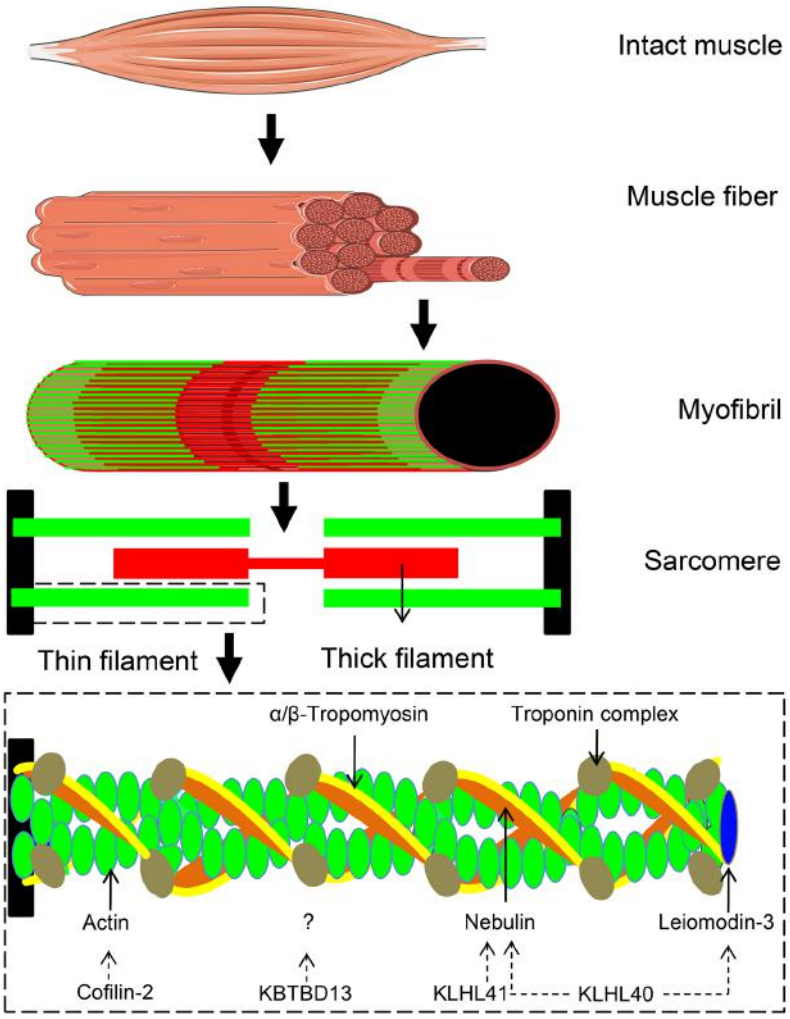

Figure 1 Schematic of the skeletal muscle thin filament

The thin filament is an essential structure in the sarcomere, the smallest contractile unit in skeletal muscle. The actin-based backbone of the thin filament is decorated with proteins that are involved in the regulation of thin filament length and in muscle activation. Tropomyosin and the troponin complex decorate the thin filament along its entire length and are important players in thin filament activation (Gordon et al., 2000). Actin, nebulin and leiomodin-3 are involved in both specifying the length of the thin filament as well as thin filament activation (Gordon et al., 2000; Ottenheijm and Granzier, 2010; Yuen et al., 2014). Both cofilin-2 and the kelch proteins –KBTBD13, KLHL40 and KHL41 – are associated with thin filament proteins: cofilin-2 by regulating actin dynamics(Agrawal et al., 2012), KLHL40 and KLHL41 by interacting with nebulin and KLHL40 by stabilizing leiomodin-3. The role of KBTBD13 has not been elucidated yet, but as it is required for the formation of a functional cullin-3 ubiquitin ligase complex, and as mutations in KBTBD13 result in thin filament myopathy, it is hypothesized to be involved in stabilizing thin filament proteins (Gupta and Beggs, 2014).

CTRL 1-8 are control subjects with no medical history. All biopsies were stored frozen and unfixed at -80°C until use.

Permeabilized muscle fiber mechanics

Small strips dissected from the muscle biopsies were permeabilized overnight as described previously (Ottenheijm et al., 2009). This procedure renders the membranous structures in the muscle fibers permeable, which enables activation of the myofilaments with exogenous calcium. Preparations were washed thoroughly with relaxing solution and stored in 50% glycerol/relaxing solution at -20°C. Small muscle bundles (cross-sectional area ~0.07 mm^2, in case of atrophic fibers in patients) and single muscle fibers (control subjects and mildly affected patients) were dissected from the permeabilized strips, and were mounted using aluminum T-clips between a length motor (ASI 403A, Aurora Scientific Inc., Ontario, Canada) and a force transducer element (ASI 315C-I, Aurora Scientific Inc., Ontario, Canada) in a single fiber apparatus (ASI 802D, Aurora Scientific Inc., Ontario, Canada) that was mounted on the stage of an inverted microscope (Zeiss Axio Observer A1). Sarcomere length was set using a high speed VSL camera and ASI 900B software (Aurora Scientific Inc., Ontario, Canada). Mechanical experiments were performed at incremental sarcomere lengths: 2.0 µm – 2.2 µm – 2.5 µm – 2.8 µm – 3.2 µm and 3.5 µm. Fiber width and diameter were measured at three points along the fiber and the cross-sectional area was determined assuming an elliptical cross-section. Three different types of bathing solutions were used during the experimental protocols: a relaxing solution (100 mM BES; 6.97 mM EGTA; 6.48 mM $MgCl_2$; 5.89 mM Na_2-ATP; 40.76 mM K-propionate; 14.5 mM creatine phosphate), a pre-activating solution with low EGTA concentration (100 mM BES; 0.1 mM EGTA; 6.42 mM $MgCl_2$; 5.87 mM Na_2-ATP; 41.14 mM K-propionate; 14.5 mM creatine phosphate; 6.9 mM HDTA), and an activating solution (100 mM BES; 7.0 mM Ca-EGTA; 6.28 mM $MgCl_2$; 5.97 mM Na_2-ATP; 40.64 mM K-propionate; 14.5 mM creatine phosphate). The temperature of the bathing solutions was kept constant at 20°C using a TEC controller (ASI 825A, Aurora Scientific Inc. Ontario, Canada).To prevent rundown of force during the protocol, muscle preparations were mounted in a relaxation solution at 1°C. Subsequently, the muscle preparations were pre-activated by switching to an activation solution at 1°C. In that way, fibers were loaded with calcium, but no force is generated. By rapid switching to an activation solution at 20°C, the fibers were activated and force was

generated. This procedure minimizes the duration of activation and force rundown. After the force plateau was reached, relaxation was induced by switching back to the bath with relaxation solution (Malfatti et al., 2014; de Winter et al., 2015).

Myosin heavy chain isoform analysis

A specialized SDS-PAGE was used to determine the myosin heavy chain isoform composition of the muscle fiber preparations that we used in our contractility experiments (Ottenheijm et al., 2009). In brief, muscles fibers were denatured by boiling for 2 minutes in SDS sample buffer and electrophoresis was performed for 24h at 15°C and a constant voltage of 275 volt using a 4% stacking gel (pH 6.7), and a 7% separating gel (pH 8.7) with 30% glycerol (v/v). Finally, the gels were silver-stained, scanned, and analyzed with One-D scan EX (Scanalytics Inc., Rockville, MD, USA) software.

Nebulin protein levels

To assess nebulin protein levels, muscle samples from CTRL (n = 5) and *NEB* (n =7) were homogenized and analyzed on 1% agarose electrophoresis gels, as previously described(Warren et al., 2003). To prevent protein degradation, all buffers contained protease inhibitors (phenylmethylsulfonyl fluoride (PMSF), 0.5mM; leupeptin, 0.04mM; E64, 0.01mM). Gels were scanned and analyzed with One-D scan EX (Scanalytics Inc., Rockville, MD, USA) software. The integrated optical density of nebulin and myosin heavy chain (MHC) was determined. For Western blot analysis, one or two-color infrared western blots were scanned (Odyssey Infrared Imaging System, Li-Cor Biosciences, NE, USA) and the images analyzed with One-D scan EX.

Confocal microscopy

Small muscle strips were dissected and permeabilized as described above in the permeabilized muscle fiber mechanics section. Immunolabelling and confocal scanning laser microscopy was performed as described previously (Ottenheijm et al., 2013). In brief, muscle bundles were stretched and fixed on a glass slide, and incubated with the following antibodies: Alexa Fluor® 488 conjugated phalloidin (A12379, Invitrogen) to stain the thin filament; a cocktail of primary antibodies against slow skeletal myosin heavy chain (ab11083, Abcam) and fast skeletal myosin heavy chain (ab51263, Abcam) followed by Alexa Fluor® 594 (goat anti-mouse, Invitrogen) as secondary

antibody to stain the thick filament. Images were captured using a Leica DM IRE2 Confocal Laser Scanning Microscope. From the acquired images, line scans were obtained using ImageJ software (National Institutes of Health). For phalloidin line scans, the half width at half maximum was used as indication of thin filament length. Thick filament length was measured from myosin line scans (full width at half maximum).

Sarcomeres in series in a conditional nebulin knockout mouse model
For the creation ofconditional nebulin knockout mice, see Li and coworkers (Li et al., 2015). In brief, for *Neb* cKO mice, a targeting vector was made with loxP sites inserted downstream of exon 3 (which contains the start codon for Nebulin and corresponds to exon 1 of Bang and coworkers (Bang et al., 2006) and in the 5' untranslated region of exon 2 upstream of the ATG. Floxed mice were bred to a *MCK-Cre* strain (#6475 Jackson Laboratory) that expresses Cre recombinase under control of the Muscle Creatine Kinase (MCK) promotor that is expressed in striated muscle (Lyons et al., 1991). Genotyping was used to determine the presence of the *MCK-Cre* transgene (following the protocol provided by the Jackson Laboratory) and the floxed nebulin allele. Mice homozygous for the floxed nebulin allele were bred to mice that were hemizygous for *MCK-Cre* and heterozygous for the floxed allele (*MCKCre+, Neb*$^{+/flox}$). Offspring that was hemizygous for MCK-Cre and homozygous for the floxed allele (*MCKCre+, Neb*$^{flox/flox}$) was deficient in nebulin and is referred to as *Neb*$^{-/-}$. We used as control offspring that had nebulin WT allele and that were either *MCK-Cre* positive or negative. All animal experiments were approved by the University of Arizona Institutional Animal Care and Use Committee and followed the U.S. National Institutes of Health "Using Animals in Intramural Research" guidelines for animal use. Similar to the methods described above for human muscle fibers, permeabilized mouse fibers were activated with exogenous calcium at incremental sarcomere lengths to investigate the force-sarcomere length relation, and confocal microscopy was used to determine thin and thick filament length.

In addition, small permeabilized strips were isolated from tendon to tendon of mouse m. soleus and were mounted in a single fiber apparatus (ASI 802D, Aurora Scientific Inc., Ontario, Canada) as described above in the permeabilized muscle fiber mechanics section. The sarcomere length was

set at 2.5 µm using a high speed VSL camera and ASI 900B software (Aurora Scientific Inc., Ontario, Canada). Muscle fiber length was determined from tendon to tendon. Muscle length was divided by the mean sarcomere length to provide the number of sarcomeres in series. This number was normalized to tibia length (note that tibia length was not different between *Neb*$^{-/-}$ and *Neb*$^{+/+}$ mice.)

To determine the sarcomere length at the muscle length that generates optimal force, intact left soleus muscles were quickly dissected from tendon to tendon and, using silk suture, mounted vertically in a tissue bath between a dual-mode lever arm (300C, Aurora Scientific Inc., Canada) and a fixed hook. Soleus muscles were chosen because of their well-defined tendons and their small size, which facilitates oxygenation. The muscle was bathed in continuously oxygenated (95% O_2–5% CO_2) mammalian Ringer solution with pH 7.40. The temperature of the solution was maintained at 30°C during the experiment. The muscle was stimulated by field stimulation with platinum plate electrodes placed in close apposition to the muscle. Optimal muscle length was determined by stimulating the muscle maximally at incremental muscle lengths, until maximal force was achieved (pulse duration of 200 µs). Then, muscle length was measured from tendon to tendon, the muscle was chemically fixed at optimal length and sarcomere length was measured with optical microscopy.

Statistical analyses

Data are presented as mean ± SEM. For statistical analyses, *t*-tests were used. A *P*-value < 0.05 was considered statistically significant.

RESULTS

Muscle fibers were isolated from biopsies of healthy controls (CTRL) (n=8) and patients (n=51) with mutations in *NEB* (n=9), *ACTA1* (n=14), *TPM3* (n=12), *TPM2* (n=3), *TNNT1* (n=1), *KBTBD13* (n=10), *KLHL40* (n=1) and *KLHL41* (n=1) (for patient characteristics, see Supplemental Table 1). From each biopsy, 3-9 muscle fiber preparations were permeabilized and maximally activated with exogenous calcium. Force was measured at incremental sarcomere lengths (2.0 – 3.5 µm) to investigate the sarcomere-length dependency of force.

Maximal force generation is lower in muscle fibers from thin filament myopathy patients

To compare the contractile strength of muscle fibers from patients – which typically are atrophic – to those from control subjects, the generated forces were normalized to the fibers' cross-sectional area (i.e., tension). Hence, maximal active tensions of muscle fibers are independent of the diameterof the fibers and reflect the intrinsic contractile capacity of the myofilament proteins. Lower maximal active tension was observed in all gene cohorts, when compared to CTRL muscle fibers (Table 1). Note that the protein product of *TPM3* is expressed predominantly in slow-twitch fibers, and, accordingly, slow-twitch fibers from patients with mutations in this gene had lower maximal active tension, whereas in fast-twitch fibers maximal active tension was similar to that of fibers from CTRL. Thus, muscle fibers from patients with thin filament myopathy exhibit lower force generation, with the most pronounced force loss in patients carrying *NEB, ACTA1* and *KLHL40* mutations.

The force-sarcomere length relation is shifted downwards in muscle fibers from patients with mutations in NEB and ACTA1

Force at incremental sarcomere lengths was fitted using a 2nd order polynomial (Udaka et al., 2008): this yielded three parameters that describe the force-sarcomere length relation: the sarcomere length at which maximum force is generated (SL_{opt}), the sarcomere length at which 50% of maximum force is generated (SL_{50}) and the sarcomere length at which the fit crosses the X-axis, thus no force is generated (SL_x, Fig 2A). The fits in figure 2B-I represent the mean of the fits of the individual patients; data from individual subjects are shown in Supplemental Table 2. In *NEB* patients, a downward shift of the descending limb of the force-sarcomere length relation was observed (Fig 2B), which was accompanied by a significant shorter SL_{opt} (2.41±0.04 in patients vs. 2.61±0.02 μm in controls), SL_{50} (3.39±0.05 in patients vs. 3.58±0.03 μm in controls) and SL_x (3.85±0.07 in patients vs. 4.02±0.03 μm in controls). Accordingly, force loss was most prominent at long sarcomere lengths, with the force deficit doubling across the operating sarcomere length range in human skeletal muscle (~2.9 μm (87% of CTRL) – 3.6μm (43% of CTRL) (Cromie et al., 2013); dashed area and right Y-axis in Fig 2B). These findings suggest that patients with *NEB* mutations have shorter thin filament lengths.

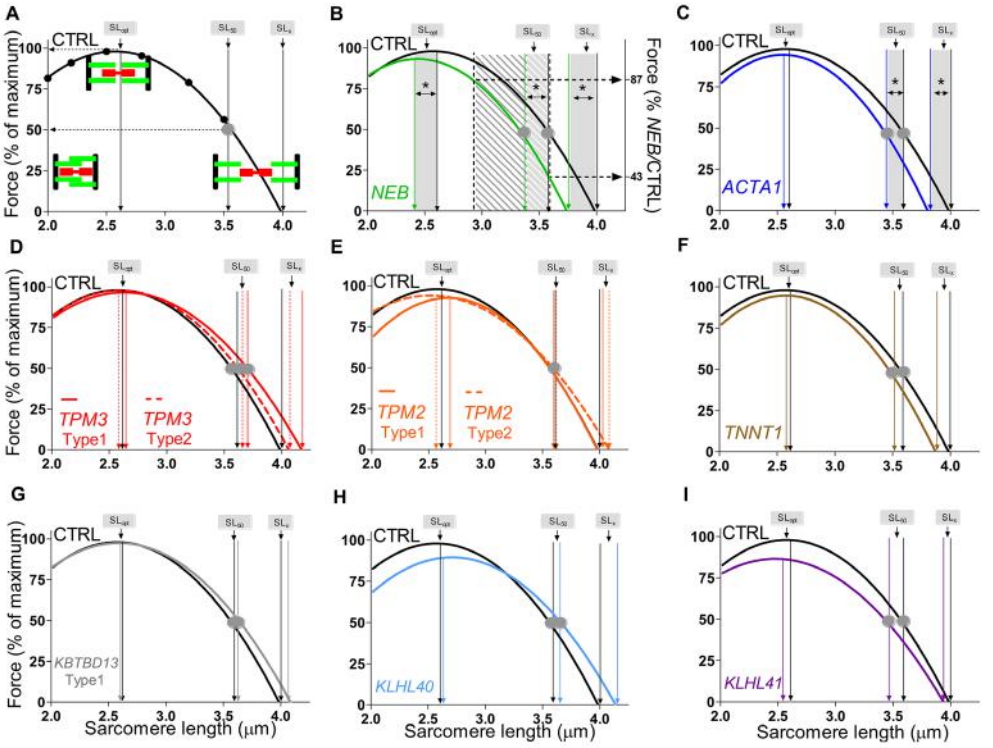

Figure 2 The force-sarcomere length relation in muscle fibers from thin filament myopathy patients and control subjects

(A) The shape of the force-sarcomere length relation is determined by the amount of overlap between the thick and thin filament. Force at incremental sarcomere lengths is fitted using a 2nd order polynomial: this yields three parameters describing the force-sarcomere length relation: the sarcomere length at which maximum force is generated (SL_{opt}), the sarcomere length at which 50% of maximum force is generated (SL_{50}) and the sarcomere length at which the fit crosses the X-axis (SL_x). Data shown is from control subjects. The fits represent the mean of individual subjects per genotype. (B-C) *NEB* (N=9) and *ACTA1* (N=13) muscle fibers exhibit a downward shift of the descending limb of the force-sarcomere length relation compared to controls. Note that in patients with mutations in *NEB* (panel B) this results in a doubling of the force deficit (right Y-axis) across the *in vivo* sarcomere length range (shaded area). (D-I) Muscle fibers from patients with mutations in *TPM3* (N=10), *TPM2* (N=3), *TNNT1* (N=1), *KBTBD13* (N=10), *KLHL40* (N=1) and *KLHL41* (N=1) exhibit a preserved force-sarcomere length relation. Note that the protein products of *TPM3* and *TPM2* are predominantly expressed in type-I fibers and that these fibers exhibited normal force-sarcomere length relations. T-tests were performed between genotype and CTRL, $p<0.05$ was considered statistically significant (indicated by*). For each biopsy (N) 3-9 muscle fibers were measured.

A novel finding of this study is that patients with mutations in *ACTA1*, encoding skeletal muscle alpha-actin, the main component of the thin filament, can also cause a significant downward shift of the descending limb of the force-sarcomere length relation, with significant shorter SL_{50} (3.47±0.02 µm in patients vs. 3.58±0.03 µm in controls) and SL_x (3.89±0.03 vs. 4.02±0.03 µm, patients vs. controls) (Fig 2C). Note that fibers from some *NEB* patients (*NEB-1, NEB-4, NEB-5, NEB-8*) and some *ACTA1* patients (*ACTA1-5, ACTA1-6, ACTA1-9, ACTA1-10*) had force-sarcomere length relations that overlapped with controls (Table 2 and Fig 3A).

For the other thin filament genes that were investigated in this study – *TPM3, TPM2, TNNT1, KBTBD13, KLHL40* and *KLHL41* - no changes in the force-sarcomere length relation were observed (Fig 2D-H and Table 1). For *KLHL40, KLHL41* and *TNNT1* only one biopsy representing each genotype was available for contractility experiments, thus these findings should be interpreted with caution.

TABLE 1. Functional data of thin filament myopathy patients and controls

Gene	N Biopsies	Maximal active tension mN/mm²	SL_{opt} µm	SL_{50} µm	SL_x µm
CTRL	8	143±16	2.61±0.03	3.59±0.02	4.03±0.04
NEB	9	* 41±11	* 2.41±0.08	* 3.39±0.07	* 3.85±0.08
ACTA1	12	* 51±7	2.57±0.02	* 3.47±0.02	* 3.89±0.03
TPM3 slow-twitch	11	* 86±12	2.64±0.04	3.67±0.04	4.14±0.05
TPM3 fast-twitch	7	161±5	2.62±0.06	3.64±0.06	4.10±0.06
TPM2 slow-twitch	2	* 56±13	2.68±0.22	3.61±0.18	4.04±0.17
TPM2 fast-twitch	3	150±15	2.56±0.09	3.75±0.07	4.27±0.09
TNNT1	1	50±3	2.60±0.03	3.53±0.12	3.98±0.20
KBTBD13	10	* 73±6	2.60±0.04	3.65±0.04	4.13±0.06
KLHL40	1	5.0±2	2.63±0.13	3.66±0.04	4.17±0.07
KLHL41	1	68±4	2.68±0.07	3.60±0.04	4.04±0.05

* Significantly different from CTRL ($P < 0.05$). Note that for *TNNT1, KLHL40* and *KLHL41* one biopsy was evaluated and therefore no statistical testing was performed. SL_{opt}: the sarcomere length at which maximum force is generated, SL_{50}: the sarcomere length at which 50% of maximum force is generated, SL_x: the sarcomere length at which the fit crosses the X-axis.

* See Supplemental Table 2 for mean values per individual subject.

Confocal microscopy reveals shorter thin filaments in patients with mutations in NEB and ACTA1

Next, we aimed to confirm that the downward shift of the descending limb of the force-sarcomere length relation in patients with mutations in *NEB* and *ACTA* was indeed caused by shorter thin filament length (note that a

downward shift of this relation can be caused by reduced length of the thin and/or thick filament). Therefore, we measured thin and thick filament length by confocal microscopy in muscle fibers from *NEB* and *ACTA1* patients exhibiting SL_{50} values that were in the range of control values (*NEB-1* and *ACTA1-6*) and in patients that had values that were markedly below this range (*NEB-2* and *ACTA1-1*) (Fig 3 A-C).

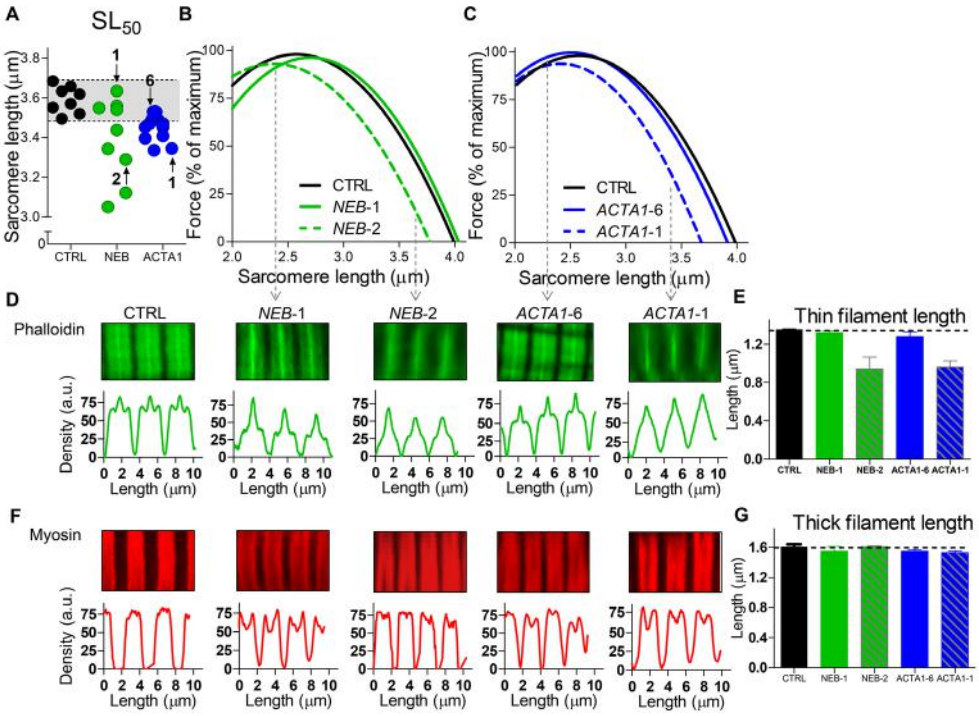

Figure 3 Confocal microscopy confirms shorter thin filament lengths in NEB and ACTA1 patients
(A-C) Within the *NEB* and *ACTA1* cohorts, fibers of some patients exhibited force-sarcomere length relation characteristics that were within the range of control values (i.e. *NEB-1, ACTA1-6*), whereas other patients (i.e., *NEB-2* and *ACTA1-1*) had values that were markedly below this range (normal SL_{50} range in grey). (D-G) FITC-labeled phalloidin (green) was used to measure thin filament length and antibodies against both slow and fast myosin heavy chain isoforms (red) were used to measure thick filament length. Thick filament length is normal in muscle fibers from CTRL, *NEB* and *ACTA1* biopsies, whereas thin filaments are shorter in fibers that revealed a downward shift of the descending limb of the force-sarcomere length relation (*NEB-2* and *ACTA1-1*) (N=4 for CTRL, >5 images per genotype).T-tests were performed between genotype and CTRL, $p<0.05$ was considered statistically significant (indicated by*).

Muscle fibers of *NEB-2* and *ACTA1-1* had shorter thin filament lengths than CTRL (0.94±0.12 in NEB-2 and 0.96±0.06 µm in *ACTA1-1* vs. 1.35±0.01 in

CTRL), while thick filament lengths were comparable to CTRL (1.62±0.02 in *NEB-2* and 1.56±0.03 µm in *ACTA1-1*, vs. 1.61±0.03 in CTRL). As expected, in muscle fibers of *NEB-1* and *ACTA1-6* normal thin filament lengths (1.32±0.02 in *NEB-1* and 1.28±0.05 µm in *ACTA1-6*) and thick filament lengths (1.55±0.06 in *NEB-1* and 1.55±0.02 µm in *ACTA1-6*) were observed. Thus, confocal microscopy reveals that thick filament length was not altered in any of the samples. This indicates that the downward shift of the descending limb of the force sarcomere length relation was indeed caused by shorter thin filament length.

A mouse model for nebulin-based thin filament myopathy suggests a compensatory mechanism for shorter thin filaments in muscle

We addressed whether muscle adds more sarcomeres in series to compensate for the sarcomere length-dependent loss of force. Adding more sarcomeres in series would blunt the effect of shorter thin filament lengths, as at a given muscle fiber length the fibers operate at a shorter sarcomere length, a length closer to their optimal length. Investigating the number of sarcomeres in series in muscle fibers of patients poses considerable technical and ethical difficulties. Therefore, we used the recently developed conditional nebulin knockout (*cNeb*$^{-/-}$) mouse, a model which represents the most frequent affected gene in thin filament myopathy, and which phenocopies several main features of human disease (Li et al., 2015). (Note that muscle fibers from thin filament myopathy patients with *NEB* mutations were also nebulin-deficient, Supplemental Table 3). This model enabled for the first time study of muscle adaptations in mature, nebulin-deficient muscle (previous *Neb*-mouse models had a life-span of maximally three weeks (Bang et al., 2006; Ottenheijm et al., 2013; Witt et al., 2006)). As expected, fibers isolated from soleus muscle of adult cNeb-/- mice revealed a downward shift of the descending limb of the force-sarcomere length relation and confocal microscopy confirmed that the observed downward shift was caused by shorter thin filaments (Fig 4A-C). Importantly, soleus muscle fibers of *cNeb*$^{-/-}$ mice contained more sarcomeres in series (7010±176 sarcomeres from tendon to tendon) compared to muscle of *cNeb*$^{+/+}$ mice (5903±209 sarcomeres from tendon to tendon, Fig 4D). Note that tibia length was comparable between *cNeb*$^{+/+}$ and *cNeb*$^{-/-}$ mice.

The addition of sarcomeres in series should enable muscle of *cNeb*$^{-/-}$ mice to operate at a shorter sarcomere length, a length closer to their optimal sarcomere length. To investigate whether muscle of *cNeb*$^{-/-}$mice indeed

operates at a shorter sarcomere length, whole intact soleus muscle was electrically activated and the optimal muscle length for force generation was determined. These studies revealed that the muscle length at optimal force generation was not different between *cNeb*$^{+/+}$ and *cNeb*$^{-/-}$ mice, and that at this muscle length the sarcomere length was shorter in cNeb-/- than in *cNeb*$^{+/+}$mice (2.51 ± 0.04 vs. 2.80 µm ± 0.03, respectively, Fig 4E). Thus, in *cNeb*$^{-/-}$mice, force loss caused by shorter thin filament lengths is compensated by increasing the number of sarcomeres in series so that the muscle can operate at shorter sarcomere lengths and the amount of overlap between the thin and thick filaments is partly restored (summarized in Fig 4F).

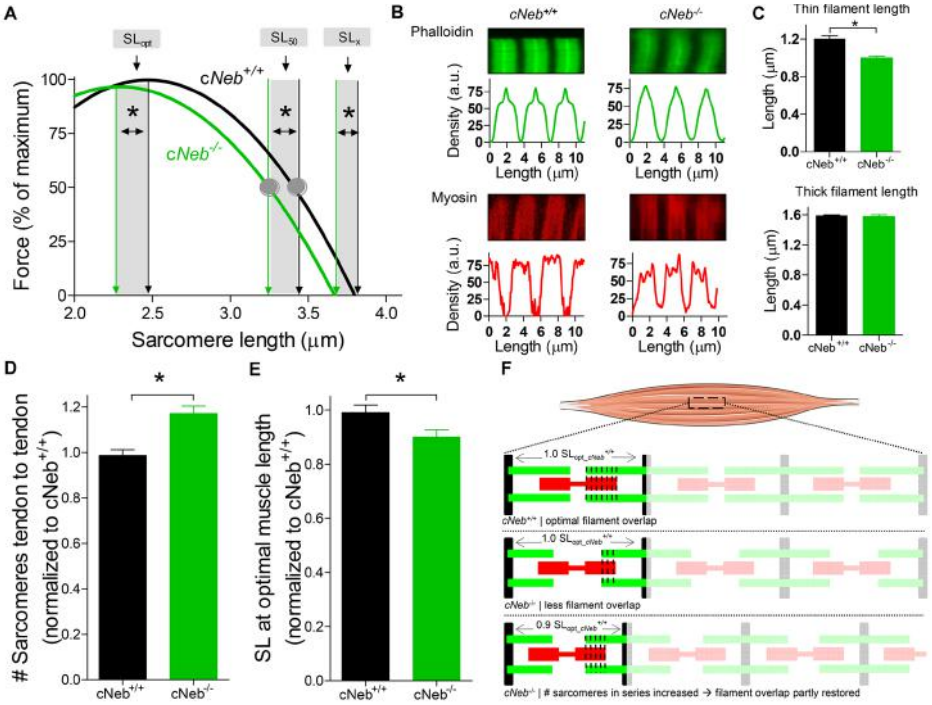

Figure 4 A mouse model for nemaline myopathy compensates for shorter thin filaments by adding more sarcomeres in series

(A) Soleus muscle fibers from a mouse model that phenocopies human nemaline myopathy (conditional nebulin knockout, *cNeb*$^{-/-}$) revealed a downward shift of the descending limb of the force-sarcomere length relation compared to muscle fibers from *cNeb*$^{-/-}$ mice (n=4 mice/group). (B-C) Confocal microscopy reveals shorter thin filaments in *cNeb*$^{-/-}$mice. (D) *cNeb*$^{-/-}$ mice compensated for the force deficit caused by shorter thin filaments by increasing the number of sarcomeres in series (n=6 mice/group). (E) At optimal length for force generation, intact soleus muscle of *cNeb*$^{-/-}$ mice operated at a shorter sarcomere length (SL) than *cNeb*$^{-/-}$ mice (n=20 mice/group). (F) The addition of sarcomeres in series increases the amount of overlap between the thin and thick filaments and enables the fibers with shorter thin filaments to operate at a length closer to their optimal length. T-tests were performed between *cNeb*$^{-/-}$ and *cNeb*$^{-/-}$ mice, p<0.05 was considered statistically significant (indicated by*).

DISCUSSION

Ten genes have been implicated in thin filament myopathy. Studies focusing on the effects of specific mutations in these genes on sarcomere function are largely lacking, mainly because patient biopsies have been limited in size and number. However, improved insight into genotype-sarcomeric phenotype correlations is essential for the development of targeted treatment strategies. Therefore, here we investigated the contractile strength of muscle fibers in fifty-one patients, covering eight of the ten implicated genes. Lower force generation was observed in muscle fibers from patients of all genotypes. Shorter than normal thin filament lengths were associated with lower force generation in patients with thin filament myopathy, but only in those that harbor specific mutations in *NEB* and *ACTA1*. A conditional Neb knock-out mouse model, which recapitulates thin filament myopathy, revealed a compensatory mechanism in muscle: force loss due to shorter thin filaments was counteracted by increasing the number of sarcomeres in series.

Mutation-specific effects on thin filament length

ACTA1 and *NEB* are the most frequently mutated genes in nemaline myopathy, the most common type of thin filament myopathy (Nowak et al., 2015). Consequently, shortened thin filaments is likely to be a phenotype that contributes to lower force generation in a large number of patients with thin filament myopathy. The effect of shorter thin filaments on force development is sarcomere- and muscle length dependent, with a more pronounced effect at larger lengths. This is illustrated in Fig 2B, where the in vivo sarcomere length range (~2.9–3.6 μm (Cromie et al., 2013)) is depicted: in patients with *NEB* mutations, the force deficit at a sarcomere length of 3.6 μm doubles compared to the deficit at a sarcomere length of 2.9 μm. This implies that muscle weakness in patients with mutations in *NEB* or *ACTA1* is more pronounced at larger joint angles, where muscle length is long. Whether this occurs in thin filament myopathy patients remains to be studied.

As some patients with *NEB* and *ACTA1* mutations, as well as the patients with mutations in *TPM3, TPM2, TNNT1, KBTBD13, KLHL40* and *KLHL41*, displayed significant force deficits without a downward shift of the force-sarcomere length relation, other mechanisms must be at play in these patients. Previous work on animal models and on biopsies from patients with

NEB, ACTA1, TPM3 and *TPM2* showed that qualitative changes in actin-myosin interactions as well as myofibrillar disarray are important contributors to lower force generation (Gineste, Duhamel, et al., 2013; Gineste, Le Fur, et al., 2013; Mokbel et al., 2013; Ottenheijm et al., 2010, 2011, 2013; Yuen et al., 2014, 2015). Similarly, not all patients with mutations in *NEB* and *ACTA1* had shorter thin filament lengths: muscle fibers of some patients (*NEB-1, NEB-4, NEB-5, NEB-8, and ACTA1-5, ACTA1-6, ACTA1-9, ACTA1-10*) had force-sarcomere length relations that overlapped with controls (Table 2 and Fig 3A). Thus, within the *NEB* and *ACTA1* cohorts, effects on thin filament length are mutation-specific. Although speculative, one could argue that mutations in *ACTA1* that reduce the binding strength between actin monomers are more likely to impact thin filament length than mutations that occur elsewhere. Similarly, although nebulin is important for thin filament length regulation (Bang et al., 2006; Witt et al., 2006), mutations in *NEB* that do not significantly affect its protein level or binding affinity of capping proteins might not disturb the regulation of thin filament length (Ochala et al., 2011). Investigating mutation-specific effects on thin filament length will be an interesting topic for future studies.

In summary, because *ACTA1* and *NEB* are the most frequently mutated genes in thin filament myopathies (Nowak et al., 2015), shortened thin filament length is likely to be a phenotype that contributes to lower force generation in a large number of patients with thin filament myopathy.

Addition of sarcomeres in series to compensate for shorter thin filament length

To date, it has been unknown if, and how, muscle responds to shorter thin filament lengths. To identify such response, we used the recently developed conditional nebulin knockout (*cNeb*$^{-/-}$) mouse, a model which closely phenocopies human thin filament myopathy (Li et al., 2015) and, importantly, which made study of muscle adaptations in mature nebulin-deficient muscle possible for the first time. Previous Neb-mouse models had a life-span of maximal three weeks, and, consequently, growth retardation and delays in muscle development could preclude meaningful explorations of response mechanisms. Adult *cNeb*$^{-/-}$ mice had muscle fibers with shorter thin filament lengths and, consequently, in isolated muscle fibers the optimal sarcomere length for force production was shorter (Fig 4A-C). However, we observed

that *cNeb*$^{-/-}$ mice increased the number of sarcomeres in series, and that as a result the optimal muscle length for force generation in intact muscle was comparable to *cNeb*$^{+/+}$ mice: the addition of sarcomeres in series allowed the muscles to operate at a shorter sarcomere length (Fig 4D-F), a length closer to their optimal sarcomere length. Adapting the number of sarcomeres in series to compensate for the changes in thin filament length suggests the existence of a compensatory mechanism in muscle. The molecular mechanisms that underlie this remain to be revealed, but might include proteins that sense suboptimal filament overlap, and in response produce more sarcomeric proteins. Previous work on animal models suggested that IGF-1, Akt, and cytosolic calcium mediate the addition of sarcomeres in series (Van Dyke et al., 2012, 2014; Yang et al., 1997). Whether these mediators are players in sensing optimal filament overlap and are involved in the regulation of sarcomeric protein expression remains to be elucidated. Future studies should address whether this compensatory mechanism is also present in human diseased muscle and whether active stretching of muscle stimulates the addition of sarcomeres in series, as observed in rodents (Riley and Van Dyke, 2012).

Study limitations

The mutations in some of the genes that are implicated in thin filament myopathy are rare, which precludes the inclusion of large numbers of patients. We were able to study only one patient with a mutation in *KLHL40,* one with a mutation in *KLHL41* and one with a mutation in *TNNT1*, and the force-sarcomere length relations in muscle fibers of these three patients were comparable to that in fibers of control subjects. Caution is warranted when drawing conclusions from this small sample size, and future studies on more patients with mutations in these genes should test whether thin filament length is indeed unaffected. Second, muscle fibers in biopsies of several patients were very small, which precluded studies on individual fibers and forced us to use multi-fiber preparations. Previous work from our group revealed that the maximal active tension determined in single fibers is comparable to that determined in multi-fiber preparations (de Winter et al., 2013). Thus, it is unlikely that our results are affected by using both single and multi-fiber preparations.

Summary
We investigated a large cohort of patients covering the majority of genes that are implicated in thin filament myopathy. Lower force generation at the sarcomere level was observed in muscle fibers from patients of all genotypes that were studied. Shorter than normal thin filament length contributes to the impaired force generation in patients with thin filament myopathy, but only in those that harbor specific mutations in *NEB* or *ACTA1*. Findings in a conditional Neb knock-out mouse model suggest that in thin filament myopathy patients adding more sarcomeres in series might be a novel direction in counteracting force loss.

REFERENCES

Agrawal PB, Joshi M, Savic T, Chen Z, Beggs AH. Normal myofibrillar development followed by progressive sarcomeric disruption with actin accumulations in a mouse Cfl2 knockout demonstrates requirement of cofilin-2 for muscle maintenance. Hum. Mol. Genet. 2012; 21: 2341–56.

Bang M-L, Li X, Littlefield R, Bremner S, Thor A, Knowlton KU, et al. Nebulin-deficient mice exhibit shorter thin filament lengths and reduced contractile function in skeletal muscle. J. Cell. Biol. 2006; 173: 905–916.

Colombo I, Scoto M, Manzur AY, Robb SA, Maggi L, Gowda V, et al. Congenital myopathies: Natural history of a large pediatric cohort. Neurology 2015; 84: 28–35.

Cromie MJ, Sanchez GN, Schnitzer MJ, Delp SL. Sarcomere lengths in human extensor carpi radialis brevis measured by microendoscopy. Muscle Nerve 2013; 48: 286–92.

Van Dyke JM, Bain JLW, Riley DA. Preserving sarcomere number after tenotomy requires stretch and contraction. Muscle Nerve 2012; 45: 367–75.

Van Dyke JM, Bain JLW, Riley DA. Stretch-activated signaling is modulated by stretch magnitude and contraction. Muscle Nerve 2014; 49: 98–107.

Gineste C, Duhamel G, Le Fur Y, Vilmen C, Cozzone PJ, Nowak KJ, et al. Multimodal MRI and (31) P-MRS investigations of the ACTA1(Asp286Gly) mouse model of nemaline myopathy provide evidence of impaired in vivo muscle function, altered muscle structure and disturbed energy metabolism. PLoS One 2013; 8: e72294.

Gineste C, Le Fur Y, Vilmen C, Le Troter A, Pecchi E, Cozzone PJ, et al. Combined MRI and 31P-MRS investigations of the ACTA1(H40Y) mouse model of nemaline myopathy show impaired muscle function and altered energy metabolism. PLoS One 2013; 8: e61517.

Gordon AM, Homsher E, Regnier M. Regulation of Contraction in Striated Muscle. Physiol Rev 2000; 80: 853–924.

Gordon AM, Huxley AF, Julian FJ. The variation in isometric tension with sarcomere length in vertebrate muscle fibres. J. Physiol. 1966; 184: 170–192.

Granzier HL, Akster HA, Ter Keurs HE. Effect of thin filament length on the force-sarcomere length relation of skeletal muscle. Am. J. Physiol. 1991; 260: C1060–70.

Gupta VA, Beggs AH. Kelch proteins: emerging roles in skeletal muscle development and diseases. Skelet. Muscle 2014; 4: 11.

Gupta VA, Ravenscroft G, Shaheen R, Todd EJ, Swanson LC, Shiina M, et al. Identification of KLHL41 Mutations Implicates BTB-Kelch-Mediated Ubiquitination as an Alternate Pathway to Myofibrillar Disruption in Nemaline Myopathy. Am. J. Hum. Genet. 2013; 93: 1108–17.

Li F, Buck D, De Winter J, Kolb J, Meng H, Birch C, et al. Nebulin deficiency in adult muscle causes sarcomere defects and muscle-type dependent changes in trophicity--novel insights in nemaline myopathy. Hum. Mol. Genet. 2015

Littlefield R, Fowler VM. Measurement of thin filament lengths by distributed deconvolution analysis of fluorescence images. Biophys. J. 2002; 82: 2548–64.

Lyons G, Muhlebach S, Moser A, Masood R, Paterson B, Buckingham M, et al. Developmental regulation of creatine kinase gene expression by myogenic factors in embryonic mouse and chick skeletal muscle. Development 1991; 113: 1017–1029.

Malfatti E, Lehtokari V-L, Böhm J, De Winter JM, Schäffer U, Estournet B, et al. Muscle histopathology in nebulin-related nemaline myopathy: ultrastructural findings correlated to disease severity and genotype. Acta Neuropathol. Commun. 2014; 2: 44.

Mokbel N, Ilkovski B, Kreissl M, Memo M, Jeffries CM, Marttila M, et al. K7del is a common TPM2 gene mutation associated with nemaline myopathy and raised myofibre calcium sensitivity. Brain 2013; 136: 494–507.

Nowak KJ, Davis MR, Wallgren-Pettersson C, Lamont PJ, Laing NG. Clinical utility gene card for: Nemaline myopathy. Eur. J. Hum. Genet. 2015

Ochala J, Lehtokari V-L, Iwamoto H, Li M, Feng H-Z, Jin J-P, et al. Disrupted myosin cross-bridge cycling kinetics triggers muscle weakness in nebulin-related myopathy. FASEB J. 2011; 25: 1903–13.

Ottenheijm CAC, Buck D, de Winter JM, Ferrara C, Piroddi N, Tesi C, et al. Deleting exon 55 from the nebulin gene induces severe muscle weakness in a mouse model for nemaline myopathy. Brain 2013; 136: 1718–31.

Ottenheijm CAC, Granzier H. Lifting the nebula: novel insights into skeletal muscle contractility. Physiology 2010; 25: 304–310.

Ottenheijm CAC, Hooijman P, DeChene ET, Stienen GJ, Beggs AH, Granzier H. Altered myofilament function depresses force generation in patients with nebulin-based nemaline myopathy (NEM2). J. Struct. Biol. 2010; 170: 334–343.

Ottenheijm CAC, Lawlor MW, Stienen GJM, Granzier H, Beggs AH. Changes in cross-bridge cycling underlie muscle weakness in patients with tropomyosin 3-based myopathy. Hum. Mol. Genet. 2011; 20: 2015–2025.

Ottenheijm CAC, Witt CC, Stienen GJ, Labeit S, Beggs AH, Granzier H. Thin filament length dysregulation contributes to muscle weakness in nemaline myopathy patients with nebulin deficiency. Hum. Mol. Genet. 2009; 18: 2359–2369.

Ravenscroft G, Miyatake S, Lehtokari V-L, Todd EJ, Vornanen P, Yau KS, et al. Mutations in KLHL40 Are a Frequent Cause of Severe Autosomal-Recessive Nemaline Myopathy. Am. J. Hum. Genet. 2013; 93: 6–18.

Riley DA, Van Dyke JM. The effects of active and passive stretching on muscle length. Phys. Med. Rehabil. Clin. N. Am. 2012; 23: 51–7.

Sambuughin N, Yau KS, Olivé M, Duff RM, Bayarsaikhan M, Lu S, et al. Dominant mutations in KBTBD13, a member of the BTB/Kelch family, cause nemaline myopathy with cores. Am. J. Hum. Genet. 2010; 87: 842–847.

Sanoudou D, Beggs AH. Clinical and genetic heterogeneity in nemaline myopathy-a disease of skeletal muscle thin filaments. Trends Mol. Med. 2001; 7: 362–368.

Udaka J, Ohmori S, Terui T, Ohtsuki I, Ishiwata S, Kurihara S, et al. Disuse-induced preferential loss of the giant protein titin depresses muscle performance via abnormal sarcomeric organization. J. Gen. Physiol. 2008; 131: 33–41.

Warren CM, Krzesinski PR, Greaser ML. Vertical agarose gel electrophoresis and electroblotting of high-molecular-weight proteins. Electrophoresis 2003; 24: 1695–1702.

de Winter JM, Buck D, Hidalgo C, Jasper JR, Malik FI, Clarke NF, et al. Troponin activator augments muscle force in nemaline myopathy patients with nebulin mutations. J. Med. Genet. 2013; 50: 383–92.

de Winter JM, Joureau B, Sequeira V, Clarke NF, van der Velden J, Stienen GJ, et al. Effect of levosimendan on the contractility of muscle fibers from nemaline myopathy patients with mutations in the nebulin gene. Skelet. Muscle 2015; 5: 12.

Witt CC, Burkart C, Labeit D, McNabb M, Wu Y, Granzier H, et al. Nebulin regulates thin filament length, contractility, and Z-disk structure in vivo. EMBO J. 2006; 25: 3843–3855.

Yang H, Alnaqeeb M, Simpson H, Goldspink G. Changes in muscle fibre type, muscle mass and IGF-I gene expression in rabbit skeletal muscle subjected to stretch. J. Anat. 1997; 190 (Pt 4: 613–22.

Yuen M, Cooper ST, Marston SB, Nowak KJ, McNamara E, Mokbel N, et al. Muscle weakness in TPM3-myopathy is due to reduced Ca2+-sensitivity and impaired acto-myosin cross-bridge cycling in slow fibres. Hum. Mol. Genet. 2015; 24: 6278–92.

Yuen M, Sandaradura SA, Dowling JJ, Kostyukova AS, Moroz N, Quinlan KG, et al. Leiomodin-3 dysfunction results in thin filament disorganization and nemaline myopathy. J. Clin. Invest. 2014; 124

SUPPLEMENTAL TABLES

Supplemental Table 1. Clinical and genetic information on subjects

Biopsy	Age (year)	Mutation	Patient ID	Disease	Clinical severity	References
Control (CTRL)						
CTRL-1	46	N/A	N/A	N/A	N/A	Yuen et al., 2015
CTRL-2	31	N/A	N/A	N/A	N/A	Yuen et al., 2015
CTRL-3	54	N/A	N/A	N/A	N/A	Yuen et al., 2015
CTRL-4	21	N/A	N/A	N/A	N/A	Yuen et al., 2015
CTRL-5	39	N/A	N/A	N/A	N/A	Yuen et al., 2015
CTRL-6	11	N/A	N/A	N/A	N/A	Yuen et al., 2015
CTRL-7	35	N/A	N/A	N/A	N/A	Yuen et al., 2015
CTRL-8	6	N/A	N/A	N/A	N/A	Yuen et al., 2015
Nebulin (*NEB*)[1]						
NEB-1	12	p.[Tyr2655Cys]; [Trp3876*]	BOS12-3 | T47[2]	NM	Typical	Lehtokari et al., 2014
NEB-2	0.1	p.[Tyr2549*]; [Arg3016*]	BOS227-1 | T159	NM	Severe	Lehtokari et al., 2014
NEB-3	5	p.[Glu666Val];[?]	BOS1027-1 | T1139	NM	Intermediate	Unpublished
NEB-4	0.5	p.[Arg8245fs];[?]	11700	NM	Intermediate	Malfatti et al., 2014
NEB-5	0.8	p.[Thr8085fs];[?]		NM	Intermediate	Malfatti et al., 2014
NEB-6	6	p.[Arg1747_Thr1778del]; [Val7425Serfs]	8536	NM	Typical	Malfatti et al., 2014
NEB-7	6	p.[Ser8193Ser];[Gln6226*]	12188	NM	Typical	Lehtokari et al., 2014, Malfatti et al., 2014
NEB-8	0.7	p.[Arg2478_Asp2512del];[?]	N/A	NM	Severe	Yonath et al., 2014
NEB-9	0.1	p.[Tyr1858*];[Leu6333_Glu6 367del]	N/A	NM	Severe	Malfatti et al., 2014
Skeletal muscle alpha-actin (*ACTA1*)[3]						
ACTA1-1	0.6	p.Gly57Arg	BOS922-1 | T866	NM	Typical	Unpublished
ACTA1-2	0.8	p.Thr79Ala	BOS95-1 | T77	NM	Typical	Laing et al., 2009
ACTA1-3	2.8	p.Glu85Lys	BOS349-1 | T256	NM	Typical	Laing et al., 2009
ACTA1-4	0.2	p.Arg258His	BOS927-1 | T865	NM	Typical	Unpublished
ACTA1-5	3	p.Ala274Glu	N/A	NM	Typical	Laing et al., 2009
ACTA1-6	60	p.Ala206Thr	N/A	NM	Mild	Laing et al., 2009
ACTA1-7	5	p.Gly270Cys	N/A	NM	Childhood onset	Ilkovski et al., 2001
ACTA1-8	0.1	p.Asp294Val	N/A	CFTD	Intermediate	Laing et al., 2004
ACTA1-9	65	p.Val165Met	N/A	NM	Mild	Hutchinson et al., 2006
ACTA1-10	17	p.Asn117Ser	N/A	NM	Childhood onset	Ilkovski et al., 2001
ACTA1-11	0.1	p.Leu223Pro	N/A	CFTD	Severe	Laing et al., 2004
ACTA1-12	0.1	p.Asp186His	N/A	NM	Severe	Unpublished
ACTA1-13	0.8	p.Pro334Ser	N/A	CFTD	Severe	Laing et al., 2004
ACTA1-14	36	p.Arg185Cys	N/A	NM	Intermediate	Nowak et al., 1999
Alpha-tropomyosin 3 (*TPM3*)[4]						
TPM3-1	10	p.Arg168Gly	N/A	CFTD	Mild	Yuen et al., 2015, Clarke et al., 2008
TPM3-2	3	p.Leu100Met	N/A	CFTD	Mild	Yuen et al., 2015, Clarke et al., 2008
TPM3-3	40	p.Arg168H	N/A	CFTD	Mild	Yuen et al., 2015
TPM3-4	30	p.Leu100Met	N/A	CFTD	Mild	Yuen et al., 2015, Clarke et al., 2008
TPM3-5	17	p.Arg168Cys	N/A	Cap	Mild	Yuen et al., 2015, Waddell et al., 2010
TPM3-6	1.3	p.Lys169Glu	N/A	CFTD	Mild	Yuen et al., 2015, Clarke et al., 2008
TPM3-7	1.7	p.Arg245Gly	N/A	CFTD	Mild to moderate	Yuen et al., 2015, Clarke et al., 2008

TPM3-8	56	p.Arg168His	N/A	CFTD	Mild	Yuen et al., 2015, Clarke et al., 2008
TPM3-9	36	p.Leu100Met	N/A	CFTD	Mild	Yuen et al., 2015, Clarke et al., 2008
TPM3-10	19	p.Arg168Cys	N/A	CFTD	Mild to moderate	Yuen et al., 2015 Clarke et al., 2008, Waddell et al., 2010
TPM3-11	0.1	p.Glu218del	N/A	N/A	Severe	Donkervoort et al., 2015
TPM3-12	1.4	p.Glu224del	N/A	N/A	Severe	Donkervoort et al., 2015
Beta-tropomyosin (*TPM2*)[5]						
TPM2-1	10	p.Glu139del	N/A	Cap	Mild	Clarke et al., 2009
TPM2-2	7	p.Lys7del	N/A	NM	Mild	Mokbel et al., 2013
TPM2-3	41	p.Lys7del	N/A	NM	Mild	Mokbel et al., 2013
Troponin T type 1 (*TNNT1*)[6]						
TNNT1-1	0.6	p.Leu203stop	N/A	NM	Severe	Abdulhaq et al., 2015
Kelch repeat and BTB (POZ) Domain Containing 13 (*KBTBD13*)[7]						
KBTBD13-1	44	p.Arg408Cys	N/A	NM	Mild	Sambuughin et al., 2010
KBTBD13-2	45	p.Arg408Cys	N/A	NM	Mild	Sambuughin et al., 2010
KBTBD13-3	42	p.Arg408Cys	N/A	NM	Mild	Unpublished
KBTBD13-4	41	p.Lys390Asn	N/A	NM	Mild	Sambuughin et al., 2010
KBTBD13-5	16	p.Arg408Cys	N/A	NM	Mild	Unpublished
KBTBD13-6	46	p.Arg408Cys	N/A	NM	Mild	Gommans et al., 2003
KBTBD13-7	55	p.Ile369Met	N/A	NM	Mild	Unpublished
KBTBD13-8	46	p.Arg408Cys	N/A	NM	Mild	Sambuughin et al., 2010
KBTBD13-9	62	p.Arg408Cys	N/A	NM	Mild	Sambuughin et al., 2010
KBTBD13-10	34	p.Arg408Cys	N/A	NM	Mild	Sambuughin et al., 2010
Kelch-like family member 40 (*KLHL40*)[8]						
KLHL40-1	0.1	p.[Asp34His];[Leu86Pro]	BOS74-4 | T545	NM	Severe	Ravenscroft et al., 2013
Kelch-like family member 41 (*KLHL41*)[9]						
KLHL41-1	4.5	p.[Ser153_Ala154insLeu]	BOS832-1 | T823	NM	Mild	Gupta et al., 2013

[1]*NEB* numbering relative to NP_001258137.1
? Note that for *NEB*-3, *NEB*-4, *NEB*-5 and *NEB*-8 only one pathogenic mutation has been identified.
[2]T number indicates biopsy number according to Boston Children's Hospital registry.
Note that the clinical scale is according to Lehtokari et al., 2015. 'Typical' NM is classified as: Onset in infancy: typical distribution of muscle weakness (weakness most pronounced in facial, bulbar, and respiratory muscles, neck flexors, and limb-girdle muscles; initially proximal, later also distal limb involvement); motor milestones delayed but reached; course slowly progressive or non-progressive.
[3]*ACTA1* numbering relative to NP_001091.1
[4]*TPM3* numbering relative to NP_689476.2
[5]*TPM2* numbering relative to NP_003280.2
[6]*TNNT1* numbering relative to NP_003274.3
[7]*KBTBD13* numbering relative to NP_001094832
[8]*KLHL40* numbering relative to NP_689606.2
[9]*KLHL41* numbering relative to NP_006054.2

Supplemental Table 2. Functional data of thin filament myopathy patients and controls

Gene	Maximal active tension mN/mm^2	SL_{opt} µm		SL_{50} µm		SL_x µm	
Control (CTRL)							
CTRL-1	151±20	2.69±0.04		3.49±0.02		3.85±0.03	
CTRL-2	120±13	2.56±0.05		3.62±0.06		4.09±0.07	
CTRL-3	125±12	2.61±0.05		3.66±0.05		4.13±0.1	
CTRL-4	238±25	2.62±0.09		3.57±0.05		3.99±0.06	
CTRL-5	154±11	2.65±0.07		3.63±0.05		4.06±0.04	
CTRL-6	109±25	2.44±0.05		3.66±0.04		4.18±0.08	
CTRL-7	143±16	2.71±0.06		3.55±0.09		3.93±0.12	
CTRL-8	82±16	2.60±0.06		3.52±0.09		3.94±0.12	
Mean	**143±16**	**2.61±0.03**		**3.59±0.02**		**4.03±0.04**	
Nebulin (*NEB*)							
NEB-1	74±25	2.73±0.06		3.63±0.05		4.05±0.06	
NEB-2	18±5	2.37±0.1		3.29±0.08		3.69±0.09	
NEB-3	9±2	2.38±0.01		3.12±0.1		3.46±0.13	
NEB-4	15±1	2.39±0.05		3.55±0.03		4.10±0.06	
NEB-5	51±18	2.75±0.21		3.56±0.19		3.96±0.22	
NEB-6	60±6	2.03±0.12		3.05±0.04		3.51±0.11	
NEB-7	108±28	2.32±0.15		3.34±0.05		3.79±0.1	
NEB-8	30±4	2.58±0.04		3.54±0.03		4.02±0.03	
NEB-9	10±2	2.16±0.52		3.44±0.13		4.05±0.4	
Mean	*** 41±11**	*** 2.41±0.08**		*** 3.39±0.07**		*** 3.85±0.08**	
Skeletal muscle alpha-actin (*ACTA1*)							
ACTA1-1	43±10	2.43±0.1		3.34±0.1		3.77±0.13	
ACTA1-2	28±7	2.52±0.08		3.49±0.06		3.93±0.05	
ACTA1-3	92±15	2.48±0.13		3.45±0.06		3.89±0.06	
ACTA1-4	31±7	2.51±0.11		3.45±0.08		3.90±0.17	
ACTA1-5	48±9	2.63±0.07		3.53±0.04		3.92±0.07	
ACTA1-6	86±22	2.57±0.05		3.53±0.06		3.96±0.09	
ACTA1-7	30±5	2.60±0.04		3.34±0.09		3.67±0.12	
ACTA1-8	33±6	2.68±0.08		3.41±0.1		3.75±0.12	
ACTA1-9	71±9	2.57±0.09		3.53±0.08		3.96±0.11	
ACTA1-10	76±14	2.45±0.06		3.49±0.1		3.97±0.15	
ACTA1-11	52±11	2.66±0.03		3.47±0.04		3.83±0.03	
ACTA1-12	5±1	2.62±0.04		3.40±0.12		3.78±0.12	
ACTA1-13	87±15	2.47±0.05		3.47±0.04		3.92±0.03	
ACTA1-14	25±15	2.72±0.1		3.71±0.09		4.17±0.13	
Mean	*** 51±7**	**2.57±0.02**		*** 3.47±0.02**		*** 3.89±0.03**	
Alpha-tropomyosin 3 (*TPM3*)							
	Slow	**Fast**	**Slow**	**Fast**	**Slow**	**Fast**	**Slow**	**Fast**
TPM3-1	71±7		2.70±0.14		3.72±0.07		4.18±0.07	
TPM3-2	144±23	156±22	2.69±0.03	2.76±0.04	3.78±0.02	3.77±0.12	4.23±0.04	4.21±0.18
TPM3-3	112	165±28	2.78	2.74±0.13	3.79	3.75±0.08	4.26	4.21±0.12
TPM3-4	95±8		2.61±0.04		3.69±0.1		4.24±0.12	
TPM3-5	66±8		2.50±0.12		3.53±0.07		4.04±0.12	
TPM3-6	22±1		2.71		3.51		3.87	
TPM3-7	74±19	176±20		2.61±0.03		3.69±0.14		4.16±0.18
TPM3-8	122±24	164±21	2.71±0.05	2.47±0.22	3.64±0.09	3.51±0.14	4.05±0.09	3.95±0.11
TPM3-9	66±10		2.44±0.1		3.66±0.11		4.21±0.13	
TPM3-10		144±12		2.53±0.04		3.48±0.04		
TPM3-11	10±1		2.28±0.15		3.51±0.04		4.12±0.09	
TPM3-12	68±8		2.54±0.06		3.47±0.05		3.90±0.05	
Mean	*** 86±12**	**161±5**	**2.64±0.04**	**2.62±0.06**	**3.67±0.04**	**3.64±0.06**	**4.14±0.05**	**4.10±0.06**
Beta-tropomyosin (*TPM2*)								
	Slow	**Fast**	**Slow**	**Fast**	**Slow**	**Fast**	**Slow**	**Fast**
TPM2-1		130±6		2.60±0.07		3.75±0.07		4.27±0.09
TPM2-2	43	140	2.89	2.68	3.79		4.21	
TPM2-3	68±9	180±19	2.46±0.06	2.39±0.09	3.43±0.19		3.87±0.27	
Mean	*** 56±13**	**150±15**	**2.68±0.22**	**2.56±0.09**	**3.61±0.18**	**3.75±0.07**	**4.04±0.17**	**4.27±0.09**
Troponin T type 1 (*TNNT1*)								
TNNT1-1	50±3		2.60±0.03		3.53±0.12		3.98±0.20	
Kelch repeat and BTB (POZ) Domain Containing 13 (*KBTBD13*)								

KBTBD13-1	93±6	2.74±0.14	3.50±0.07	3.84±0.07
KBTBD13-2	64	2.37	3.63	4.24
KBTBD13-3	51±6	2.58±0.05	3.51±0.07	3.91±0.07
KBTBD13-4	87±5	2.52±0.16	3.52±0.1	3.94±0.01
KBTBD13-5	74±7	2.68±0.08	3.67±0.05	4.12±0.06
KBTBD13-6	68±13	2.63±0.06	3.85±0.07	4.37±0.08
KBTBD13-7	45±9	2.73±0.10	3.78±0.07	4.27±0.10
KBTBD13-8	71±14	2.50±0.13	3.73±0.05	4.28±0.10
KBTBD13-9	71±9	2.52±0.05	3.66±0.05	4.16±0.07
KBTBD13-10	103±13	2.72±0.07	3.68±0.07	4.15±0.07
Mean	*** 73±6**	**2.60±0.04**	**3.65±0.04**	**4.13±0.06**
Kelch-like family member 40 (*KLHL40*)				
KLHL40-1	5.0±2	2.63±0.13	3.66±0.04	4.17±0.07
Kelch-like family member 41 (*KLHL41*)				
KLHL41-1	68±4	2.68±0.07	3.60±0.04	4.04±0.05

* Significantly different from CTRL ($P < 0.05$). Note that for *TNNT1*, *KLHL40* and *KLHL41* one biopsy was evaluated and therefore no statistical testing was performed. SL_{opt}: the sarcomere length at which maximum force is generated, SL_{50}: the sarcomere length at which 50% of maximum force is generated, SL_x: the sarcomere length at which the fit crosses the X-axis.

Supplemental Table 3. Nebulin levels by Western blot analysis

Genotype	Number of biopsies	Nebulin levels by Western blot / Myosin heavy chain levels by PonceauS staining
CTRL	5	2.67±0.3
NEB	7	*1.55±0.3

*Significantly different from CTRL ($P < 0.05$).

CHAPTER 3

MUSCLE HISTOPATHOLOGY IN NEBULIN-RELATED NEMALINE MYOPATHY: ULTRASTRUCTURAL FINDINGS CORRELATED TO DISEASE SEVERITY AND GENOTYPE

Edoardo Malfatti, Vilma-Lotta Lehtokari, Johann Böhm, Josine M De Winter, Ursula Schaffer, Brigitte Estournet, Susana Quijano-Roy, Soledad Monges, Fabiana Lubieniecki, Remi Bellance, Mai Thao Viou, Angéline Madelaine, Bin Wu, Ana Lía Taratuto, Bruno Eymard, Katarina Pelin, Michel Fardeau, Coen Ottenheijm, Carina Wallgren-Pettersson, Jocelyn Laporte, Norma B Romero

Acta Neuropathologica Communications, 2014

ABSTRACT

Background | Nemaline myopathy (NM) is a rare congenital myopathy characterised by hypotonia, muscle weakness, and often skeletal muscle deformities with the presence of nemaline bodies (rods) in the muscle biopsy. The nebulin (*NEB*) gene is the most commonly mutated and is thought to account for approximately 50% of genetically diagnosed cases of NM.

Methods | We undertook a detailed muscle morphological analysis of 14 *NEB*-mutated NM patients with different clinical forms to define muscle pathological patterns and correlate them with clinical course and genotype. Three groups were identified according to clinical severity. Group 1 (n = 5) comprises severe/lethal NM and biopsy in the first days of life. Group 2 (n = 4) includes intermediate NM and biopsy in infancy. Group 3 (n = 5) comprises typical/mild NM and biopsy in childhood or early adult life. Biopsies underwent histoenzymological, immunohistochemical and ultrastructural analysis. Fiber type distribution patterns, rod characteristics, distribution and localization were investigated. Contractile performance was studied in muscle fiber preparations isolated from seven muscle biopsies from each of the three groups.

Results | G1 showed significant myofibrillar dissociation and smallness with scattered globular rods in one third of fibers; there was no type 1 predominance. G2 presented milder sarcomeric dissociation, dispersed or clustered nemaline bodies, and type 1 predominance/uniformity. In contrast, G3 had well-delimited clusters of subsarcolemmal elongated rods and type 1 uniformity without sarcomeric alterations. In accordance with the clinical and morphological data, functional studies revealed markedly low forces in muscle bundles from G1 and a better contractile performance in muscle bundles from biopsies of patients from G2, and G3.

Interpretation | In conclusion *NEB*-mutated NM patients present a wide spectrum of morphological features. It is difficult to establish firm genotype phenotype correlation. Interestingly, there was a correlation between clinical severity on the one hand and the degree of sarcomeric dissociation and contractility efficiency on the other. By contrast the percentage of fibers occupied by rods, as well as the quantity and the sub sarcolemmal position of rods, appears to inversely correlate with severity. Based on our observations, we propose myofibrillar dissociation and changes in contractility as an important cause of muscle weakness in *NEB*-mutated NM patients.

INTRODUCTION

Nemaline myopathy (NM) is a congenital muscle disorder associated with hypotonia, muscle weakness, and often skeletal muscle deformities with the presence of numerous nemaline bodies (rods) in muscle biopsy (Romero et al., 2013). Clinically the disorder has a marked clinical variability, ranging from neonatal lethal to mild non-progressive forms with onset in childhood and adulthood. NM has been classified into six clinical categories according to the severity of the disease, the age of onset and the pattern of muscle weakness (Wallgren-Pettersson and Laing, 2001). To date at least nine genes have been implicated in NM (*ACTA1*, MIM#161800; *NEB*, MIM#256030; *TPM2*, MIM#609285; *TPM3*, MIM#609284; *TNNT1*, MIM#605355; *KBTBD13*, MIM#609273; *CFL2*, MIM#610687; *KLHL40* MIM#615340; and *KLHL41*) encoding proteins of the thin filament of skeletal muscle sarcomere or the Kelch domain associated proteins (Agrawal et al., 2007; Donner et al., 2002; Gupta et al., 2013; Johnston et al., 2000; Laing et al., 1995; Nowak et al., 1999; Pelin et al., 1999; Ravenscroft et al., 2013; Sambuughin et al., 2010). *ACTA1, TPM2* and *TPM3* NM is inherited both as autosomal dominant or recessive trait, with de novo dominant mutations being common in all three genes. *KBTBD13* NM is an autosomal dominant disorder. The other five genes present autosomal recessive mode of inheritance.

Nebulin is a sarcomeric structural protein crucial for the proper assembly and function of thin filaments (Wallgren-Pettersson et al., 2011). One molecule spans nearly the entire length of the thin filament, making nebulin one of the largest polypeptides in nature. The nebulin (*NEB*) gene is the most commonly mutated and is thought to account for approximately 50% of genetically diagnosed cases of NM (Wallgren-Pettersson et al., 2011). It is composed by 183 exons of which at least 17 (Donner et al., 2004) have been shown to be alternatively spliced, giving rise to several different nebulin isoforms in skeletal muscle (Pelin and Wallgren-Pettersson, 2008). Molecular diagnosis has mostly been based on dHPLC and confirmed by exon Sanger sequencing which are time-consuming, laborious, and expensive (Böhm et al., 2013). Recently next generation sequencing technology in combination with microarray methodology (Kiiski et al., 2013) has been demonstrated to be a fast and reliable tool for analysis of large genes such as *NEB* (Böhm et al., 2013). Patients are usually compound heterozygous for two different mutations (Lehtokari et al., 2006). The mechanisms leading to the alteration

of muscle structure or rod formation are largely unknown.

Nemaline bodies are the pathologic hallmarks of congenital NM, even if these structures may sometimes be found associated with other conditions (Romero and Clarke, 2013). These are protein aggregates staining red with the modified Gomori trichrome technique. They can appear within the fibers as fine isolated/diffuse structures, compact subsarcolemmal clusters, or both (Gurgel-Giannetti et al., 2003). On electron microscopy, nemaline bodies are electron dense and generally measure 1–7 μm in length and 0.3-2 μm in width. Due to their structural continuity with the Z-disk, and their resemblance to Z-disk lattice pattern, they are considered to be lateral expansions of the Z-disk (Fardeau, 1969; Goebel, 1996; North et al., 1997). In the case of nebulin mutation the rod formation could be due to a defect of the nebulin C-terminal, and serine-rich (SH3) domains. Concordantly, the nebulin C-terminal region, or part of it, may extend into the Z-disk (Ryan et al., 2003). Another common histologic finding of NM is type 1 predominance or type 1 uniformity (Goebel, 1996; North et al., 1997). Based on observations from consecutive muscle biopsies done in the same patient, a substitution of type 2 to type 1 fibers has been suggested to occur with increasing age (Fardeau, 1982; Gurgel-Giannetti et al., 2003). All congenital NM patients seem to present a homogeneous morphological phenotype characterized by the presence of rods and type I predominance. However the largest series reporting on histologic NM findings were published before the identification of specific NM genes or they included patients harbouring mutations in other genes (Goebel, 1996; Wallgren-Pettersson et al., 1988). For this reason it is difficult to assess the existence of specific genotype-morphological phenotype correlations in the nine genetically identified forms of NM. A systematic morphological analysis of each entity is therefore pivotal in order to reveal pathogenetic mechanisms.

With the aim of characterizing different patterns of muscle involvement, defining the relationship between morphological changes, genotype, and disease severity, we describe muscle morphology and functional studies of a large cohort of clinically heterogeneous *NEB*-mutated NM patients.

MATERIAL AND METHODS

Patients

Fourteen patients from 13 unrelated families from France, the French Antilles, and Argentina were included in the present study. Patients were classified into three groups according to their clinical disease severity. P4 and P5 are brothers. P1 to P5 (Group 1) presented a severe/lethal congenital myopathy leading to death in the first days of life. Their muscle biopsy was performed between 2 days and 15 days of life. P6 to P9 presented an intermediate congenital myopathy and a biopsy effectuated between 2 and 10 months (Group 2); P10 to P14 presented typical or mild (P13, and P14) nemaline myopathy and a muscle biopsy performed during childhood or adolescence/ early adult life (6 months-21 years; Group 3). The clinical data of these patients were systematically retrieved and retrospectively analyzed. Patients were personally examined by one of 6 of the authors. Clinical and genetic characterization of P1, P2, P4, and P5 has been previously reported (Böhm et al., 2013; Lehtokari et al., 2009; Pelin et al., 1999).

Mutation analysis

Patients or parents gave informed consent for the genetic analysis according to French legislation (Comité de Protection des Personnes Est IV DC-2012-1693). Genomic DNA was extracted from blood by standard methods. As nemaline myopathy (NM) is genetically heterogeneous and as the immense size of the nebulin gene significantly impedes classical sequences approaches (Wallgren-Pettersson et al., 2011), we performed exome sequencing on 5 µg of genomic DNA from the patients and their parents as in Bohm et al. (Böhm et al., 2013).

Exome sequencing was performed at the BGI (Shenzhen) on a Hiseq 2000 (Illumina) by using the Agilent 44 M v2 SureSelect Exon enrichment kit. Variant calling was done with the SOAP software. Variants filtering and prioritization were performed by comparison with SNP databases and with the VaRank program (Vasli et al., 2012). We discarded polymorphisms with a minor allele frequency (MAF) of more than 0.5% and excluded all variants with a frequency <20% of the total reads for a specific position. Additionally dHPLC and Sanger sequencing was performed in 7 patients as reported in Lehtokari et al. (Lehtokari et al., 2006). The mutations are reported according to the coding sequence of the nebulin cDNA reference sequence NM_001164508.1, and its translation.

RT-PCR

RNA was extracted from muscle biopsies with TRI-Reagent (Sigma), and cDNA was reverse transcribed using the SuperScript II Reverse Transcriptase (Invitrogen) and random hexamer primers. The PCR fragments of selected cDNA regions were cloned into the pGEM-T easy vector (Promega) and transformed into E. coli DH5alpha cells. Plasmid DNA was then extracted from single colonies and Sanger sequenced.

Morphological studies

An open muscle biopsy was performed in all patients after informed consent. Age at biopsy varied from 29 weeks of adjusted gestational age to 21 years. The biopsied muscle is reported in Table 1 and was deltoid in 9 patients (P1, P2, P3, P5, P6, P9, P10, P13, and P14) and vastus lateralis in 5 (P4, P7, P8, P11, and P12). In order to make a precise and comparative study of muscle biopsy findings in Group 1 we standardized the age of new-borns calculating their 'gestational adjusted age' as described in Shichiji et al. (Shichiji et al., 2013) (Table 1). Samples were analyzed in our research laboratory at the Myology Institute in Paris or in the Neuropathology laboratory of FLENI Institute and Garrahan Hospital in Buenos Aires, Argentina. For conventional histochemical techniques 10 µm thick cryostat sections were stained with haematoxylin and eosin (H&E), modified Gomori trichrome (mGT), Periodic acid Schiff technique (PAS), Oil red O, reduced nicotinamide adenine dinucleotide dehydrogenase-tetrazolium reductase (NADH-TR), succinic dehydrogenase (SDH), cytochrome c oxidase (COX), and adenosine triphosphatase (ATPase) preincubated at pH 9.4, 4.63, 4.35. Digital photographs of each biopsy were obtained with a Zeiss AxioCam HRc linked to a Zeiss Axioplan Bright Field Microscope and processed with the Axio Vision 4.4 software (Zeiss, Germany). The fiber type pattern was determined by counting 1000 fibers from each patient in ATPase 9.4 and 4.35 reactions, and by calculating the percentage of type 1 and type 2 fibers.

Based on our experience, the fiber type proportion reported in the literature regarding the muscle analyzed, we considered type 1 fibers predominance to be present when there were more than of 60% type 1 fiber in deltoid muscles, and more than 40% in vastus lateralis muscle (Dubowitz et al., 2013). Fiber type distribution in G1 patients was analyzed comparing the data on muscle fiber patterns during the main phases of skeletal muscle development obtained from individual with no neumuscular disorder (Farkas-Bargeton

et al., 1977; Romero et al., 2013). Moreover, where possible, we analyzed fiber type proportion in age-matched control biopsies corresponding to G2, and G3 patients. For the analysis of the proportion of fibers with rods, 800–1000 fibers of the muscle sections of each patient were analyzed, and the percentage of fibers appearing with and without rods on the total number of fibers of a muscle sections was calculated; four consecutive, non-overlapping fields were counted. In addition, a classification of the rods and their pattern was effectuated. We defined the rods as being cytoplasmic when localized mainly inside the fibers sparing the subsarcolemmal areas, scattered when they were randomly distributed in the muscle fiber, diffuse, when several small rods were distributed across the whole fibers homogenously occupying the majority of their area, central when distributed mainly in the centre of the cytoplasm, and subsarcolemmal when they were localized in a compact manner close to the fiber membrane (as clusters). We also evaluated the shape of nemaline bodies being mainly globular/ovoid, squared, or elongated.

Immunohistochemistry and immunofluorescence

Frozen muscle samples for immunohistochemical and immunofluorescence analyzes were available for 7 patients (P1, P6, P7, P9, P10, P11, and P14). Myosin heavy chain fast (NCL-MHCf, Novocastra Laboratories, Newcastle Upon Tyne, United Kingdom), myosin heavy chain slow (NCL-MHCs, Novocastra Laboratories, Newcastle Upon Tyne, United Kingdom), myosin heavy chain developmental (NCL-MHCd, Novocastra Laboratories, Newcastle Upon Tyne, United Kingdom), myosin heavy chain neonatal (NCL-MHCn, Novocastra Laboratories, Newcastle Upon Tyne, United Kingdom). Antibodies were visualized using immunoperoxidase techniques (Shichiji et al., 2013). Myosin alpha and beta-slow heavy chain, fast 2A heavy chain, and 2X myosin heavy chain (BA-D5, SC-71, and 6H1, Developmental Studies Hybridoma Bank, University of Iowa, Iowa City, USA) immunofluorescence were assessed on 10-µm-thick cryosections over night at 4°C. Subsequently, sections were incubated with appropriate conjugated secondary antibodies for one hour (Alexa Fluor-488 green goat anti-rabbit antibody, and Alexa Fluor-594 red goat anti-mouse antibody, Molecular Probes, Cergy Pontoise France). A set of control slides was prepared with omission of the primary antibodies.

Electron microscopy

Detailed electron microscopy analysis was prospectively performed in thirteen patients. Small muscle specimens were fixed with glutaraldehyde (2.5%, pH 7.4), post fixed with osmium tetroxide (2%), dehydrated and embedded in resin (EMBed-812, Electron Microscopy Sciences, USA). Ultra-thin sections from at least three small blocks from each patient were stained with uranyl acetate and lead citrate. The grids were observed using a Philips CM120 electron microscope (80 kV; Philips Electronics NV, Eindhoven, The Netherlands) and were photo documented using a Morada camera (Soft Imaging System, France).

Muscle contractility experiments

To investigate whether the contractile performance is affected in muscle biopsies from patients with mutations in the nebulin gene, we performed skinned muscle fiber contractility experiments. Small strips were dissected from muscle biopsies of patients P1 (Group 1), P7, P8 and P9 (Group 2), and P10, P11 and P14 (Group 3) and were skinned overnight as described previously (Ottenheijm et al., 2009). The skinning procedure renders the membranous structures in the muscle fibers permeable, which enables activation of the myofilaments with exogenous Ca^{2+}. Preparations were washed thoroughly with relaxing solution and stored in 50% glycerol/ relaxing solution at −20°C. Small muscle preparations (cross-sectional area ~0.002 mm2) were dissected from the skinned strips, and were mounted using aluminum T-clips between a length motor (ASI 403A, Aurora Scientific Inc., Ontario, Canada) and a force transducer element (ASI 315C-I, Aurora Scientific Inc., Ontario, Canada) in a single fiber apparatus (ASI 802D, Aurora Scientific Inc., Ontario, Canada) that was mounted on an inverted microscope (Zeiss Axio Observer A1). Sarcomere length was set using a high speed VSL camera and ASI 900B software (Aurora Scientific Inc., Ontario, Canada). Mechanical experiments were performed at a sarcomere length of ~2.2 μm, a length selected to minimize force differences due to shorter thin filaments in fibers from nemaline myopathy patients with nebulin mutations (Ottenheijm et al., 2009). Fiber width and diameter were measured at three points along the fiber and the cross-sectional area was determined assuming an elliptical cross-section. Two different types of bathing solutions were used during the experimental protocols: a relaxing solution (40 mM BES; 10 mM EGTA; 6.86 mM $MgCl_2$; 5.96 mM Na-ATP; 3.28 mM K-propionate; 33 mM creatine phosphate; 1 mM DTT; 0.5 mM PMSF; 0.2 mM Leupeptin; 0.05

mM E64) and an activating solution (40 mM BES; 10 mM $CaCO_3$-EGTA; 6.64 mM $MgCl_{2;}$ 6.23 mM Na-ATP; 2.1 mM K-propionate; 15 mM creatine phosphate; 1 mM DTT; 0.5 mM PMSF; 0.2 mM Leupeptin; 0.05 mM E64). The temperature of the bathing solutions was controlled by a TEC controller (ASI 825A, Aurora Scientific Inc. Ontario, Canada). Muscle preparations were mounted in a relaxation solution at 1°C. Subsequently, the muscle preparations were pre-activated by switching to an activation solution at 1°C. In that way the myofibers are loaded with calcium, but no force is generated. By rapid switching to an activation solution at 20°C, the fibers were activated and force was generated. When the force trace reached a plateau, the muscle fibers were slacked to 70% of their original length followed by a rapid restretch to the original length after 30 milliseconds. This procedure allows the force to redevelop from zero (Ottenheijm et al., 2010). The rate of tension redevelopment was calculated by fitting a bi-exponentional through the force redevelopment curve. The first-order rate constant k1 reflects cross-bridge cycling kinetics and was therefore used in the analyses (Caremani et al., 2008).

Myosin heavy chain composition of bundles used for contractility experiments

For determination of the myosin heavy chain isoform composition of the muscle fiber preparations we used specialized SDS-PAGE (Ottenheijm et al., 2009). In brief, muscles fibers were denatured by boiling for 2 minutes in SDS sample buffer. The stacking gel contained a 4% acrylamide concentration (pH 6.7), and the separating gel contained 7% acrylamide (pH 8.7) with 30% glycerol (v/v). The gels were run for 24 h at 15°C and a constant voltage of 275 V. Lastly, the gels were silver-stained, scanned, and analyzed with One-D scan EX software (Scanalytics Inc., Rockville, MD, USA).

The ethical committee of La Pitié-SalpêtrièreHospital (CCPPRB) approved this study.

Table 1 Clinical, laboratory, and genetic features of patients

Patient sex current age	Ethnic origin consanguinity	Age at onset (Gestational age)	Biopsied muscle Age at biopsy	Morphological methods (Functional studies)	Clinical phenotype	Permanent mechanical ventilation/age	NEB mutation: nucleotide/protein change	Effect of the mutations	Reference
P1, F, deceased 10 days	French Caucasian, Yes	Antenatal (38 weeks)	Deltoid 2 days	IHC, IF, EM (Yes)	Group 1/Severe congenital nemaline myopathy Polyhydramnios, fœtal akinesia. Severe global hypotonia, respiratory distress, arthrogryposis, hip hyperlaxity, club feet and dysmorphic features.	Yes From birth	ex45; c.5574C > G; p.Tyr1858Stop; int122; c.19101 + 5G > A; p.Leu6333_Glu6367del	exon 45: nonsense mRNA decay (by RTPCR) exon 122: skipping confirmed by RTPCR and sequencing cDNA	Böhm et al., [15]
P2, F, deceased at 1 month	French Jewish (Ashkenazi) Yes	Antenatal, (36 weeks)	Deltoid 5 days	IHC, EM (No)	Group 1/Severe congenital nemaline myopathy Polyhydramnios, fœtal akinesia. Severe global hypotonia, respiratory distress, arthrogryposis, club feet and dysmorphic features.	Yes From birth	homozygous deletion of exon 55 c.7432 + 1916_7535 + 372del p.Arg2478_ Asp2512del	Ashkenazi founder mutation; deletion of exon 55	Lehtokari et al., [26]
P3, M, deceased at 6 days	French Caucasian, No	Antenatal (38 weeks)	Deltoid 6 days	IHC, EM (No)	Group 1/Severe congenital nemaline myopathy Polyhydramnios, fœtal akinesia. Severe global hypotonia, respiratory distress, arthrogryposis, club feet, and dysmorphic features.	Yes From birth	ex86 (triplicated region); c.13066delT; p.Tyr4356Thrfs*8 ex110; c.17535G > A; p.Glu5845Glu	exon 86: frameshift mutation leading to either truncation or degradation. exon 110: splice site mutation	Present paper
P4, M, deceased at 5 days, Brother of P5	French Caucasian, Yes	Antenatal (29 weeks)	Vastus lateralis 3 days	IHC (No)	Group 1/Severe congenital nemaline myopathy Polyhydramnios, fœtal akinesia. Severe global hypotonia, absence of spontaneous movements at birth, respiratory distress, macrosomy and macrocephaly.	Yes From birth	ex177; c.24686_ 24687del; p.Glu8229 Glufs*18 ex163; c.23420_ 23421del; p.Arg7807 Serfs*16	both mutations truncating/degrading	Pelin et al., [4] Lehtokari et al., [17]
P5, M, deceased at 29 days, Brother of P4	French Caucasian, Yes	Antenatal (36 weeks)	Deltoid 15 days	IHC, EM (No)	Group 1/Severe congenital nemaline myopathy Polyhydramnios, macrosomy Severe global hypotonia, respiratory distress, reduced spontaneous movements, ptosis, arthrogryposis, hypetrichosis, and macrocephaly.	Yes From birth	ex177; c.24686_ 24687del; p.Glu8229 Glufs*18 ex163; c.23420_ 23421del; p.Arg7807 Serfs*16	both mutations truncating/degrading	Pelin et al., [4] Lehtokari et al., [17]
P6, M, deceased at 5 months	French Caucasian, No	Birth (39 weeks)	Deltoid 9 weeks	IHC, IF, EM (No)	Group 2/Intermediate congenital nemaline myopathy Hypotonia and poor spontaneous	Yes From 1 month	ex6; c.300dup; p.Tyr101fs*5 int49, c.6496-G > A, p.2166_2234del	exon 6: truncating/ degrading exon 50 skiping by RT and cDNA sequencing	Present paper

Table 1 Clinical, laboratory, and genetic features of patients *(Continued)*

					movements at birth. At one month respiratory distress and deglutition problems. Elongated face. High-arched palate. Low-set ears. Facial diplegia.				
P7, F, deceased at 2 and half yrs	African, Yes	11 days (39 weeks)	Vastus lateralis 6 months	IHC, IF, EM (Yes)	Group 2/Intermediate congenital nemaline myopathy. Apparently normal at birth. Successively hypotonia and deglutition problems. At 1.5 months development of progressive respiratory failure followed by recuperated cardiac arrest.	Yes From 2 months	homozygous 177; c.24735-24736DelA_ fsx1 is this c.24735_ 24736del (AG) p.Arg8245fs*1	truncating/degrading	Present paper
P8, M 5 yrs	Argentinian, No	6 months (40 weeks)	Vastus lateralis 6 months	IHC, EM (Yes)	Group 2/Intermediate congenital nemaline myopathy Hypotonia, motor delay. High-arched palate. Proximal and distal muscle weakness. Retractions of fingers. Mild hyperlaxity. At 1 year development of progressive respiratory involvement necessitating tracheostomy.	Yes From 1 month	ex139; c.20928G > T; p.Gly6976Gly ex172; c.24269del p.Arg8090fs*54	RTPCR and Sanger sequencing of cDNA showed that instead of 105 nt, exon 139 contains only 34 nt: frameshift and a premature stop codon. Exon 172; truncating/degrading	Present paper
P9, M, 11 yrs	French Caucasian, Yes	Birth (39 weeks)	Deltoid 10 months	IHC, IF, EM (Yes)	Group 2/Intermediate congenital nemaline myopathy Shortly after birth severe respiratory failure. Tracheostomy and gastrostomy at five months. Facial diplegia, drooling, deglutition problems. Axial hypotonia and weakness of all limb muscles.	Yes From 5 months	homozygous ex174; c.24440_24441insGTCA, p.Pro8148Serfs*15	truncating/degrading	Present paper
P10, M, 17 yrs	French Caucasian, No	6 years (At term)	Deltoid 6 years	IHC, IF, EM (Yes)	Group 3/Typical congenital nemaline myopathy. Global hypotonia, deglutition problems. Proximal muscle weakness. Facial diplegia. Nasal voice. Mild respiratory	No	int43; c.5343 + 5G > A p.Arg1747_Thr1778del ex153; c.22273del p.Val7425Serfs49*	intron 43: a splice site mutation exon153: truncating/degrading	Present paper

Table 1 Clinical, laboratory, and genetic features of patients *(Continued)*

					insufficiency treated with discontinuous non-invasive ventilation.				
P11, M, 19 years	French Antillean No	1 yrs (At term)	Vastus lateralis 6 yrs	IHC, IF, EM (Yes)	Group 3/Typical congenital nemaline myopathy. Hypotonia and feeding difficulties. Delayed motor milestones. Facial weakness with open mouth. Axial and limb girdle proximal weakness. Mild respiratory involvement treated with discontinuous non-invasive ventilation.	No	ex175; c.24579G > A, p.Ser8193Ser ex119; c.18676C > T, p.Gln6226*	ex175: a splice site mutation ex119: a nonsense mutation (truncating/degrading)	Present paper
P12, M, 20 yrs	French Caucasian, No	2-3 years (At term)	Vastus lateralis 6 years	IHC, EM (No)	Group 3/Typical congenital nemaline myopathy. Difficulties in running and rising stairs. Facial weakness with open mouth. Mild upper and lower limb girdle weakness.	No	int155; c.22591-3C > G; p.7531Val_ Ser7564del; ex148; c.21796_21810delinsT; p.Pro7266fs*30	intron 155: a splice site mutation exon 148: truncating/degrading	Present paper
P13, F, 52 yrs	French Caucasian, No	6 yrs (At term)	Deltoid 18 years	IHC, EM (No)	Group 3/Mild congenital nemaline myopathy. Difficulties in sport activities in school. Bilateral pes cavus. Presence of mild upper girdle musle weakness. Diffuse muscle pain.	No	ex69; c.10043_ 10046del, p.Val3348Alafs *43 ex49; c.6388G > C p.Ala2130Pro	ex69: truncating/ degrading ex49: missense on the acting binding site	Present paper
P14, F, 37 yrs	French Caucasian, No	2 yrs (At term)	Deltoid 21 yrs	IHC, IF, EM (Yes)	Group 3/Mild congenital nemaline myopathy. Frequent falls. Difficulties in running , rising stairs. Jaw contractures. Nasal voice. Elongated face. Respiratory involvement. Axial weakness with difficulties in neck flexion. Asymmentrical distal weaakness with foot drop (right > left). Proximo-distal weakness.	No	int17; c.1569 + 1G > A p.His491_Asp523del ex176; c.24606del p.Ala8203Glnfs*13	intron 17: a splice site mutation exon 176: truncating/ degrading	Present paper

RESULTS

Clinical findings

Five patients were female and 9 were male. Clinical summary, laboratory features, a complete list of morphological methods, functional studies applied to muscle biopsies, and genetic characterization of all patients is provided in Table 1. Patient 6 and 7 were classified to be a part of intermediate congenital nemaline myopathy group because they were breathing and moving at birth. However, these patients developed soon after birth a severe clinical picture and they were never able to achieve respiratory independence and/or ambulation. They eventually deceased at 5 months, and 32 months respectively. They therefore present a phenotype in between a severe and an intermediate congenital nemaline myopathy.

Molecular data

To identify the genetic cause in this cohort of patients, we performed exome enrichment and sequencing on genomic DNA from the patients and their parents. Exome sequencing allows a rapid and parallel screening of most human genes, and is suitable and efficient for the diagnosis of neuromuscular diseases and the analysis of large genes such as *NEB*, frequently mutated in NM (Böhm et al., 2013). This approach also covers any newly discovered gene for the disorder. For all patients presented here we found known or novel variations in the *NEB* gene. These changes were confirmed by Sanger sequencing, and their familial segregation validated when parent DNA available. In all the patients, at least one of the two compound heterozygous mutations was a truncating mutation (frameshift or nonsense mutation) leading to protein truncation or degradation, or both (Table 1). The second mutations were, either a frameshift mutation, deletion of several amino acids in frame (splice site mutations), a non-conservative missense change close to an actin binding site (P13), or synonymous variants in P3, P8, and P11 that all impacted on splicing. Most of the mutations (18) affected ubiquitously expressed exons, while six were in the alternatively spliced exons and one in an exon of the triplicated region of eight exons. Overall, most mutations were predicted to lead to a truncated or absent protein. There was no obvious correlation between the type of mutation or its location on the protein and the clinical severity.

Morphological findings

Histological and histochemical features

Group 1

A similar morphological pattern characterized by marked fiber size variability was noted in all biopsies from G1. We constantly identified two populations of fibers; the first characterized by muscle fibers of predictably normal or slightly augmented size, and the second one consisting of severely atrophic fibers (Figure 1A; arrows).

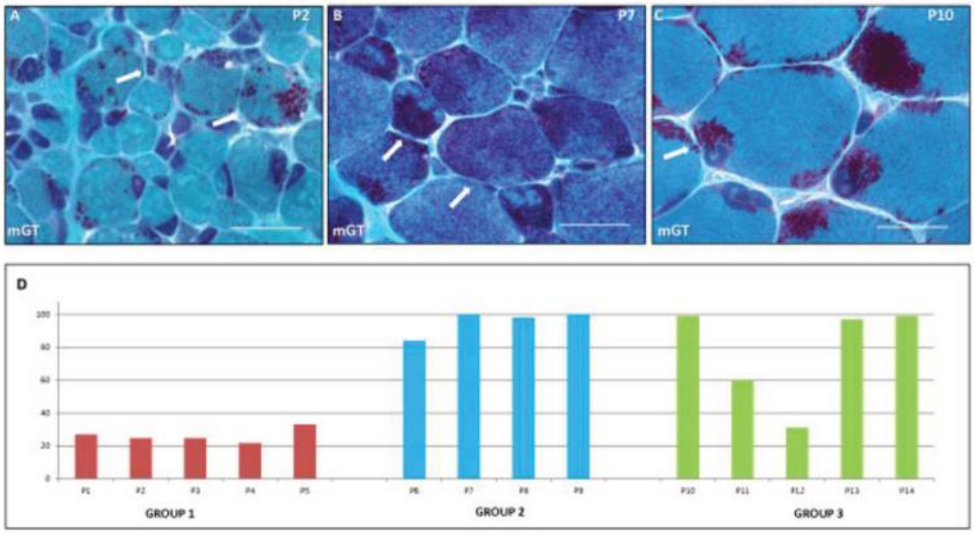

Figure 1 Light microscopy and percentage of fibers with rods

Modified Gomori trichrome stainings. A and B. Nemaline bodies in muscle biopsies from P2 (G1) and P7 (G2) have a rounded/ovoid shape. They are present in both normal size, and atrophic fibers (indicated by arrows). C. Nemaline bodies in muscle biopsy from P11 have an elongated shape (indicated by arrows) and they are localized in subsarcolemmal and perinuclear areas. Scale bars represent 20 µm for mGT stainings. D. Representation of percentage of rod occupied fibers in Group 1 (red), Group 2 (blue), and Group 3 (green). See text for explanations

Small rounded/globular inclusions staining red by the mGT, corresponding to nemaline bodies, were present in less than half of muscle fibers (Figure 1 A). Nemaline bodies occupied both normal-sized and atrophic fibers (Figure 1A). They presented a dispersed or, more often, a subsarcolemmal distribution (Figure 1A). Some atrophic fibers appeared completely occupied by nemaline bodies. The percentage of muscle fibers harbouring rods was to 22% to 33%

(Figure 1D, Group 1, red). The oxidative enzyme reactions revealed more than 30% of fibers presenting uneven staining of the intermyofibrillar network (not shown). The latter did not always correspond to the areas occupied by nemaline bodies, suggesting the presence of some degree of sarcomeric disruption. ATPase techniques did not reveal type 1 fiber predominance in any of the patients in G1. The majority of fibers staining differently from type 1 are probably undifferentiated fibers (not shown).

Group 2

The morphological pattern found in this group was heterogeneous compared with G1 biopsies. While in P6, and P7 samples we noticed the presence of two populations of muscle fibers (predictably normal size and severely atrophic) (Figure 1B; arrows), P8, and P9 showed a mild variation of fibers size without any particular topography (not shown). Conversely to G1 nemaline bodies were present in the vast majority of fibers (mean: 95% to 100%; Figure 1D, Group 2, blue) and presented a variable shape varying from oval to elongated. The oxidative enzyme reactions revealed some alteration of the intermyofibrillar network, probably corresponding to rod accumulation or myofibrillar disorganization with oxidative techniques. ATPase techniques showed type 1 fiber predominance in P6, and P8. Type 1 uniformity was noted in P7 and P9.

Group 3

In this group we noticed mild variation of fiber size except in P12 where some atrophic rounded fibers were identified (not shown). Nemaline bodies presented a constant elongated shape and formed well separated clusters both in subsarcolemmal and cytoplasmic areas (Figure 1C). There was a large variability in the percentage of fibers harbouring rods. While P10, P13 and P14 presented rods in almost all fibers (97-99%), P11 had 60% and P12 31% of fibers with rods, respectively (Figure 1D, Group 3, green). ATPase techniques showed almost complete type 1 uniformity in G3 muscle biopsies. The areas of muscle fibers containing rods lacked ATPase staining.

Summary

Overall, severe NM was associated with a fiber size variability, presence of rods in about 1/3 of fibers, and a high percentage of undifferentiated fibers. By contrast a higher percentage of fibers with rods, and a type 1 fiber predominance/uniformity was noted in the intermediate and typical NM patients. The amount of nemaline bodies seems to be inversely related to

clinical severity.

Immunohistochemistry and immunofluorescence

Group 1
In P1 we identified many fibers expressing developmental, neonatal, fast and/or slow myosin. Immunofluorescence studies showed absence of type 2X myosin.

Group 2
In P6 we identified many fibers co-expressing slow and fast myosins. Developmental and neonatal myosins were expressed in a minority of fibers. In P8 we identified occasional fibers expressing developmental myosin and less than 5% of fibers expressing neonatal myosin; there was partial co-expression of fast and slow myosins. P9 showed unique expression of slow myosin both in immunohistochemical, and immunofluorescence studies.

Group 3
P10, P11, and P14 showed slow myosin uniformity using both techniques. No fibers expressing developmental and/or neonatal myosins were noted.

Electron microscopy

Group 1
The prominent ultrastructural finding in all G1 patients was the diffuse myofibrillar dissociation. The myofibrils appeared thinner, and smaller than in age-matched controls (Figure 2A). The latter suggested either a defect in sarcomeric structure establishment either the lost of it. Remnants of sarcomeres were intermingled with organelles (e.g. mitochondria) or glycogen granules (Figure 2A). Globular/ovoid nemaline bodies were scattered or distributed in subsarcolemmal and perinuclear areas (Figure 2B, and C). Some fibers were completely occupied by them (Figure 2C). At higher magnification globular/ovoid rods presented thin filaments projecting from their thinnest edges (Figure 2D).

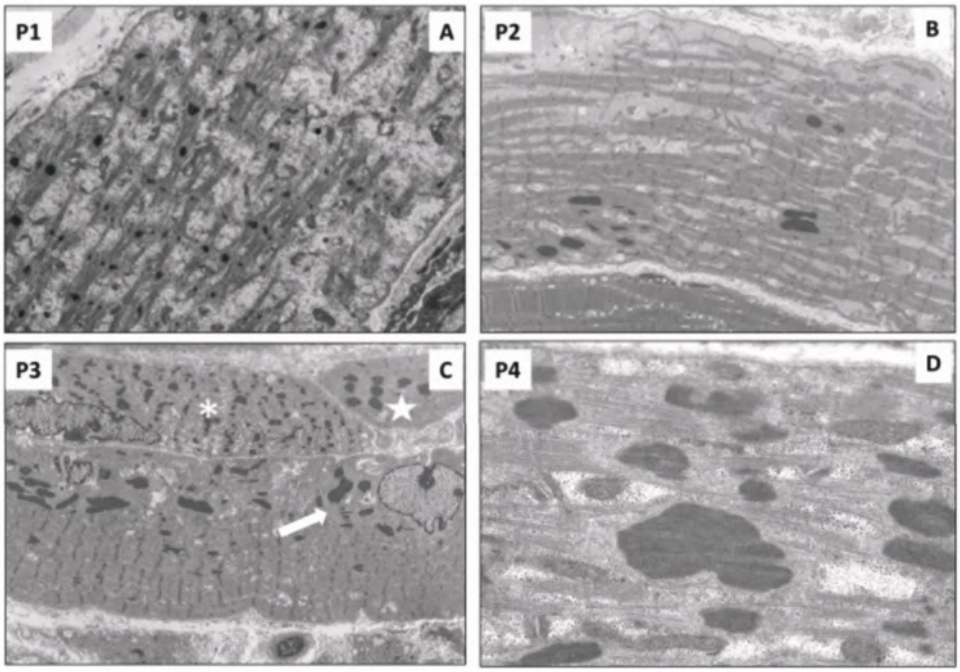

Figure 2 Electron microscopy for group G1- Severe NM.
(A) P1. Sarcomeric structure is completely disrupted. Fragment of sarcomeres are intermingled with amorphous material containing organelles and glycogen granules. (B) P2. Scattered globular ovoidal nemaline bodies are found inside a fiber showing partial sarcomeric alteration. (C) P3. Presence of three muscle fibers presenting different degree of alterations. Nemaline bodies are found in subsarcolemmal areas (indicated by an arrow). The fiber above the first one shows sarcomeric disarray and thicknened Z-lines probably leading to globular rods formation (indicated by an asterisk). A small atrophic fiber is completely invaded by rounded nemaline bodies (indicated by a star). (D) P4. Globular nemaline bodies present thin filaments coming out from the thinner edges. Original magnification: A. 11,000x . B. 7,000x C. 8,400x D. 51,000x.

Group 2

This group presented a milder degree of myofibrillar dissociation accompanying dispersed or clustered nemaline bodies (Figure A, and 3B). Rods showed the typical lattice structure resembling Z-disc material at very high magnification (Figure 3C). In P9 we noticed the presence of some typical cytoplasmic bodies with a dense core, and a clear halo of fine filaments (not shown).

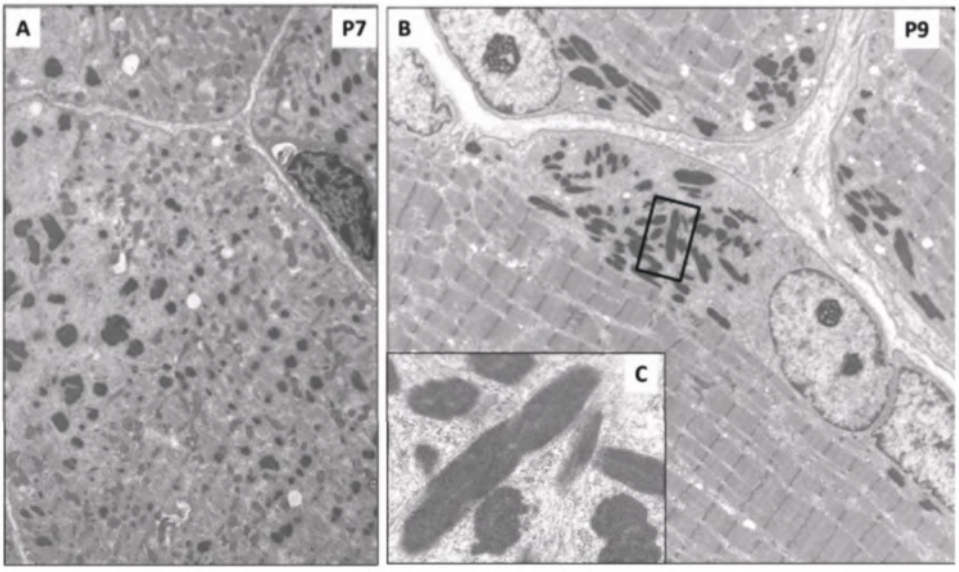

Figure 3 Electron microscopy for group G2-Intermediate NM.
(A) P7. Globular ovoid nemaline bodies associated with partial sarcomeric disarray strongly resembling the pathologic picture of G1. (B) P9. Presence of elongated nemaline bodies in perinuclear and subsarcolemmal areas. The latter are well separated from well-preserved sarcomeric structure. (C) P9. Higher magnification of an elongated nemaline body. The typical periodic net structure composing rods is clearly recognisable. Thin filament spread out of the thinnest edges of rods. Sparse thin filaments are found around the rods intermingled with glycogen granules. Original magnification: A. 11,000x . B. 6,400x C. 94,000x

Group 3

We found a homogenous picture characterized by the presence of well-separated clusters of subsarcolemmal (Figure 4A), perinuclear, and less often cytoplasmic nemaline bodies (Figure 4B). The rods were always surrounded by thin filaments and amorphous material. The sarcomeric structure was overall conserved (Figure A, and 4B).

Taken together, our results suggest that myofibrillar dissociation correlated with clinical severity.

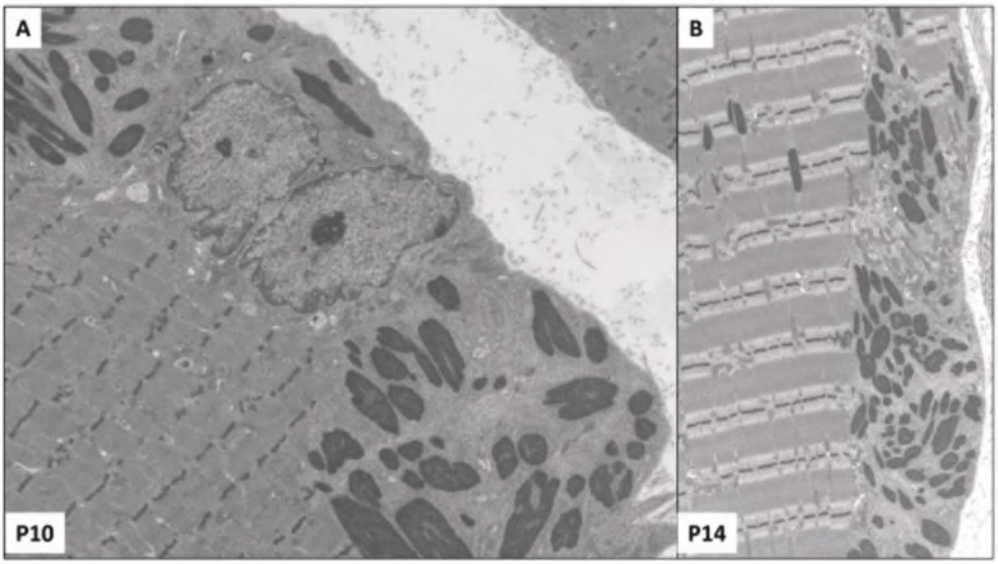

Figure 4 Electron microscopy for group G3-Typical-Mild NM.
(A) P10, G3. Presence of globally preserved sarcomeric structure associated with a cluster of elongated nemaline bodies in the subsarcolemmal areas of muscle fibers. P10. (B) P14. Well-delimited clusters of rods surrounded by thin filaments. Original magnification: A. 9,000x B. 8,200x

Muscle contractility experiments

The maximal force generation capacity of the muscle fiber preparations was normalized to their cross-sectional area (i.e. maximal active tension) (Figure 5). An overview of the maximal active tension and the rate of tension redevelopment of the muscle fibers are summarized in Table 2. Data are presented as mean ± SEM.

	P1	P7	P8	P9	P10	P11	P14
Maximal active tension (mN/mm^2)	8.1 ± 1.5	18.8 ± 2.7	76.9 ± 10.0	90.9 ± 10.5	55.5 ± 7.1	102.2 ± 21.2	61.4 ± 12.2
Rate of tension redevelopment (k_1 (s^{-1}))	5.1 ± 0.4	4.5 ± 0.7	5.0 ± 0.5	3.4 ± 0.2	3.6 ± 0.2	4.0 ± 0.6	3.8 ± 0.5

Table 2 Muscle contractility data of permeabilized fibers from nemaline myopathy patients with *NEB* mutations

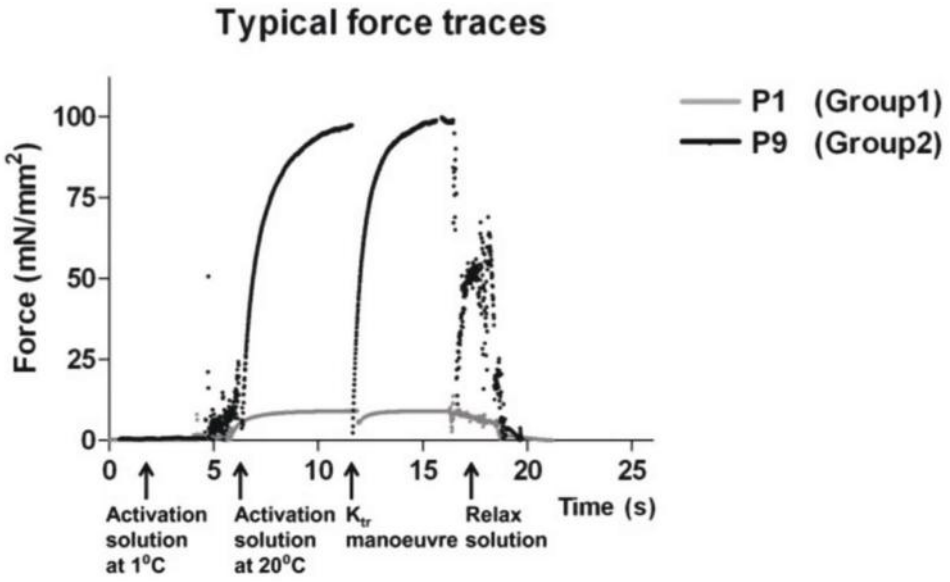

Figure 5 Typical force traces of skinned myofibers from nemaline myopathy patients with nebulin mutations

Typical examples from force traces of a skinned muscle preparation from P1 from Group1 (in grey) and P9 from group2 (in black). Myofibers are pre-activated by exposure to an activation solution at 1°C. By rapid switching to an activation solution at 20°C, the fibers are activated and force is generated. When the force trace reaches a plateau, the myofibers are slacked to 70% of their original length followed by a rapid restretch to the original length after 30 milliseconds (K_{tr} manouvre). When force generation has reached a plateau again, the muscle preparation is exposed to a calcium-free solution to induce relaxation.

Myosin heavy chain analyzes

The myosin heavy chain (MHC) gel electrophoresis experiments revealed that muscle preparations from biopsies from patient P1 contained both neonatal isoforms as well as type 1 and type 2A isoforms: (9.2 ± 2.8% MHC neonatal; 40.0 ± 3.2% MHC type 1; 50.8 ± 1.3% MHC type 2A). Muscle preparations from biopsies of P7 and P8 (group 2) contained both MHC type 1 and MHC type 2A isoforms: P7 (66.6 ± 6.6% MHC type 1 and 33.4 ± 6.6% MHC type 2A) and P8 (40.8 ± 12.0% MHC type 1 and 59.2 ± 12.0% MHC type 2A), respectively. All other patient biopsies (P9, P10, P11 and P14) showed exclusively myosin heavy chain type 1 isoforms.

DISCUSSION

In our tertiary Center for Neuromuscular Disorders we perform a detailed clinical, morphological, and genetic analysis of large cohorts of patients presenting NM. Due to the genetic heterogeneity of NM, and the difficulties encountered in the molecular screening of the 'giant' *NEB* gene (Böhm et al., 2013; Vasli and Laporte, 2013), in France and Finland an integrated approach combining next generation sequencing and dHPLC/Sanger sequencing was set-up. Our strategy allowed the identification of ten new families harbouring *NEB* mutations. All patients presented autosomal recessive pattern of inheritance and either homozygous or compound heterozygous pathogenic variants. Our results confirm that *NEB* is one of the most frequently mutated NM genes, accounting for almost half of the genetically identified NM patients screened for the known genes associated with NM (Agrawal et al., 2007; Donner et al., 2002; Gupta et al., 2013; Johnston et al., 2000; Laing et al., 1995; Nowak et al., 1999; Pelin et al., 1999; Ravenscroft et al., 2013; Sambuughin et al., 2010).

We undertook a detailed clinical histological, and, when possible, muscle functional analysis in a cohort of fourteen *NEB*-mutated subjects whose muscle biopsy was available in our laboratory. We comment on relevant findings encountered.

NEB-mutated patients revealed a wide pathological spectrum and showed recurrent morphological pattern with some overlap among the clinical groups. Lethal/severe NM subjects (G1) presented: high degree of myofibrillar dissociation and smallness revealed by electron microscopy, scattered globular/ovoid nemaline bodies occupying one third of muscle fibers, and absence of type 1 predominance with myosins ATPases techniques (Figure 2). Intermediate congenital myopathy patients (G2) showed features similar to G1 in P6 and P7, even though the presented higher percentage of rods and type 1 predominance, and well-separated clusters of rods associated with type 1 predominance or uniformity in the other patients. It is noteworthy that P6 and P7 deceased at 5 months, and 2 and a half year, respectively. For this reason these patients could be considered as a 'Longer survivor severe congenital NM' subgroup due to their 'midway' clinical and morphological features between G1 and G2. Group 3 had a preserved sarcomeric structure with clusters of elongated rods invariantly associated with type 1 predominance/uniformity.

In summary we show a large pathological spectrum ranging from severely damaged sarcomeres with scattered nemaline bodies to globally preserved muscle with clusters of well separated rods occupying the majority of myofibers. Interestingly the degree of sarcomeric disruption directly related to clinical severity whereas the number of rod invaded fibers seemed to be inversely correlated.

We undertook this study to search for genotype-phenotype correlations. Taken together, the vast majority of *NEB* mutations are predicted to lead to a degradation and or denaturation of many nebulin isoforms. Markedly reduced amounts of nebulin in muscle samples from patients homozygous for exon 55 deletions have been reported previously (Lawlor et al., 2011). P2 in this study is homozygous for the same exon 55 deletion, resulting in an in-frame deletion of 35 amino acids, and subsequent protein degradation. Nonsense mRNA-mediated decay was demonstrated by RT-PCR in P1, who carries a heterozygous nonsense mutation in exon 45. P1 is also heterozygous for a splice site mutation in intron 122, which was shown to cause exon 122 skipping, resulting in in-frame deletion of 35 amino acids (Böhm et al., 2013). Splice site mutations are, however, often “leaky”, i.e. some transcripts are spliced correctly, whereas others are incorrectly spliced. Therefore, it seems plausible that P1, as well as the other patients with splice site mutations (P3, P6, P8, P10, P11, P12 and P14) express small amounts of normal nebulin in their muscles. Markedly reduced amounts of nebulin in muscle have been reported in one patient compound heterozygous for a splice site mutation and a frameshift mutation in constitutively expressed exons (de Winter et al., 2013). The mutations in alternatively spliced exons (exons 174, 175, 176 and 177) only affect nebulin isoforms expressing these exons, leaving other isoforms unaffected. Consequently reduced amounts of nebulin and absence of some isoforms, precluding an appropriate thin filaments assembly, might be responsible for the drastic myofibrillar dissociation revealed in G1 [Figure 4]. Functional studies confirmed that G1 patients’ muscle fibers generate very low force. Although one could argue that age confounded our findings, previous work from our group revealed no major differences in the contractile performance of myofibers isolated from young (age 2–5 years) versus adult (age 20–30) human control biopsies (de Winter et al., 2013). Note that G1 patients’ muscle fibers expressed only very low levels of neonatal myosin heavy chain isoforms; such low levels are unlikely to account for the major loss of force in this patient. We therefore suggest

that nebulin degradation/absence translates into sarcomeric disarray and/or altered actomyosin interaction. This could be responsible for low force generation producing global hypotonia, muscle akinesia, and arthrogryposis. Concordantly, a recent study reported that low levels of nebulin in skeletal muscle are probably responsible for the foetal akinesia and arthrogryposis sequence phenotype (Lawlor et al., 2011).

How nebulin deficiency results in nemaline bodies formation is yet to be understood. Some authors suggested that a truncated nebulin would disrupt myofibrillar connectivity leading to Z-disc displacement and, eventually, rods formation (Millevoi et al., 1998). Analysis of nemaline bodies features in our cohort revealed differences in shape across the three groups. These tended to be globular/ovoid in G1, elongated in the other groups. The specificity of this finding is uncertain. What is more striking is that in P8, and P9 from G2 and in all G3 patients, the majority of fibers harboured rod clusters confined to subsarcolemmal and/or perinuclear areas. The myofibrillar structure surrounding them was overall preserved. Some unknown process could try to circumscribe the protein aggregates and avoid a perturbation of muscle contraction. This could explain why muscle fibers in G2 and G3 patients showed a better contractile performance, probably translating into a milder clinical phenotype. It is tempting to speculate that mutations encountered in these groups affect only specific nebulin isoforms, which is certainly true for patients P7, P8, P9, P11, and P14 who all have at least one mutation in an alternatively spliced exon. In this scenario, residual normal isoforms could allow a proper thin filament assembly, while the altered ones might be responsible for protein aggregation/rod formation. If this turned to be true, the presence of rods might be considered unrelated to muscle contractility disturbances. Following this reasoning we could imagine that an additive effect of degraded nebulin isoforms would determine clinical severity.

Type 1 predominance or type uniformity has been reported as a very common feature associated with NM, and many other structural congenital myopathies (Ottenheijm and Granzier, 2010). It is speculated that this is due to a disturbance of fiber differentiation before phase three of muscle differentiation (35th weeks) (Sewry, 1998). A severe *NEB* mutated family composed by two brothers has been reported as not having type 1 fiber predominance. However, biopsied muscle and age at muscle biopsy were not specified (Wallgren-Pettersson et al., 2002). In the present study we

performed type fiber distribution analysis on ATPase techniques. Surprisingly, all G1 patients failed to show type 1 predominance and constantly showed absence of 2B fibers. Immunostainings for different myosins isoforms (foetal neonatal, fast and slow) revealed a certain degree of myosin isoforms co-expression in numerous fibers suggesting the presence of undifferentiated fibers. This contrasted with the other groups where type 1 predominance/ uniformity was present. This finding suggests that G1 *NEB*-mutated patients were not able to switch towards type 1 predominance due to a possible alteration of muscle maturation. It is tempting to speculate that aberrations in fiber-typing, and absence of type 2B seen with ATPase techniques are due to changes in isoforms imbalance more than related to age at muscle biopsy. Additionally the presence of high percentages of undifferentiated fibers encountered in G1 might turn out to be an important prognostic factor. In fact muscle biopsy analysis of new-borns presenting artrhogryposis and a pathological picture characterized by sarcomeric dissociation, scattered nemaline bodies absence of type 1 predominance and type 2B fibers with ATPases techniques might orientate toward *NEB* mutations. This is something distinctive from other severe form of congenital myopathies commonly showing type 1 predominance as a prominent feature (Romero and Bitoun, 2011). In particular we recently demonstrated that *MTM1*-mutated boys presenting an extremely severe clinical phenotype all had type 1 predominance in their biopsies, regardless of the biopsied muscle, and the gestational age (Shichiji et al., 2013).

In conclusion, this study adds on the clinical, morphological and functional characterization of the most recurrent form of NM. We assessed morphological and functional heterogeneity in *NEB*-mutated NM patients and identified a correlation between disease severity on the one hand, and ultrastructural myofibrillar abnormalities and contractility on the other. We suggest that myofibrillar dissociation and smallness is a primary defect causing the disease while nemaline bodies could be due to a collateral mechanism.

REFERENCES

Agrawal PB, Greenleaf RS, Tomczak KK, Lehtokari V-L, Wallgren-Pettersson C, Wallefeld W, et al. Nemaline myopathy with minicores caused by mutation of the CFL2 gene encoding the skeletal muscle actin-binding protein, cofilin-2. Am. J. Hum. Genet. 2007; 80: 162–7.

Böhm J, Vasli N, Malfatti E, Le Gras S, Feger C, Jost B, et al. An integrated diagnosis strategy for congenital myopathies. PLoS One 2013; 8: e67527.

Caremani M, Dantzig J, Goldman YE, Lombardi V, Linari M. Effect of Inorganic Phosphate on the Force and Number of Myosin Cross-Bridges During the Isometric Contraction of Permeabilized Muscle Fibers from Rabbit Psoas. Biophys. J. 2008; 95: 5798–5808.

Donner K, Ollikainen M, Ridanpää M, Christen H-J, Goebel HH, de Visser M, et al. Mutations in the β-tropomyosin (TPM2) gene – a rare cause of nemaline myopathy. Neuromuscul. Disord. 2002; 12: 151–158.

Donner K, Sandbacka M, Lehtokari V-L, Wallgren-Pettersson C, Pelin K. Complete genomic structure of the human nebulin gene and identification of alternatively spliced transcripts. Eur. J. Hum. Genet. 2004; 12: 744–51.

Dubowitz V, Sewry CA, Oldfors A. Muscle Biopsy: A Practical Approach. 2013.

Fardeau M. Etude d'une nouvelle observation de 'Nemaline Myopathy'. Acta Neuropathol. 1969; 13: 250–266.

Fardeau M. Congenital myopathies. In: Mastaglia FL, Walton S, editor(s). Skeletal muscle pathology. London: Churchill Livingston; 1982. p. 161–203.

Farkas-Bargeton E, Diebler MF, Arsénio-Nunes ML, Wehrlé R, Rosenberg B. Etude de la maturation histochimique, quantitative et ultrastructurale du muscle foetal humain. J. Neurol. Sci. 1977; 31: 245–259.

Goebel HH. Congenital myopathies. Semin. Pediatr. Neurol. 1996; 3: 152–161.

Gupta VA, Ravenscroft G, Shaheen R, Todd EJ, Swanson LC, Shiina M, et al. Identification of KLHL41 Mutations Implicates BTB-Kelch-Mediated Ubiquitination as an Alternate Pathway to Myofibrillar Disruption in Nemaline Myopathy. Am. J. Hum. Genet. 2013; 93: 1108–17.

Gurgel-Giannetti J, Reed U, Marie S, Zanoteli E, Fireman M, Oliveira A, et al. Rod distribution and muscle fiber type modification in the progression of nemaline myopathy. J Child Neurol 2003; 18

Johnston JJ, Kelley RI, Crawford TO, Morton DH, Agarwala R, Koch T, et al. A novel nemaline myopathy in the Amish caused by a mutation in troponin T1. Am. J. Hum. Genet. 2000; 67: 814–21.

Kiiski K, Laari L, Lehtokari V-L, Lunkka-Hytönen M, Angelini C, Petty R, et al. Targeted array comparative genomic hybridization--a new diagnostic tool for the detection of large copy number variations in nemaline myopathy-causing genes. Neuromuscul. Disord. 2013; 23: 56–65.

Laing NG, Wilton SD, Akkari PA, Dorosz S, Boundy K, Kneebone C, et al. A mutation in the alpha tropomyosin gene TPM3 associated with autosomal dominant nemaline myopathy. Nat. Genet. 1995; 9: 75–9.

Lawlor MW, Ottenheijm CA, Lehtokari V-L, Cho K, Pelin K, Wallgren-Pettersson C, et al. Novel mutations in NEB cause abnormal nebulin expression and markedly impaired muscle force generation in severe nemaline myopathy. Skelet. Muscle. 2011; 1: 23.

Lehtokari V-L, Greenleaf RS, DeChene ET, Kellinsalmi M, Pelin K, Laing NG, et al. The exon 55 deletion in the nebulin gene--one single founder mutation with world-wide occurrence. Neuromuscul. Disord. 2009; 19: 179–81.

Lehtokari V-L, Pelin K, Sandbacka M, Ranta S, Donner K, Muntoni F, et al. Identification of 45 novel mutations in the nebulin gene associated with autosomal recessive nemaline myopathy. Hum. Mutat. 2006; 27: 946–56.

Millevoi S, Trombitas K, Kolmerer B, Kostin S, Schaper J, Pelin K, et al. Characterization of nebulette and nebulin and emerging concepts of their roles for vertebrate Z-discs. J. Mol. Biol. 1998; 282: 111–23.

North KN, Laing NG, Wallgren-Pettersson C. Nemaline myopathy: current concepts. The ENMC International Consortium and Nemaline Myopathy. J. Med. Genet. 1997; 34: 705–13.

Nowak KJ, Wattanasirichaigoon D, Goebel HH, Wilce M, Pelin K, Donner K, et al. Mutations in the skeletal muscle alpha-actin gene in patients with actin myopathy and nemaline myopathy. Nat. Genet. 1999; 23: 208–12.

Ottenheijm CAC, Granzier H. New insights into the structural roles of nebulin in skeletal muscle. J. Biomed. Biotechnol. 2010; 2010: 968139.

Ottenheijm CAC, Hooijman P, DeChene ET, Stienen GJ, Beggs AH, Granzier H. Altered myofilament function depresses force generation in patients with nebulin-based nemaline myopathy (NEM2). J. Struct. Biol. 2010; 170: 334–343.

Ottenheijm CAC, Witt CC, Stienen GJ, Labeit S, Beggs AH, Granzier H. Thin filament length dysregulation contributes to muscle weakness in nemaline myopathy patients with nebulin deficiency. Hum. Mol. Genet. 2009; 18: 2359–2369.

Pelin K, Hilpelä P, Donner K, Sewry C, Akkari PA, Wilton SD, et al. Mutations in the nebulin gene associated with autosomal recessive nemaline myopathy. Proc. Natl. Acad. Sci. 1999; 96: 2305–2310.

Pelin K, Wallgren-Pettersson C. Nebulin--a giant chameleon. Adv. Exp. Med. Biol. 2008; 642: 28–39.

Ravenscroft G, Miyatake S, Lehtokari V-L, Todd EJ, Vornanen P, Yau KS, et al. Mutations in KLHL40 Are a Frequent Cause of Severe Autosomal-Recessive Nemaline Myopathy. Am. J. Hum. Genet. 2013; 93: 6–18.

Romero NB, Bitoun M. Centronuclear myopathies. Semin. Pediatr. Neurol. 2011; 18: 250–6.

Romero NB, Clarke NF. Congenital myopathies. Handb. Clin. Neurol. 2013; 113: 1321–36.

Romero NB, Mezmezian M, Fidziańska A. Main steps of skeletal muscle development in the human: morphological analysis and ultrastructural characteristics of developing human muscle. Handb. Clin. Neurol. 2013; 113: 1299–310.

Romero NB, Sandaradura SA, Clarke NF. Recent advances in nemaline myopathy. Curr. Opin. Neurol. 2013; 26: 519–26.

Ryan MM, Ilkovski B, Strickland CD, Schnell C, Sanoudou D, Midgett C, et al. Clinical course correlates poorly with muscle pathology in nemaline myopathy. Neurology 2003; 60: 665–673.

Sambuughin N, Yau KS, Olivé M, Duff RM, Bayarsaikhan M, Lu S, et al. Dominant mutations in KBTBD13, a member of the BTB/Kelch family, cause nemaline myopathy with cores. Am. J. Hum. Genet. 2010; 87: 842–847.

Sewry C. The role of immunocytochemistry in congenital myopathies. Neuromuscul. Disord. 1998; 8: 394–400.

Shichiji M, Biancalana V, Fardeau M, Hogrel J-Y, Osawa M, Laporte J, et al. Extensive morphological and immunohistochemical characterization in myotubular myopathy. Brain Behav. 2013; 3: 476–86.

Vasli N, Böhm J, Le Gras S, Muller J, Pizot C, Jost B, et al. Next generation sequencing for molecular

diagnosis of neuromuscular diseases. Acta Neuropathol. 2012; 124: 273–83.

Vasli N, Laporte J. Impacts of massively parallel sequencing for genetic diagnosis of neuromuscular disorders. Acta Neuropathol. 2013; 125: 173–85.

Wallgren-Pettersson C, Donner K, Sewry C, Bijlsma E, Lammens M, Bushby K, et al. Mutations in the nebulin gene can cause severe congenital nemaline myopathy. Neuromuscul. Disord. 2002; 12: 674–679.

Wallgren-Pettersson C, Laing NG. Report of the 83rd ENMC International Workshop: 4th Workshop on Nemaline Myopathy, 22–24 September 2000, Naarden, The Netherlands. Neuromuscul. Disord. 2001; 11: 589–595.

Wallgren-Pettersson C, Rapola J, Donner M. Pathology of congenital nemaline myopathy. J. Neurol. Sci. 1988; 83: 243–257.

Wallgren-Pettersson C, Sewry CA, Nowak KJ, Laing NG. Nemaline myopathies. Semin. Pediatr. Neurol. 2011; 18: 230–8.

de Winter JM, Buck D, Hidalgo C, Jasper JR, Malik FI, Clarke NF, et al. Troponin activator augments muscle force in nemaline myopathy patients with nebulin mutations. J. Med. Genet. 2013; 50: 383–92.

CHAPTER 4

IN VIVO AND *IN VITRO* INVESTIGATIONS OF HETEROZYGOUS NEBULIN KNOCK-OUT MICE DISCLOSE A MILD SKELETAL MUSCLE PHENOTYPE

De Winter JM*, Gineste C*, Kohl C, Witt CC, Giannesini B, Brohm K, Le Fur Y, Gretz N, Vilmen C, Pecchi E, Jubeau M, Cozzone PJ, Stienen GJM, Granzier H, Labeit S, Ottenheijm CAC, Bendahan D and Gondin J.

* Contributed equally

Neuromuscular Disorders, 2013

ABSTRACT

Background | Nemaline myopathy is the most common non-dystrophic skeletal muscle congenital disease, and mutations in the nebulin gene account for ~ 50% of all nemaline myopathy cases. Recent studies reported that the disease severity might be related to the nebulin expression levels. Considering that mutations in the nebulin gene are typically recessive, one could suggest that a single functional nebulin allele would allow to maintain nebulin protein expression to normal levels which would result in preserved skeletal muscle function.

Methods | We investigated skeletal muscle function of heterozygous *Neb*-KO (i.e., nebulin$^{+/-}$) mice using a multidisciplinary approach including protein and gene expression analysis and combined in vivo and in vitro force measurements. Skeletal muscle anatomy and energy metabolism were studied strictly non-invasively using magnetic resonance imaging and 31P-magnetic resonance spectroscopy.

Results | Maximal force production was reduced by ~16% in isolated muscle of nebulin$^{+/-}$ mice while in vivo force generating capacity was preserved. Muscle weakness was associated with a shift toward a slower proteomic phenotype, but was not related to nebulin protein deficiency or to an impaired energy metabolism.

Interpretation | Further studies would be warranted in order to determine the mechanisms leading to a mild skeletal muscle phenotype resulting from the expression of a single nebulin allele.

INTRODUCTION

Nemaline Myopathy (NM) is the most common non-dystrophic skeletal muscle congenital disease (Clarkson et al., 2004). While muscle weakness and hypotonia are the main clinical symptoms, the hallmark feature is the presence of nemaline (rod-like) bodies in muscle fibers (Schnell et al., 2000). From a clinical point of view, six different categories have been identified ranging from neonatal-lethal forms to late only slowly-progressive weakness (North et al., 1997; Wang et al., 2012). So far, seven genes have been associated with NM in humans i.e. alpha-tropomyosin-3 and beta-tropomyosin (*TPM3* and *TPM2*), nebulin (*NEB*), actin alpha 1 (*ACTA1*), troponin T type 1 (*TNNT1*), cofilin-2 (*CFL2*), and kelch repeat and BTB (POZ) domain containing 13 (*KBTBD13*) (Sanoudou and Beggs, 2001; Wallgren-Pettersson et al., 2011). Given that six out of these genes encode proteins associated with the sarcomeric thin filament, NM has been considered as a thin filament myopathy. The function of the protein product of the seventh gene *KBTBD13* is still to be discovered (Sambuughin et al., 2010).

Human mutations in the *NEB* gene are the most common causes of autosomal recessive NM, accounting for ~ 50% of all NM cases (Pelin and Wallgren-Pettersson, 2008). Although often associated with the non-progressive or slowly-progressive “typical” form of congenital NM, *NEB* mutations may also lead to “intermediate” and “severe” forms of NM which are characterized by lack of ambulation or neonatal death (Lehtokari et al., 2009; Wallgren-Pettersson et al., 2002). To date, 64 different *NEB* mutations have been identified in 55 NM families and most of the patients are compound heterozygous for two different *NEB* mutations (Lehtokari et al., 2006; Wallgren-Pettersson et al., 2011).

Nebulin is a giant sarcomeric protein (depending on splice isoform, 600-900 kDa in size) which spans nearly the entire length (~1 μm) of the thin filament (Kruger, 1991; Labeit et al., 2011; Wang, 1988). The C-terminal region of nebulin is anchored in the Z-disk while its N-terminal region is located near the thin filament pointed end (Bang et al., 2002; Gokhin et al., 2012; Labeit and Kolmerer, 1995). The physiological function of nebulin in skeletal muscle has been recently highlighted thanks to the generation of nebulin knock-out (*Neb*-KO) mouse models (Bang et al., 2006; Pappas et al., 2010). It has been consistently reported that nebulin plays a critical role in the regulation of thin filament length (Bang et al., 2006; Pappas et al., 2010; Witt et al.,

2006). When compared to wild-type muscle fibers, thin filaments are on average shorter in nebulin-deficient skeletal muscle fibers, thereby leading to a reduced thin-thick filament overlap and resulting in an impaired force generating capacity. Interestingly, nebulin is not merely a structural protein but is also involved in the regulation of muscle contraction by modulating both cross-bridge cycling kinetics and the calcium sensitivity of force generation (Bang et al., 2009; Chandra et al., 2009; Ottenheijm et al., 2010).

Interestingly, muscle characteristics observed in *Neb*-KO mice, i.e., shorter and non-uniform thin filament lengths, altered cross-bridge cycling kinetics, reduced calcium-sensitivity of force generation and impaired force generating capacity are similar to those observed in muscle of NM patients (Ottenheijm et al., 2008; Ottenheijm, Witt, et al., 2009). Additionally, it has been recently suggested that disease severity might be related to the nebulin expression levels. Indeed, myofibers force production was severely decreased in a NM patient with ~10% of the normal nebulin level due to compound heterozygous *NEB* mutations. This impaired contractile performance largely exceeded what has been reported in patients for whom the nebulin protein level was roughly 28% of control values as a result of a deletion of exon 55 (Lawlor et al., 2011; Ottenheijm, Witt, et al., 2009). On the contrary, a mild muscle weakness has been reported in a patient with 70% of the control protein level while single muscle fibers analysis showed no changes in both the force-sarcomere length relationship and in the calcium-sensitivity of force generation (Ochala et al., 2011). Considering that *NEB* mutations are typically recessive and that two mutations are required for the development of NM, one could suggest that one functional nebulin allele would be sufficient to preserve the normal nebulin level which would result in an unaltered skeletal muscle function.

We aimed therefore at characterizing protein and gene expression, *in vivo* and *in vitro* muscle contractile performance, anatomical and metabolic characteristics in heterozygous *Neb*-KO (nebulin$^{+/-}$) in order to determine the functional impact of the expression of a single nebulin allele. Our data suggested that the expression of a single functional allele resulted both in mild muscle weakness at the *in vitro* level and in a shift toward a slower proteomic phenotype, which were not related to nebulin protein deficiency.

MATERIALS AND METHODS

Animals

Three-month old male nebulin$^{+/-}$ and nebulin$^{+/+}$ littermates were used for the experiments conducted in agreement with the German and French guidelines for animal care, in conformity with the European convention for the protection of vertebrate animals used for experimental purposes and institutional guidelines n° 86/609/CEE November 24, 1986 and followed the U.S. National Institutes of Health "Using Animals in Intramural Research" guidelines for animal use. All animal experiments were approved by The University of Arizona IACUC Office (permit number: #07-090), by the "Regierungspräsidium Karlsruhe" (permit number: AZ-35-9185.81/G-108/07) and by the "Préfecture des Bouches du Rhône" (permit number: #13-441 & #13-475). Mice were housed in an environment-controlled facility (12-12 hour light-dark cycle, 22°C) and received water and standard food ad libitum. Mice were identified through PCR genotyping from mouse tail DNA as previously described (Witt et al., 2006).

Gene expression

RNA isolation and Microarray Analysis: Expression profiling with Affymetrix gene chips was performed as described previously (Witt et al., 2005, 2006). Briefly, total RNA was prepared with the RNeasy Kit (Qiagen) from quadriceps (n = 3 for both groups), reverse transcribed with Superscript II (Invitrogen), as recommended by the manufacturer, and labeled and hybridized as described in the Affymetrix manual. We used the Affymetrix Mouse Genome 430 2.0 microarrays. A Custom CDF Version 13 with Entrez based gene definitions was used to annotate the arrays. The Raw fluorescence intensity values were normalized applying quantile normalization. All data have been deposited onto the Gene Expression Omnibus (GEO accession number: GSE36743).

miRNA isolation and miRNA Microarray Analysis: Total RNA was prepared from quadriceps using Trizol® reagent (Gibco). Microarray analysis was performed using Affymetrix miRNA-1_0 – type arrays. Samples were labeled using the FlashTag™ Biotin HSR Kit from Genisphere (Genisphere, Hatfield, PA, USA) starting with 1 µg of total RNA according to the protocol of the manufacturer. Biotin-labelled samples were hybridized to GeneChipmiRNA Arrays at 48 °C and 60 r.p.m. for 16 h. After washing at a Fluidics Station 450 using fluidics script, FS450_0003 arrays were scanned with an

AffymetrixGeneChip Scanner 3000. Raw data were background corrected and quantile normalized using the miRNAQCTool from Affymetrix with default parameters recommended by Affymetrix (RMA normalization). All of the equipment used was from the Affymetrix-Company (Affymetrix, High Wycombe, UK). Only mouse miRNAs were considered in the analysis. All arrays were pre-processed using Robust Multiarray Average (RMA). RMA was performed on all probe sets after which nonmouse probe sets were removed leaving 609 mousemiRNA probe sets. All data have been deposited onto the Gene Expression Omnibus (GEO accession number: GSE36741).

In vitro experiments

Left soleus (SOL) muscles (n = 7 for nebulin$^{+/+}$ group ; n = 6 for nebulin$^{+/-}$ group) were quickly dissected and, using silk suture, mounted vertically in a tissue bath between a dual-mode lever arm and a fixed hook (1200A Intact Muscle Test System, Aurora Scientific Inc., Canada). SOL muscles were chosen because of their well-defined tendons and their small size, which facilitates oxygenation. The muscle was bathed in continuously oxygenated (95% O_2–5% CO_2) mammalian Ringer solution with pH 7.40. The temperature of the solution was maintained at 30°C during the experiment. The muscle was stimulated directly with platinum plate electrodes placed in close apposition to the muscle. Muscle length was adjusted until maximal twitch force was achieved (pulse duration of 200 μs). A twitch and tetanus (150 Hz) were generated in order to determine twitch and maximal force prior to the experimental protocols. After completion of the contractility measurements, length and weight of the SOL muscles were determined. Cross-sectional area (CSA; in mm^2) was calculated by dividing muscle weight (g) by muscle length (mm) multiplied by specific density (1.056 g/ml) × 100.

Force-frequency protocol: The muscle was stimulated with incremental stimulation frequencies (1, 10, 20, 30, 50, 70, 100, 150 Hz) as previously described (Ottenheijm, Hidalgo, et al., 2009). Data were discarded when stimulation at 150 Hz rendered a force that was less than 95% of the force generated during the first stimulation at 150 Hz. Stimuli were applied with a train duration of 600 ms. The resting interval was 30 sec between the stimulations at 1 and 10 Hz; 60 sec after stimulation at 20 Hz; 90 sec after stimulation at 30 Hz; and 120 sec between stimulations at 50, 70, 100 and 150 Hz.

Fatigue protocol: Five minutes after completion of the force-frequency protocol, the fatigue protocol was started. For a period of 4 min, a one-second 40 Hz pulse train was applied to the muscle, with resting intervals of two seconds.

In vivo experiments

Animal preparation: Mice were initially anesthetized in an induction chamber using 4% isoflurane in 33% O_2 (0.5 l/min) and 66% NO_2 (1 l/min). The left hindlimb was shaved before an electrode cream was applied at the knee and heel regions to optimize electrical stimulation. Each anaesthetized mouse was placed supine in a home-built cradle which has been specially designed for the strictly non-invasive functional investigation of the left hindlimb muscles (Giannesini et al., 2010). Throughout a typical experiment, anaesthesia was maintained by gas inhalation through a facemask continuously supplied with 1.75% isoflurane in 33% O_2 (0.2 l/min) and 66% N_2O (0.4 l/min). Exhaled and excess gases were removed through a canister filled with activated charcoal (Smiths Industries Medical System, Sheffield, UK) mounted on an electrical pump extractor (Equipement Vétérinaire Minerve, Esternay, France). Physiological temperature was adjusted with an electrical heating blanket. The foot was positioned on the pedal of the ergometer with a 90° flexion ankle joint. The hindlimb was centered inside a 20 mm-diameter 1H Helmholtz imaging coil and the belly of the gastrocnemius muscle was located above an elliptical (8 x 12 mm) 31P-magnetic resonance spectroscopy (MRS) surface coil. Muscle contractions were achieved by transcutaneous electrical stimulation using two rod-shaped 1.5 mm-diameter surface electrodes integrated in the cradle and connected to an electrical stimulator (type 215/T; Hugo Sachs Elektronik-Harvard Apparatus GmbH, March-Hugstetten, Germany). One electrode was placed at the heel level and the other one was located just above the knee joint. The gastrocnemius muscle was chosen because it is easily accessible for 31P-MRS measurements and preferentially activated using our in vivo experimental set-up (Giannesini et al., 2010).

Study design: Mice were tested twice over a one-week period in order to assess mechanical performance, muscle fatigability, muscle volume and metabolic changes during a standardized stimulation protocol.

During the first testing session, transcutaneous stimulation was first elicited with square-wave pulses (0.5 ms duration) on the gastrocnemius muscle. The individual maximal stimulation intensity was determined on the basis of a progressive stimulation intensity increase until there was no further peak twitch force increase. This intensity was then maintained to elicit tetanic stimulations (0.75 sec duration, 30 sec resting interval; n = 18 for nebulin$^{+/+}$ group; n = 19 for nebulin$^{+/-}$ group) at various incremental frequencies (from 1 to 150 Hz). After a 20 min resting period, a fatigue protocol (n = 12 for nebulin$^{+/+}$ group; n = 10 for nebulin$^{+/-}$ group) was performed using the same stimulation parameters as the in vitro experiments.

During the second testing session, magnetic resonance imaging (MRI) measurements were performed at rest to get information about muscle volume. Additionally, metabolic changes were investigated using 31P-MRS during a standardized stimulation protocol (n = 15 for nebulin$^{+/+}$ group; n = 17 for nebulin$^{+/-}$ group) consisting of 6 min of repeated single twitch isometric contractions delivered at a frequency of 1.7 Hz (Giannesini et al., 2010).

Force output measurements: The analog electrical signal from the force transducer was amplified with a home-built device (Operational amplifier AD620; Analog Devices, Norwood, MA, USA; gain = 70 dB; bandwidth = 0-5 kHz), converted to a digital signal (PCI-6220; National Instruments, Austin, TX, USA) and recorded on a personal computer using the WinATS software (Sysma, Aix-en-Provence, France).

MR acquisition: Investigations were performed in a 4.7-Tesla horizontal superconducting magnet (47/30 Biospec Avance, Bruker, Karlsruhe, Germany) equipped with a Bruker 120-mm BGA12SL (200 mT/m) gradient insert.

T2-weighted anatomic imaging: Ten contiguous axial slices (thickness = 1 mm), covering the region from the knee to the ankle, were acquired at rest using a spin echo sequence (TE = 10.6 ms; TR = 1000 ms; one accumulation; field of view = 42 x 30 mm; matrix size = 256 x 192; acquisition time = 3 min 12 sec).

31P-MRS measurements: Spectra (8-kHz sweep width; 2048 data points) from the gastrocnemius region were continuously acquired at rest and throughout the standardized stimulation protocol. A fully relaxed spectrum

(12 accumulations, TR = 20 sec) was acquired at rest followed by a total of 256 free induction decays (FID) (TR = 1.875 sec). The first 64 FIDs were acquired at rest and summed together. The next 192 FIDs were acquired during the stimulation period and were summed by packets of 32, allowing a temporal resolution of ~ 60 sec.

Biochemical and Molecular analyses

Intracellular ATP concentration: Mice were anesthetized intra-peritoneally with a pentobarbital injection (50 mg/kg). Gastrocnemius muscles were harvested and freeze-clamped with liquid nitrogen-chilled metal tongs before mice were submitted to a cervical dislocation. The corresponding tissue sample was used in order to measure intracellular ATP concentration. Water soluble metabolites were extracted from 20-40 mg of freeze-clamped gastrocnemius muscle sample using perchloric acid solution (0.6 M) as previously described (Giannesini et al., 2007). ATP concentration was determined using a bioluminescence assay according to the manufacturer's instructions (ATP Determination Kit (A22066), Invitrogen, Eugene, Oregon, USA).

Gel Electrophoresis: SDS-agarose electrophoresis studies on nebulin$^{+/-}$ and nebulin$^{+/+}$ SOL muscles were performed as previously described (Ottenheijm, Hidalgo, et al., 2009). Wet gels were scanned and analyzed with One-D scan EX (Scanalytics Inc., Rockville, MD, USA) software. The integrated optical density (intOD) of nebulin, titin, and myosin heavy chain (MHC) isoforms were determined as a function of the volume of solubilized protein sample that was loaded (a range of volumes was loaded on each gel). The slope of the linear range of the relation between integrated optical density and loaded volume was obtained for each protein. Nebulin and titin slopes were normalized over MHC slopes.

Data processing

Mechanical performance: For each stimulation train, isometric peak force was calculated and the corresponding data were fitted to the Hill equation providing f_{50} (frequency giving 50% of the maximal force). Regarding the fatigue protocol, the peak force of each contraction was measured and the corresponding mean tetanic force was calculated every 5 contractions A fatigue index corresponding to the ratio between the first five and the last five contractions was determined. For the standardized stimulation protocol, the amplitude of each peak twitch was measured and was then averaged every

15 sec of stimulation.

For all stimulation protocols, force was divided by muscle CSA or by the corresponding hindlimb muscles volume (see below) in order to obtain normalized force (in mN/mm^2 for *in vitro* investigations or in mN/mm^3 for *in vivo* investigations, respectively).

MR data: The hindlimb muscles volume (in mm3) was calculated as the sum of the five cross-sectional areas of the six consecutive largest slices. 31P-MRS data were processed using a proprietary software developed using IDL (Interactive Data Language, Research System, Inc., Boulder, CO, USA) (Le Fur et al., 2010). Relative concentrations of phosphocreatine (PCr), inorganic phosphate (Pi) and ATP were obtained with a 60 sec time-resolution by a time-domain fitting routine using the AMARES-MRUI Fortran code and appropriate prior knowledge of the ATP multiplets. Absolute amounts of phosphorylated compounds were expressed relative to a resting ATP concentration determined in vitro (see above). PCr to ATP ratios were calculated from the peak areas of the fully relaxed spectrum. Intracellular pH (pHi) was calculated from the chemical shift of the Pi signal relative to PCr (Moon and Richards, 1973).

Statistical analyses

RNA isolation and Microarray Analysis: Differential gene expression was analysed based on loglinear mixed model ANOVA, using a commercial software package SAS JMP7 Genomics, version 4.0, from SAS (SAS Institute, Cary, NC, USA). A false positive rate of alpha = 0.05 with FDR correction was taken as the level of significance.

miRNA isolation and miRNA Microarray Analysis: Differential miRNA expression was analysed based on one-way ANOVA using a commercial software package SAS JMP7 Genomics, version 4, from SAS (SAS Institute, Cary, NC, USA). A false positive rate of alpha = 0.05 with FDR correction was taken as the level of significance.

In vitro and in vivo experiments: Statistical analyses were performed with Statistica software version 9 (StatSoft, Tulsa, OK, USA). Normality was checked using a Kolmogorov-Smirnov test. Two-factor (group x time) analysis of variance (ANOVAs) with repeated measures on time were used to compare isometric force production, metabolites concentrations and pHi.

Two-factor (group x contraction number or stimulation frequency) ANOVAs with repeated measures on contraction number or stimulation frequency were used to compare force production. When a main effect or a significant interaction was found, Newman–Keuls post-hoc analysis was used. Unpaired t-tests were used for other comparisons. Data are presented as mean ± standard error of mean (SEM). Significance was accepted when $P < 0.05$.

RESULTS

Gene, miRNA and protein expression profiles

The quadriceps transcriptome disclosed a group of 159 dysregulated genes in nebulin$^{+/-}$ mice as compared to nebulin$^{+/+}$ mice. 85 genes were up-regulated (Table 1) and 74 down- regulated (Table 2). The fold changes ranged from 1.1 to 8.0 with a p value < 0.00065. The most up-regulated genes were Myosin Heavy Chain 7 (β-MHC) with an 8-fold increase and the slow isoforms of the Troponins (Tn) C, I, and T with a 5-fold increase (Table 1). Although a slightly lower nebulin mRNA level was observed in nebulin$^{+/-}$ mice (- 14%) as compared to controls, the corresponding difference was far from the threshold of significance ($P = 0.25$). Additionally, no significant difference was detected in the miRNA profiles between the two genotypes.

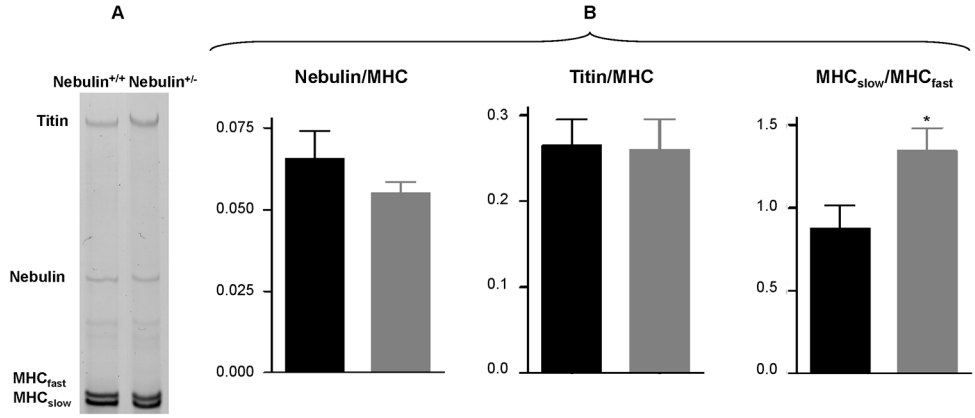

Figure 1 SDS-agarose gel electrophoresis

(A) and a typical gel result example of nebulin$^{+/+}$ and nebulin$^{+/-}$ mice. (B) Nebulin, titin, and myosin heavy chain (MHC) isoforms protein levels were measured by SDS-agarose from soleus muscles (for nebulin n = 8 for both groups; for titin n = 6 for both groups; for MHC n = 10 for nebulin$^{+/+}$ group and n = 7 for nebulin$^{+/-}$ group). MHC protein was used as a loading control. The ratio MHC_{slow}/MHC_{fast} was higher in nebulin+/- (grey) compared to nebulin$^{+/+}$ mice (black). Values are presented as mean ± SEM. Significantly different between groups * $P < 0.05$.

Table 1
List of the 85 upregulated genes in nebulin$^{+/-}$ mice.

Gene symbol	Gene name	Fold change
Myh7	Myosin, heavy polypeptide 7, cardiac muscle, beta	8.0
Tnnc1	Troponin C, cardiac/slow skeletal	5.4
Tnni1	Troponin I, skeletal, slow 1	5.3
Tnnt1	Troponin T1, skeletal, slow	5.2
Ddit4	DNA-damage-inducible transcript 4	4.7
Ctgf	Connective tissue growth factor	2.6
Arrdc2	Arrestin domain containing 2	2.6
Arrdc3	Arrestin domain containing 3	2.1
Mt2	Metallothionein 2	2.0
Cebpb	CCAAT/enhancer binding protein (C/EBP), beta	1.9
1810011O10Rik	RIKEN cDNA 1810011O10 gene	1.8
Errfi1	ERBB receptor feedback inhibitor 1	1.7
Fgfbp1	Fibroblast growth factor binding protein 1	1.6
Ccrn4l	CCR4 carbon catabolite repression 4-like (*Saccharomyces cerevisiae*)	1.6
Myl3	Myosin, light polypeptide 3	1.5
Rhob	Ras homolog gene family, member B	1.5
Btg2	B-cell translocation gene 2, anti- proliferative	1.4
Timp4	Tissue inhibitor of metalloproteinase 4	1.4
Slc10a6	Solute carrier family 10 (sodium/bile acid cotransporter family), member 6	1.4
Dnajb1	DnaJ (Hsp40) homolog, subfamily B, member 1	1.4
Cdc14a	CDC14 cell division cycle 14A	1.4
Fam107a	Family with sequence similarity 107, member A	1.3
Lypd6	LY6/PLAUR domain containing 6	1.3
Dusp16	Dual specificity phosphatase 16	1.3
Camk2n1	Calcium/calmodulin-dependent protein kinase II inhibitor 1	1.3
Sars2	Seryl-aminoacyl-tRNA synthetase 2	1.3
Wee1	WEE 1 homolog 1 (*Schizosaccharomyces pombe*)	1.3
Hbegf	Heparin-binding EGF-like growth factor	1.3
Tspan4	Tetraspanin 4	1.3
Npy1r	Neuropeptide Y receptor Y1	1.3
Rasl11b	RAS-like, family 11, member B	1.3
Cntnap2	Contactin associated protein-like 2	1.3
Als2cr12	Amyotrophic lateral sclerosis 2 (juvenile) chromosome region, candidate 12	1.3
Scin	Scinderin	1.3
Map4k3	Mitogen-activated protein kinase kinase kinase kinase 3	1.2
6430527G18Rik	RIKEN cDNA 6430527G18 gene	1.2
Skil	SKI-like	1.2
Cnn3	Calponin 3, acidic	1.2
Map3k6	Mitogen-activated protein kinase kinase kinase 6	1.2
Lgi1	Leucine-rich repeat LGI family, member 1	1.2
Adh1	Alcohol dehydrogenase 1 (class I)	1.2
Lin52	Lin-52 homolog (*Caenorhabbitis elegans*)	1.2
Lonrf3	LON peptidase N-terminal domain and ring finger 3	1.2
Ptprd	Protein tyrosine phosphatase, receptor type, D	1.2
Pcyt2	Phosphate cytidylyltransferase 2, ethanolamine	1.2
Phgdh	3-Phosphoglycerate dehydrogenase	1.2
A530082C11Rik	RIKEN cDNA A530082C11 gene	1.2
Rnf145	Ring finger protein 145	1.2
Mybpc3	Myosin binding protein C, cardiac	1.2
Tle4	Transducin-like enhancer of split 4, homolog of *Drosophila E* (spl)	1.2
Slc46a3	Solute carrier family 46, member 3	1.2
Fhl3	Four and a half LIM domains 3	1.2
Epc1	Enhancer of polycomb homolog 1 (*Drosophila*)	1.2
Mpv17	MpV17 mitochondrial inner membrane protein	1.2
Ablim3	Actin binding LIM protein family, member 3	1.2
Serpini1	Serine (or cysteine) peptidase inhibitor, clade I, member 1	1.2
Hmgcl	3-Hydroxy-3-methylglutaryl-Coenzyme A lyase	1.2
Fam102b	Family with sequence similarity 102, member B	1.2
Chodl	Chondrolectin	1.2
Bcap29	B-cell receptor-associated protein 29	1.2
Sfrs13a	Splicing factor, arginine/serine-rich 13A	1.2
Lrtm2	Leucine-rich repeats and transmembrane domains 2	1.2
Gucy2g	Guanylate cyclase 2g	1.2

Ahnak	AHNAK nucleoprotein (desmoyokin)	1.2
5930434B04Rik	RIKEN cDNA 5930434B04 gene	1.2
Gm7517	Predicted gene 7517	1.2
Crispld2	Cysteine-rich secretory protein LCCL domain containing 2	1.2
1700003E16Rik	RIKEN cDNA 1700003E16 gene	1.1
Yjefn3	YjeF N-terminal domain containing 3	1.1
Cyp39a1	Cytochrome P450, family 39, subfamily a, polypeptide 1	1.1
Tap1	Transporter 1, ATP-binding cassette, sub-family B (MDR/TAP)	1.1
Bat1a	HLA-B-associated transcript 1A	1.1
Smcr7	Smith-Magenis syndrome chromosome region, candidate 7 protein homolog	1.1
Hsd3b3	Hydroxy-delta-5-steroid dehydrogenase, 3 beta- and steroid delta-isomerase 3	1.1
Dlc1	Deleted in liver cancer 1	1.1
Tef	Thyrotroph embryonic factor	1.1
Pkd1	Polycystic kidney disease 1 homolog	1.1
BC031781	CDNA sequence BC031781	1.1
D10Jhu81e	DNA segment, Chr 10, Johns Hopkins University 81 expressed	1.1
Pisd	Phosphatidylserine decarboxylase	1.1
Pbk	PDZ binding kinase	1.1
Smarce1	SWI/SNF related, matrix associated, actin dependent regulator of chromatin, subfamily e, member 1	1.1
Capn11	Calpain 11	1.1
Vax2os2	Vax2 opposite strand transcript 2	1.1
Dnajc8	DnaJ (Hsp40) homolog, subfamily C, member 8	1.1

Nebulin protein level, normalized to MHC, was not significantly different between nebulin$^{+/+}$ and nebulin$^{+/-}$ mice (0.066 ± 0.02 vs. 0.055 ± 0.01, respectively). In addition, no significant changes were observed in titin protein levels between nebulin$^{+/+}$ and nebulin$^{+/-}$ mice (0.26 ± 0.08 vs. 0.26 ± 0.09, respectively) (Fig 1).

MHC isoform composition was assessed using the MHC_{slow} to MHC_{fast} ratio. This ratio was higher in nebulin$^{+/-}$ mice as compared to nebulin$^{+/+}$ (1.34 ± 0.44 vs. 0.88 ± 0.37, respectively; $P < 0.05$) (Fig 1).

In vitro experiments

No significant difference was observed between nebulin$^{+/+}$ and nebulin$^{+/-}$ mice for body weight (28.0 ± 6.5 g vs. 29.5 ± 5.6 g, respectively) and SOL CSA (0.61 ± 0.09 mm2 vs. 0.64 ± 0.07 mm^2, respectively). As illustrated in figure 2A, normalized maximal tetanic force was significantly reduced ($p < 0.05$) in nebulin$^{+/-}$ as compared to nebulin$^{+/+}$ mice at 30, 50, 70, 100 and 150 Hz. A relative force-frequency curve was constructed using force values expressed as a percentage of the maximally generated force at 150 Hz. As shown in figure 2B, no difference was observed in the relative force-frequency curve of nebulin$^{+/-}$ mice as compared to nebulin$^{+/+}$ mice. Accordingly, the f_{50} was not different between groups. No significant change was observed during the fatigue protocol, as illustrated by a comparable fatigue index between nebulin$^{+/+}$ and nebulin$^{+/-}$ mice (2.00 ± 0.21 vs. 1.94 ± 0.27, respectively) (Fig 4A).

Table 2
List of the 74 downregulated genes in nebulin$^{+/-}$ mice.

Gene symbol	Gene name	Fold change
Sh2d6	SH2 domain containing 6	−1.1
Rxrg	Retinoid X receptor gamma	−1.1
Xpa	Xeroderma pigmentosum, complementation group A	−1.1
Zfand3	Zinc finger, AN1-type domain 3	−1.1
Itfg3	Integrin alpha FG-GAP repeat containing 3	−1.1
Sgpp1	Sphingosine-1-phosphate phosphatase 1	−1.1
Ifnar2	Interferon (alpha and beta) receptor 2	−1.1
Elmod3	ELMO/CED-12 domain containing 3	−1.1
Galnt2	UDP-N-acetyl-alpha-D-galactosamine: polypeptide N-acetylgalactosaminyltransferase 2	−1.1
Ccdc59	Coiled-coil domain containing 59	−1.1
Fam82a1	Family with sequence similarity 82, member A1	−1.1
Zfand5	Zinc finger, AN1-type domain 5	−1.1
Tmem37	Transmembrane protein 37	−1.2
Oscp1	Organic solute carrier partner 1	−1.2
Dym	Dymeclin	−1.2
Atf1	Activating transcription factor 1	−1.2
Agpat3	1-Acylglycerol-3-phosphate o-acyltransferase 3	−1.2
Creld1	Cysteine-rich with EGF-like domains 1	−1.2
Ccl7	Chemokine (C–C motif) ligand 7	−1.2
Slc16a3	Solute carrier family 16 (monocarboxylic acid transporters), member 3	−1.2
Klhl29	Kelch-like 29 (Drosophila)	−1.2
Skp1a	S-phase kinase-associated protein 1A	−1.2
Sep-04	Septin 4	−1.2
V1rd6	Vomeronasal 1 receptor, D6	−1.2
Pax5	Paired box gene 5	−1.2
Crot	Carnitine o-octanoyltransferase	−1.2
Cysltr1	Cysteinyl leukotriene receptor 1	−1.2
Psme4	Proteasome (prosome, macropain) activator subunit 4	−1.2
Fut8	Fucosyltransferase 8	−1.2
Mtx2	Metaxin 2	−1.2
Schip1	Schwannomin interacting protein 1	−1.2
Asb5	Ankyrin repeat and SOCs box-containing 5	−1.2
Mthfd2	Methylenetetrahydrofolate dehydrogenase (NAD + dependent), methenyltetrahydrofolate cyclohydrolase	−1.2
Slc40a1	Solute carrier family 40 (iron-regulated transporter), member 1	−1.2
Pola2	Polymerase (DNA directed), alpha 2	−1.2
Rab10	RAB10, member RAS oncogene family	−1.2
Phlda3	Pleckstrin homology-like domain, family A, member 3	−1.2
Dync1li1	Dynein cytoplasmic 1 light intermediate chain 1	−1.2
9030617O03Rik	RIKEN cDNA 9030617O03 gene	−1.2
Slc15a4	Solute carrier family 15, member 4	−1.2
D4Bwg0951e	DNA segment, Chr 4, Brigham & Women's Genetics 0951 expressed	−1.2
Kif3c	Kinesin family member 3C	−1.2
Golph3	Golgi phosphoprotein 3	−1.2
Sorl1	Sortilin-related receptor, LDLR class A repeats-containing	−1.2
AI317395	Expressed sequence AI317395	−1.2
H2afz	H2A histone family, member Z	−1.2
Arl2bp	ADP-ribosylation factor-like 2 binding protein	−1.2
Hist1h2bc	Histone cluster 1, H2bc	−1.3
Supt3h	Suppressor of Ty 3 homolog (*S. cerevisiae*)	−1.3
Xrcc5	X-ray repair complementing defective repair in Chinese hamster cells 5	−1.3
Hipk2	Homeodomain interacting protein kinase 2	−1.3
Prdx1	Peroxiredoxin 1	−1.3
Comtd1	Catechol-o-methyltransferase domain containing 1	−1.3
Kcnj12	Potassium inwardly-rectifying channel, subfamily J, member 12	−1.3
Lrrc52	Leucine rich repeat containing 52	−1.3
Tnfaip2	Tumor necrosis factor, alpha-induced protein 2	−1.3
Oxct1	3-Oxoacid CoA transferase 1	−1.3
Sh3bp5	SH3-domain binding protein 5 (BTK-associated)	−1.3
Rabgef1	RAB guanine nucleotide exchange factor (GEF) 1	−1.3
Tinag	Tubulointerstitial nephritis antigen	−1.3
Actr3b	ARP3 actin-related protein 3 homolog B	−1.3
Entpd4	Ectonucleoside triphosphate diphosphohydrolase 4	−1.3
Gpr177	G protein-coupled receptor 177	−1.4

Grem2	Gremlin 2 homolog, cysteine knot superfamily (*Xenopus laevis*)	−1.4
Arntl	Aryl hydrocarbon receptor nuclear translocator-like	−1.4
Fgl2	Fibrinogen-like protein 2	−1.4
Pde7a	Phosphodiesterase 7A	−1.4
Bdh1	3-Hydroxybutyrate dehydrogenase, type 1	−1.5
Prkcd	Protein kinase C, delta	−1.5
Cd24a	CD24a antigen	−1.5
Neto2	Neuropilin (NRP) and tolloid (TLL)-like 2	−1.5
Slc15a5	Solute carrier family 15, member 5	−1.6
Igh-1b	Immunoglobulin heavy chain 1b	−1.8
1700001O22Rik	RIKEN cDNA 1700001O22 gene	−2.0

In vivo experiments

No significant difference ($p > 0.05$) was observed between nebulin$^{+/+}$ and nebulin$^{+/-}$ mice for body weight (29.8 ± 1.0 g vs. 29.4 ± 0.6 g, respectively) and hindlimb muscles volume (193 ± 6 mm^3 vs. 197 ± 4 mm^3, respectively).

Mechanical performance: Normalized maximal tetanic force was similar between nebulin$^{+/+}$ (1.44 ± 0.08 mN/mm^3) and nebulin$^{+/-}$ mice (1.38 ± 0.04 mN/mm^3). Force production was similar between nebulin$^{+/+}$ and nebulin^{-} groups regardless of the stimulation frequency used (Fig 3A). The f50 was also similar for the two groups (Fig 3B).

No significant difference was observed during the fatigue protocol between the two groups leading to a similar fatigue index for nebulin$^{+/+}$ and nebulin$^{+/-}$ mice (5.0 ± 0.5 vs. 5.2 ± 0.5, respectively) (Fig 4B). Additionally, force production during the 6-min stimulation protocol was similar in both groups (data not shown).

Metabolic changes: Both [PCr] and [PCr]/[ATP] resting values were similar between nebulin+/+ (23 ± 4 mM and 4.1 ± 0.7, respectively) and nebulin$^{+/-}$ groups (20 ± 2 mM and 3.9 ± 0.3, respectively). For both groups, [PCr] fell rapidly throughout the standardized stimulation protocol and reached a steady state at the end of the stimulation bout. No significant difference was observed between the two groups throughout the stimulation period (Fig 5A). As expected, the [Pi] time-course evolved as a mirror of the [PCr] time-dependent changes. [Pi] resting values were not different between the two groups and increased similarly during the first part of the exercise. For both groups, [Pi] reached a plateau after 3 min of exercise (Fig 5B). At rest, pHi was not significantly different for nebulin$^{+/+}$ (7.07 ± 0.04) and nebulin$^{+/-}$ groups (7.16 ± 0.02). pHi decreased significantly throughout the stimulation session so that the acidosis extent was similar for the two groups at the end

of the stimulation protocol (Fig 5C). [ATP] resting value was similar between nebulin$^{+/+}$ (5.9 ± 0.2 mM) and nebulin$^{+/-}$ (5.4 ± 0.4 mM) groups. [ATP] slightly decreased during the exercise without any significant difference between the two groups (Fig 5D).

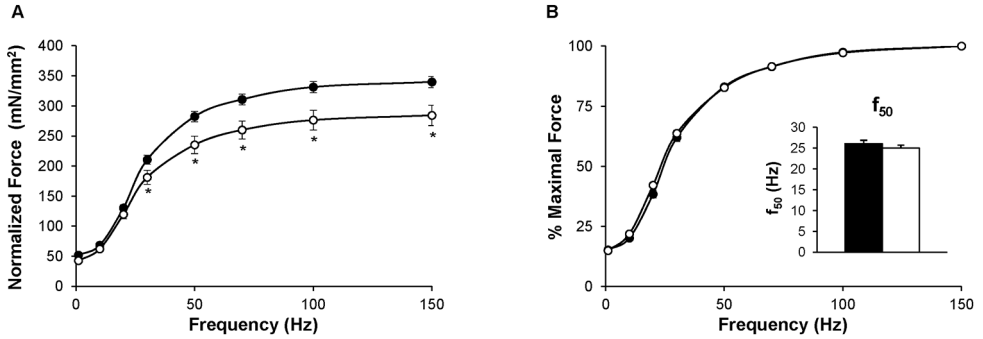

Figure 2 Normalized (A) and relative (B) force production during the force-frequency protocol performed *in vitro*

Maximal force was reduced in nebulin$^{+/-}$ group (n = 7) compared to nebulin$^{+/+}$ group (n = 6) while force-frequency curves were not different between the two groups. Force is normalized to muscle CSA (A) and to maximal force obtained at 150 Hz (B). Values are presented as mean ± SEM. Significantly different between groups * $P < 0.05$.

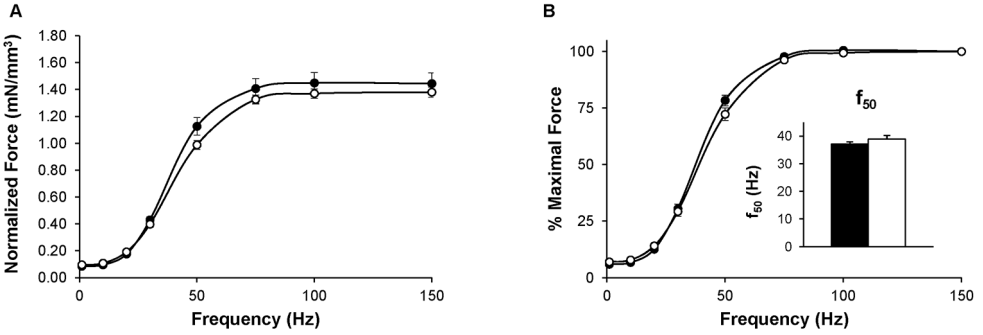

Figure 3 Normalized (A) and relative (B) force production during the force-frequency protocol performed *in vivo*

Maximal force and force-frequency curves were similar in nebulin$^{+/-}$ group (; n = 19) compared to nebulin$^{+/+}$ group (; n = 18). Force is normalized to muscle volume (A) and to maximal force obtained at 150 Hz (B). Values are presented as mean ± SEM.

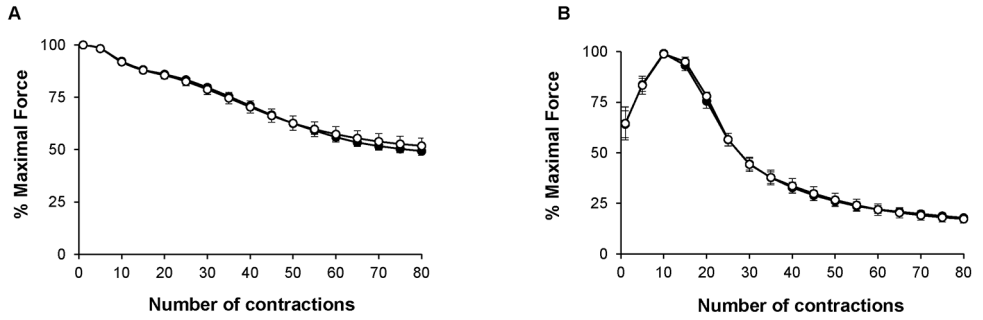

Figure 4 Force production during the fatigue protocol *in vitro* (A) and *in vivo* (B)
Fatigability was similar both *in vivo* and *in vitro* in nebulin$^{+/-}$ group (*in vitro n* = 6; *in vivo n* = 10) as compared to nebulin$^{+/+}$ group (*in vitro n* = 7; *in vivo n* = 12). Force is normalized to maximal force. Values are presented as mean ± SEM.

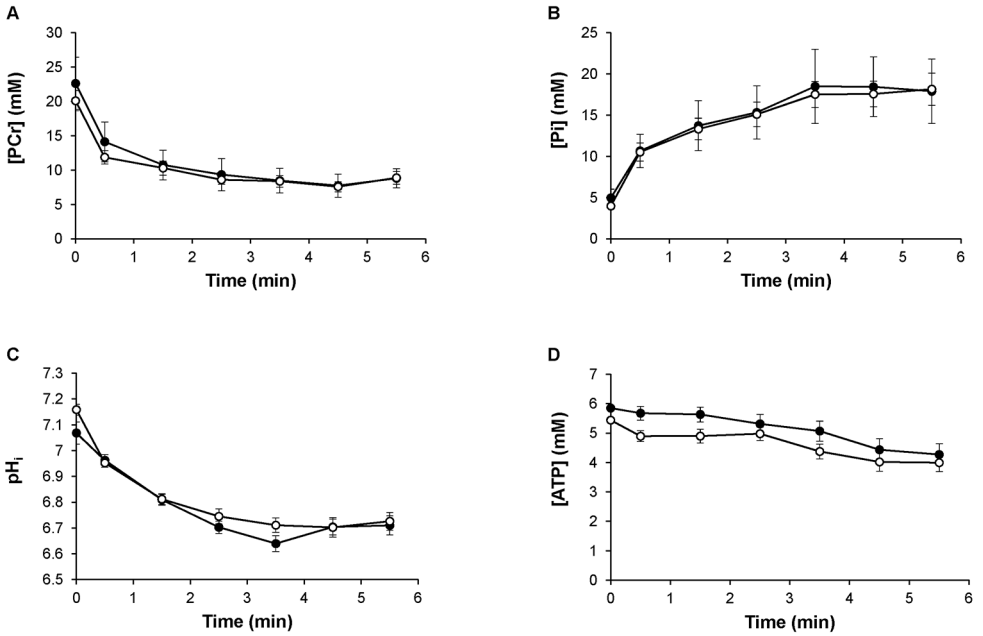

Figure 5 Changes in gastrocnemius [PCr] (A), [Pi] (B), pHi (C) and [ATP] (D)
The 6 min stimulation at 1.7 Hz disclosed no difference in metabolic variations for nebulin$^{+/-}$ group (; n = 17) as compared to nebulin$^{+/+}$ group (; n = 15). Values are presented as mean ± SEM.

DISCUSSION

We aimed at providing a comprehensive picture of the skeletal muscle phenotype of heterozygous *Neb*-KO mice through a combination of both *in vivo* and *in vitro* analyses. We demonstrated that the expression of a single functional nebulin allele resulted in a reduced force *in vitro* while this variable was not altered *in vivo*. Muscle weakness was associated with a shift toward a slower proteomic phenotype, but was not related to nebulin protein deficiency or to an impaired energy metabolism.

One of the key findings of the present study was that maximal force production was significantly reduced by ~16% in isolated muscle of nebulin$^{+/-}$ mice while *in vivo* force generating capacity was preserved. A larger decrease in maximal force, ranging from 50% to 90%, has been previously reported in muscle fibers from both *Neb*-KO mice (Bang et al., 2006; Gokhin and Bang, 2009; Ottenheijm et al., 2008) and severely affected patients (Lawlor et al., 2011; Ottenheijm et al., 2010), thereby indicating that the expression of a single functional allele led to a mild skeletal muscle phenotype as compared to either homozygous null mutation (Bang et al., 2006; Gokhin and Bang, 2009; Ottenheijm et al., 2008) or to the compound heterozygosity for two different *NEB* mutations (Lawlor et al., 2011; Ottenheijm et al., 2010). The fact that our *in vitro* and *in vivo* force measurements were performed on two different muscles with different fiber-type composition (i.e., slow soleus vs. fast gastrocnemius muscles, respectively) might be considered as a potential methodological limitation. However, it should also be pointed out that previous MRI studies have reported a selective muscle involvement of both the fast tibialis anterior and the slow soleus muscles with a relatively mild effect in the fast gastrocnemius muscles of patients with *NEB*-related NM (Jungbluth et al., 2004; Quijano-Roy et al., 2011). As a consequence, a specific muscle involvement, independent of the muscle fiber-type composition, might also occur in nebulin$^{+/-}$ mice and might explain the differences in terms of maximal force production between *in vivo* and *in vitro* conditions. Taken together, the combined *in vivo* and *in vitro* measurements of force production indicate that the expression of a single allele of the *NEB* gene led to a mild muscle weakness.

Recent studies on human biopsies from NM cases suggested that disease severity might be correlated with nebulin deficiency levels. Indeed, myofiber force production was severely decreased in a NM patient with ~10% of the

normal nebulin level due to compound heterozygous *NEB* mutations (Lawlor et al., 2011). This impaired contractile performance largely exceeded that observed in patients in whom nebulin protein levels were roughly 28% of control values as a result of a deletion of exon 55 (Ottenheijm, Witt, et al., 2009). Finally, only a mild muscle weakness was reported in a patient with 70% of the control protein level while single muscle fibers analysis showed unchanged force-sarcomere length relationship and calcium-sensitivity of force generation (Ochala et al., 2011). For our heterozygous mouse model, we observed a significant force loss, despite normal nebulin transcript and protein levels. Indeed, SDS-agarose experiments did not reveal any nebulin content alteration in nebulin$^{+/-}$ mice and array profiling indicated non-significantly reduced NEB transcript levels. The lack of a significant reduction in nebulin protein level might explain why the magnitude of force reduction observed *in vitro* in soleus muscle fibers from nebulin$^{+/-}$ mice was lower than that previously reported in both severe NM patients (Lawlor et al., 2011; Ottenheijm et al., 2010) and *Neb*-KO mice (Bang et al., 2006; Gokhin and Bang, 2009; Ottenheijm et al., 2008). It should be pointed out that in another model, despite similar total actin levels, newborn heterozygous actin KO mice also showed a slight reduction of force production as compared to wild-type littermates data (~9 mN/mm² vs. ~11.5 mN/mm², respectively) even though no statistical analysis was performed on the corresponding data (Crawford et al., 2002).

In order to determine the underlying mechanisms responsible for the mild muscle weakness in nebulin$^{+/-}$ mice, calcium sensitivity was assessed on the basis of both *in vitro* and *in vivo* measurements of force production resulting from incremental stimulation frequencies. The resulting force frequency curves were not different between the two groups. These findings suggested that calcium homeostasis was unaffected in nebulin$^{+/-}$ mice which is consistent with the absence of variation in the nebulin protein level. Indeed, it has been recently demonstrated that nebulin plays a role in calcium regulation (Ottenheijm et al., 2012). For example, calcium-sensitivity of force generation was reduced in both *Neb*-KO mice and NM patients (Chandra et al., 2009; Ottenheijm et al., 2010). Additionally, sarcolipin, an inhibitor of SERCA, was upregulated in nebulin-deficient muscle (Gokhin and Bang, 2009; Ottenheijm et al., 2008). Interestingly, our results are in line with those reported in a mildly affected patient which had only a slightly reduced protein level and an unaffected calcium-sensitivity of force generation (Ochala et

al., 2011). Furthermore, our gene expression profiling did not demonstrate any change in genes involved in calcium regulation, thereby indicating that calcium homeostasis is preserved in nebulin$^{+/-}$ mice.

Transcriptome-wide array studies clearly showed a five to eight-fold upregulation of slow Tn complexes (I, T and C) and slow isoform β-MHC, indicating a shift toward a slower proteomic phenotype in nebulin$^{+/-}$ mice. In support of this, a shift in the MHCslow/MHCfast ratio was observed in nebulin$^{+/-}$ mice as compared to nebulin$^{+/+}$ mice. These findings are in line with the predominance of type 1 fibers typically observed in NM patients (North et al., 1997; Ryan et al., 2003) and in animal models mimicking mild and severe forms of NM (Corbett, 2001; Nguyen et al., 2011; Ravenscroft, Jackaman, et al., 2011). Indeed, muscle tissues from NM patients had a slower Tn profile and contained only fibers expressing slow MHC isoforms as compared to healthy muscles (Ottenheijm et al., 2010). Despite that, the content of slow troponin T and I was also found higher in *Neb*-KO mice as compared to control mice (Chandra et al., 2009) whereas no difference was noted in terms of MHC composition between the two groups (Bang et al., 2006; Chandra et al., 2009; Gokhin and Bang, 2009). Nevertheless, the corresponding results were obtained from 1 and 7-day old nebulin deficient mice since they typically die within the first three weeks after birth. Considering that newborn mouse muscles mostly expressed embryonic and neonatal MHC isoforms (Agbulut et al., 2003), one could assume that the short life expectancy of *Neb*-KO mice might have precluded the transition in the MHC isoform observed in both the nebulin$^{+/-}$ mouse model and the adult NM patients.

Considering the large shift toward a slower proteomic phenotype in heterozygous *Neb*-KO mice, one could hypothesize that nebulin directly or indirectly regulates muscle typology. While it has been reported that nebulin expression controls the thin filament length and regulates muscle contraction (Bang et al., 2006; Chandra et al., 2009; Witt et al., 2006), there is so far no compelling evidence for a role of nebulin in the regulation of fiber-type composition. It should also be pointed out that a slower phenotype has been reported as a result of mutations in other genes implicated in NM (Bouldin et al., 2007; Clarke et al., 2008; Donner et al., 2002; Ilkovski et al., 2001; Ohlsson et al., 2004; Pénisson-Besnier et al., 2007; Ravenscroft, Wilmshurst, et al., 2011; Wattanasirichaigoon et al., 2002) and in genes encoding thick filament proteins (i.e., myosin) (Tajsharghi et al., 2010). Thus, the shift towards a

slow phenotype might be a general mechanism during the development of myopathic changes. Surprisingly, the shift toward a slower proteomic phenotype was not linked to an improved muscle fatigability in nebulin$^{+/-}$ mice. Similar findings have been reported in a mouse model mimicking a mild form of NM (de Haan et al., 2002).

Regarding the metabolic changes, our 31P-MRS results showed a similar PCr consumption, Pi accumulation and acidosis during the stimulation exercise between the two groups. We also found no significant dysregulation in genes coding for proteins involved in energy metabolism in nebulin$^{+/-}$ mice. Consistently, no major change was observed for the expression of genes encoding the proteins involved in metabolic pathways in a mouse model which displays a late onset, mild form of NM (Sanoudou et al., 2006). On the contrary, abnormal glycogen accumulation as well as a marked variation in the size, number and shape of mitochondria have been observed, in a mouse model with *ACTA1* mutation (Nguyen and Hardeman, 2008) and in patients with typical or severe forms of NM (Ryan et al., 2003; Sanoudou et al., 2003). In this latter case, several genes directly or indirectly involved in the glycolytic pathway also had significantly altered expression (Sanoudou et al., 2003). Additionally, the severe muscle weakness in *Neb*-KO mice was also associated with accumulation of glycogen and alteration at the mitochondrial level (Bang et al., 2006). Considering the mild phenotype of the nebulin$^{+/-}$ mice as compared to the *Neb*-KO mice, our results are in line with the fact that defects in energy consumption might only be related to a severe phenotype.

In the present study, we demonstrated that despite normal protein levels, *in vitro* force production was altered in nebulin$^{+/-}$ mice. Considering the large shift toward a slower phenotype in nebulin$^{+/-}$ mice, one could suggest that the decrease of *in vitro* force generation may be, at least in part, related to the fact that maximal isometric tension output is typically lower in slow-twitch as compared to fast-twitch fibers (Andruchov et al., 2004; Bottinelli et al., 1991). We also observed that nebulin mRNA levels were slightly but not significantly reduced in nebulin$^{+/-}$ mice so that one could speculate that muscle weakness was probably not related to a reduced nebulin protein turnover. Finally, the large number of dysregulated genes is a striking finding. One could suggest that the physical deletion of nebulin might affect the neighboring genes, thereby leading to this large dysregulation of gene expression. This would be

of utmost importance for genetic disorders involving disruption of the nebulin gene (Pelin and Wallgren-Pettersson, 2008).

In conclusion, we provided a comprehensive picture of skeletal muscle phenotype of heterozygous *Neb*-KO mice through a combination of both *in vivo* and *in vitro* analyses. We demonstrated that (i) nebulin$^{+/-}$ mice displayed a slight reduction in force production *in vitro* whereas this variable was not altered *in vivo*; and (ii) a shift toward a slower proteomic phenotype occurred in nebulin$^{+/-}$ mice, while both nebulin protein content and energy metabolism were not altered. Overall, these data demonstrated that the expression of a single functional allele led to a mild skeletal muscle phenotype.

REFERENCES

Agbulut O, Noirez P, Beaumont F, Butler-Browne G. Myosin heavy chain isoforms in postnatal muscle development of mice. Biol. Cell 2003; 95: 399–406.

Andruchov O, Andruchova O, Wang Y, Galler S. Kinetic properties of myosin heavy chain isoforms in mouse skeletal muscle: comparison with rat, rabbit, and human and correlation with amino acid sequence. Am. J. Physiol. Cell Physiol. 2004; 287: C1725–32.

Bang M-L, Caremani M, Brunello E, Littlefield R, Lieber RL, Chen J, et al. Nebulin plays a direct role in promoting strong actin-myosin interactions. FASEB J. 2009; 23: 4117–4125.

Bang M-L, Gregorio C, Labeit S. Molecular dissection of the interaction of desmin with the C-terminal region of nebulin. J. Struct. Biol. 2002; 137: 119–27.

Bang M-L, Li X, Littlefield R, Bremner S, Thor A, Knowlton KU, et al. Nebulin-deficient mice exhibit shorter thin filament lengths and reduced contractile function in skeletal muscle. J. Cell. Biol. 2006; 173: 905–916.

Bottinelli R, Schiaffino S, Reggiani C. Force-velocity relations and myosin heavy chain isoform compositions of skinned fibres from rat skeletal muscle. J. Physiol. 1991; 437: 655–72.

Bouldin AA, Parisi MA, Laing N, Patterson K, Gospe SM. Variable presentation of nemaline myopathy: novel mutation of alpha actin gene. Muscle Nerve 2007; 35: 254–8.

Chandra M, Mamidi R, Ford S, Hidalgo C, Witt CC, Ottenheijm CA, et al. Nebulin alters cross-bridge cycling kinetics and increases thin filament activation: a novel mechanism for increasing tension and reducing tension cost. J. Biol. Chem. 2009; 284: 30889–30896.

Clarke NF, Kolski H, Dye DE, Lim E, Smith RLL, Patel R, et al. Mutations in TPM3 are a common cause of congenital fiber type disproportion. Ann. Neurol. 2008; 63: 329–37.

Clarkson E, Costa CF, Machesky LM. Congenital myopathies: diseases of the actin cytoskeleton. J. Pathol. 2004; 204: 407–17.

Corbett MA. A mutation in alpha-tropomyosinslow affects muscle strength, maturation and hypertrophy in a mouse model for nemaline myopathy. Hum. Mol. Genet. 2001; 10: 317–328.

Crawford K, Flick R, Close L, Shelly D, Paul R, Bove K, et al. Mice Lacking Skeletal Muscle Actin Show Reduced Muscle Strength and Growth Deficits and Die during the Neonatal Period. Mol. Cell. Biol. 2002; 22: 5887–5896.

Donner K, Ollikainen M, Ridanpää M, Christen H-J, Goebel HH, de Visser M, et al. Mutations in the β-tropomyosin (TPM2) gene – a rare cause of nemaline myopathy. Neuromuscul. Disord. 2002; 12: 151–158.

Le Fur Y, Nicoli F, Guye M, Confort-Gouny S, Cozzone PJ, Kober F. Grid-free interactive and automated data processing for MR chemical shift imaging data. MAGMA 2010; 23: 23–30.

Giannesini B, Izquierdo M, Dalmasso C, Le Fur Y, Cozzone PJ, Verleye M, et al. Endotoxemia causes a paradoxical intracellular pH recovery in exercising rat skeletal muscle. Muscle Nerve 2007; 36: 505–14.

Giannesini B, Vilmen C, Le Fur Y, Dalmasso C, Cozzone PJ, Bendahan D. A strictly noninvasive MR setup dedicated to longitudinal studies of mechanical performance, bioenergetics, anatomy, and muscle recruitment in contracting mouse skeletal muscle. Magn. Reson. Med. 2010; 64: 262–70.

Gokhin D, Bang M. Reduced thin filament length in nebulin-knockout skeletal muscle alters isometric contractile properties. Am. J. Resp. Crit. Care 2009; 296: 1123–1132.

Gokhin DS, Kim NE, Lewis SA, Hoenecke HR, D'Lima DD, Fowler VM. Thin-filament length correlates with fiber type in human skeletal muscle. Am. J. Physiol. Cell Physiol. 2012; 302: C555–65.

de Haan A, van der Vliet M., Gommans IM., Hardeman E., van Engelen BG. Skeletal muscle of mice with a mutation in slow α-tropomyosin is weaker at lower lengths. Neuromuscul. Disord. 2002; 12: 952–957.

Ilkovski B, Cooper ST, Nowak K, Ryan MM, Yang N, Schnell C, et al. Nemaline myopathy caused by mutations in the muscle alpha-skeletal-actin gene. Am. J. Hum. Genet. 2001; 68: 1333–43.

Jungbluth H, Sewry CA, Counsell S, Allsop J, Chattopadhyay A, Mercuri E, et al. Magnetic resonance imaging of muscle in nemaline myopathy. Neuromuscul. Disord. 2004; 14: 779–84.

Kruger M. Nebulin as a length regulator of thin filaments of vertebrate skeletal muscles: correlation of thin filament length, nebulin size, and epitope profile. J. Cell Biol. 1991; 115: 97–107.

Labeit S, Kolmerer B. The complete primary structure of human nebulinand its correlation to muscle structure. J. Mol. Biol. 1995; 248: 308–315.

Labeit S, Ottenheijm CAC, Granzier H. Nebulin, a major player in muscle health and disease. FASEB J. 2011; 25: 822–9.

Lawlor MW, Ottenheijm CA, Lehtokari V-L, Cho K, Pelin K, Wallgren-Pettersson C, et al. Novel mutations in NEB cause abnormal nebulin expression and markedly impaired muscle force generation in severe nemaline myopathy. Skelet. Muscle. 2011; 1: 23.

Lehtokari V-L, Greenleaf RS, DeChene ET, Kellinsalmi M, Pelin K, Laing NG, et al. The exon 55 deletion in the nebulin gene--one single founder mutation with world-wide occurrence. Neuromuscul. Disord. 2009; 19: 179–81.

Lehtokari V-L, Pelin K, Sandbacka M, Ranta S, Donner K, Muntoni F, et al. Identification of 45 novel mutations in the nebulin gene associated with autosomal recessive nemaline myopathy. Hum. Mutat. 2006; 27: 946–56.

Moon RB, Richards JH. Determination of Intracellular pH by 31P Magnetic Resonance. J. Biol. Chem. 1973; 248: 7276–7278.

Nguyen M-AT, Hardeman EC. Mouse models for thin filament disease. Adv. Exp. Med. Biol. 2008; 642: 66–77.

Nguyen M-AT, Joya JE, Kee AJ, Domazetovska A, Yang N, Hook JW, et al. Hypertrophy and dietary tyrosine ameliorate the phenotypes of a mouse model of severe nemaline myopathy. Brain 2011; 134: 3516–29.

North KN, Laing NG, Wallgren-Pettersson C. Nemaline myopathy: current concepts. The ENMC International Consortium and Nemaline Myopathy. J. Med. Genet. 1997; 34: 705–13.

Ochala J, Lehtokari V-L, Iwamoto H, Li M, Feng H-Z, Jin J-P, et al. Disrupted myosin cross-bridge cycling kinetics triggers muscle weakness in nebulin-related myopathy. FASEB J. 2011; 25: 1903–1913.

Ohlsson M, Tajsharghi H, Darin N, Kyllerman M, Oldfors A. Follow-up of nemaline myopathy in two patients with novel mutations in the skeletal muscle alpha-actin gene (ACTA1). Neuromuscul. Disord. 2004; 14: 471–5.

Ottenheijm CAC, Fong C, Vangheluwe P, Wuytack F, Babu GJ, Periasamy M, et al. Sarcoplasmic reticulum calcium uptake and speed of relaxation are depressed in nebulin-free skeletal muscle. FASEB J. 2008; 22: 2912–9.

Ottenheijm CAC, Granzier H, Labeit S. The sarcomeric protein nebulin: another multifunctional giant in charge of muscle strength optimization. Front. Physiol. 2012; 3: 37.

Ottenheijm CAC, Hidalgo C, Rost K, Gotthardt M, Granzier H. Altered contractility of skeletal muscle in mice deficient in titin's M-band region. J. Mol. Biol. 2009; 393: 10–26.

Ottenheijm CAC, Hooijman P, DeChene ET, Stienen GJ, Beggs AH, Granzier H. Altered myofilament function depresses force generation in patients with nebulin-based nemaline myopathy (NEM2). J. Struct. Biol. 2010; 170: 334–343.

Ottenheijm CAC, Witt CC, Stienen GJ, Labeit S, Beggs AH, Granzier H. Thin filament length dysregulation contributes to muscle weakness in nemaline myopathy patients with nebulin deficiency. Hum. Mol. Genet. 2009; 18: 2359–2369.

Pappas CT, Krieg PA, Gregorio CC. Nebulin regulates actin filament lengths by a stabilization mechanism. J. Cell. Biol. 2010; 189: 859–870.

Pelin K, Wallgren-Pettersson C. Nebulin--a giant chameleon. Adv. Exp. Med. Biol. 2008; 642: 28–39.

Pénisson-Besnier I, Monnier N, Toutain A, Dubas F, Laing N. A second pedigree with autosomal dominant nemaline myopathy caused by TPM3 mutation: a clinical and pathological study. Neuromuscul. Disord. 2007; 17: 330–7.

Quijano-Roy S, Carlier RY, Fischer D. Muscle imaging in congenital myopathies. Semin. Pediatr. Neurol. 2011; 18: 221–9.

Ravenscroft G, Jackaman C, Sewry CA, McNamara E, Squire SE, Potter AC, et al. Actin nemaline myopathy mouse reproduces disease, suggests other actin disease phenotypes and provides cautionary note on muscle transgene expression. PLoS One 2011; 6: e28699.

Ravenscroft G, Wilmshurst JM, Pillay K, Sivadorai P, Wallefeld W, Nowak KJ, et al. A novel ACTA1 mutation resulting in a severe congenital myopathy with nemaline bodies, intranuclear rods and type I fibre predominance. Neuromuscul. Disord. 2011; 21: 31–6.

Ryan MM, Ilkovski B, Strickland CD, Schnell C, Sanoudou D, Midgett C, et al. Clinical course correlates poorly with muscle pathology in nemaline myopathy. Neurology 2003; 60: 665–673.

Sambuughin N, Yau KS, Olivé M, Duff RM, Bayarsaikhan M, Lu S, et al. Dominant mutations in KBTBD13, a member of the BTB/Kelch family, cause nemaline myopathy with cores. Am. J. Hum. Genet. 2010; 87: 842–847.

Sanoudou D, Beggs AH. Clinical and genetic heterogeneity in nemaline myopathy-a disease of skeletal muscle thin filaments. Trends Mol. Med. 2001; 7: 362–368.

Sanoudou D, Corbett MA, Han M, Ghoddusi M, Nguyen M-AT, Vlahovich N, et al. Skeletal muscle repair in a mouse model of nemaline myopathy. Hum. Mol. Genet. 2006; 15: 2603–12.

Sanoudou D, Haslett JN, Kho AT, Guo S, Gazda HT, Greenberg SA, et al. Expression profiling reveals altered satellite cell numbers and glycolytic enzyme transcription in nemaline myopathy muscle. Proc. Natl. Acad. Sci. U. S. A. 2003; 100: 4666–71.

Schnell C, Kan A, North KN. 'An artefact gone awry': Identification of the first case of nemaline myopathy by Dr R.D.K. Reye. Neuromuscul. Disord. 2000; 10: 307–312.

Tajsharghi H, Hilton-Jones D, Raheem O, Saukkonen AM, Oldfors A, Udd B. Human disease caused by loss of fast IIa myosin heavy chain due to recessive MYH2 mutations. Brain 2010; 133: 1451–9.

Wallgren-Pettersson C, Donner K, Sewry C, Bijlsma E, Lammens M, Bushby K, et al. Mutations in the nebulin gene can cause severe congenital nemaline myopathy. Neuromuscul. Disord. 2002; 12: 674–679.

Wallgren-Pettersson C, Sewry CA, Nowak KJ, Laing NG. Nemaline myopathies. Semin. Pediatr. Neurol. 2011; 18: 230–8.

Wang CH, Dowling JJ, North K, Schroth MK, Sejersen T, Shapiro F, et al. Consensus statement on standard of care for congenital myopathies. J. Child Neurol. 2012; 27: 363–82.

Wang K. Architecture of the sarcomere matrix of skeletal muscle: immunoelectron microscopic evidence that suggests a set of parallel inextensible nebulin filaments anchored at the Z line. J. Cell Biol. 1988; 107: 2199–2212.

Wattanasirichaigoon D, Swoboda KJ, Takada F, Tong H-Q, Lip V, Iannaccone ST, et al. Mutations of the slow muscle -tropomyosin gene, TPM3, are a rare cause of nemaline myopathy. Neurology 2002; 59: 613–617.

Witt CC, Burkart C, Labeit D, McNabb M, Wu Y, Granzier H, et al. Nebulin regulates thin filament length, contractility, and Z-disk structure in vivo. EMBO J. 2006; 25: 3843–3855.

Witt SH, Granzier H, Witt CC, Labeit S. MURF-1 and MURF-2 target a specific subset of myofibrillar proteins redundantly: towards understanding MURF-dependent muscle ubiquitination. J. Mol. Biol. 2005; 350: 713–22.

CHAPTER 5

NEW KELCH ON THE NM BLOCK: ELUCIDATING THE PATHOPHYSIOLOGY OF NEM6

J. M. de Winter, M. van Willigenburg, B. Joureau, J. Strom, R. van der Pijl, S. Lassche, M.L. Lawlor, G.J.M. Stienen, H. Granzier, B.G. van Engelen, N.C. Voermans, C.A.C. Ottenheijm

In preparation

ABSTRACT

Background | Nemaline myopathy (NM) is among the most common non-dystrophic congenital neuromuscular disorders. Hallmark features of NM are muscle weakness and the presence of nemaline bodies in the muscle fibers. Strikingly, all genes that are implicated in NM are associated with the skeletal muscle thin filament, a major constituent of the sarcomere. Recently, a novel gene was discovered to be implicated in NM - *KBTBD13* – which protein product is expressed in both skeletal and cardiac muscle tissue. Mutations in *KBTBD13* result in a new form of NM, NEM6, which is characterized by a typical form of muscle slowness.

Methods | To elucidate the pathophysiology of NEM6, we investigated the contractile performance of muscle fibers isolated from biopsies of NEM6 patients and studied a newly-developed mouse model that lacks *Kbtbd13*.

Results | Permeabilized muscle fiber mechanics revealed a fiber-type dependent force loss in fibers from NEM6 patients, slower cross-bridge cycling kinetics, lower active stiffness and an increase in the calcium-sensitivity of force generation. The passive properties of NEM6 muscle fibers and the length-dependence of force were unaltered. Intact soleus muscle of *Kbtbd13*-KO revealed lower muscle mass and mildly progressive muscle weakness. Echocardiography revealed a lower contractile reserve in *Kbtbd13*-KO mice upon stress.

Interpretation | The contractile data of NEM6 muscle fibers indicate that alterations at the level of the sarcomere contribute to muscle weakness and slowness in NEM6 patients. Muscle characteristics of the *Kbtbd13*-KO mouse model partly phenocopy the muscle weakness of NEM6 patients. Hence, the mouse model allows to further unravel the role of KBTBD13 in health and disease and to test therapeutic strategies for NEM6.

INTRODUCTION

Nemaline myopathy (NM) is among the most common non-dystrophic neuromuscular disorders (Colombo et al., 2015). Hallmark features are muscle weakness and the presence of nemaline bodies in muscle fibers. In 2002, a new form of NM was described, NEM6, characterized by a typical muscle slowness and stiffness. In vivo force measurements revealed that NEM6 patients have a lower maximal torque generation, a hypercontractile phenotype at submaximal stimulation frequencies and slower muscle activation and relaxation rates (Pauw-Gommans et al., 2006). The muscle slowness is manifested by the inability to run and jump and by having difficulties taking the stairs (Gommans et al., 2002). Genetic screening revealed that none of the implicated NM genes at that time – *TPM3, ACTA1, NEB* and *TPM2* - harbored pathological mutations. In 2003, the specific locus was identified – 15q21-23 (Gommans et al., 2003) -, however it was not until 2010 that the associated gene was identified: kelch repeat and BTB (POZ) Domain Containing 13 (*KBTBD13*) – (Olivé et al., 2010; Sambuughin et al., 2010). *KBTBD13* is expressed in both skeletal and cardiac muscle tissue. The function of the protein product of *KBTBD13* remains unknown.

Genes that are implicated in NM encode proteins that are either components of the skeletal muscle thin filament, including nebulin (*NEB*), skeletal muscle alpha-actin1 (*ACTA1*), beta-tropomyosin 2 (*TPM2*), alpha-tropomyosin 3 (*TPM3*), troponin T type 1 (*TNNT1*), cofilin-2 (*CFL2*), and leiomodin-3 (*LMOD3*), or are thought to contribute to the stability or turnover of thin filament proteins, such as kelch-like family members 40 (*KLHL40*) and -41 (*KLHL41*) (Gupta et al., 2013; Ravenscroft et al., 2013; Sambuughin et al., 2010; Sanoudou and Beggs, 2001; Yuen et al., 2014). Therefore, NM is considered a thin filament disease. The thin filament is a major constituent of the sarcomere, the smallest contractile unit in muscle, hence essential for the generation of muscle force (Gordon et al., 2000). To elucidate the contribution of sarcomere function to muscle weakness and muscle slowness in NEM6, here we studied the contractile properties of individual, permeabilized muscle fibers of NEM6 patients. In addition, we generated a *Kbtbd13*-deficient mouse model to study the role of its protein product in the structure and function of intact skeletal and cardiac muscle.

The present study reveals that alterations at the level of the sarcomere contribute to muscle weakness and slowness in NEM6 patients. The *Kbtbd13*-

KO mouse model partly recapitulates the typical NEM6 phenotype, making this a suitable model to further unravel the role of KBTBD13 in muscle and to test therapeutic strategies for NEM6 patients.

METHODS

Skeletal muscle biopsies of NEB-NM patients

Quadriceps muscle specimens, remaining from diagnostic procedures or obtained during clinically indicated surgical procedures, were collected from twelve NEM6 patients with confirmed *KBTBD13* mutations, and from six adult control subjects with no medical history. All biopsies were collected following informed consent supervised by the Radboud University Institutional Review Board. Details on the clinical and genetic data of the subjects are shown in Table 1. All biopsies were stored frozen and unfixed at -80°C until use.

Permeabilized muscle fiber mechanics

Small strips were dissected from the muscle biopsies and permeabilized overnight as described previously (Donkervoort et al., 2015; Ottenheijm et al., 2009; de Winter et al., 2015). This procedure renders the membranous structures in the muscle fibers permeable, which enables activation of the myofilaments with exogenous calcium. Preparations were washed thoroughly with relaxing solution and stored in 50% glycerol/relaxing solution at ?20°C. Single muscle fibers were dissected from the permeabilized strips, and were mounted using aluminum T-clips between a length motor (ASI 403A, Aurora Scientific Inc., Ontario, Canada) and a force transducer element (ASI 315C-I, Aurora Scientific Inc., Ontario, Canada) in a single fiber apparatus (ASI 802D, Aurora Scientific Inc., Ontario, Canada) that was mounted on the stage of an inverted microscope (Zeiss Axio Observer A1). Sarcomere length was set using a high speed VSL camera and ASI 900B software (Aurora Scientific Inc., Ontario, Canada). Mechanical experiments were performed at a sarcomere length of 2.5 µm, to ensure that the sarcomeres operate at an optimal length (middle of the plateau phase). Fiber width and diameter were measured at three points along the fiber and the cross-sectional area was determined assuming an elliptical cross-section. Various bathing solutions were used during the experimental protocols: a relaxing solution (100 mM BES; 6.97 mM EGTA; 6.48 mM $MgCl_2$; 5.89 mM Na_2-ATP; 40.76 mM K-propionate; 14.5 mM creatine phosphate), a pre-activating solution with low EGTA concentration (100 mM BES; 0.1 mM EGTA; 6.42 mM $MgCl_2$; 5.87 mM Na_2-ATP; 41.14 mM K-propionate; 14.5 mM creatine phosphate;

6.9 mM HDTA), and an activating solution (100 mM BES; 7.0 mM Ca-EGTA; 6.28 mM $MgCl_2$; 5.97 mM Na2-ATP; 40.64 mM K-propionate; 14.5 mM creatine phosphate). The temperature of the bathing solutions was kept constant at 20°C using a TEC controller (ASI 825A, Aurora Scientific Inc. Ontario, Canada). To investigate the sarcomere-length dependency of force, maximal active tension was measured at incremental sarcomere lengths (2.0 – 3.5 µm).

Table 1 Characteristics of NEM 6 patients and control subjects

Biopsy	ID# Radboud UMC	Mutation	Sex	Age	References
NEM6-1	T09_13176	Arg408Cys*	F	42	De Winter *et al.*, 2016 *ID: KBTBD13-3*
NEM6-2	T12_26869	Arg408Cys	F	44	Sambuughin *et al.*, 2010; De Winter *et al.*, 2016 *ID: KBTBD13-1*
NEM6-3	T04_00344	Arg408Cys	F	16	De Winter *et al.*, 2016 *ID: KBTBD13-5*
NEM6-4	T04_00343	Arg408Cys	F	46	Sambuughin *et al.*, 2010; De Winter *et al.*, 2016 *ID: KBTBD13-8*
NEM6-5	SN_01162	Arg408Cys	M	62	Sambuughin *et al.*, 2010; De Winter *et al.*, 2016 *ID: KBTBD13-9*
NEM6-6	SN_00160	Arg408Cys	F	34	Sambuughin *et al.*, 2010; De Winter *et al.*, 2016 *ID: KBTBD13-10*
NEM6-7	T11_07212	Arg408Cys	F	29	
NEM6-8	O2_T2204	Arg408Cys	M	68	
NEM6-9	O2_T1664	Arg408Cys	F	46	Gommans *et al.*, 2003; De Winter *et al.*, 2016 *ID: KBTBD13-6*
NEM6-10	SN_99035	Arg408Cys	F		Sambuughin *et al.*, 2010; De Winter *et al.*, 2016 *ID: KBTBD13-2*
NEM6-11	T10_12160	Lys390Asn	F	41	Sambuughin *et al.*, 2010; De Winter *et al.*, 2016 *ID: KBTBD13-4*
NEM6-12	T12_14968	Ile369Met	M	55	De Winter *et al.*, 2016 *ID: KBTBD13-7*
CTRL-1	70682	N/A	F	65	
CTRL-2	70653	N/A	M	50	
CTRL-3	70620	N/A	M	44	
CTRL-4	70641	N/A	M	50	
CTRL-5	70204	N/A	F	52	
CTRL-6	70205	N/A	F	51	

*Note that Arg408Cys is the Dutch founder mutation for NEM6.

Cross-bridge cycling kinetics

To investigate mechanisms underlying maximal force generation, we determined the cross-bridge cycling kinetics by measuring the rate of tension redevelopment and active stiffness. The rate of tension redevelopment indicates the number of strongly bound cross-bridges and the active stiffness is an estimate of the number of available cross-bridges. To measure the rate of tension redevelopment, muscle fibers were maximally activated and when the force trace reached a plateau, the muscle fibres were slacked to 70% of their original length followed by a rapid restretch to the original length after 30 milliseconds. This procedure allows the force to redevelop from zero (Brenner and Eisenberg, 1986). The rate of tension redevelopment was calculated by fitting a bi-exponential through the force redevelopment curve. The first-order rate constant k_1 reflects the cross-bridge cycling kinetics most accurate and was therefore used in the analyses (Caremani et al., 2008). Active stiffness was obtained by applying small length perturbations on the fibers, while the fibers were maximally activated, and fit to a linear curve through the data points. By dividing the maximal active tension by active stiffness, the force generation per cross-bridge is estimated (Manders et al., 2014).

Calcium-sensitivity of force generation

To investigate submaximal force generating capacities at the sarcomere level, force-pCa relations were established. To determine the force-pCa relation (pCa = -log of molar free Ca^{2+} concentration), permeabilized muscle fibers were sequentially bathed in solutions with pCa values ranging from 4.5 to 9.0 and the steady-state force was measured. Force values were normalized to the maximal force obtained at pCa 4.5. The obtained force-pCa data were fit to the Hill equation, providing the pCa_{50} and the Hill coefficient, nH, an index of myofilament cooperativity.

Passive stiffness

To investigate the origin of the muscle stiffness that NEM6 patients experience, we determined the passive tension-sarcomere length relation. The muscle fiber was stretched in relaxation solution from its slack sarcomere length to a sarcomere length of 3.2 µm. The stretching velocity was kept constant for all muscle fibers. A hold phase of 90 seconds followed after the sarcomere length of 3.2 µm was reached. Here, the sarcomere length of 3.2 µm was maintained, while the passive tension was allowed to stabilize (irrespective

of the velocity-dependent viscous component) (Manders et al., 2015).

Myosin heavy chain isoform composition

As the contractile properties of muscle fibers are influenced by the myosin heavy chain composition of the muscle fibers, we determined this composition of the muscle fibers that we used in our contractility experiments. A specialized SDS-PAGE was used to determine the myosin heavy chain isoform composition (Ottenheijm et al., 2009). In brief, muscles fibers were denatured by boiling for 2 minutes in SDS sample buffer. The stacking gel contained a 4% acrylamide concentration (pH 6.7), and the separating gel contained 7% acrylamide (pH 8.7) with 30% glycerol (v/v). The gels were run for 24h at 15°C and a constant voltage of 275 volt. Finally, the gels were silver-stained, scanned, and analyzed with One-D scan EX (Scanalytics Inc., Rockville, MD, USA) software.

Generation of a Kbtbd13-KO mouse model

This strain was generated at the Genetically Engineered Mouse Models (GEMM) core facility at the University of Arizona and completely deletes the entire *Kbtbd13* (Kelch Repeat and BTB Domain #13) gene. Deletion of the *Kbtbd13* gene was achieved by homologous recombination replacing the *Kbtbd13* locus with a floxed neoR cassette in 129S6 ES cells. Genotyping was performed using tail digests using GoTaq® Green Master Mix (Promega). The following primer sets were used: (P1) Kbtbd13-Wt forward 5'- GAAGACTTCAGGAGGCAAGG -3'; (P2) Kbtbd13-KO forward 5'- CACGCGTCACCTTAATATGC -3'; (P3) reverse 5'- CCCACGCTCAGAGGTAGC -3'. Mice used were in a mixed 129/SvEvTAC and C57BL/6J background. All experiments were approved by IACUC and followed the NIH Guidelines 'Using Animals in Intramural Research' for animal use.

Electron microscopy

For electron microscopy, samples were fixed and processed per standard histological techniques for either routine histochemical staining or ultrastructural examination at the time of biopsy, and all slides and ultrastructural images were reviewed by a neuropathologist (MWL).

Intact muscle mechanics

The characterization of intact muscle function was performed as described previously (Gineste et al., 2013). In brief, left soleus (SOL) muscles were

quickly dissected and, using silk suture, mounted vertically in a tissue bath between a dual-mode lever arm and a fixed hook (1200A Intact Muscle Test System, Aurora Scientific Inc., Canada). SOL muscles were chosen because of their well-defined tendons and their small size, which facilitates oxygenation. The muscle was bathed in continuously oxygenated (95% O_2 –5% CO_2) mammalian Ringer solution with pH 7.40. The temperature of the solution was maintained at 30°C during the experiment. The muscle was stimulated directly with platinum plate electrodes placed in close apposition to the muscle. Muscle length was adjusted until maximal twitch force was achieved (pulse duration of 200 μs). A twitch and tetanus (150 Hz) were generated in order to determine twitch and maximal force prior to the experimental protocols. The experimental protocols consisted of a full tetanus at 150 Hz, a force-frequency protocol and a fatigue protocol.

For the force-frequency protocol, the muscle was stimulated with incremental stimulation frequencies (1, 10, 20, 30, 50, 70, 100, 150 Hz). Data were discarded when stimulation at 150 Hz rendered a force that was less than 95% of the force generated during the first stimulation at 150 Hz. Stimuli were applied with a train duration of 600 ms. The resting interval was 30 sec between the stimulations at 1 and 10 Hz; 60 sec after stimulation at 20 Hz; 90 sec after stimulation at 30 Hz; and 120 sec between stimulations at 50, 70, 100 and 150 Hz.

The fatigue protocol was performed five minutes after completion of the force-frequency protocol. For a period of 4 min, a one-second 40 Hz pulse train was applied to the muscle, with resting intervals of two seconds.

After completion of the contractility measurements, length and weight of the SOL muscles were determined. Cross-sectional area (CSA; in mm^2) was calculated by dividing muscle weight (g) by muscle length (mm) multiplied by specific density (1.056 g/ml) × 100.

Echocardiography

Echocardiography was performed using a Vevo 2100 High Resolution Imaging System (Visual-Sonics, Toronto, Canada) with an MS550D scan head designed for murine cardiac imaging. Following anesthetic induction in 3% isoflurane, mice were placed in a supine position on a heated platform for echocardiography. Body temperature was maintained at 37°C and anesthesia was maintained with 1.5% isoflurane (USP, Phoenix) in 100%

oxygen. Imaging was performed at a depth setting of 1 cm. Images were collected and stored as digital cine loops for off-line calculations. Standard imaging planes, M-mode, Doppler, and functional calculations were obtained according to American Society of Echocardiography guidelines. A short axis M-mode cine loop was recorded at the level of the papillary muscles to asses chamber dimensions (LV systolic and diastolic dimensions (LVIDs, LVIDd)) posterior wall thickness (PWT), and cardiac function via fractional shortening (%FS). Doppler imaging was obtained from an apical 4-chamber view to assess LV filling and tissue velocity of the septal mitral valve annulus. Suitable cine loops were selected based on adequate visualization of the epi- and endocardial borders. Semi-automated tracing of the endocardial and epicardial borders were averaged over 3 consecutive cardiac cycles.

The echo stress test assessed systolic performance following administration of the β1-specific adrenergic agonist dobutamine. Briefly, baseline echocardiographic parameters were assessed as outlined above, followed by administration of dobutamine (2.5μg/kg, IP). Cardiac parameters (HR, %FS, and LVID) stabilized by 5 minutes post-administration, at which point the echo exam was repeated.

RESULTS

To investigate whether alterations at the sarcomere level contribute to muscle weakness in NEM6, muscle fibers were isolated from quadriceps biopsies of healthy controls (CTRL) (n=6) and NEM6 patients (n=12) (for patient characteristics, see Table 1). Next, muscle fibers were permeabilized and activated with exogenous calcium solutions. First, force was measured at incremental calcium concentrations to investigate the calcium-sensitivity of force generation, followed by a slack-release manoeuvre and an active stiffness protocol to study the cross-bridge cycling kinetics. After collecting these parameters that describe active components of muscle fiber contractility, the passive properties of the muscle fiber were studied in a calcium-free solution. As the force-generating capacity of muscle fibers depends on the myosin heavy chain isoform composition, for each muscle fiber this composition was determined using specialized SDS-PAGE gels. Per biopsy 3 – 15 muscle fibers were measured for each fiber type.

Alterations in NEM6 muscle fiber size

Light microscopy images reveal that the ultrastructure of NEM6 muscle fibers is largely preserved (typical examples in Figure 1). However, the diameter of slow- and fast-twitch NEM6 muscle fibers is different from that of CTRL fibers. Whereas CTRL slow- and fast-twitch muscle fibers are of similar size (4733±413 μm^2 for slow-twitch fibers vs. 4369±500 μm^2 for fast-twitch fibers) (Fig A-C), in NEM6 the diameter of slow-twitch fibers is significantly larger than that of fast-twitch fibers (5911±663 μm^2 for slow-twitch fibers vs. 3772±472 μm^2 for fast-twitch fibers) (Fig 1D-F). Note that there is no significant interaction effect (P-interaction = 0.15), hence the diameter in NEM6 fibers does not deviate from CTRL values. Thus, NEM6 fibers have a preserved ultrastructure, but display fiber-type specific changes in muscle fiber size.

Lower maximal active tension in permeabilized muscle fibers of NEM6 patients

At a saturating calcium concentration (pCa 4.5), no force deficit is observed in slow-twitch NEM6 muscle fibers compared to CTRL (0.49±0.07 mN for CTRL vs. 0.39±0.05 mN for NEM6). However, fast-twitch NEM6 muscle fibers generate lower absolute forces than fast-twitch muscle fibers of CTRL (0.59±0.1 mN for CTRL vs. 0.25±0.06 mN for NEM6) (Fig 2A, F). As, typically, force scales with the diameter of the muscle fiber, absolute forces were normalized to the fiber's cross-sectional area to determine the maximal active tension. These data provide insight into the contractile performance of the sarcomeres. The active tension of both slow- and fast-twitch fibers of NEM6 patients was lower compared to those of CTRL (slow-twitch fibers: 64±8 mN/mm^2 for NEM6 vs. 101±8 mN/mm^2 for CTRL; fast-twitch fibers: 64±10 mN/mm^2 for NEM6 vs. 131±8 mN/mm^2 for CTRL) (Fig 2B, G). Thus, both slow- and fast-twitch NEM6 muscle fibers display contractile weakness at the sarcomere level.

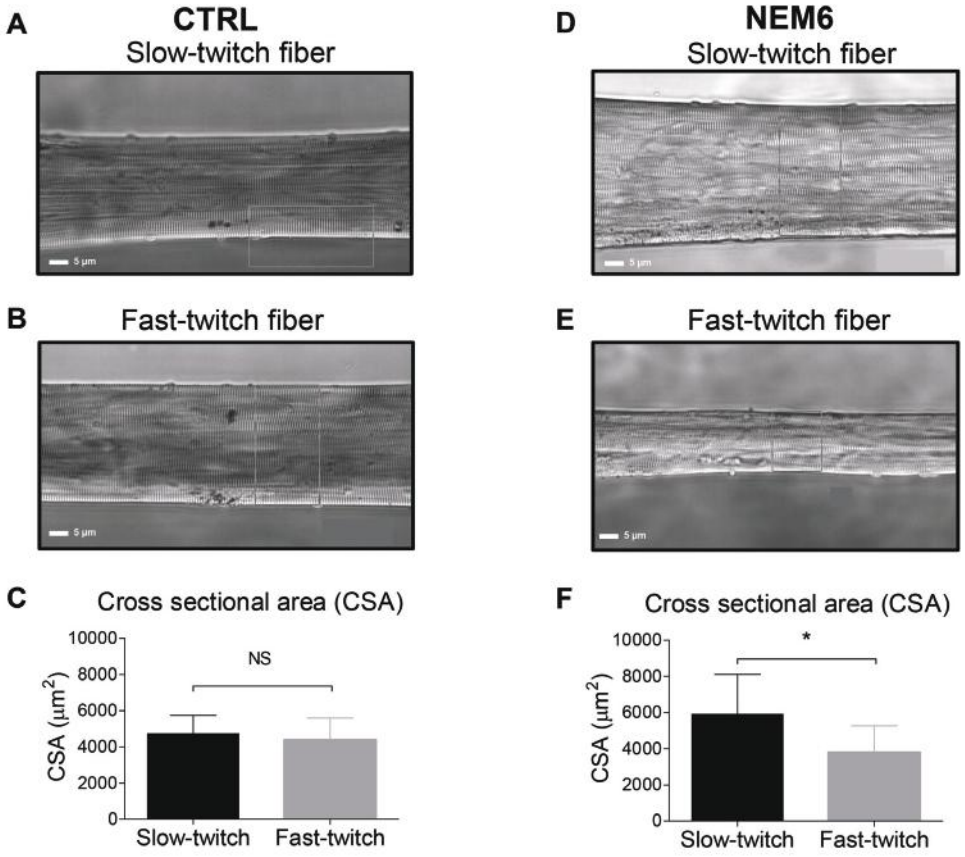

Figure 1 Cross-sectional area of CTRL and NEM6 muscle fibers
Typical examples of slow-twitch and fast-twitch muscle fibers of CTRL (A-B) and NEM6 patients (D-E) by light microscopy. No change in fiber size diameter was found between slow- and fast twitch muscle fibers of CTRL (C), whereas in muscle fibers of NEM6 patients the diameter of slow-twitch fibers was significantly larger than that of fast-twitch fibers.

Lower number of bound cross-bridges in NEM6 muscle fibers

To elucidate the mechanisms underlying the contractile weakness in NEM6 muscle fibers, we studied the cross-bridge cycling kinetics - an important parameter of force generation — by measuring the rate of tension redevelopment and the active stiffness. Lower active stiffness was found in both slow- and fast-twitch NEM6 fibers compared to CTRL (slow-twitch fibers: 33 ± 4 mN/mm^2 for NEM6 vs. 58±3 mN/mm^2 for CTRL; fast-twitch fibers: 31±5 mN/mm^2 for NEM6 vs. 58±2 mN/mm^2 for CTRL), suggesting that the number of bound cross-bridges is reduced in muscle fibers of NEM6

patients (Fig 3C). Both slow- and fast twitch NEM6 fibers revealed a lower rate of tension redevelopment compared to CTRL fibers (slow-twitch fibers: 4.5±0.3 s^{-1} for NEM6 vs. 5.3±0.2 s^{-1} for CTRL; fast-twitch fibers: 6.9±0.7 s^{-1} for NEM6 vs. 11.6±0.9 s^{-1} for CTRL), suggesting that the reduced number of bound cross-bridges is a result of a reduced fraction of attached cross-bridges (Fig 3B). (Note that caution is warranted: to conclusively establish that this fraction is reduced, stiffness measurements during rigor conditions or measurements of the rate of cross-bridge detachment are necessary). Normalizing the active tension over the active stiffness reflects the force generated per cross-bridge. This ratio is not altered in muscle fibers of NEM6 compared to muscle fibers of controls (Fig 3D). Note that in a subset of biopsies the myosin heavy chain concentration was measured and the

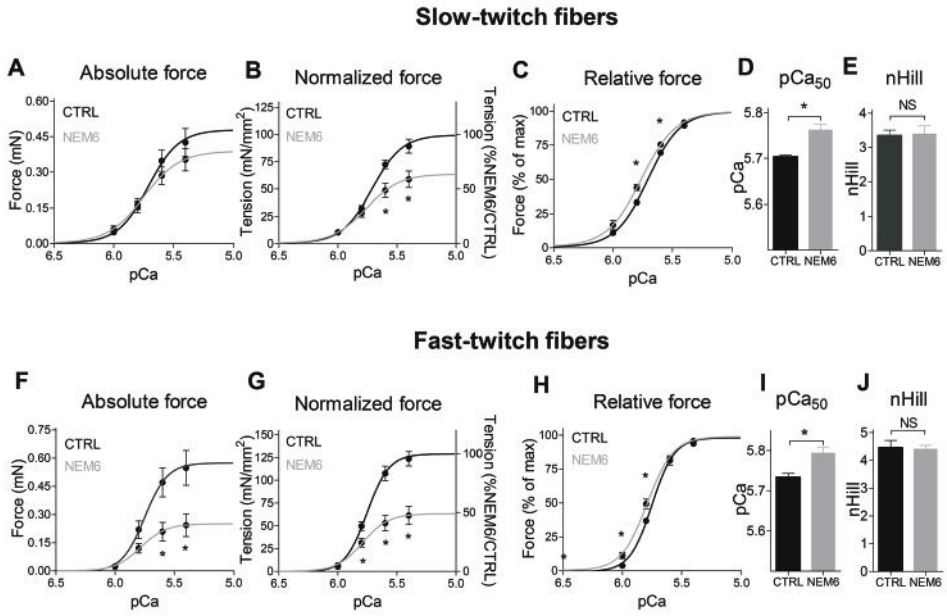

Figure 2 The calcium-sensitivity of force generation in CTRL and NEM6 muscle fibers
(A) No changes in absolute force generation were found in slow-twitch fibers of NEM6 patients (in grey) compared to those of CTRL (in black). (B) However, from pCa 5.5 – 4.5, tension generation was lower in muscle fibers from slow-twitch fibers of NEM6 patients compared to those of CTRL. (C) Relative tension was higher at submaximal calcium levels in slow-twitch fibers of NEM6 patients compared to those of CTRL, accompanied by (D) an increase in the pCa_{50} value and (E) the absence of changes in nHill, an index for myofilament cooperativity. (F) Fast-twitch fibers of NEM6 patients revealed lower absolute force and (G) active tension compared to those of CTRL. (H) At submaximal calcium levels, relative tension was higher in fast twitch fibers of NEM6 patients compared to those of CTRL, accompanied by (I) an increase in the pCa50 value in (J) the absence of changes in nHill.

myosin content per half sarcomere was calculated (n= 4 for both CTRL and NEM6). No significant changes were found for both the myosin concentration and the myosin content per half sarcomere between CTRL and NEM6 muscle. Thus, a lower number of bound cross-bridges is associated with the impaired force generation in both slow- and fast-twitch muscle fibers of NEM6 patients.

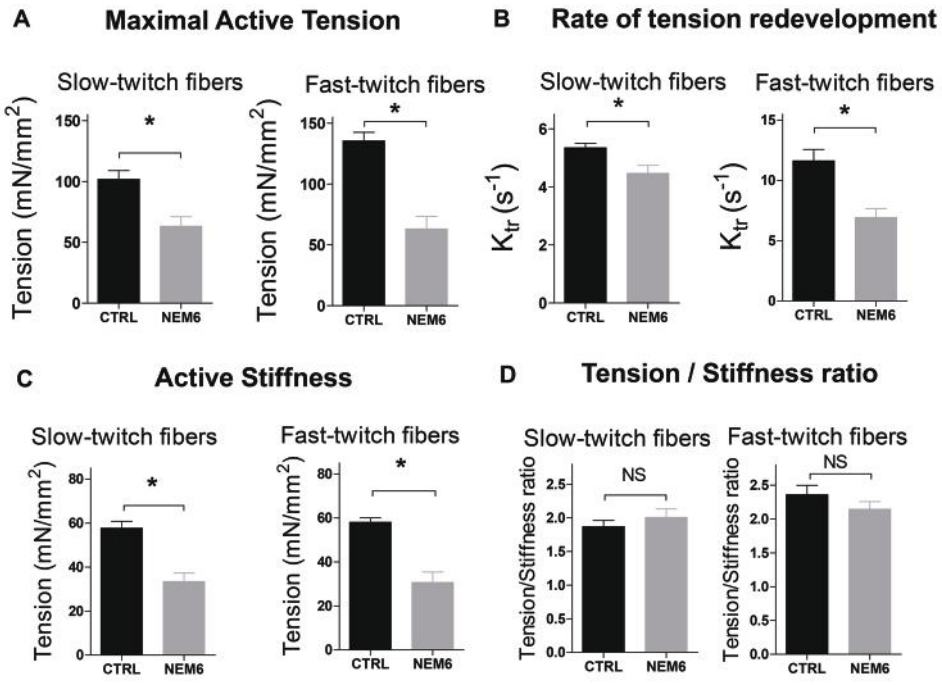

Figure 3 Cross-bridge cycling kinetics in CTRL and NEM6 muscle fibers
(A) Maximal active tension, (B) cross-bridge cycling kinetics and (C) active stiffness were lower in both slow-twitch and fast-twitch muscle fibers of NEM6 patients compared to those of CTRL. (D) No changes in the tension/stiffness ratio were found in both slow- and fast-twitch fibers of NEM6 compared to those of CTRL.

Preserved thin and thick filament length in muscle fibers of NEM6 patients

The length of the thin filament is an important determinant of the amount of force that a muscle can generate, as the overlap between the thin filament and the thick filament determines the number of cross-bridges that can be formed. We measured the force-sarcomere length relation in permeabilized muscle fibers, a functional assay that provides insight in thin (and thick) filament length. Maximal active tension was lower in NEM6 muscle fibers

at all sarcomere lengths (Fig 4A), however the relative force deficit was independent of sarcomere length (Fig 4B). This suggests that thin (and thick) filament length is not affected in NEM6 muscle fibers.

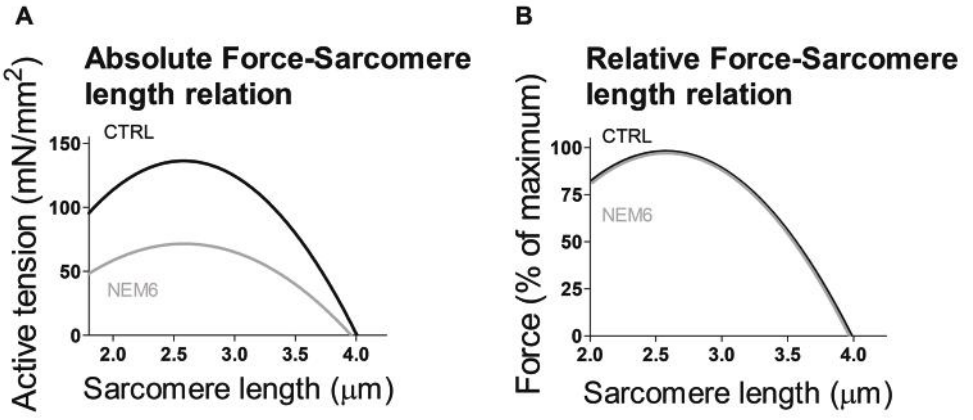

Figure 4 Force-sarcomere length relation in CTRL and NEM6 muscle fibers
(A-B) Both the absolute and the relative force-sarcomere length relation did not indicate changes in thin and/or thick filament length in NEM6 muscle fibers compared to those of CTRL.

Hypercontractile phenotype at submaximal activation levels in muscle fibers of NEM6 patients

To investigate the force generating capacity at submaximal activation levels, tension-[Ca^{2+}] relations of permeabilized muscle fibers were constructed. At submaximal calcium levels, relative tension was higher in NEM6 muscle fibers compared to CTRL, reflected by a higher pCa50 in both slow-twitch and fast-twitch fibers (pCa_{50}, slow-twitch fibers: 5.87±0.05 for NEM6 vs. 5.73±0.01 for CTRL; fast-twitch fibers: 5.90±0.07 for NEM6 vs. 5.76±0.01 for CTRL) (Fig 2C-E, H-J). Note that nHill - a measure of cooperativity – was not altered in both slow-twitch and fast-twitch muscle fibers of NEM6 (slow-twitch fibers: 3.0±0.3 for NEM6 vs. 3.0±0.1 for CTRL; fast-twitch fibers: 3.8±0.2 for NEM6 vs. 4.1±0.3 for CTRL). Thus, muscle fibers of NEM6 patients exhibit a hypercontractile phenotype at submaximal calcium levels.

No changes in the passive properties of NEM6 muscle fibers

To investigate whether changes in the passive properties of NEM6 muscle fibers contribute to the muscle stiffness that patients experience, a protocol was executed that gives insight in both the elastic and visco-elastic properties of muscle fibers. First, the muscle fiber is stretched from its slack length to a sarcomere length of 3.2 μm, with the force reflecting both the viscous and

elastic properties of the muscle fiber. Next, the muscle fiber is held at the sarcomere length of 3.2 µm for 90 seconds. The force at the end of this hold phase represents the pure elastic properties of the muscle fiber (Fig 5A-B). The passive force-sarcomere length relation of NEM6 muscle fibers (i.e. the visco-elastic component) resembles that of CTRL muscle fibers in both slow-twitch and fast-twitch muscle fibers (Fig 5C). In addition, the passive tension that was measured at the end of the hold phase at a sarcomere length of 3.2 µm (i.e. the elastic component) was not significantly different between NEM6 and CTRL in both slow-twitch and fast-twitch muscle fibers (Fig 5D). Thus, the passive-elastic properties of NEM6 muscle fibers resemble those of CTRL muscle fibers.

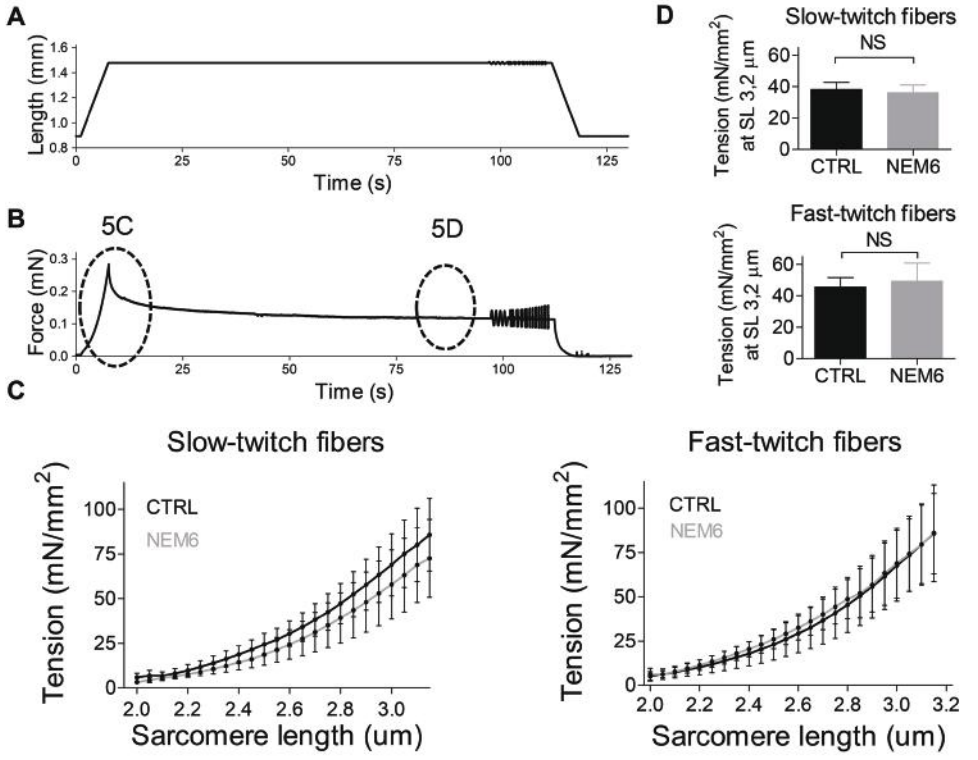

Figure 5 Passive properties of CTRL and NEM6 muscle fibers

Typical example of (A) the applied changes in length of a CTRL muscle fiber and (B) the development of passive tension in time. (C) No changes in passive tension were observed at incremental sarcomere lengths between muscle fibers of CTRL and NEM6. (D) In addition, the passive tension that was measured at the end of the hold phase at a sarcomere length of 3,2 µm was not different between slow- and fast-twitch muscle fibers of NEM6 and CTRL.

Characteristics of the Kbtbd13-KO mouse model

Mice were viable and were monitored up to a year. At birth, body weights of *Kbtbd13*-KO mice were similar to those of *Kbtbd13*-Wt mice, but upon ageing *Kbtbd13*-KO mice had lower body weights than *Kbtbd13*-Wt mice at all 3-month time points (Fig 6A). Gomori trichrome staining revealed no abnormalities in *Kbtbd13*-KO mice, suggesting the absence of nemaline bodies (Fig 6B). Electron microscopy confirmed the absence of nemaline bodies, and revealed a preserved ultrastructure in *Kbtbd13*-KO mice: Z-disks were well aligned and myofilament organization resembled that of *Kbtbd13*-Wt mice (Fig 6C). Subtle changes in mitochondrial organization and shape were found in *Kbtbd13*-KO mice. In healthy muscle, the Z-disk is flanked by round-shaped mitochondria and the sarcoplasmic reticulum. However, in *Kbtbd13*-KO mice disrupted sarcoplasmic reticula were found, and odd-shaped elongated mitochondria (Fig 6D). These changes might hamper calcium-handling and energetic supply in *Kbtbd13*-deficient muscle.

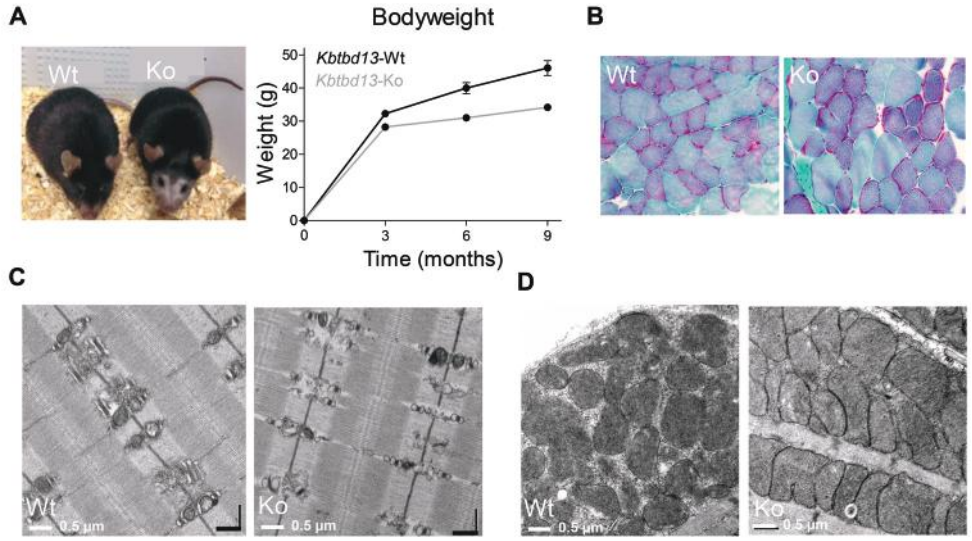

Figure 6 Characteristics of *Kbtbd13*-Wt and *Kbtbd13*-KO

(A-B) *Kbtdb13*-KO mice have a normal life span, but display a reduced bodyweight upon ageing. (C) Gomori trichrome staining revealed no abnormalities in *Kbtbd13*-KO mice. (D) Electron microscopy confirmed the absence of nemaline bodies and revealed a preserved ultrastructure in *Kbtbd13*-KO mice. (E) Subtle changes in mitochondrial organization and shape were found in *Kbtbd13*-KO mice, which suggests that less mitochondria are in contact with calcium release units.

Reduced mass was observed in soleus, gastrocnemius, extensor digitorum longus and tibialis cranialis muscle of 3 month old *Kbtbd13*-KO mice, also after normalization of muscle mass to the length of the tibia bone (Fig 7). At 6 and 9 months, no differences in the mass of gastrocnemius, extensor digitorum longus and tibialis cranialis muscle were observed, whereas the mass of soleus of *Kbtbd13*-KO mice remained lower than that of *Kbtbd13*-Wt mice at 6 and 9 months. Thus, *Kbtbd13*-KO mice display selective soleus muscle atrophy upon ageing.

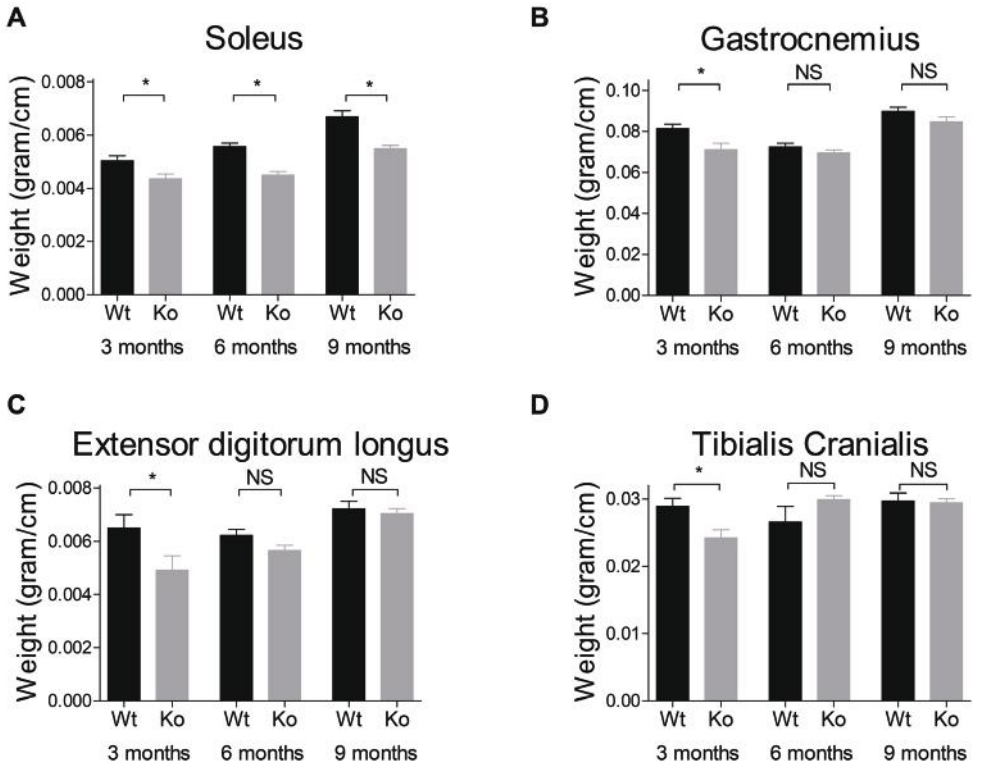

Figure 7 Muscle mass of hindlimb muscles of *Kbtbd13*-Wt and *Kbtbd13*-KO
(A-D) In 3 month old *Kbtbd13*-KO mice, reduced mass was observed in soleus, gastrocnemius, extensor digitorum longus and tibialis cranialis muscle, also after normalization of muscle mass to the length of the tibia bone. At 6 and 9 months, no differences in the mass of gastrocnemius, extensor digitorum longus and tibialis cranialis muscle were observed anymore, whereas the mass of soleus of *Kbtbd13*-KO mice remained lower than that of *Kbtbd13*-Wt mice.

Mildly progressive muscle weakness in intact soleus muscle of Kbtbd13-KO mice

At 3 months of age, soleus muscle of *Kbtbd13*-KO mice trends towards lower force generation at maximum stimulation frequency (150 Hz) (198±9 mN for *Kbtbd13*-KO vs. 225±10 mN for *Kbtbd13*-Wt p=0.108) (Fig 8A). When force at 150 Hz is normalized to the muscle's cross-sectional area (i.e. maximal active tension), no weakness is observed in 3 month old *Kbtbd13*-KO mice (297±18 mN/mm^2 for *Kbtbd13*-KO vs. 302±13 mN/mm^2 for *Kbtbd13*-Wt) (Fig 8B). Upon ageing (i.e. at 9 months of age), both force and tension are significantly lower in *Kbtbd13*-KO mice (Force: 170±9 mN for *Kbtbd13*-KO vs. 204±13 mN for *Kbtbd13*-Wt; Active tension: 240±9 mN/mm^2 for *Kbtbd13*-KO vs. 278±13 mN/mm^2 for *Kbtbd13*-Wt) (Fig 8F-G). Thus, a mildly progressive muscle weakness is observed in *Kbtbd13*-KO mice.

Hypercontractile phenotype at submaximal activation levels in intact muscle of young Kbtbd13-KO mice

The force-frequency relation provides insight into submaximal muscle performance. In 3-month-old *Kbtbd13*-KO mice, the relative force-frequency relationship is shifted leftwards compared to *Kbtbd13*-Wt mice (Fig 8C). Thus, at submaximal frequencies, *Kbtbd13*-KO mice have a hypercontractile phenotype. The cause of the augmented force generation at submaximal frequencies can relate to changes in the myosin heavy chain composition and/or to intrinsic changes in the activation and relaxation kinetics of muscle fibers of *Kbtbd13*-KO mice. No shift in the myosin heavy chain isoform composition in soleus muscle of *Kbtbd13*-KO was observed (data not shown). This prompted us to investigate the activation and relaxation kinetics of intact muscle. *Kbtbd13*-KO mice revealed slower activation kinetics and slower relaxation kinetics, reflected by an increased time to reach a force plateau (923±27 ms for *Kbtbd13*-KO vs. 742±49 ms for *Kbtbd13*-Wt) and an increased half-relaxation time (57±1 ms for *Kbtbd13*-KO vs. 51±1 ms for *Kbtbd13*-Wt) at 3 months (Fig 8D-E). Slowed activation and relaxation kinetics in *Kbtbd13*-KO mice will cause twitches to fuse at lower stimulation frequencies, shifting the force-frequency relation leftward.

In soleus muscle of 9 month old *Kbtbd13*-KO mice, no shift of the relative force-frequency relationship is observed (Fig 8H). In line with this observation, no significant differences in the activation (985±4 ms for *Kbtbd13*-KO vs. 992±4 ms for *Kbtbd13*-Wt) and relaxation kinetics were found (65±2 ms for

Kbtbd13-KO vs. 68±2 ms for *Kbtbd13*-Wt) (Fig 8I-J). Thus, soleus muscle of 3 month old *Kbtbd13*-KO mice displays a hypercontractile phenotype that can be explained by altered activation and relaxation kinetics. This phenotype restores to normal upon ageing.

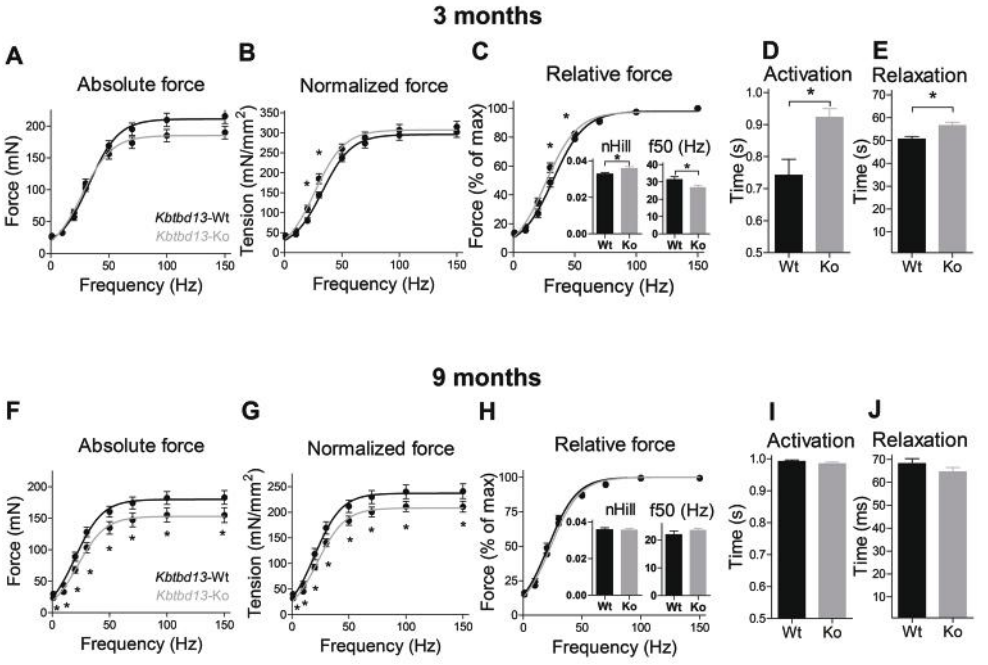

Figure 8 Calcium-sensitivity of force generation in intact soleus muscle of *Kbtbd13-Wt and Kbtbd13-KO mice*

(A) No changes in absolute force generation were found in intact soleus muscle of 3 month old *Kbtbd13*-KO mice (in grey) compared to *Kbtbd13*-Wt mice (in black). (B) However, at submaximal calcium levels, tension generation was higher in intact soleus muscle of *Kbtbd13*-KO mice compared to *Kbtbd13*-Wt mice. (C) Also, relative tension was higher at submaximal calcium levels in intact soleus muscle of *Kbtbd13*-KO mice compared to *Kbtbd13*-Wt mice, accompanied by an increase in the nHill and pCa_{50} value. (D-E) Both activation and relaxation times were longer in *Kbtbd13*-KO mice compared to *Kbtbd13*-Wt mice. Intact soleus muscle of 9 month old *Kbtbd13*-KO mice displayed (F) lower absolute force generation and (G) lower tension generation than *Kbtbd13*-Wt mice at all stimulation frequencies. (H) However, no changes in relative force generation were found between intact soleus muscle of *Kbtbd13*-KO mice and *Kbtbd13*-Wt mice, accompanied by comparable nHill and pCa_{50} values in both groups. In addition, both activation and relaxation times were not different in *Kbtbd13*-KO and *Kbtbd13*-Wt mice.

Kbtbd13-KO mice display a cardiac phenotype

Kbtbd13-KO mice have a lower muscle mass of the heart, the left ventricle and the right ventricle when normalized to tibia length upon ageing (Fig 9A-C and Table 2). This is in line with echocardiography data that indicated

a lower left ventricular posterior wall thickness in diastole in *Kbtbd13*-KO mice compared to *Kbtbd13*-Wt mice at all time points (Fig 9D). Note that - to conclusively establish atrophy - histological evaluation is necessary to confirm whether cardiomyocytes of *Kbtbd13*-KO mice have a lower cross-sectional area. Functional evaluation by echocardiography revealed no changes in the heart rate and fractional shortening at baseline (for typical M-mode examples by echo see Fig 10A), however upon dobutamine administration *Kbtbd13*-KO mice had a reduced increase in heart rate (P-interaction < 0.01) and fractional shortening (P-interaction < 0.05) (Fig 10B-C). Thus, echo data indicate that *Kbtbd13*-KO mice have a thinner left ventricular wall thickness and a lower contractile reserve.

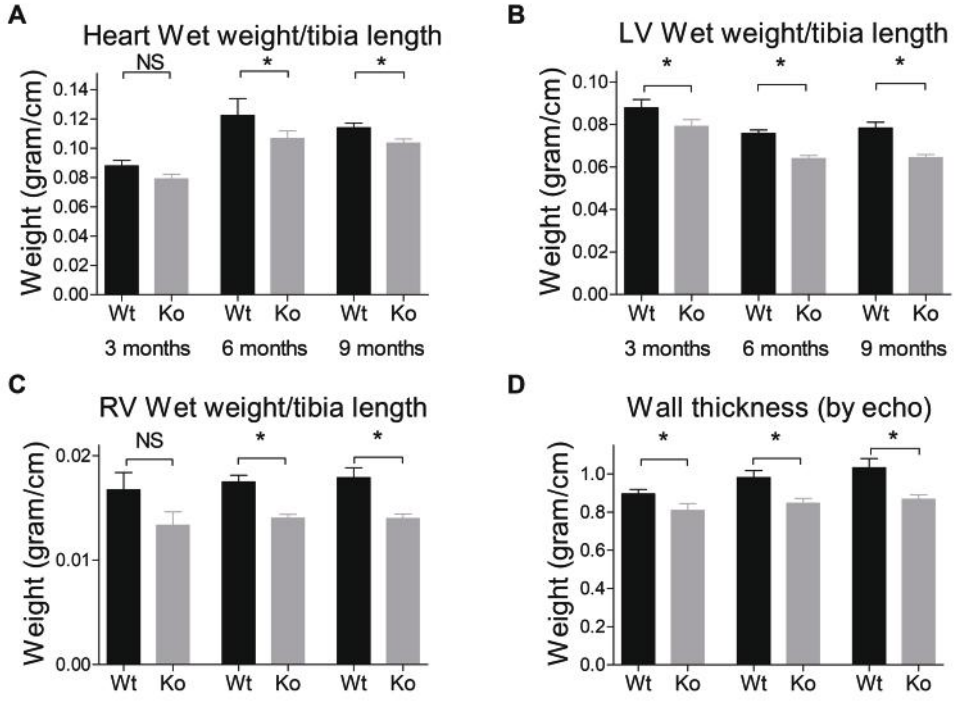

Figure 9 Muscle mass of cardiac muscle of *Kbtbd13*-Wt and *Kbtbd13*-KO mice
(A-C) *Kbtbd13*-KO mice have a lower muscle mass of the heart, the left ventricle and the right ventricle when normalized to tibia length upon ageing. (D) Echocardiography revealed a lower left ventricular posterior wall thickness in diastole in *Kbtbd13*-KO mice compared to *Kbtbd13*-Wt mice at all time points.

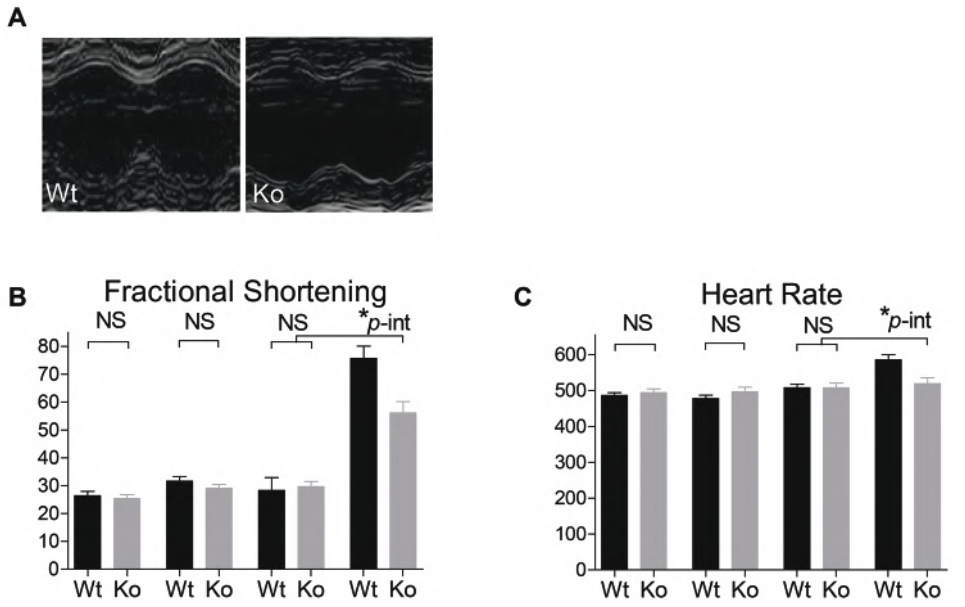

Figure 10 Stress-echocardiography in *Kbtbd13*-Wt and *Kbtbd13*-KO mice

(A) Typical M-mode examples by echocardiography of *Kbtbd13*-Wt and *Kbtbd13*-KO mice. (B-C) Echocardiography revealed no changes in the heart rate and fractional shortening at baseline in *Kbtbd13*-KO mice compared to *Kbtbd13*-Wt mice upon ageing, however upon dobutamine administration 9 month old *Kbtbd13*-KO mice had a reduced increase in heart rate and fractional shortening compared to *Kbtbd13*-Wt mice.

	Kbtbd13-Wt (n=12)			Kbtbd13-KO (n=15)		
Age	3 months	6 months	9 months	3 months	6 months	9 months
Heart weight/TL (gram/cm)	0.088±0.004	0.13±0.006	0.11±0.003	0.079±0.003	0.11±0.005*	0.10±0.003*
Left ventricle/TL (gram/cm)	0.057±0.002	0.076±0.002	0.078±0.003	0.049±0.002*	0.064±0.001*	0.064±0.001*
Right ventricle/TL (gram/cm)	0.017±0.002	0.017±0.001	0.018±0.001	0.013±0.001	0.014±0.0003*	0.014±0.0004*
Wall Thickness (mm)	0.90±0.02	0.98±0.04	1.0±0.05	0.81±0.04*	0.85±0.02*	0.87±0.02*
%Fractional shortening	26.4±1.6	31.6±1.7	28.3±4.5	25.4±1.4	29.1±1.3	29.6±1.9
+ Dobutamine	69.0±1.0	76.2±1.7	75.7±4.4	58.0±3.3*	50.8±1.8*	56.1±4.1*
Heart rate (beats per minute)	486±8	478±9	508±10	494±10	497±13	508±13
+ Dobutamine	606±7	579±8	586±14	549±27*	561±8	519±16*

Table 2 Cardiac characteristics of *Kbtbd13-Wt* and *Kbtbd13-KO* mice

DISCUSSION

NM patients that harbor mutations in the *KBTBD13* gene exhibit muscle weakness and a typical muscle slowness. As to date the role of KBTBD13 in muscle structure and function is unknown, the mechanisms underlying this particular NM phenotype are poorly understood. Hence, we investigated the contractile performance of permeabilized muscle fibers isolated from biopsies of NEM6 patients and we assessed the phenotype of a newly-generated *Kbtbd13*-KO mouse model. Permeabilized muscle fiber mechanics revealed contractile alterations at the sarcomere level in NEM6 patients, including a lower maximal active tension, lower cross-bridge cycling kinetics and an increased calcium-sensitivity of force generation: changes that contribute to the observed muscle weakness and slowness *in vivo*. The *Kbtbd13*-KO mouse partly recapitulates the clinical phenotype of NEM6 patients, reflected by a mildly progressive muscle weakness and atrophy of the soleus muscle. In addition, the *Kbtbd13*-KO mouse revealed a cardiac phenotype: a reduced left ventricular wall thickness and a lower contractile reserve. Hence, these studies gained insight in the pathophysiology of NEM6.

Muscle weakness at the intact muscle and sarcomere level

Permeabilized muscle fibers of NEM6 patients had lower maximal active tension than muscle fibers of CTRL. The impaired force generation at the sarcomere level was associated with a lower number of bound cross-bridges in both slow- and fast-twitch muscle fibers of NEM6 patients. In addition, at the intact muscle level, weakness slowly progressed in ageing *Kbtbd13*-KO mice. These findings are in line with the in vivo muscle function characteristics of NEM6 patients (Pauw-Gommans et al., 2006), which revealed muscle weakness at maximal stimulation frequencies. Note that these patients show no signs of neurological abnormalities (Gommans et al., 2002; Sambuughin et al., 2010). Although changes in excitation-contraction coupling might be at play as well, the present study strongly indicates that at least part of the muscle weakness in NEM6 is sarcomere-based. As the ultrastructure of muscle from both NEM6 patients and *Kbtbd13*-KO mice is largely preserved, we hypothesize that intrinsic changes in contractile proteins contribute to weakness. The lower number of bound cross-bridges in slow and fast-twitch muscle fiber of NEM6 patients is most likely not due to a lower availability of myosin, as the myosin content per half sarcomere is similar to that in CTRL fibers. Hence, we propose that alterations in cross-bridge cycling

kinetics result in a lower recruitment of cross-bridges which contribute to a lower number of bound cross-bridges. To further elucidate the contribution of alterations in cross-bridge cycling kinetics to contractile weakness, additional experiments implicating the activation and relaxation kinetics are necessary; i.e. myofibril kinetics and stiffness measurements during rigor conditions.

Hypercontractile phenotype at the intact and sarcomere level

Studies on intact soleus muscle revealed a leftward shift of the force-frequency relation in 3 month old *Kbtbd13*-KO mice; i.e. more force is generated at submaximal stimulation frequencies. These data are in line with *in vivo* data on NEM6 patients: i.e. increased force generation at submaximal stimulation frequencies and impaired activation and relaxation kinetics. The leftward shift of the force-frequency relation in *Kbtbd13*-KO mice is most likely due to changes in calcium-handling and/or sarcomere function, as the myosin heavy chain composition – a factor that influences the force-frequency relationship- was not altered between *Kbtbd13*-KO mice and *Kbtbd13*-Wt mice. Sarcomere function was investigated in muscle fibers isolated from NEM6 patients and revealed an increase in the calcium-sensitivity of force generation in both slow and fast fibers of NEM6 patients compared to CTRL. An increase in the calcium-sensitivity of force generation has been reported previously in muscle fibers from NM patients with other implicated genes (Mokbel et al., 2013; Ottenheijm et al., 2011). However, these patients did not reveal muscle slowness; hence it is likely that other mechanisms accompany the increase calcium-sensitivity of force generation, resulting in muscle slowness. A likely player in muscle slowness is disturbed calcium handling (Ottenheijm et al., 2008). Therefore, KBTBD13's role in calcium-handling is an interesting topic for future studies. In addition, the increase in the calcium-sensitivity of force generation is in line with the muscle stiffness that NEM6 patients experience (Gommans et al., 2002; Sambuughin et al., 2010). As the present study reveals that the passive properties of muscle fibers of NEM6 patients are not affected, the increase in muscle stiffness is most likely based on changes in thin filament activation. Thus, the hypercontractile phenotype at the intact muscle and the sarcomere level contributes to the clinical phenotype of NEM6 patients.

Does KBTBD13 encode a thin filament protein?

To date, all genes that are implicated in NM encode proteins that are associated with the skeletal muscle thin filament or modulate the stability

of thin filament proteins. Therefore, it is presumed that thin filament function is compromised in NM patients with mutations in *KBTBD13*. However, little is known about the role of KBTBD13 in muscle function and its interaction partners. A recent paper postulates that KBTBD13 acts as a substrate adaptor for specific proteins through interaction with Cullin-3, an ubiquitin ligase (Sambuughin et al., 2012). To date, target proteins for KBTBD13 are not known yet, but as KLHL40 binds to nebulin and leiomodin-3 and KLHL41 interacts with nebulin - hence promoting the stability of these proteins through their interaction with Cullin-3 (Cenik et al., 2015; Garg et al., 2014; Gupta et al., 2013; Ravenscroft et al., 2013) -, it has been hypothesized that KBTBD13 stabilizes a specific thin filament protein. As our contractile data on NEM6 muscle fibers reveal substantial changes in the calcium-sensitivity of force generation and cross-bridge cycling kinetics, we speculate that regulatory thin filament proteins are candidates to interact with KBTBD13. Note that a previous study on NM muscle fibers harboring *TPM3* mutation revealed a contractile functional phenotype that resembled that of NEM6 muscle fibers, i.e. lower maximal active tension, slower cross-bridge cycling kinetics, increased calcium-sensitivity of force generation and a preserved force-sarcomere length relationship (Ottenheijm et al., 2011). In addition to tropomyosins, also nebulin, tropomodulins and leiomodins are interesting candidate proteins as interaction partner of KBTBD13. Thus, KBTBD13 might interact with a regulatory thin filament protein.

The localization of KBTBD13

To date, the localization of KBTBD13 remains unclear. However, KLHL40 and KLHL41 – the other two kelch proteins that are implicated in NM – colocalize with the sarcoplasmic reticulum (Gupta et al., 2013), an essential player in muscle contraction as it modulates calcium release and calcium re-uptake (Gordon et al., 2000). As NEM6 patients reveal impaired muscle activation and relaxation, the sarcoplasmic reticulum is an interesting putative localization for KBTBD13. Of interest, muscle biopsies of NEM6 patients reveal remarkable cores that are devoid of mitochondria (Olivé et al., 2010; Sambuughin et al., 2010) – the energy suppliers of muscle that are in close vicinity with the sarcoplasmic reticulum (Boncompagni et al., 2009). In line with these findings on NEM6 biopsies, electron microscopy on *Kbtbd13*-KO mouse muscle reveals mitochondrial abnormalities. Whether KBTBD13 is directly associated with altered function of the sarcoplasmic reticulum and/or mitochondria or whether changes in the contractile properties of the muscle

fibers result in an increased demand on the mitochondria and the sarcoplasmic reticulum remains unknown (Maclennan and Zvaritch, 2011; Paolini et al., 2015). Hence, both the localization of KBTBD13 and its role in the function of the sarcoplasmic reticulum are key topics for future studies. Note that the lack of a proper antibody against KBTBD13 hampered the identification of the location of this novel protein in muscle. A second consequence is that KBTBD13 protein levels could not be assessed in muscle of NEM6 patients. Hence, caution is warranted translating the findings on Kbtbd13-deficient mouse tissue to the contractile data from biopsies of NEM6 patients harboring a missense mutation in *KBTBD13*.

Cardiac involvement of Kbtbd13

KBTBD13 is expressed in both skeletal and cardiac muscle tissue. However to date, only a skeletal muscle phenotype has been reported in NEM6 patients. The newly developed *Kbtbd13*-KO mouse is a unique tool to assess the effect of *Kbtbd13*-deficiency on cardiac structure and function. Lower cardiac muscle mass was found in *Kbtbd13*-KO mice, accompanied by a limited potential of increasing contractile performance upon stress. The cause of this lower contractile reserve is not elucidated yet, but we speculate that a similar mechanism as observed in skeletal muscle of *Kbtbd13*-KO mice can be at play: at submaximal levels of activation a relative higher force is generated. Therefore, *Kbtbd13*-KO mice have a smaller potential to increase muscle force upon maximal stimulation. Note that caution is warranted interpreting the contractile data on the heart, as the myosin heavy chain isoform composition is an important factor influencing contractility (Tardiff et al., 2000; Krenz et al., 2004), which has not been determined yet. Thus far, a cardiac phenotype has not been reported in NEM6 patients, but the current data strongly suggest to evaluate cardiac function in NEM6 patients, especially under stress conditions.

In conclusion, our data indicate that alterations at the level of the sarcomere contribute to muscle weakness and slowness in NEM6 patients. Muscle characteristics of the *Kbtbd13*-KO mouse model partly phenocopy the muscle weakness and slowness of NEM6 patients. In addition, cardiac evaluation of the *Kbtbd13*-KO mouse model suggests a role for *Kbtbd13* in cardiac structure and function. Hence, this novel NM mouse model is a useful tool to further unravel the role of KBTBD13 in health and disease and to test therapeutic strategies to combat NEM6.

REFERENCES

Boncompagni S, Rossi AE, Micaroni M, Beznoussenko G V, Polishchuk RS, Dirksen RT, et al. Mitochondria are linked to calcium stores in striated muscle by developmentally regulated tethering structures. Mol. Biol. Cell 2009; 20: 1058–67.

Brenner B, Eisenberg E. Rate of force generation in muscle: correlation with actomyosin ATPase activity in solution. Proc. Natl. Acad. Sci. U. S. A. 1986; 83: 3542–6.

Caremani M, Dantzig J, Goldman YE, Lombardi V, Linari M. Effect of Inorganic Phosphate on the Force and Number of Myosin Cross-Bridges During the Isometric Contraction of Permeabilized Muscle Fibers from Rabbit Psoas. Biophys. J. 2008; 95: 5798–5808.

Cenik BK, Garg A, McAnally JR, Shelton JM, Richardson JA, Bassel-Duby R, et al. Severe myopathy in mice lacking the MEF2/SRF-dependent gene leiomodin-3. J. Clin. Invest. 2015; 125: 1569–78.

Colombo I, Scoto M, Manzur AY, Robb SA, Maggi L, Gowda V, et al. Congenital myopathies: Natural history of a large pediatric cohort. Neurology 2015; 84: 28–35.

Donkervoort S, Papadaki M, de Winter JM, Neu MB, Kirschner J, Bolduc V, et al. TPM3 deletions cause a hypercontractile congenital muscle stiffness phenotype. Ann. Neurol. 2015; 78: 982–94.

Garg A, O'Rourke J, Long C, Doering J, Ravenscroft G, Bezprozvannaya S, et al. KLHL40 deficiency destabilizes thin filament proteins and promotes nemaline myopathy. J. Clin. Invest. 2014; 124: 3529–3539.

Gineste C, De Winter JM, Kohl C, Witt CC, Giannesini B, Brohm K, et al. In vivo and in vitro investigations of heterozygous nebulin knock-out mice disclose a mild skeletal muscle phenotype. Neuromuscul. Disord. 2013; 23: 357–69.

Gommans, Davis M, Saar K, Lammens M, Mastaglia F, Lamont P, et al. A locus on chromosome 15q for a dominantly inherited nemaline myopathy with core-like lesions. Brain 2003; 126: 1545–51.

Gommans IMP, van Engelen BGM, ter Laak HJ, Brunner HG, Kremer H, Lammens M, et al. A new phenotype of autosomal dominant nemaline myopathy. Neuromuscul. Disord. 2002; 12: 13–18.

Gordon AM, Homsher E, Regnier M. Regulation of Contraction in Striated Muscle. Physiol Rev 2000; 80: 853–924.

Gupta VA, Ravenscroft G, Shaheen R, Todd EJ, Swanson LC, Shiina M, et al. Identification of KLHL41 Mutations Implicates BTB-Kelch-Mediated Ubiquitination as an Alternate Pathway to Myofibrillar Disruption in Nemaline Myopathy. Am. J. Hum. Genet. 2013; 93: 1108–17.

Maclennan DH, Zvaritch E. Mechanistic models for muscle diseases and disorders originating in the sarcoplasmic reticulum. Biochim. Biophys. Acta 2011; 1813: 948–64.

Manders E, Bogaard H-J, Handoko ML, van de Veerdonk MC, Keogh A, Westerhof N, et al. Contractile dysfunction of left ventricular cardiomyocytes in patients with pulmonary arterial hypertension. J. Am. Coll. Cardiol. 2014; 64: 28–37.

Manders E, Ruiter G, Bogaard H-J, Stienen GJM, Vonk-Noordegraaf A, de Man FS, et al. Quadriceps muscle fibre dysfunction in patients with pulmonary arterial hypertension. Eur. Respir. J. 2015: 09031936.00205114–.

Mokbel N, Ilkovski B, Kreissl M, Memo M, Jeffries CM, Marttila M, et al. K7del is a common TPM2 gene mutation associated with nemaline myopathy and raised myofibre calcium sensitivity. Brain 2013; 136: 494–507.

Olivé M, Goldfarb LG, Lee H-S, Odgerel Z, Blokhin A, Gonzalez-Mera L, et al. Nemaline myopathy type 6: clinical and myopathological features. Muscle Nerve 2010; 42: 901–7.

Ottenheijm CAC, Fong C, Vangheluwe P, Wuytack F, Babu GJ, Periasamy M, et al. Sarcoplasmic reticulum calcium uptake and speed of relaxation are depressed in nebulin-free skeletal muscle. FASEB J. 2008; 22: 2912–9.

Ottenheijm CAC, Lawlor MW, Stienen GJM, Granzier H, Beggs AH. Changes in cross-bridge cycling underlie muscle weakness in patients with tropomyosin 3-based myopathy. Hum. Mol. Genet. 2011; 20: 2015–2025.

Ottenheijm CAC, Witt CC, Stienen GJ, Labeit S, Beggs AH, Granzier H. Thin filament length dysregulation contributes to muscle weakness in nemaline myopathy patients with nebulin deficiency. Hum. Mol. Genet. 2009; 18: 2359–2369.

Paolini C, Quarta M, Wei-LaPierre L, Michelucci A, Nori A, Reggiani C, et al. Oxidative stress, mitochondrial damage, and cores in muscle from calsequestrin-1 knockout mice. Skelet. Muscle 2015; 5: 10.

Pauw-Gommans, Gerrits, de Haan A, van Engelen BGM. Muscle slowness in a family with nemaline myopathy. Neuromuscul. Disord. 2006; 16: 477–480.

Ravenscroft G, Miyatake S, Lehtokari V-L, Todd EJ, Vornanen P, Yau KS, et al. Mutations in KLHL40 Are a Frequent Cause of Severe Autosomal-Recessive Nemaline Myopathy. Am. J. Hum. Genet. 2013; 93: 6–18.

Sambuughin N, Swietnicki W, Techtmann S, Matrosova V, Wallace T, Goldfarb L, et al. KBTBD13 interacts with Cullin 3 to form a functional ubiquitin ligase. Biochem. Biophys. Res. Commun. 2012; 421: 743–9.

Sambuughin N, Yau KS, Olivé M, Duff RM, Bayarsaikhan M, Lu S, et al. Dominant mutations in KBTBD13, a member of the BTB/Kelch family, cause nemaline myopathy with cores. Am. J. Hum. Genet. 2010; 87: 842–847.

Sanoudou D, Beggs AH. Clinical and genetic heterogeneity in nemaline myopathy-a disease of skeletal muscle thin filaments. Trends Mol. Med. 2001; 7: 362–368.

de Winter JM, Joureau B, Sequeira V, Clarke NF, van der Velden J, Stienen GJ, et al. Effect of levosimendan on the contractility of muscle fibers from nemaline myopathy patients with mutations in the nebulin gene. Skelet. Muscle 2015; 5: 12.

Yuen M, Sandaradura SA, Dowling JJ, Kostyukova AS, Moroz N, Quinlan KG, et al. Leiomodin-3 dysfunction results in thin filament disorganization and nemaline myopathy. J. Clin. Invest. 2014; 124

CHAPTER 6

EFFECT OF LEVOSIMENDAN ON THE CONTRACTILITY OF MUSCLE FIBERS FROM NEMALINE MYOPATHY PATIENTS WITH MUTATIONS IN THE NEBULIN GENE

Josine M. de Winter, Barbara Joureau, Vasco Sequeira, Nigel F. Clarke, Jolanda van der Velden, Ger J.M. Stienen, Henk Granzier, Alan H. Beggs and Coen A.C. Ottenheijm

Skeletal Muscle, 2015

ABSTRACT

Background | Nemaline myopathy (NM), the most common non-dystrophic congenital myopathy, is characterized by generalized skeletal muscle weakness, often from birth. To date, no therapy exists that enhances the contractile strength of muscles of NM patients. Mutations in *NEB*, encoding the giant protein nebulin, are the most common cause of NM. The pathophysiology of muscle weakness in NM patients with *NEB* mutations (*NEB*-NM) includes a lower calcium-sensitivity of force generation. We propose that the lower calcium-sensitivity of force generation in *NEB*-NM offers a therapeutic target. Levosimendan is a calcium sensitizer that is approved for use in humans, and has been developed to target cardiac muscle fibers. It exerts its effect through binding to slow skeletal/cardiac troponin C. As slow skeletal/cardiac troponin C is also the dominant troponin C isoform in slow-twitch skeletal muscle fibers, we hypothesized that levosimendan improves slow-twitch muscle fiber strength at submaximal levels of activation in patients with *NEB*-NM.

Methods | To test whether levosimendan affects force production, permeabilized slow-twitch muscle fibers isolated from biopsies of *NEB*-NM patients and controls were exposed to levosimendan and the force response was measured.

Results | No effect of levosimendan on muscle fiber force in *NEB*-NM and control skeletal muscle fibers was found, both at a submaximal calcium level using incremental levosimendan concentrations, and at incremental calcium concentrations in the presence of levosimendan. In contrast, levosimendan did significantly increase the calcium-sensitivity of force in human single cardiomyocytes. Protein analysis confirmed that the slow skeletal/cardiac troponin C isoform was present in the skeletal muscle fibers tested.

Interpretation | These findings indicate that levosimendan does not improve the contractility in human skeletal muscle fibers, and do not provide rationale for using levosimendan as a therapeutic to restore muscle weakness in *NEB*-NM patients. We stress the importance of searching for compounds that improve the calcium-sensitivity of force generation of slow-twitch muscle fibers. Such compounds provide an appealing approach to restore muscle force in patients with *NEB*-NM, and also in patients with other neuromuscular disorders.

INTRODUCTION

Nemaline myopathy (NM) is the most common non-dystrophic congenital myopathy (incidence ~1:50,000) (Wallgren-Pettersson and Laing, 2000). Hallmark features of NM include muscle weakness and the presence of nemaline bodies in muscle fibers (North et al., 1997). To date, ten genes have been implicated in NM. Seven of these genes encode proteins of the skeletal muscle thin filament (alpha-tropomyosin-3 and beta-tropomyosin (*TPM3* and *TPM2*), nebulin (*NEB*), actin alpha 1 (*ACTA1*), troponin T type 1 (*TNNT1*), cofilin-2 (*CFL2*)) and leiomodin-3 (*LMOD3*) (Ryan et al., 2003; Yuen et al., 2014), and three genes encode kelch domain proteins that are associated with thin filament proteins and may be involved in regulating thin filament protein stability or turnover (kelch repeat and BTB (POZ) Domain Containing 13 (*KBTBD13*), (kelch-like family member 40 (*KLHL40*) and kelch-like family member 41 (*KLHL41*)) (Garg et al., 2014; Gupta and Beggs, 2014; Gupta et al., 2013; Olivé et al., 2010; Ravenscroft et al., 2013; Sambuughin et al., 2010, 2012).

Mutations in *NEB* are the most common cause of NM, accounting for more than 50% of NM cases (Lehtokari et al., 2014; Pelin et al., 1999). Nebulin is a giant sarcomeric protein (~800 kDa) and a single nebulin molecule spans nearly the entire length of the thin filament. Previous studies of a nebulin knockout mouse model showed that nebulin stabilizes the thin filament and specifies its length (Bang et al., 2006; Castillo et al., 2009; Gokhin and Bang, 2009; Pappas et al., 2010; Witt et al., 2006). Evidence also suggests that nebulin modulates both the kinetics of actomyosin cross-bridge formation (Bang et al., 2009; Chandra et al., 2009) and the calcium-sensitivity of thin filament activation (Chandra et al., 2009; Ottenheijm et al., 2013). Recent work revealed that skeletal muscle fibers of NM patients with *NEB* mutations (NEB-NM) develop muscle weakness due to loss of these functions of nebulin; their myofibers contain thin filaments of shorter length, they show altered actomyosin cross-bridge kinetics (Lawlor et al., 2011; Ottenheijm et al., 2009, 2010), and they have a lower calcium-sensitivity of force generation (Ottenheijm et al., 2010).

To date, no therapy exists that enhances force generation in *NEB*-NM. We propose that the lower calcium-sensitivity of force generation in *NEB*-NM offers a therapeutic target. Recent work from our group addressed the ability of a fast skeletal muscle troponin activator to enhance the calcium-sensitivity

of force generation in skeletal muscle fibers from *NEB*-NM patients. These troponin activators target fast-twitch muscle fibers (Russell et al., 2012), and it was demonstrated that the compound increased the calcium-sensitivity of force generation in fast-twitch fibers of *NEB*-NM patients (de Winter et al., 2013). As human skeletal muscles consist of a mixture of fast- and slow-twitch muscle fibers, it would be desirable to also target the calcium-sensitivity of slow-twitch muscle fibers in NM patients, especially as these patients have been shown to have a predominance of slow-twitch muscle fibers (North et al., 1997). Levosimendan is a calcium sensitizer that is approved for use in humans, and has been developed to target cardiac muscle fibers. It exerts its effect through binding to slow skeletal/cardiac troponin C and improves cardiac contractility in vivo (Follath et al., 2002) and in vitro (Edes et al., 1995). Slow skeletal/cardiac troponin C is also the dominant troponin C isoform in slow-twitch skeletal muscle fibers, and recent work suggested that levosimendan improves submaximal contractility of slow-twitch muscle fibers in the diaphragm of animal models and in humans (Doorduin et al., 2012; van Hees et al., 2009, 2011).

Based on these findings, we hypothesized that levosimendan improves slow-twitch muscle fiber strength at submaximal levels of activation in patients with *NEB*-NM. To test this hypothesis, we exposed muscle fibers isolated from biopsies of *NEB*-NM patients to levosimendan and measured the force response. Our findings suggest that levosimendan does not improve the in vitro contractility of slow-twitch muscle fibers at submaximal activation levels in patients with *NEB*-NM.

METHODS

Skeletal muscle biopsies of NEB-NM patients

Quadriceps muscle specimens, remaining from diagnostic procedures or obtained during clinically indicated surgical procedures, were collected from four NM patients with confirmed *NEB* gene mutations, and from three adult control subjects with no medical history. Ethical approval for study of the NM biopsies was granted by the Institutional Review Board of Boston Children's Hospital and these biopsies were obtained from discarded clinical specimens following informed consent under protocol 03-08-128R. Details on the clinical and genetic data of the subjects have been published previously (biopsy ID's T33, T1033, T1069 and T887 (de Winter et al., 2013)). The three adult control muscle biopsies were obtained under supervision of the HREC, Children's

Hospital at Westmead (CHW/10/45). All biopsies were stored frozen and unfixed at −80°C until use.

Skeletal muscle mechanics

Small strips dissected from the muscle biopsies were permeabilized overnight as described previously (Ottenheijm et al., 2009). This procedure renders the membranous structures in the muscle fibers permeable, which enables activation of the myofilaments with exogenous calcium. Preparations were washed thoroughly with relaxing solution and stored in 50% glycerol/relaxing solution at −20°C. Small muscle bundles (cross-sectional area ~0.07 mm^2, NEB-NM patients) and single muscle fibers (control subjects) were dissected from the permeabilized strips, and were mounted using aluminum T-clips between a length motor (ASI 403A, Aurora Scientific Inc., Ontario, Canada) and a force transducer element (ASI 315C-I, Aurora Scientific Inc., Ontario, Canada) in a single fiber apparatus (ASI 802D, Aurora Scientific Inc., Ontario, Canada) that was mounted on the stage of an inverted microscope (Zeiss Axio Observer A1). Sarcomere length was set using a high speed VSL camera and ASI 900B software (Aurora Scientific Inc., Ontario, Canada). Mechanical experiments were performed at a sarcomere length of 2.1 μm, a length selected to minimize force differences due to shorter thin filaments in fibers from NEB-NM patients (Ottenheijm et al., 2009). Fiber width and diameter were measured at three points along the fiber and the cross-sectional area was determined assuming an elliptical cross-section. Three different types of bathing solutions were used during the experimental protocols: a relaxing solution (100 mM BES; 6.97 mM EGTA; 6.48 mM $MgCl_2$; 5.89 mM Na_2-ATP; 40.76 mM K-propionate; 14.5 mM creatine phosphate), a pre-activating solution with low EGTA concentration (100 mM BES; 0.1 mM EGTA; 6.42 mM $MgCl_2$; 5.87 mM Na_2-ATP; 41.14 mM K-propionate; 14.5 mM creatine phosphate; 6.9 mM HDTA), and an activating solution (100 mM BES; 7.0 mM Ca-EGTA; 6.28 mM $MgCl_2$; 5.97 mM Na2-ATP; 40.64 mM K-propionate; 14.5 mM creatine phosphate). The temperature of the bathing solutions was kept constant at 20°C using a TEC controller (ASI 825A, Aurora Scientific Inc. Ontario, Canada).

Concentrated stock solutions of levosimendan (a kind gift from Orion Pharma, Espoo, Finland) were prepared in dimethyl sulfoxide (DMSO). Before use, levosimendan stock solutions were diluted with experimental solutions. The final concentration of DMSO did not exceed 0.03%. Control experimental

solutions contained 0.03% DMSO (vehicle). To determine a dose-response curve for levosimendan in muscle fibers from controls (CTRL) and from NEB-NM patients, tissue was exposed to an activating solution with a pCa of 5.8 (CTRL) or pCa 5.6 (*NEB*-NM) – these pCa's yielded ~40% of maximal active tension – with vehicle (to establish the submaximal force generation at that calcium concentration). Subsequently, tissue was exposed to a similar activating solution, but which contained increasing concentrations of levosimendan (0.1, 1, 10, 25 and 100 μM). After exposure to the final levosimendan concentration, the fibers were once more activated in vehicle to rule out rundown of force. Note that 0.03% DMSO did not affect muscle fiber contractility (data not shown).

Finally, to determine the effect of levosimendan (100 μM) on the force-pCa relation, permeabilized muscle fiber bundles or single fibers were sequentially bathed in a relaxing solution, a pre-activation solution and solutions with pCa values ranging from 9.0 to 4.5 – all containing 100 μM levosimendan - and the steady-state force was measured. Measured force values were normalized to the maximal force obtained at pCa 4.5. The obtained force-pCa data were fit to the Hill equation ($Y=1/(1+10nH(pCa-pCa_{50}))$) where the pCa_{50} corresponds to the calcium concentration that yields half-maximal force and the Hill coefficient, nH, to myofilament cooperativity (Sun and Irving, 2010).

Myocardial human biopsies

Human left ventricular tissue was obtained from three non-failing donors of whom the myocardium was not required for transplantation. Donors had no history of cardiac abnormalities, normal ECG and normal ventricular function on echocardiography within 24 hours of heart transplantation. Tissue was collected in cardioplegic solution and immediately frozen and stored in liquid nitrogen. Samples were obtained after written informed consent and with approval of the local Human Research Ethics Committee of the University of Sydney (#7326). The investigation conforms with the principles outlined in the Declaration of Helsinki (1997).

Cardiomyocyte mechanics

Cardiac tissue samples were thawed in relaxing solution (5.95 mM Na_2-ATP, 6.04 mM $MgCl_2$, 2 mM EGTA, 139.6 mM KCl, 10 mM Imidazole, pH 7.0) and cardiomyocytes were mechanically isolated by tissue disruption. Thereafter, cardiomyocytes were chemically permeabilized by incubation for 5 minutes in relaxing solution containing 0.5% (v/v) Triton-X100 and glued between

a force transducer and a piezoelectric motor as described previously (van der Velden et al., 1998). Isometric force measurements were performed at a submaximal calcium concentration (pCa 5.6), which generates 44±5% of maximal force at saturating calcium levels (pCa 4.5). Sarcomere length was adjusted to 1.8 µm and determined by means of a spatial Fourier transformation as described previously (van der Velden et al., 1998).

Levosimendan was dissolved in DMSO and diluted in pCa 5.6 calcium-batches to a final concentration ranging from 0.1-100 µM. The final DMSO concentration did not exceed 0.03%. To control for artificial side-effects resulting from DMSO, the latter was diluted in pCa 5.6 (DMSO final concentration <0.03%) and served as control, herein termed as vehicle. No difference in developed force was found between pCa 5.6 compared with vehicle up to the maximum concentration levosimendan used.

Myosin heavy chain composition

A specialized SDS-PAGE was used to determine the myosin heavy chain isoform composition of the muscle fiber preparations that we used in our contractility experiments (Ottenheijm et al., 2009). In brief, muscles fibers were denatured by boiling for 2 minutes in SDS sample buffer. The stacking gel contained a 4% acrylamide concentration (pH 6.7), and the separating gel contained 7% acrylamide (pH 8.7) with 30% glycerol (v/v). The gels were run for 24h at 15°C and a constant voltage of 275 volt. Finally, the gels were silver-stained, scanned, and analyzed with One-D scan EX (Scanalytics Inc., Rockville, MD, USA) software.

Troponin C Western blotting

Muscle samples were solubilized as described previously (Zaremba et al., 2007). In brief, frozen muscle samples were homogenized in a liquid nitrogen cooled mortar and re-suspended in 1 ml cold 10% trichloracetic acid (TCA) solution dissolved in acetone containing dithiothreitol (DTT) (0.2% w/v) and stored at -80°C for 60 minutes. Subsequently, homogenates were brought to room temperature stepwise: 20 minutes at -20°C, 20 minutes at 4°C and 20 minutes at room temperature (while being mixed on a vortex in between all steps). Then, muscle homogenates were centrifuged at 12,000 g for 15 minutes followed by washing the tissue pellets with 1 mL of 0.2% w/v DTT-acetone solution and shaking them for 5 min at room temperature. This cycle of centrifugation, washing and shaking was repeated five times. Tissue pellets were freeze-dried overnight and homogenized in sample buffer containing

15% glycerol, 62.5 mM Tris (pH 6.8), 1% w/v SDS and 2% w/v DTT (final concentration 5 µg dry weight/µL).

To discriminate between both slow skeletal/cardiac troponin C and fast skeletal troponin C isoforms, 4 µL of muscle homogenates in 1-D sample buffer (20 µg of dry weight tissue) were loaded on a 15% acrylamide SDS-PAGE gel. Subsequently, the gel ran first for 20 minutes at 200 volt and thereafter 160 minutes at 400 volt at 15°C. After completion of the run, the gel was blotted for 90 minutes at constant amperage of 320 mA using a semidry blotting system (Trans-Blot SD Cell, Bio-Rad, USA). After staying overnight in blocking solution (5% milk in TBS-T), the blot was incubated at room temperature for 90 minutes in a pan-specific antibody directed against Troponin C (#4002, Cell Signaling, USA) (1:500 in blocking solution), washed for 30 minutes and put in secondary antibody goat anti-rabbit HRP (Dako, Denmark) (1:2500 in blocking solution) for 60 minutes at room temperature. Thereafter, the blot was washed with TBS-T for 30 minutes and treated with ECL prima reagents (GE Healthcare, UK) for 5 minutes. The blot was scanned using a LAS 3000 (Fujifilm Medical Systems, USA).

Statistical analyses

Data are presented as mean ± SEM. For statistical analyses, t test, 1-way ANOVA and 2-way ANOVA were used. For dose-response tests, 1-way Repeated Measures ANOVA was used, with Dunnett's Multiple Comparison Test as post-hoc test. $P < 0.05$ was considered to be statistically significant.

RESULTS

The contractile performance of permeabilized muscle fibers from nemaline myopathy patients with nebulin mutations

Muscle contractility experiments

The force generating capacity of permeabilized muscle fiber bundles isolated from nemaline myopathy biopsies with mutations in the nebulin gene (*NEB*-NM) was lower compared to muscle fibers from healthy controls at both maximal and submaximal calcium levels (for typical force traces see Figure 1A). At pCa 4.5 – corresponding to a calcium concentration that yielded maximal force generation - *NEB*-NM muscle fiber bundles revealed a significant lower force generating capacity (19 ± 3 mN/mm^2) compared to slow-twitch single fibers from control biopsies ($CTRL_{slow}$) (133 ± 11 mN/mm^2) and fast-twitch single fibers from control biopsies ($CTRL_{fast}$) (172 ± 8 mN/mm^2) (Figure 1B). In addition, at submaximal calcium levels (pCa 5.8) *NEB*-NM muscle fibers (7 ± 2 mN/mm^2) were significantly weaker than $CTRL_{slow}$ (58 ± 6 mN/mm^2) and $CTRL_{fast}$ fibers (49 ± 4 mN/mm^2) (Figure 1C).

Interestingly, when expressing the force generating capacity of the muscle fibers at a submaximal calcium concentration (pCa 5.8) as a percentage of the maximal force generating capacity (pCa 4.5, Fmax), *NEB*-NM muscle fibers reveal a significant lower relative contractile performance at submaximal calcium levels (24 ± 2 %Fmax) compared to $CTRL_{slow}$ (43 ± 2 %Fmax) and $CTRL_{fast}$ fibers (37 ± 3 %Fmax) (Figure 1D). This observation indicates that *NEB*-NM muscle fibers have a lower calcium-sensitivity of force than fibers from controls.

Myosin heavy chain composition

As the force generating capacity of muscle fibers depends on the myosin heavy chain isoform composition, we determined the relative abundance of slow myosin isoforms (MHC_{slow}) and fast myosin isoforms MHC 2A and 2X (MHC_{fast}) in the single fibers of control subjects and the muscle fiber bundles of *NEB*-NM patients that were used for the contractility experiments. Our analyses showed that *NEB*-NM muscle bundles were composed of 75 ± 6% MHC_{slow} and of 25 ± 6% MHC_{fast} (Figure 1E). Thus, the biopsies of the *NEB*-NM patients contained predominantly slow-twitch muscle fibers.

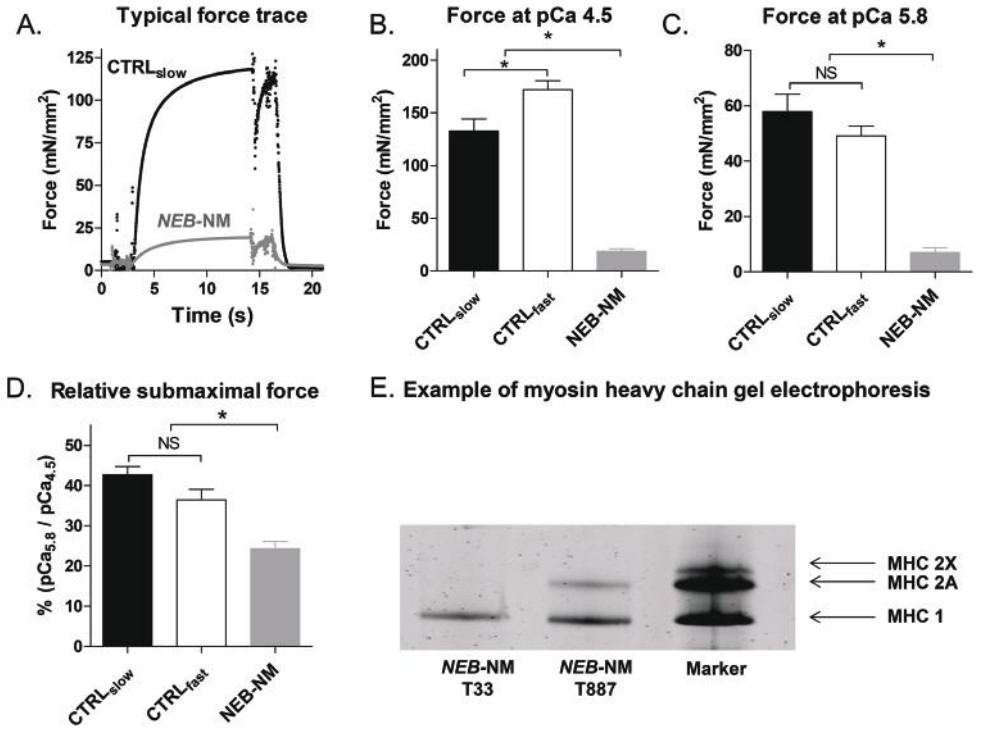

Figure 1

(A) Typical force trace of a slow-twitch single muscle fiber of a control subject and of a muscle fiber bundle of a *NEB*-NM patient (biopsy ID T33 is shown) during exposure to an experimental solution with pCa 4.5. Note the severely reduced maximal tension of the muscle fibers of the *NEB*-NM patient. (B) Maximal tension (pCa 4.5) of muscle fibers of healthy controls and *NEB*-NM patients. (C) Submaximal tension (pCa 5.8) of muscle fibers of healthy controls and *NEB*-NM patients. (D) Relative submaximal tension (pCa 5.8/4.5). Note that the relative submaximal tension of muscle fibers of *NEB*-NM patients is reduced, indicating a reduced calcium- sensitivity of force. (E) Example of a specialized SDS-PAGE gel that was used to determine the myosin heavy chain isoform composition of the muscle fiber preparations that we used in our contractility experiments. Here, the bundle from *NEB*-NM T33 is composed of type 1 myosin heavy chain isoforms (MHC 1), the bundle from *NEB*-NM T887 contains both MHC 1 and type 2A myosin heavy chain isoforms (MHC 2A) and the marker exhibits both MHC 1, MHC 2A as myosin 2X isoforms (MHC 2X).

The effect of levosimendan on force in permeabilized skeletal muscle fibers

Dose-response relation

We tested levosimendan at a range of concentrations and at a pCa that yielded ~40% of maximal force in both *NEB*-NM fibers and CTRL fibers. In

both *NEB*-NM muscle bundles that expressed solely MHC_{slow} and *NEB*-NM muscle bundles that expressed a mix of MHC_{slow} and MHC_{fast}, no effect of levosimendan on force was observed at any of the concentrations tested (Figure 2A-B). Muscle of these *NEB*-NM patients is nebulin-deficient (as reported previously (de Winter et al., 2013)). To verify whether an effect of levosimendan on force was blunted by nebulin-deficiency of *NEB*-NM muscle fibers, we also performed dose-response experiments on $CTRL_{slow}$ and $CTRL_{fast}$ muscle fibers at ~40% Fmax. Again, at none of the concentrations tested an effect of levosimendan on muscle fiber force was observed (Figure 2C-D).

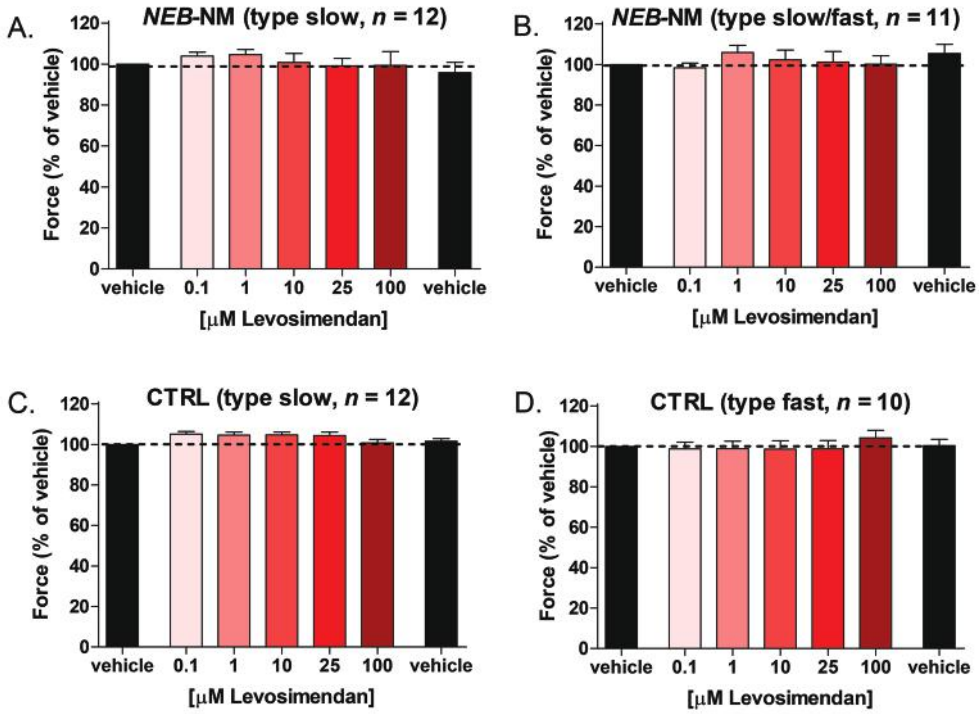

Figure 2

The effect of incremental concentrations of levosimendan on submaximal force (~40% of maximal force) of *NEB*-NM slow-twitch (A) and mixed (B) muscle fibers. Prior to and directly after exposure to the levosimendan concentrations. fibers were exposed to vehicle to rule out confounding effects of force rundown during the protocol. Note that levosimendan did not increase force compared to vehicle. Similar results were observed in slow-twitch (C) and fast-twitch (D) muscle fibers of control subjects.

Force-pCa curve

The dose-response experiments were performed at a single pCa, and

therefore we also studied the effect of levosimendan on fiber force at a range of calcium concentrations. In *NEB*-NM muscle fibers, no shift of the force-pCa curve was observed upon exposure to 100 µM levosimendan (Figure 3A-B), as reflected by no change in the pCa_{50} value (5.52 ± 0.01 vs. 5.53 ± 0.02, levosimendan in vehicle vs. vehicle alone respectively), and no change in nH, a measure of cooperativity of activation (2.06 ± 0.16 vs. 2.07 ± 0.12, levosimendan in vehicle vs. vehicle alone respectively).

Thus, we observed no effect of levosimendan on muscle fiber force in *NEB*-NM and CTRL skeletal muscle fibers, neither at a submaximal calcium level using incremental levosimendan concentrations nor at incremental calcium concentrations in the presence of levosimendan.

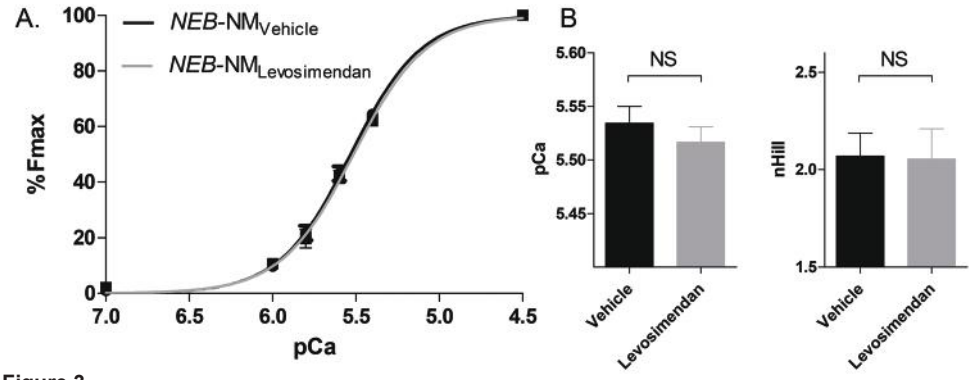

Figure 3

(A) Levosimendan (100 µM) did not affect the force-pCa relation of muscle fibers of *NEB*-NM patients, as reflected by the unaltered pCa50 (B, left panel) and nHill (B, right panel).

The effect of levosimendan on force in human cardiomyocytes

As previous work showed that levosimendan augments submaximal force in cardiomyocytes (Edes et al., 1995), we next studied whether – in our hands – levosimendan affects submaximal force in cardiomyocytes (see Figure 4A for a typical force traces). These experiments revealed a significant dose-dependent increase of submaximal force in human cardiomyocytes at levosimendan concentrations of 1 µM (115 ± 2 % of vehicle), 25 µM (125 ± 4 % of vehicle) and 100 µM (131 ± 8 % of vehicle) (Figure 4B). Thus, we confirmed the efficacy of levosimendan in human cardiomyocytes.

Slow skeletal/cardiac troponin C levels in skeletal muscle fibers of NEB-NM patients

Levosimendan exerts its calcium-sensitizing effect by binding to slow skeletal/

cardiac troponin C. As we observed no effect of levosimendan in slow-twitch skeletal muscle fibers, we tested whether these fibers indeed expressed slow skeletal/cardiac troponin C isoforms. Figure 5 shows that *NEB*-NM_{slow} muscle fibers, *NEB*-NM_{mixed} muscle fibers and $CTRL_{slow}$ muscle fibers express the slow skeletal/cardiac troponin C isoform. Thus, slow skeletal/cardiac troponin C, the isoform through which levosimendan exerts its effect, was abundantly expressed in *NEB*-NM and $CTRL_{slow}$ muscle samples.

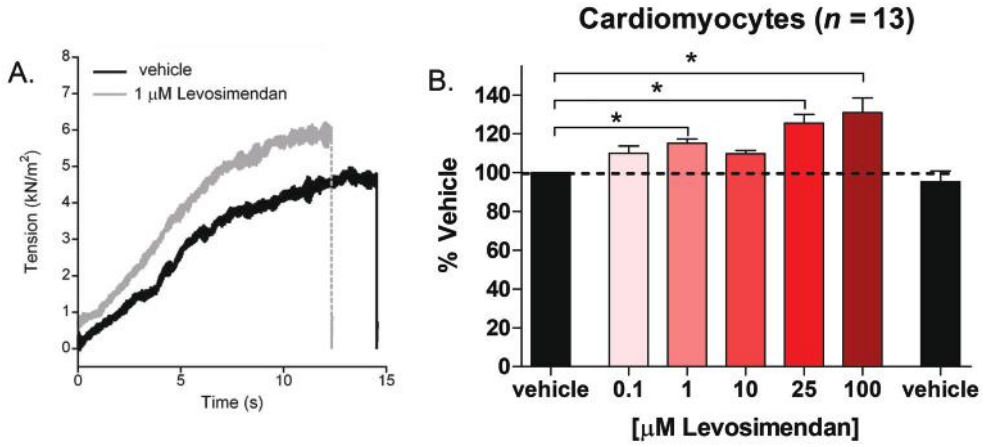

Figure 4

(A) Typical force trace of a human cardiomyocyte. Force increases while exposing the cardiomyocyte to an experimental solution with submaximal exogeneous calcium levels (pCa 6.5). Relaxation is induced by exposing the cardiomyocyte to an experimental solution with a very low calcium concentration (pCa 9.0). (B) The effect of incremental concentrations of levosimendan on submaximal force (~40% of maximal force) of human cardiomyocytes. Prior to and directly after exposure to the levosimendan concentrations cardiomyocytes were exposed to vehicle to rule out confounding effects of force rundown during the protocol. Note that at various concentrations (1, 25, and 100 μM) levosimendan significantly increased submaximal force.

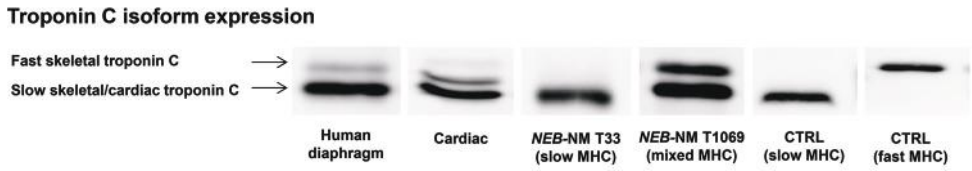

Figure 5

Western blot example, with anti-TnC antibody, including muscle homogenates of human diaphragm muscle (which is known to contain both slow skeletal/cardiac troponin C and fast skeletal troponin C), human left ventricle (which also contains slow skeletal/cardiac troponin C), and quadriceps muscle of *NEB*-NM patients (biopsy IDs T33 and T1069 are shown) and healthy controls. Note that slow skeletal/cardiac troponin C is abundant in *NEB*-NM muscle.

DISCUSSION

A reduced calcium-sensitivity of force generation contributes to muscle weakness in *NEB*-NM muscle. Therefore, in the present study we aimed to test the ability of levosimendan, the only calcium sensitizer approved for use in humans, to improve the calcium-sensitivity of force generation in slow-twitch muscle fibers of *NEB*-NM patients. Our findings indicate that levosimendan does not improve the calcium-sensitivity of force generation of slow-twitch muscle fibers isolated from biopsies of *NEB*-NM patients.

Submaximal force generation is lower in muscle fibers from NEB-NM patients compared to those from controls

The severe reductions in force levels generated by fibers of *NEB*-NM patients are caused by contractile deficits due to defects in sarcomeric proteins (Sanoudou and Beggs, 2001), rather than lower neural activation, ineffective excitation-contraction coupling, or other non-contractile defects. Mechanisms that contribute to weakness of muscle fibers in *NEB*-NM include myofibrillar disarray (Lawlor et al., 2011; Ryan et al., 2003), shorter thin filaments (Ottenheijm et al., 2009), altered cross-bridge cycling kinetics (Bang et al., 2009; Chandra et al., 2009), and a reduced calcium-sensitivity of force generation (Chandra et al., 2009; Ottenheijm et al., 2013).

The *NEB*-NM samples studied here were from the same cohort as studied recently by de Winter and coworkers (de Winter et al., 2013). In that study, it was shown that muscle fibers of *NEB*-NM patients have a lower calcium-sensitivity of force generation compared to fibers from control subjects (de Winter et al., 2013). Here, we confirmed these findings on freshly isolated fibers from biopsies of these patients. Figure 1 illustrates that at pCa 5.8 – a pCa that yields submaximal force – the force generated, relative to maximal force, is lower in *NEB*-NM fiber bundles when compared to fibers from control subjects. As discussed previously, the lower calcium-sensitivity of force in *NEB*-NM fibers is likely to be caused, at least in part, by nebulin deficiency (Chandra et al., 2009; Ottenheijm et al., 2013). Note that previous work indicated that muscle fibers in the biopsies of these patients contained ~25% of normal nebulin levels (de Winter et al., 2013).

Levosimendan does not improve the submaximal force of NEB-NM muscle fibers

Targeting the reduced calcium-sensitivity of force is an appealing approach to combat muscle weakness in *NEB*-NM patients. Recently, we tested the ability of a fast skeletal troponin activator to restore force of fast-twitch muscle fibers of NM patients (de Winter et al., 2013) and of a mouse model for *NEB*-NM (Ottenheijm et al., 2013). Fast skeletal troponin activators selectively sensitize the sarcomeres of fast-twitch skeletal muscle fibers to calcium ions by increasing the affinity of fast skeletal troponin C to calcium (Russell et al., 2012). As neuromuscular input results in calcium release in the muscle, the increased calcium-sensitivity will enhance submaximal muscle strength. We have shown that fast skeletal troponin activators augment the *in vitro* contractile strength of muscle fibers of *NEB*-NM patients and *NEB*-NM mice; the calcium-sensitivity of force generation even increased to levels higher than observed in healthy, untreated, control muscle (Ottenheijm et al., 2013; de Winter et al., 2013).

Skeletal muscles are, however, composed of a mixture of fast- and slow-twitch fibers, and their proportion varies between muscles. For instance, in healthy humans, the quadriceps muscle contains approximately fifty percent slow-twitch fibers, while in the soleus muscle more than eighty percent of fibers are of the slow-twitch type. During activation of an individual muscle, first the motor units that comprise of slow-twitch muscle fibers are the first ones recruited. Subsequently, and only if required, the larger motor units that consist of fast-twitch fibers are recruited. In addition, NM patients typically exhibit a shift towards a larger proportion of slow-twitch fibers (North et al., 1997). These factors highlight the therapeutic opportunity of improving the calcium-sensitivity of force of slow-twitch muscle fibers in *NEB*-NM patients.

Levosimendan was developed to increase the calcium-sensitivity of cardiac muscle to enhance contractility in the failing heart (Edes et al., 1995; Sorsa et al., 2003). It binds to slow skeletal/cardiac troponin C, encoded by the *TNNC1* gene, and stabilizes the conformation of the troponin complex (Sorsa et al., 2003). Slow skeletal/cardiac troponin is also the dominant troponin C isoform in slow-twitch skeletal muscle fibers, suggesting that levosimendan could also improve the calcium-sensitivity of slow-twitch muscle fibers. Indeed, recent work showed that slow-twitch diaphragm muscle fibers of patients with chronic obstructive pulmonary disease had an increased submaximal force

after exposure to levosimendan (van Hees et al., 2009). Furthermore, *in vivo* administration of levosimendan improved diaphragm contractility in healthy subjects (Doorduin et al., 2012). More specifically, the latter study showed that levosimendan improved the neuromechanical efficiency and reduced the development of fatigue of the human diaphragm during loading tasks in vivo (Doorduin et al., 2012). These findings highlight that the potential benefit of calcium sensitizers includes not only increased force development, but also increased efficiency by reducing the amount of cytosolic calcium that is required to generate a given level of force. The energy utilization of SERCA accounts for 30-40% of total ATP consumption during muscle contraction (Barclay et al., 2007) (Szentesi et al., 2001). Therefore, the use of a calcium sensitizer has the potential to reduce the amount of calcium that cycles each contraction and thereby reduce muscle fatigue. This might be especially beneficial for the respiratory muscles in patients with NM, considering that respiratory failure due to diaphragm weakness is the main cause of death in neonates with NM (North et al., 1997).

These previous findings with levosimendan provided an impetus to study its effect on slow-twitch muscle fibers of *NEB*-NM fibers. However, to our surprise, we observed no effect of levosimendan on submaximal force of slow-twitch muscle fibers of *NEB*-NM patients (Figures 2 and 3). Similarly, slow-twitch fibers of control subjects showed no response to levosimendan. Note that we also tested levosimendan in slow-twitch human diaphragm muscle fibers – the muscle type that revealed positive results in previous studies (van Hees et al., 2009, 2011) – but we observed no effect on the calcium-sensitivity of force generation (see Additional Figure 1). It should be noted that the lack of a response to levosimendan was not caused by 'defective' levosimendan. We ruled out this possibility by testing the effect of levosimendan on human cardiomyocytes, and in line with extensive previous work (for instance (Edes et al., 1995; Papp et al., 2004; Szilágyi et al., 2004)), we observed a significant increase in the calcium-sensitivity of force after exposure to levosimendan (Figure 4). Furthermore, we evaluated whether slow-twitch muscle fibers of control and *NEB*-NM biopsies contained slow skeletal/cardiac troponin C isoforms. As shown in Figure 5, these fibers did indeed contain slow skeletal/cardiac troponin C. Thus, the absence of a response to levosimendan in slow-twitch muscle fibers was not caused by deficiency of slow skeletal/cardiac troponin C. Unfortunately, we cannot provide a plausible explanation for the discrepancy between our findings and

those from previous studies that did show a response of slow-twitch fibers to levosimendan (van Hees et al., 2009, 2011).

In conclusion, the ex-vivo findings with isolated muscle fibers do not provide rationale for levosimendan as a therapeutic to restore muscle weakness in *NEB*-NM patients. Future studies, to be performed by independent laboratories, should confirm these findings. We stress the importance of searching for compounds that improve the calcium-sensitivity of force of slow-twitch muscle fibers. For instance, future research could test the efficacy of, not yet registered, compounds such as EMD57033 and pimobendan (Ochala, 2010). These compounds may be able to restore muscle force in patients with *NEB*-NM, but also in patients with other neuromuscular disorders.

REFERENCES

Bang M-L, Caremani M, Brunello E, Littlefield R, Lieber RL, Chen J, et al. Nebulin plays a direct role in promoting strong actin-myosin interactions. FASEB J. 2009; 23: 4117–4125.

Bang M-L, Li X, Littlefield R, Bremner S, Thor A, Knowlton KU, et al. Nebulin-deficient mice exhibit shorter thin filament lengths and reduced contractile function in skeletal muscle. J. Cell. Biol. 2006; 173: 905–916.

Barclay CJ, Woledge RC, Curtin N a. Energy turnover for Ca2+ cycling in skeletal muscle. J. Muscle Res. Cell. M. 2007; 28: 259–274.

Castillo A, Nowak R, Littlefield KP, Fowler VM, Littlefield RS. A nebulin ruler does not dictate thin filament lengths. Biophys. J. 2009; 96: 1856–1865.

Chandra M, Mamidi R, Ford S, Hidalgo C, Witt CC, Ottenheijm CA, et al. Nebulin alters cross-bridge cycling kinetics and increases thin filament activation: a novel mechanism for increasing tension and reducing tension cost. J. Biol. Chem. 2009; 284: 30889–30896.

Doorduin J, Sinderby C a, Beck J, Stegeman DF, van Hees HWH, van der Hoeven JG, et al. The calcium sensitizer levosimendan improves human diaphragm function. Am. J. Resp. Crit. Care 2012; 185: 90–95.

Edes I, Kiss E, Kitada Y, Powers FM, Papp JG, Kranias EG, et al. Effects of Levosimendan, a Cardiotonic Agent Targeted to Troponin C, on Cardiac Function and on Phosphorylation and Ca2+ Sensitivity of Cardiac Myofibrils and Sarcoplasmic Reticulum in Guinea Pig Heart. Circ. Res. 1995; 77: 107–113.

Follath F, Cleland J, Just H, Papp J, Scholz H, Peuhkurinen K, et al. Efficacy and safety of intravenous levosimendan compared with dobutamine in severe low-output heart failure (the LIDO study): a randomised double-blind trial. Lancet 2002; 360: 196–202.

Garg A, O'Rourke J, Long C, Doering J, Ravenscroft G, Bezprozvannaya S, et al. KLHL40 deficiency destabilizes thin filament proteins and promotes nemaline myopathy. J. Clin. Invest. 2014; 124: 3529–3539.

Gokhin D, Bang M. Reduced thin filament length in nebulin-knockout skeletal muscle alters isometric contractile properties. Am. J. Resp. Crit. Care 2009; 296: 1123–1132.

Gupta VA, Beggs AH. Kelch proteins: emerging roles in skeletal muscle development and diseases. Skelet. Muscle 2014; 4: 11.

Gupta VA, Ravenscroft G, Shaheen R, Todd EJ, Swanson LC, Shiina M, et al. Identification of KLHL41 Mutations Implicates BTB-Kelch-Mediated Ubiquitination as an Alternate Pathway to Myofibrillar Disruption in Nemaline Myopathy. Am. J. Hum. Genet. 2013; 93: 1108–17.

van Hees H, Andrade Acuña G, Linkels M, Dekhuijzen P, Heunks L. Levosimendan improves calcium sensitivity of diaphragm muscle fibres from a rat model of heart failure. Br. J. Pharmacol. 2011; 162: 566–573.

van Hees HWH, Dekhuijzen PNR, Heunks LM. Levosimendan enhances force generation of diaphragm muscle from patients with chronic obstructive pulmonary disease. Am. J. Resp. Crit. Care 2009; 179: 41–47.

Lawlor MW, Ottenheijm CA, Lehtokari V-L, Cho K, Pelin K, Wallgren-Pettersson C, et al. Novel mutations in NEB cause abnormal nebulin expression and markedly impaired muscle force generation in severe nemaline myopathy. Skelet. Muscle. 2011; 1: 23.

Lehtokari V-L, Kiiski K, Sandaradura SA, Laporte J, Repo P, Frey JA, et al. Mutation update: the spectra of nebulin variants and associated myopathies. Hum. Mutat. 2014; 35: 1418–26.

North KN, Laing NG, Consortium I. Nemaline myopathy: current concepts. The ENMC International Consortium and Nemaline Myopathy. J. Med. Genet. 1997; 34: 705–713.

Ochala J. Ca2+ sensitizers: An emerging class of agents for counterbalancing weakness in skeletal muscle diseases? Neuromusc. Dis. 2010; 20: 98–101.

Olivé M, Goldfarb LG, Lee H-S, Odgerel Z, Blokhin A, Gonzalez-Mera L, et al. Nemaline myopathy type 6: clinical and myopathological features. Muscle Nerve 2010; 42: 901–7.

Ottenheijm CAC, Buck D, de Winter JM, Ferrara C, Piroddi N, Tesi C, et al. Deleting exon 55 from the nebulin gene induces severe muscle weakness in a mouse model for nemaline myopathy. Brain 2013; 136: 1718–31.

Ottenheijm CAC, Hooijman P, DeChene ET, Stienen GJ, Beggs AH, Granzier H. Altered myofilament function depresses force generation in patients with nebulin-based nemaline myopathy (NEM2). J. Struct. Biol. 2010; 170: 334–343.

Ottenheijm CAC, Witt CC, Stienen GJ, Labeit S, Beggs AH, Granzier H. Thin filament length dysregulation contributes to muscle weakness in nemaline myopathy patients with nebulin deficiency. Hum. Mol. Genet. 2009; 18: 2359–2369.

Papp Z, Van Der Velden J, Borbély A, Édes I, Stienen GJM. Effects of Ca 2+ -Sensitizers in Permeabilized Cardiac Myocytes from Donor and End-Stage Failing Human Hearts. J. Muscle Res. Cell Motil. 2004; 25: 219–224.

Pappas CT, Krieg PA, Gregorio CC. Nebulin regulates actin filament lengths by a stabilization mechanism. J. Cell. Biol. 2010; 189: 859–870.

Pelin K, Hilpelä P, Donner K, Sewry C, Akkari PA, Wilton SD, et al. Mutations in the nebulin gene associated with autosomal recessive nemaline myopathy. Proc. Natl. Acad. Sci. 1999; 96: 2305–2310.

Ravenscroft G, Miyatake S, Lehtokari V-L, Todd EJ, Vornanen P, Yau KS, et al. Mutations in KLHL40 Are a Frequent Cause of Severe Autosomal-Recessive Nemaline Myopathy. Am. J. Hum. Genet. 2013; 93: 6–18.

Russell AJ, Hartman JJ, Hinken AC, Muci AR, Kawas R, Driscoll L, et al. Activation of fast skeletal muscle troponin as a potential therapeutic approach for treating neuromuscular diseases. Nat. Med. 2012; 18: 452–455.

Ryan MM, Ilkovski B, Strickland CD, Schnell C, Sanoudou D, Midgett C, et al. Clinical course correlates poorly with muscle pathology in nemaline myopathy. Neurology 2003; 60: 665–673.

Sambuughin N, Swietnicki W, Techtmann S, Matrosova V, Wallace T, Goldfarb L, et al. KBTBD13 interacts with Cullin 3 to form a functional ubiquitin ligase. Biochem. Biophys. Res. Commun. 2012; 421: 743–9.

Sambuughin N, Yau KS, Olivé M, Duff RM, Bayarsaikhan M, Lu S, et al. Dominant mutations in KBTBD13, a member of the BTB/Kelch family, cause nemaline myopathy with cores. Am. J. Hum. Genet. 2010; 87: 842–847.

Sanoudou D, Beggs AH. Clinical and genetic heterogeneity in nemaline myopathy-a disease of skeletal muscle thin filaments. Trends Mol. Med. 2001; 7: 362–368.

Sorsa T, Pollesello P, Permi P, Drakenberg T, Kilpeläinen I. Interaction of levosimendan with cardiac troponin C in the presence of cardiac troponin I peptides. J. Mol. Cell. Cardiol. 2003; 35: 1055–1061.

Sun Y-B, Irving M. The molecular basis of the steep force-calcium relation in heart muscle. J. Mol. Cell. Cardiol. 2010; 48: 859–65.

Szentesi P, Zaremba R, van Mechelen W, Stienen GJ. ATP utilization for calcium uptake and force production in different types of human skeletal muscle fibres. J. Physiol. 2001; 531: 393–403.

Szilágyi S, Pollesello P, Levijoki J, Kaheinen P, Haikala H, Édes I, et al. The effects of levosimendan and OR-1896 on isolated hearts, myocyte-sized preparations and phosphodiesterase enzymes of the guinea pig. Eur. J. Pharmacol. 2004; 486: 67–74.

van der Velden J, Klein L, van der Bijl M, Huybregts M, Stooker W, Witkop J, et al. Force production in mechanically isolated cardiac myocytes from human ventricular muscle tissue. Cardiovasc. Res. 1998; 38: 414–423.

Wallgren-Pettersson C, Laing NG. Report of the 70th ENMC International Workshop: Nemaline myopathy, 11-13 June 1999, Naarden, The Netherlands. Neuromuscul. Disord. 2000; 10: 299–306.

de Winter JM, Buck D, Hidalgo C, Jasper JR, Malik FI, Clarke NF, et al. Troponin activator augments muscle force in nemaline myopathy patients with nebulin mutations. J. Med. Genet. 2013; 50: 383–92.

Witt CC, Burkart C, Labeit D, McNabb M, Wu Y, Granzier H, et al. Nebulin regulates thin filament length, contractility, and Z-disk structure in vivo. EMBO J. 2006; 25: 3843–3855.

Yuen M, Sandaradura SA, Dowling JJ, Kostyukova AS, Moroz N, Quinlan KG, et al. Leiomodin-3 dysfunction results in thin filament disorganization and nemaline myopathy. J. Clin. Invest. 2014; 124

Zaremba R, Merkus D, Hamdani N, Lamers JMJ, Paulus WJ, dos Remedios C, et al. Quantitative analysis of myofilament protein phosphorylation in small cardiac biopsies. Proteomics – Clin. Appl. 2007; 1: 1285–1290.

SUPPLEMENT

Dose-force response experiments were performed according to the protocol reported in the methods section. Single muscle fibers were isolated from a diaphragm muscle biopsy that was obtained from a patient that underwent resection of an early lung malignancy (male, age 64). The biopsy protocol was approved by the institutional review board at VU University Medical Center Amsterdam (#2010/69). Written informed consent was obtained from the patient.

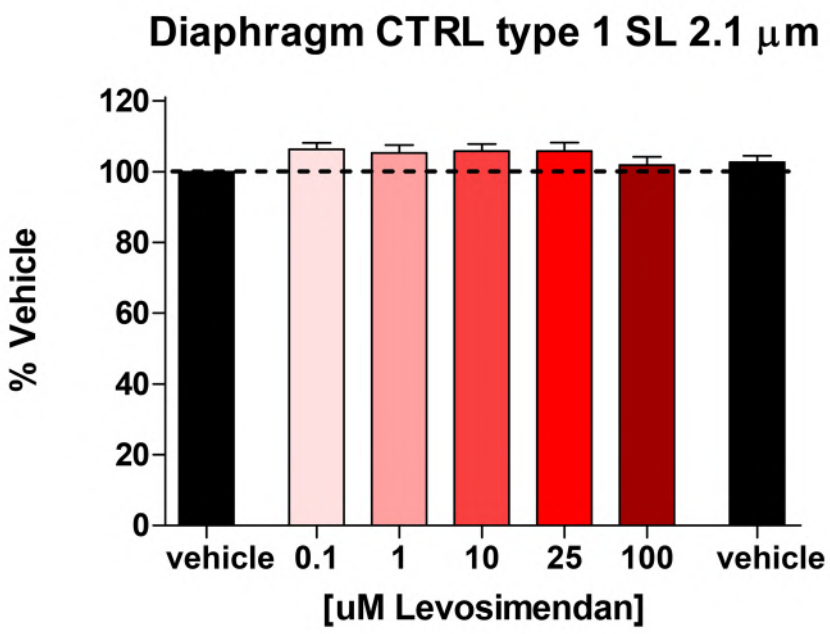

Supplemental Figure 1
The effect of incremental concentrations of levosimendan on submaximal force (pCa 5.8, which yielded ~40% of maximal force) of individual slow-twitch fibers from human diaphragm (n = 7).

CHAPTER 7

THE FAST SKELETAL MUSCLE TROPONIN ACTIVATOR, CK-2066260, AMELIORATES WEAKNESS OF MOUSE FAST MUSCLE FIBERS THAT ARE DEFICIENT IN NEBULIN.

Eun-Jeong Lee, Josine M. De Winter, Jeffrey R Jasper, Fady I Malik, Siegfried Labeit, Coen C.A. Ottenheijm and Henk Granzier.

PLoS ONE, 2013

ABSTRACT

Background | The effect of the fast skeletal muscle troponin activator, CK-2066260, on calcium-induced force development was studied in skinned fast skeletal muscle fibers from wildtype (WT) and nebulin deficient (NEB KO) mice. Nebulin is a sarcomeric protein that has recently been shown to play crucial roles in force development. When nebulin is absent (NEB KO mouse) or is present at low levels (nemaline myopathy (NM) patients with *NEB* mutations), severe muscle weakness ensues. The goal of this work was to study whether fast skeletal troponin activation might be a potential therapeutic mechanism to increase muscle strength in nebulin deficient muscle.

Methods & Results | We measured tension–pCa relations with and without added CK-2066260. Maximal active tension in NEB KO tibialis cranialis fibers in the absence of CK-2066260 was ~60% less than in WT fibers, consistent with earlier work. CK-2066260 at mM levels shifted the tension-calcium relationship leftwards in skinned muscle fibers, with the largest relative increase (up to 8-fold) at low to intermediate calcium levels. This effect was present in both WT and NEB KO fibers; at pCa levels above ~6.0 (i.e., calcium concentrations <1 mM), CK-2066260 increased tension of NEB KO fibers to beyond that of WT fibers. Crossbridge cycling kinetics were studied by measuring Ktr (rate constant of force redevelopment following a rapid shortening/restretch). CK-2066260 increased K_{tr} in NEB KO fibers only. We also studied the sarcomere length (SL) dependence of the CK-2066260 effect (SL 2.1 mm and 2.6 mm) and found that in the NEB KO fibers, CK-2066260 had a larger effect on calcium sensitivity at the long SL.

Interpretation | We conclude that fast skeletal muscle troponin activation is a potential therapeutic mechanism for increasing force in NM and other skeletal muscle diseases with loss of muscle strength.

INTRODUCTION

The skeletal muscle sarcomere is a highly organized and intricate structure that consists of a regular array of actin-based thin filaments that interdigitate with myosin-based thick filaments; these filaments slide past each other as muscles contract, a process driven by the mechano-chemical cycling of the thick-filament based myosin cross-bridges (Huxley, 2004). The force level that is generated by the sarcomere depends on the degree to which the thin and thick filaments overlap, the degree of thin filament activation, and on the kinetics of the cross-bridge cycle that determine the fraction of the cross-bridges that develops force. Recent studies on mouse models deficient in nebulin (Bang et al., 2006; Chandra et al., 2009; Witt et al., 2006) indicate that the large filamentous protein nebulin plays an important role in each of these force determinants and, importantly, that when nebulin levels are reduced in nemaline myopathy (NM) patients, severe muscle weakness ensues (Lawlor et al., 2011; Ottenheijm et al., 2009, 2010).

The C-terminus of nebulin is anchored at the Z-disk, the majority of the nebulin filament is co-extensive with the thin filament, and the N-terminus is near the pointed end of the thin filament (Fig. 1A) (Castillo et al., 2009; Kruger, 1991; Pappas et al., 2010; Wright et al., 1993). The human *NEB* (nebulin) gene is large, containing 183 exons in human that encode a ~800 kDa protein (Kazmierski et al., 2003; Labeit and Kolmerer, 1995). The bulk of the molecule is comprised of small modules that are organized into seven-module super-repeats that match the 38.5 nm repeat of the actin filament (J P Jin and Wang, 1991; Jian Ping Jin and Wang, 1991; Kazmierski et al., 2003; Labeit and Kolmerer, 1995). This arrangement allows each nebulin module to interact with a single actin monomer, and each nebulin super-repeat to associate with a single tropomyosin/troponin complex (J P Jin and Wang, 1991; Jian Ping Jin and Wang, 1991). Recent work indicates that nebulin's C-terminus interacts with the actin nucleating protein N-WASP, that this interaction plays an important role in skeletal muscle hypertrophy, and that this process is controlled by phosphorylation of nebulin's serine rich domain (Takano et al., 2010).

Studies using nebulin KO mouse models have shown that thin filaments are shorter in nebulin deficient muscle, indicating that nebulin contributes to thin filament length specification (Bang et al., 2006; Witt et al., 2006). Furthermore, on the descending limb of the force-sarcomere length relationship, the shorter

thin filaments of nebulin deficient muscle give rise to reduced filament overlap and reduced force (Bang et al., 2006; Granzier et al., 1991; Ottenheijm et al., 2009). Finally, nebulin plays a role in increasing calcium sensitivity and, importantly, in increasing the fraction of the cross-bridges that generates force, by altering cross-bridge cycling kinetics (Bang et al., 2009; Chandra et al., 2009). Subsequent studies on biopsies from NM patients support that nebulin's compromised role in augmenting force generation contributes to the muscle weakness of nebulin-based NM patients (Chandra et al., 2009; Ottenheijm et al., 2010). Therapeutic approaches to lessen force impairment in NM patients are currently unavailable.

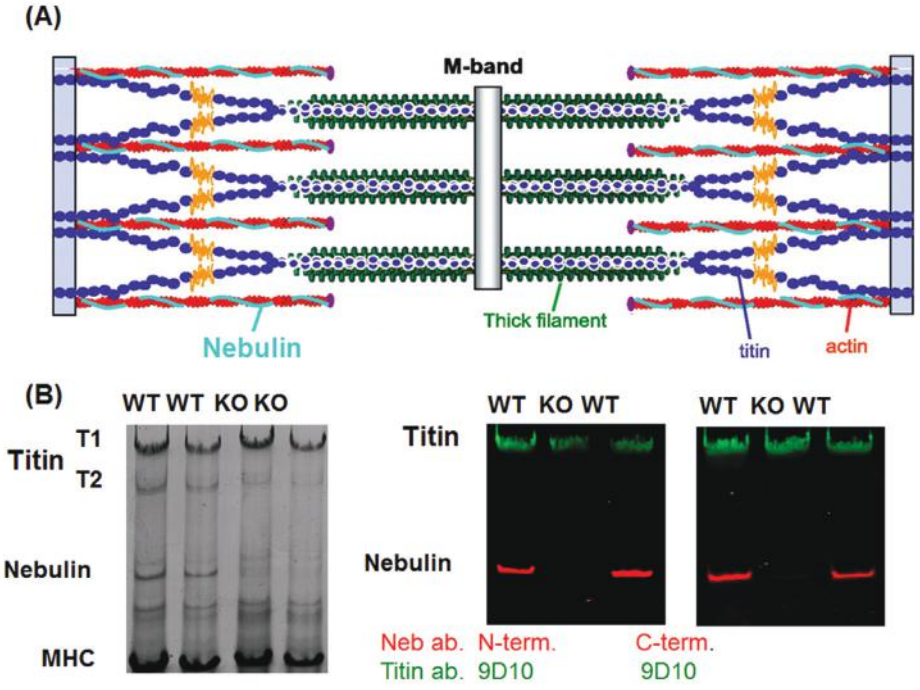

Figure 1 Location of nebulin in the sarcomere and protein expression in WT and NEB KO mouse TC muscle

(A) Nebulin is a large sarcomeric protein that is coextensive with the actin filament. (B) Protein expression in WT and NEB KO mouse TC muscle. (1% agarose gel). Left coomassie blue stained gel. Right: Westernblot with anti-titin antibody 9D10 (green) and anti-nebulin antibody raised to nebulin's N-terminus (left) and anti-nebulin antibody raised to nebulin's C-terminus. Nebulin is a ~800 kDa protein that is only present in WT mice

A class of fast skeletal troponin activators was recently discovered that can augment force development of skeletal muscle by slowing the dissociation rate of calcium from the troponin complex and enhancing cross-bridge formation at a given calcium concentration (Russell et al., 2012). Given that deficits in force production described above in NM might be improved by this mechanism of action, the purpose of this study was to establish the effect of the fast skeletal troponin activator, CK-2066260, on force generation in 1) skinned fibers from WT mice, and 2) skinned fibers from NEB-KO mice.

METHODS

Ethics Statement

Experiments were approved by the University of Arizona Institutional Animal Care and Use Committee (protocol 07-090) and followed the U.S. National Institutes of Health "Using Animals in Intramural Research" guidelines for animal use.

Animal model

We used wildtype (WT) and nebulin-deficient (NEB KO) mice in which the nebulin gene is inactivated by targeting its promoter region (Witt et al., 2006). Inactivation of the nebulin gene and genotyping of mice was as described previously (Witt et al., 2006). NEB KO mice die at early age (Witt et al., 2006) and we were restricted to comparing ~1 week old WT and NEB KO mice. We focused our studies on the tibialis cranialis (TC) muscle which is a fast fiber muscle type that is convenient to use for skinned fiber studies. Mice were anesthetized using isoflurane and the TC muscles were dissected. For the mechanical studies, the muscle was chemically skinned using 1% Triton X-100 in relaxing solution. For protein expression studies, muscles were quick-frozen in liquid nitrogen and stored at -80 oC. In addition to PCR genotyping, absence of nebulin expression was also confirmed by 1% agarose protein gels (Fig. 1B shows examples).

Muscle preparations

Skinned TC muscles were dissected into small strips (cross-sectional area (CSA) ~0.02 mm^2; length ~1.5mm) and small aluminum clips were glued at each end of the muscle strip. Note that fiber bundles were used for ease of experimentation (single fibers are only ~ 10 μm in diameter). Because the bundles contain different types that express neonatal myosin, MHC type IIA and IIB, and small amounts of MHC type I (Chandra et al., 2009), to know

the effect of CK-2066260 on the individual fiber types requires future follow-up studies at the single fiber level. The muscles were attached to a force transducer (model 405A, Aurora Scientific) and a length controller (model 322C, Aurora Scientific) (Muhle-Goll et al., 2001). We used a custom-designed experimental setup (model 802D, Aurora Scientific) with an experimental stage that was mounted on top of an inverted microscope with 8 isolated wells that were pre-loaded with activating solutions that contain a range of calcium concentrations. The fiber bundles were visualized via a CCD camera, and from the video images the sarcomere length was measured on-line using a spatial autocorrelation function (model 901, Aurora Scientific). The experimental stage was temperature controlled at 15 ^{o}C. The thickness and width of the preparation were measured and the CSA was calculated by assuming an elliptical cross-section. The CSA was used to convert measured forces into tension (in mN/mm^2).

Skinned muscle solutions

We used relaxing solution (RS), pre-activating solution (Pre-A), and maximal activating solution (AS, pCa 4.5). Sub-maximal activating solutions were obtained by mixing RS and AS according to Fabiato and Fabiato (Fabiato and Fabiato, 1979). All solutions contained the following: BES, 40 mM; DTT, 1 mM; creatine phosphate (PCr), 33 mM; creatine phosphokinase (CPK), 200 U/ml; the ionic strength was adjusted to 180mM with K-proprionate; pH 7.0 at 15°C. Relaxing solution, pre-activating solution and activating solution contains 6.9, 6.7, 6.6 mM MgCl2, respectively. For Na-ATP the values were 6.0, 6.0 and 6.2 mM, for EGTA 10.0, 1.0 and 0.0 mM, for Ca-EGTA 0, 0 and 10 mM and for K-proprionate 3.3, 30.4, and 2.1 mM, respectively.

Fast skeletal troponin activator

CK-2066260 belongs to a class of fast skeletal troponin activators discovered by Cytokinetics (Russell et al., 2012) and was provided by the Research and Early Development department at Cytokinetics (South San Francisco, CA). CK-2066260 selectively binds to and activates the fast skeletal troponin complex by increasing its sensitivity to calcium. CK-2066260 was added to all experimental solutions (relaxing, pre-activating and activating solutions) from a DMSO stock (final DMSO concentration 1%). Control solutions contained 1% DMSO with no CK-2066260 (vehicle control).

Tension-pCa measurements

Fiber bundles while in relaxing solution were stretched to either sarcomere length (SL) 2.1 μm or 2.6 μm, were held at the extended length for 7 min, and were then released. During the hold phase the preparation was first incubated in a pre-activating solution and was then activated in the following sequence pCa 6.4, 6.25, 6.1, 5.95, 5.75 and 4.5 (see Fig. 2A). The muscle was then relaxed again and released. To study the length-dependence of activation (LDA), we first obtained a tension-pCa curve at SL of 2.1μm, then a relation at 2.6 μm both without CK-2066260 and after that the same sequence was repeated in the presence of 10 μM CK-2066260. Experiments were also performed in which the tension-pCa curves were constructed by activating the fiber bundles at a certain pCa solution (randomly selected) followed by relaxation and a repeat with activation at a different pCa.

Active tension was measured at the plateau of each activation (Fig 2A). Active tension was normalized by the maximal active tension at pCa 4.5 (Tmax), and plotted against the pCa to determine the tension-pCa curve. The tension-pCa curves were fit to the Hill equation: T/Tmax (relative tension) = $[Ca^{2+}]^{nH}$ / (K+$[Ca^{2+}]^{nH}$), where nH is the Hill coefficient, and pCa_{50} (pCa value that results in 50% of the maximal activate tension measured at pCa 4.5) was calculated as (-logK)/nH. In the LDA experiments, we determined the differences between pCa_{50} of the tension-pCa curves measured at SL 2.1 and 2.6 μm and used this as an index of length-dependent activation (i.e. ΔpCa_{50}). Rundown was determined from a maximal activation (pCa 4.5; SL 2.1 μm) prior to measurement of the first tension-pCa curve and once more after the last curve (typically we measured 4 curves). Experiments in which rundown was less than 10% were accepted in this study (on average rundown was absent).

Ktr measurement

The rate constant of tension redevelopment (K_{tr}) was measured at pCa 5.95, 5.75 and 4.5 by using the large release, rapid shortening, rapid re-stretch approach (Brenner, 1988). First, the muscle preparation was activated and once the steady-state was reached, the preparation was rapidly shortened by 20% of the initial length, which reduced tension to zero. This was followed by unloaded shortening lasting 30 msec. The remaining bound cross-bridges were mechanically detached by rapidly (1 msec) re-stretching the muscle fiber bundles to its original length, after which tension redevelops.

Measurements were performed by controlling fiber length as the quality of the striation patterns did not permit control of sarcomere length. Ktr was determined by fitting the rise of tension redevelopment following re-stretch by a mono-exponential equation: $T=T_{ss}(1^{-e\text{-}Ktr.t})$, where T is tension at time t, T_{ss} is steady-state tension, and K_{tr} is the rate constant of tension redevelopment.

Protein gels and Westernblots

The anti-titin antibody (9D10 (Wang and Greaser, 1985; Wang, 1988)) was obtained from the Developmental Studies Hybridoma Bank, University of Iowa. For details on nebulin antibodies, see acknowledgements. Nebulin antibodies were obtained from Myomedix, Mannheim Germany (www.myomedix.com). For additional technical details, please see (Lahmers et al., 2004; Ottenheijm et al., 2006; Warren et al., 2003).

Statistical analysis

Data are shown as mean ± SEM. Paired or unpaired t-tests or ANOVA was used, as appropriate, to test for statistical significance with $p<0.05$.

RESULTS

We performed tension-pCa studies on skinned muscle fiber bundles from ~1 week old WT and NEB KO mice (for protocol see Fig. 2A) and studied the effect of the fast skeletal muscle activator CK-2066260 on tension. The initial studies were performed at a sarcomere length (SL) of 2.1 μm because at this sarcomere length WT and NEB KO fibers have a similar degree of filament overlap (Chandra et al., 2009), which simplifies interpretation of results. We first established the CK-2066260 dose-response curve by measuring active tension in skinned WT fibers at pCa 6.25 and adding CK-2066260 at concentrations that ranged from 0-20 μM. Tension in the absence of CK-2066260 was ~25% of the maximal tension at pCa 4.5 and the addition of CK-2066260 increased tension in a dose-dependent manner (Fig. 2B) with 20 μM CK-2066260 resulting in a tension that was near the maximal tension, Tmax (pCa 4.5). Thus, in the μM range CK-2066260 is highly effective in increasing submaximal active tensions of wildtype mouse skeletal muscle.

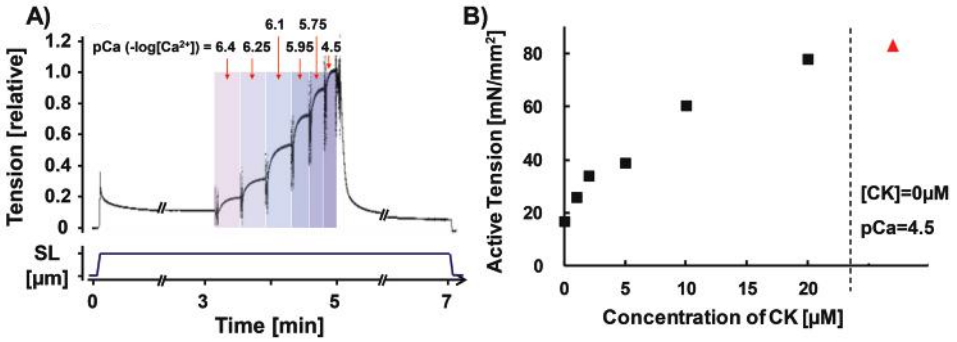

Figure 2 Experimental Protocol and effect of CK-2066260 on active tension at submaximal activation

(A) Skinned skeletal muscle fibers (TC muscle) were stretched, held for 7 min, and were then released During the hold phase, the muscle was exposed to various pCa activating solutions, and was then relaxed again. (B) Effect of CK-2066260 on active tension at submaximal activation level (pCa=6.25). Active tensions at a range of CK-2066260 concentrations (black symbols). The maximal active tension (pCa 4.5) at 0 µM CK-2066260 is shown to the right in red.

Effect of CK-2066260 on calcium sensitivity of active tension

We measured the full tension – pCa relations in WT and NEB KO fiber bundles, normalized tensions to Tmax and used the normalized curves to derive the pCa50 (pCa that results in a tension that is 50% of Tmax). Tmax in KO fiber bundles was only 42% of WT fibers (Table 1, 0 µM CK-2066260). This finding is consistent with previous work on nebulin deficient mouse muscle that reported the tension in KO fibers to be ~45% of WT fibers (Chandra et al., 2009). In the present study, calcium sensitivity was found to be increased in the NEB KO (Table 1), whereas previously a reduction was found (Chandra et al., 2009). Increased calcium sensitivity might be explained by the upregulation of a low level (~10%) of slow skeletal muscle TnT (sTnT) and slow TnI (sTnI) in nebulin KO TC muscle (Chandra et al., 2009), or a change in their post-translational modification. This notion is supported by experiments in which in both NEB KO and WT fibers the native troponin complex was replaced by recombinant troponin and calcium sensitivity was reduced (Chandra et al., 2009). Next we studied the effect of CK-2066260 on the tension-pCa curve and selected, based on the measured dose-response curve, 5 and 10 µM CK-2066260. In both genotypes CK-2066260 substantially shifted the tension-calcium relationship to the left as compared to vehicle alone (0 µM CK-2066260), with the most prominent tension increase observed at lower activation levels, while peak tension (Tmax) was not affected (Fig. 3A). To highlight the effect of CK-2066260 on

submaximal active tension, we plotted the relative increase in active tension in the presence of 10 µM CK-2066260 over that measured in absence of CK-2066260, at various pCa levels (Fig. 3B). The increase in tension was ~800% at pCa 6.4 and decreased as calcium concentration increased, with only a small ~5% increase in WT and a ~10% increase in KO at pCa 4.5 ($p > 0.05$ compared to the absence of CK-2066260). There were no differences between the genotypes in the relative increase in tension in CK-2066260. In summary, CK-2066260 was highly effective in increasing active tension levels with very large effects at low to intermediate levels of activation.

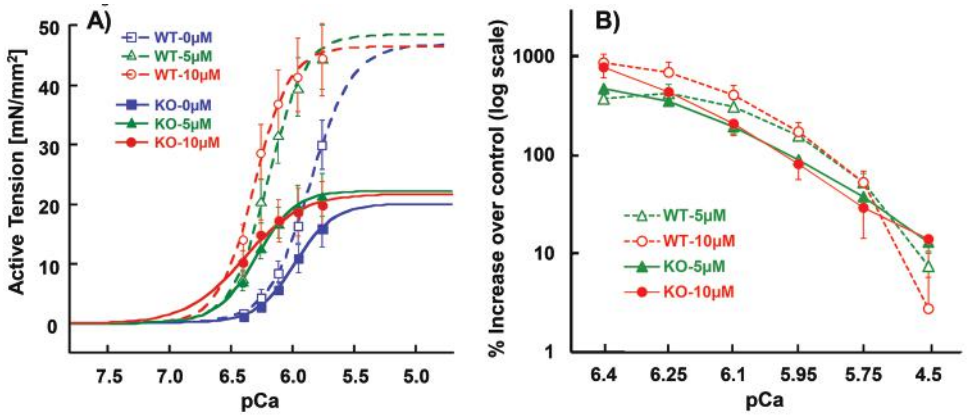

Figure 3 Tension–pCa relations in WT and NEB KO skinned TC muscle fibers
(A) Average active tension-pCa curves in WT (open symbols, dashed) and KO (closed symbols, solid) mice with 0 (blue), 5 µM (green) and 10 µM (red) CK-2066260 at SL = 2.1 µm. Curves in CK were shifted to the left in both WT and KO, i.e. calcium sensitivity is increased. Note that at pCa>6.0, CK-2066260 increased active tension of NEB-KO muscle beyond that of WT. (B) Relative active tension increase (plotted on a log scale) in 5 and 10 µM of CK over 0 µM of CK at various pCa levels. Regardless of genotype, active tensions were significantly increased from ~800% at the pCa 6.4 to ~10% at pCa 4.5. Results from five WT and five KO mice.

In WT muscle fibers, pCa50 was significantly increased by 0.34 and 0.45 pCa units in 5 µM and 10 µM CK-2066260, respectively. In nebulin deficient fibers, a similar increase occurred with values of 0.31 and 0.45 pCa units (Table 1). We also determined the cooperativity of activation (Hill coefficient, nH) and found this to be unchanged (Table 1). Thus, CK-2066260 alters the activation characteristics of mouse skinned fibers by greatly increasing calcium sensitivity.

Genotype/parameter	CK-2066260 concentration		
	0 μM	**5 μM**	**10 μM**
WT- T_{max} (mN/mm^2)	46.6±5.5	49.7±5.1	47.8±6.0
KO- T_{max} (mN/mm^2)	19.9±4.0**	22.1±4.1**	22.2±4.5**
WT- pCa_{50}	5.85±0.04	6.18±0.04# #	6.30±0.04# #√√
Δ from 0 CK (pCa unit)		0.34±0.02	0.45±0.02√√
KO- pCa_{50}	5.98±0.03*	6.29±0.01* # #	6.43±0.05# #√√
Δ from 0 CK(pCa unit)		0.31±0.02	0.45±0.04√
WT- n_H	2.64±0.07	3.21±0.20	3.29±0.34
KO- n_H	2.83±0.15	3.14±0.38	2.16±0.58
WT- Tmax (SL 2.6 μm)	58.7±6.0	NA	66.7±6.4#
KO- Tmax (SL 2.6 μm)	34.0±5.7**	NA	44.5±8.0**# #
WT- nH (SL 2.6 μm)	2.7±0.28	NA	2.31±0.24
KO- nH (SL 2.6 μm)	3.09±0.11	NA	1.47±0.24*# #

Table 1. T_{max} (tension at pCa 4.5); calcium sensitivity (pCa_{50}) and Hill coefficient (n_H) of WT and KO in 0, 5, and 10 μM CK-2066260.

Because all studies were performed in the presence of 1% DMSO (CK-2066260 solvent) we studied whether DMSO itself affects tension. We compared the tension-pCa relation in solutions without and with 1 % DMSO (but no CK-2066260) and measured for each muscle preparation multiple tension-pCa relations (as in our CK-2066260 experiments). DMSO did cause a small increase in active tension, but the same relative increase occurred at all pCa levels. Consequently 1% DMSO did not cause a change in pCa50 nor in nH (measurement of cooperativity) and is therefore a safe concentration to use in our experiments. Finally, we also evaluated whether the activation protocol with progressively increasing calcium levels (explained in Fig. 2A) gave the same results as when performing experiments in which the tension-pCa curves were constructed by activating the fiber bundles by a single pCa solution (randomly selected) followed by relaxation, and repeating this

sequence at different pCa values. Figure S1 shows both protocols gave the same results.

In summary, CK-2066260 increases tension in both WT and nebulin deficient fibers, with large effects at submaximal activation levels. Thus, CK-2066260 is a highly effective calcium sensitizer.

Effect of CK-2066260 on rate constant of tension development (Ktr)
To gain insights in the effect of CK-2066260 on cross-bridge cycling kinetics we measured K_{tr}, the rate constant of force redevelopment following a release/shortening/restretch protocol. This rate constant reflects the sum of the apparent rate constant of conversion of non-force generating to force generating cross-bridges, fapp, and the apparent rate constant of conversion of force generating to non-force generating cross-bridges, gapp (Brenner and Eisenberg, 1986). K_{tr} was measured at three pCa levels (5.95, 5.75 and 4.5) and the effect of 10 μM CK-2066260 was determined. Fig. 4A shows example experiments and Fig. 4B and 4C summarized results of WT (B) and NEB KO (C) fiber bundles. Under all experimental conditions was ktr less in NEB KO than WT fiber bundles. K_{tr} increased with activation level and, importantly, was significantly increased by CK-2066260. The largest effects were present at submaximal activation level where K_{tr} was increased by more than 150% (Fig 4D). These results indicate that in WT and NEB KO fibers CK-2066260 alters cross-bridge cycling kinetics.

Length Dependent Effects of CK-2066260.
Because muscle operates at a range of sarcomere lengths, a separate set of studies was performed in which tension-pCa curves were measured at SL 2.1 μm and 2.6 μm. To keep rundown to a minimum during the experiment we tested only 10 μM CK-2066260, which required a manageable four force-pCa curves per muscle preparation. An increase in SL caused a leftward shift in the tension pCa relation (see the small shifts between the pair of broken lines and between the pair of solid lines in Fig. 5), which reflects the well-known phenomenon of length dependence of activation in striated muscle (John P Konhilas et al., 2002). This SL-induced shift was characterized by determining the delta pCa_{50} (pCa50 at SL 2.6 μm minus pCa_{50} at SL 2.1 μm) and the result is shown in Fig. 6A. The data did not reveal a significant difference between the genotypes. However, within genotype a significant difference was found in the KO fibers as the SL effect was larger in fibers that were exposed to CK-2066260 (Fig 6A).

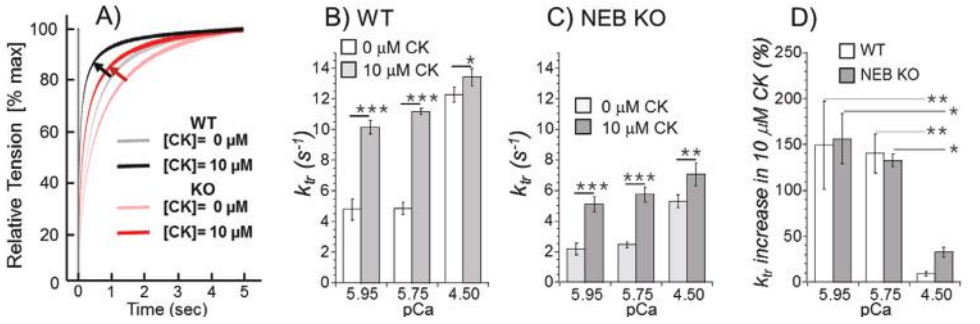

Figure 4 Effect of CK 2066260 on the rate constant of force redevelopment (k_{tr})
(A) Examples of k_{tr} experiments on WT and NEB KO fiber bundles activated at pCa 5.95 before (control) and after the addition of 10 µM CK-2066260. Shown is the tension recovery phase following the re-stretch (see Methods for details). In the presence of 10 µM CK-2066260 (darker traces) tension recovery is faster than in absence of CK-2066260. B) and C) k_{tr} results of WT (B) and NEB KO fibers (C). Addition of 10 µM CK-2066260 increases k_{tr} in both WT and NEB-KO fibers. A two-way ANOVA reveals in WT bundles significant effects of pCa and CK-2066260 on ktr with a significant interaction between pCa and CK ($p<0.001$). The same is the case for the KO data, except that the p-value of the interaction term is $p=0.02$. D) Change in ktr in CK 2066260 (as percentage of control values). Results from six WT and six KO mice.

We also determined the length-dependence of the CK-2066260 effect on calcium sensitivity by determining the deltapCa50 (pCa50 in 10 µM CK-2066260 minus pCa50 in 0 µM CK-2066260, see shift between same color broken and solid curves in Figure 5). The results (Fig. 6B) reveal deltapCa50 values of 0.4-0.6 pCa units, which is several times larger than the values obtained by increasing SL (compare Figure 6B with Figure 6A). Thus compared to SL increase, CK-2066260 is a much more efficacious calcium sensitizer. Furthermore, CK-2066260 at a SL of 2.6 µm increases calcium sensitivity to a significantly higher degree in KO fibers than in WT fibers and the CK-2066260 effect on KO fibers is significantly larger at long SL than at short SL (Fig. 6B). Tmax was increased by CK-2066260 at the long SL in both genotypes (WT: 58.7± 6.0 to 66.7 ± 6.4 mN/mm2; KO: 34.0± 5.7 to 44.5 ± 8.0 mN/mm2 (see Table 1, near bottom)). Finally, we also determined the cooperatively of activation (nH) at SL 2.6 µm and found that CK-2066260 did not affect nH of WT fibers but that nH was reduced in KO fibers (Table 1, bottom two rows).

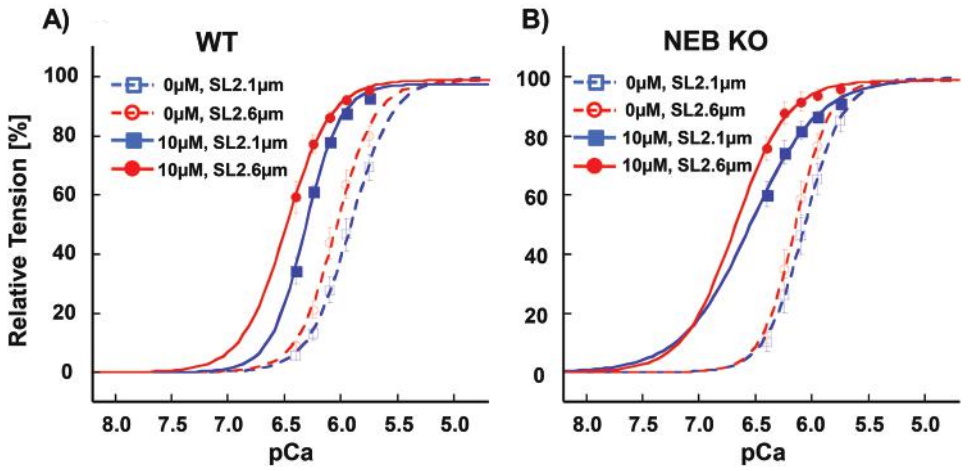

Figure 5 Effect of 10 μM CK-2066260 on tension-pCa curves at short (2.1 μm) and long SL (2.6 μm) Result in WT in A and in NEB KO fibers in B. Increasing SL slightly shifts the curves left-ward (i.e., calcium sensitivity is increased) and CK results in an additional large shift. Results from six WT and six KO mice.

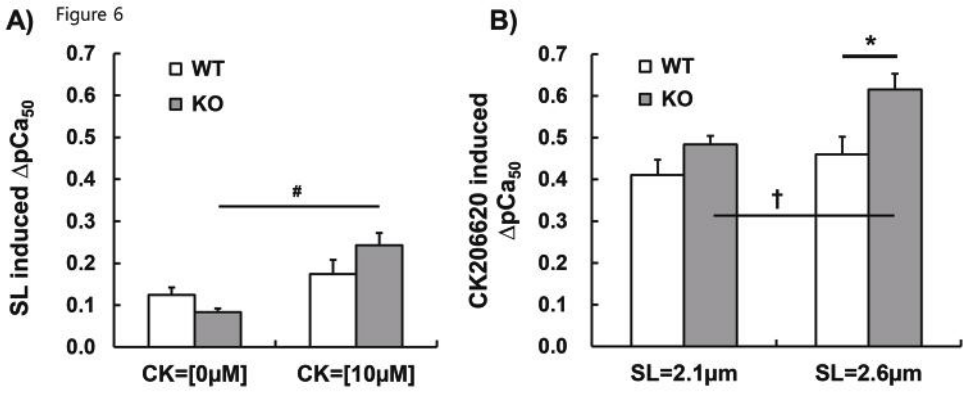

Figure 6 SL-induced ΔpCa50 at 0 and 10 μM CK-2066260 and CK 2066260-induced ΔpCa50 at SL 2.1 μm and SL 2.6 μm

(A) Effect of increasing SL from 2.1 to 2.6 μm on calcium sensitivity (SL-induced ΔpCa50) without and with 10 μM CK 2066260. In KO fibers CK-2066260 increased the SL-induced ΔpCa50 (#, $p<0.05$). (B) CK-2066260 (10 μM) induced ΔpCa50 at SL 2.1 μm and 2.6 μm. Only in KO fibers CK 2066260-induced ΔpCa50 was significantly greater at SL 2.6 μm compared to 2.1 μm (†, $p<0.05$). Furthermore, at SL 2.6 μm CK 2066260-induced ΔpCa50 in KO fibers was significantly greater than in WT (*, $p<0.05$). Results from six WT and six KO mice.

DISCUSSION

Compromised neural input and excitation-contraction coupling is well-known to underlie muscle weakness in many skeletal muscle diseases. However, reduced force production can also result from alterations in sarcomeric proteins (Laing and Nowak, 2005). A prime example is nemaline myopathy (NM), the most common non-dystrophic congenital skeletal muscle myopathy (Sanoudou and Beggs, 2001), that is caused by mutations in six genes that all encode thin filament proteins (*TMP2* (Donner et al., 2002), *TMP3* (Laing et al., 1995), *NEB* (Pelin et al., 1999), *ACTA1* (Nowak et al., 1999), *TNNT1* (Johnston et al., 2000), *CFL2* (Agrawal et al., 2007)). Of these NM genes *NEB* is most important as it accounts for ~50 percent of NM cases (Pelin et al., 1999). Treatment options for NM currently do not exist and gene therapy is still far away. Considering that a hallmark feature of NM is muscle weakness (North et al., 1997) we studied whether the fast skeletal muscle troponin activator CK-2066260 can restore muscle strength in skinned fast skeletal muscle fiber bundles from wildtype and nebulin deficient mice. In both genotypes CK-2066260 causes a large increase in calcium sensitivity of force development with a ~8-fold increase in force at low activating calcium levels.

CK-2066260 is structurally and functionally closely related to the fast skeletal muscle troponin activator CK-2017357 that is currently in phase II clinical trials for Amyotrophic Lateral Sclerosis (Russell et al., 2012). CK-2017357 slows the dissociation rate of calcium from troponin thereby stabilizing the open-conformation of the troponin/tropomyosin complex and enhancing cross-bridge formation at a given calcium concentration (Russell et al., 2012); the analogue CK-2066260 acts similarly (data not shown). In the present study, we observed that CK-2066260 greatly increases the calcium-sensitivity of force generation with an increase in pCa50 of 0.4-0.6 pCa units (Fig 6B). A large effect is already seen at low doses with a 2 μM dose nearly doubling force at a pCa of 6.25 (Fig. 2B). This effect of CK-2066260 is similar to that of CK-2017357 in human and rabbit fast skeletal muscle fibers (Russell et al., 2012), indicating that this class of troponin activators is effective in a wide range of species.

Nebulin deficient muscle fibers produced active tensions that were much less than in WT muscle; for example the deficit in Tmax (maximal active tension at pCa 4.5) was ~60% at a SL of 2.1 μm (Table 1), which is consistent with

earlier findings (Chandra et al., 2009). Nebulin deficiency results in thin filaments that are on average shorter than in WT muscle (Bang et al., 2006; Witt et al., 2006); however, it is unlikely that this explains the large tension deficit because the effect of the shorter thin filament length on active tension is minimal at the SL of 2.1 μm where KO fibers reach their optimal sarcomere length and WT fibers are on the ascending limb of the force-sarcomere length relation (Chandra et al., 2009). An additional known effect of nebulin deficiency that impacts Tmax is an increase in gapp (apparent rate constant with which force generating cross-bridges detach) and a decrease in fapp (apparent rate constant with which cross-bridges enter the force generating state) with the net effect being a reduction in the fraction of cross-bridges that generate force (Bang et al., 2009; Chandra et al., 2009; Lawlor et al., 2011). These earlier conclusions were based on an increased tension cost (which reflects gapp) and a reduction in k_{tr} in NEB KO fibers, (k_{tr} represents the sum of fapp and gapp (Brenner, 1988)) and a similar k_{tr} reduction was found in the present study (Fig. 4). We consider it likely therefore that the tension deficit of nebulin KO fibers in the present study has a large contribution from altered cross-bridge cycling kinetics.

We found that k_{tr} increases with activation level (Fig. 4B and C), consistent with the work of others (Metzger and Moss, 1990; Metzger, 1989; Moreno-Gonzalez et al., 2007). This Ca^{2+}-dependence of k_{tr} is likely due to complex kinetic interactions between cross-bridge cycling and Ca^{2+}-dependent thin-filament dynamics that increase fapp as sub-maximal calcium levels are increased (Brenner, 1988; Moreno-Gonzalez et al., 2007). TnC likely plays an important role in force kinetics since previous studies have provided evidence that TnC mutants with a slower Ca^{2+} dissociation increase k_{tr} at submaximal activation levels (Moreno-Gonzalez et al., 2007; Regnier et al., 1996). Similarly, we found that CK-2066260 causes a pronounced increase in ktr (Fig. 4), consistent with the slowing of Ca2+ dissociation from TnC caused by skeletal muscle troponin activators (Russell et al., 2012). We propose that the greater calcium sensitivity of the thin filament induced by CK-2066260 increases k_{tr} because of an increase in f_{app}. Considering that force is proportional to $f_{app}/(f_{app}+g_{app})$ (the fraction of cycling cross-bridges that develops force (Brenner, 1988)), the effect of CK-2066260 will not only be a more rapid rise in force but also an increase in peak force at submaximal activation levels. Thus, both effects are consequences of the increase in calcium sensitivity of the sarcomere caused by CK-2066260.

Our finding that in the NEB KO muscle, CK-2066260 increased Tmax at SL 2.6 µm (13% in WT muscle fibers and 30% in the NEB KO muscle fibers) was unexpected considering that the effect of the activator is thought to be an increase in calcium sensitivity only. The increase in Tmax suggests that a saturating level of calcium does not cause a maximal number of cross-bridges to attach and develop force. It has been reported that even a maximal tetanic contraction in normal healthy muscle has only ~40% of the available cross-bridges attached (Nowak et al., 1999). Furthermore, a reduction in the number of force generating cross-bridges was previously reported in nebulin-deficient muscle both in the mouse KO model and in NM patients. If underlying the CK-2066260 induced increase in ktr at saturating calcium levels (Fig. 4B-D) is solely an increase in fapp, then an increase in Tmax would be expected. A reduction in the number of force generating cross-bridges was previously reported in nebulin-deficient muscle both in the mouse KO model and in NM patients (Chandra et al., 2009); this finding might underlie the larger effect of CK-2066260 at maximal activation on both ktr (increase 9% in WT and 34% in KO) and Tmax (increase 13% in WT and 30% in KO). Finally, the finding that the coefficient of cooperatively (nH) is reduced (at 10 µM CK-2066260) in only the NEB KO fibers (Table 1) suggests that the absence of nebulin alters the CK-2066260-thin filament interactions and its downstream effects.

The conclusion that absence of nebulin alters the effect of CK-2066260 on the thin filament is also supported by the length dependency of the CK-2066260 effect on calcium sensitivity. It is well known that increasing SL causes an increase in calcium sensitivity (Kentish et al., 1986), a phenomenon that is especially prominent in cardiac muscle (where it underlies the Frank-Starling mechanism of the heart) but that also occurs in skeletal muscle (J. P Konhilas et al., 2002). In the present study, an increase in SL caused a left-shift in the force-pCa relation of ~0.1 pCa units, with no difference between the genotypes (Fig. 6A). Although calcium sensitivity is already increased at the long SL, CK-2066260 causes a further increase and this increase exceeds the one at short length (Fig. 6B). At the long SL (2.6 µm) CK-2066260 had a larger effect in NEB KO fibers than in WT fibers (Fig. 6B) which suggests that nebulin deficiency sensitizes troponin to CK-2066260. Although additional studies are required to fully understand the mechanistic basis of these findings, our results establish that CK-2066260 is a potent activator of fast skeletal muscle, especially of nebulin deficient muscle.

In summary, we investigated the effect of the fast skeletal muscle troponin activator CK-2066260 on force development in fast skeletal muscle of wildtype and NEB KO mice. CK-2066260 was found to greatly increase force development at submaximal activation levels. Considering that most muscles during normal activity operate in the submaximal activation regime (Jasmin and Gardiner, 1987) the beneficial effect of CK-2066260 on in vivo muscle force may be substantial. It is also noteworthy that the class of troponin activators to which CK-206620 belongs is specific to fast skeletal troponin and does not affect cardiac muscle (Russell et al., 2012), which is an important consideration in terms of therapeutic index. The beneficial effect of CK-2066260 on fast skeletal muscle can be well visualized by our finding that at pCa levels above ~6.0 (i.e., calcium levels < 1 μM) CK-2066260 increases the tension of NEB KO fibers to beyond that of WT fibers (compare red and green solid curves in Fig. 3A with blue broken line). We conclude that fast skeletal troponin activators may ameliorate muscle weakness in NM and other patients with compromised muscle strength.

REFERENCES

Agrawal PB, Greenleaf RS, Tomczak KK, Lehtokari V-L, Wallgren-Pettersson C, Wallefeld W, et al. Nemaline myopathy with minicores caused by mutation of the CFL2 gene encoding the skeletal muscle actin-binding protein, cofilin-2. Am. J. Hum. Genet. 2007; 80: 162–7.

Bang M-L, Caremani M, Brunello E, Littlefield R, Lieber RL, Chen J, et al. Nebulin plays a direct role in promoting strong actin-myosin interactions. FASEB J. 2009; 23: 4117–4125.

Bang M-L, Li X, Littlefield R, Bremner S, Thor A, Knowlton KU, et al. Nebulin-deficient mice exhibit shorter thin filament lengths and reduced contractile function in skeletal muscle. J. Cell. Biol. 2006; 173: 905–916.

Brenner B, Eisenberg E. Rate of force generation in muscle: correlation with actomyosin ATPase activity in solution. Proc. Natl. Acad. Sci. U. S. A. 1986; 83: 3542–6.

Brenner B. Effect of Ca2+ on cross-bridge turnover kinetics in skinned single rabbit psoas fibers: implications for regulation of muscle contraction. Proc. Natl. Acad. Sci. 1988; 85: 3265–3269.

Castillo A, Nowak R, Littlefield KP, Fowler VM, Littlefield RS. A nebulin ruler does not dictate thin filament lengths. Biophys. J. 2009; 96: 1856–1865.

Chandra M, Mamidi R, Ford S, Hidalgo C, Witt CC, Ottenheijm CA, et al. Nebulin alters cross-bridge cycling kinetics and increases thin filament activation: a novel mechanism for increasing tension and reducing tension cost. J. Biol. Chem. 2009; 284: 30889–30896.

Donner K, Ollikainen M, Ridanpää M, Christen H-J, Goebel HH, de Visser M, et al. Mutations in the β-tropomyosin (TPM2) gene – a rare cause of nemaline myopathy. Neuromuscul. Disord. 2002; 12: 151–158.

Fabiato A, Fabiato F. Calculator programs for computing the composition of the solutions containing multiple metals and ligands used for experiments in skinned muscle cells. J. Physiol. (Paris). 1979

Granzier HL, Akster HA, Ter Keurs HE. Effect of thin filament length on the force-sarcomere length relation of skeletal muscle. Am. J. Physiol. 1991; 260: C1060–70.

Huxley A. Muscle structure and theories of contraction. Prog. Biophys. Biophys. Chem 1957

Huxley HE. Fifty years of muscle and the sliding filament hypothesis. Eur. J. Biochem. 2004; 271: 1403–15.

Jasmin BJ, Gardiner PF. Patterns of EMG activity of rat plantaris muscle during swimming and other locomotor activities. J. Appl. Phys. 1987; 63: 713–718.

Jin JP, Wang K. Nebulin as a giant actin-binding template protein in skeletal muscle sarcomere Interaction of actin and cloned human nebulin fragments. FEBS Lett. 1991; 281: 93–96.

Jin JP, Wang K. Cloning, expression, and protein interaction of human nebulin fragments composed of varying numbers of sequence modules. J. Biol. Chem. 1991; 266: 21215–23.

Johnston JJ, Kelley RI, Crawford TO, Morton DH, Agarwala R, Koch T, et al. A novel nemaline myopathy in the Amish caused by a mutation in troponin T1. Am. J. Hum. Genet. 2000; 67: 814–21.

Kazmierski ST, Antin PB, Witt CC, Huebner N, McElhinny AS, Labeit S, et al. The Complete Mouse Nebulin Gene Sequence and the Identification of Cardiac Nebulin. J. Mol. Biol. 2003; 328: 835–846.

Kentish JC, ter Keurs HE, Ricciardi L, Bucx JJ, Noble MI. Comparison between the sarcomere length-force relations of intact and skinned trabeculae from rat right ventricle. Influence of calcium concentrations on these relations. Circ. Res. 1986; 58: 755–768.

Konhilas JP, Irving TC, de Tombe PP. Length-dependent activation in three striated muscle types of the rat. J. Phys. 2002; 544: 225–236.

Konhilas JP, Irving TC, de Tombe PP. Frank-Starling law of the heart and the cellular mechanisms of length-dependent activation. Pflügers Arch. Eur. J. Physiol. 2002; 445: 305–10.

Kruger M. Nebulin as a length regulator of thin filaments of vertebrate skeletal muscles: correlation of thin filament length, nebulin size, and epitope profile. J. Cell Biol. 1991; 115: 97–107.

Labeit S, Kolmerer B. The complete primary structure of human nebulinand its correlation to muscle structure. J. Mol. Biol. 1995; 248: 308–315.

Lahmers S, Wu Y, Call DR, Labeit S, Granzier H. Developmental control of titin isoform expression and passive stiffness in fetal and neonatal myocardium. Circ. Res. 2004; 94: 505–13.

Laing NG, Nowak KJ. When contractile proteins go bad: the sarcomere and skeletal muscle disease. Bioessays 2005; 27: 809–22.

Laing NG, Wilton SD, Akkari PA, Dorosz S, Boundy K, Kneebone C, et al. A mutation in the alpha tropomyosin gene TPM3 associated with autosomal dominant nemaline myopathy. Nat. Genet. 1995; 9: 75–9.

Lawlor MW, Ottenheijm CA, Lehtokari V-L, Cho K, Pelin K, Wallgren-Pettersson C, et al. Novel mutations in NEB cause abnormal nebulin expression and markedly impaired muscle force generation in severe nemaline myopathy. Skelet. Muscle. 2011; 1: 23.

Metzger J, Moss R. Calcium-sensitive cross-bridge transitions in mammalian fast and slow skeletal muscle fibers. Science (80-.). 1990; 247: 1088–1090.

Metzger JM. Variations in cross-bridge attachment rate and tension with phosphorylation of myosin in mammalian skinned skeletal muscle fibers. Implications for twitch potentiation in intact muscle. J. Gen. Physiol. 1989; 93: 855–883.

Moreno-Gonzalez A, Gillis TE, Rivera AJ, Chase PB, Martyn DA, Regnier M. Thin-filament regulation of force redevelopment kinetics in rabbit skeletal muscle fibres. J. Physiol. 2007; 579: 313–26.

Muhle-Goll C, Habeck M, Cazorla O, Nilges M, Labeit S, Granzier H. Structural and functional studies of titin's fn3 modules reveal conserved surface patterns and binding to myosin S1--a possible role in the Frank-Starling mechanism of the heart. J. Mol. Biol. 2001; 313: 431–47.

North KN, Laing NG, Consortium I. Nemaline myopathy: current concepts. The ENMC International Consortium and Nemaline Myopathy. J. Med. Genet. 1997; 34: 705–713.

Nowak KJ, Wattanasirichaigoon D, Goebel HH, Wilce M, Pelin K, Donner K, et al. Mutations in the skeletal muscle alpha-actin gene in patients with actin myopathy and nemaline myopathy. Nat. Genet. 1999; 23: 208–12.

Ottenheijm CAC, Heunks LMA, Hafmans T, van der Ven PFM, Benoist C, Zhou H, et al. Titin and diaphragm dysfunction in chronic obstructive pulmonary disease. Am. J. Respir. Crit. Care Med. 2006; 173: 527–34.

Ottenheijm CAC, Hooijman P, DeChene ET, Stienen GJ, Beggs AH, Granzier H. Altered myofilament function depresses force generation in patients with nebulin-based nemaline myopathy (NEM2). J. Struct. Biol. 2010; 170: 334–343.

Ottenheijm CAC, Witt CC, Stienen GJ, Labeit S, Beggs AH, Granzier H. Thin filament length dysregulation contributes to muscle weakness in nemaline myopathy patients with nebulin deficiency. Hum. Mol. Genet. 2009; 18: 2359–2369.

Pappas CT, Krieg PA, Gregorio CC. Nebulin regulates actin filament lengths by a stabilization mechanism. J. Cell. Biol. 2010; 189: 859–870.

Pelin K, Hilpelä P, Donner K, Sewry C, Akkari PA, Wilton SD, et al. Mutations in the nebulin gene associated with autosomal recessive nemaline myopathy. Proc. Natl. Acad. Sci. 1999; 96: 2305–2310.

Regnier M, Martyn DA, Chase PB. Calmidazolium alters Ca2+ regulation of tension redevelopment rate in skinned skeletal muscle. Biophys. J. 1996; 71: 2786–94.

Russell AJ, Hartman JJ, Hinken AC, Muci AR, Kawas R, Driscoll L, et al. Activation of fast skeletal muscle troponin as a potential therapeutic approach for treating neuromuscular diseases. Nat. Med. 2012; 18: 452–455.

Sanoudou D, Beggs AH. Clinical and genetic heterogeneity in nemaline myopathy-a disease of skeletal muscle thin filaments. Trends Mol. Med. 2001; 7: 362–368.

Takano K, Watanabe-Takano H, Suetsugu S, Kurita S, Tsujita K, Kimura S, et al. Nebulin and N-WASP cooperate to cause IGF-1-induced sarcomeric actin filament formation. Science 2010; 330: 1536–40.

Wang S-M, Greaser ML. Immunocytochemical studies using a monoclonal antibody to bovine cardiac titin on intact and extracted myofibrils. J. Muscle Res. Cell Motil. 1985; 6: 293–312.

Wang SM. Studies on cardiac myofibrillogenesis with antibodies to titin, actin, tropomyosin, and myosin. J. Cell Biol. 1988; 107: 1075–1083.

Warren CM, Krzesinski PR, Greaser ML. Vertical agarose gel electrophoresis and electroblotting of high-molecular-weight proteins. Electrophoresis 2003; 24: 1695–1702.

Witt CC, Burkart C, Labeit D, McNabb M, Wu Y, Granzier H, et al. Nebulin regulates thin filament length, contractility, and Z-disk structure in vivo. EMBO J. 2006; 25: 3843–3855.

Wright J, Huang Q-Q, Wang K. Nebulin is a full-length template of actin filaments in the skeletal muscle sarcomere: an immunoelectron microscopic study of its orientation and span with site-specific monoclonal antibodies. J. Muscle Res. Cell Motil. 1993; 14: 476–483.

CHAPTER 8

TROPONIN ACTIVATOR AUGMENTS MUSCLE FORCE IN NEMALINE MYOPATHY PATIENTS WITH NEBULIN MUTATIONS

Josine M. de Winter, Danielle Buck, Carlos Hidalgo, Jeffrey R.Jasper, Fady I. Malik, Nigel F. Clarke, Ger J.M. Stienen, Michael W Lawlor, Alan H. Beggs, Henk Granzier and Coen A.C. Ottenheijm

Journal of Medical Genetics, 2013

ABSTRACT

Background | Nemaline myopathy - the most common non-dystrophic congenital myopathy - is caused by mutations in thin filament genes, of which the nebulin gene is the most frequently affected one. The nebulin gene codes for the giant sarcomeric protein nebulin, which plays a crucial role in skeletal muscle contractile performance. Muscle weakness is a hallmark feature of nemaline myopathy patients with nebulin mutations, and is caused by changes in contractile protein function, including a lower calcium-sensitivity of force generation. To date no therapy exists to treat muscle weakness in nemaline myopathy. Here, we studied the ability of the novel fast skeletal muscle troponin activator, CK-2066260, to augment force generation at submaximal calcium levels in muscle cells from nemaline myopathy patients with nebulin mutations.

Methods | Contractile protein function was determined in permeabilized muscle cells isolated from frozen patient biopsies. The effect of 5 μM CK-2066260 on force production was assessed.

Results | Nebulin protein levels were severely reduced in muscle cells from these patients compared to controls, while myofibrillar ultrastructure was largely preserved. Both maximal active tension and the calcium-sensitivity of force generation were lower in patients compared to controls. Importantly, CK-2066260 greatly increased the calcium-sensitivity of force generation – without affecting the cooperativity of activation - in patients to levels that exceed those observed in untreated control muscle.

Interpretation | Fast skeletal troponin activation is a therapeutic mechanism to augment contractile protein function in nemaline myopathy patients with nebulin mutations and with other neuromuscular diseases.

INTRODUCTION

Nemaline myopathy (NM) is the most common non-dystrophic congenital myopathy (incidence ~1:50,000) (Wallgren-Pettersson and Laing, 2000). Hallmark features of NM are muscle weakness and the presence of nemaline bodies in skeletal muscle fibers (North et al., 1997). To date, seven genes have been implicated in NM. Strikingly, six of these genes code for proteins of the skeletal muscle thin filament: alpha-tropomyosin-3 and beta-tropomyosin (*TPM3* and *TPM2*), nebulin (*NEB*), actin alpha 1 (*ACTA1*), troponin T type 1 (*TNNT1*), and cofilin-2 (*CFL2*). The seventh implicated gene, *KBTBD13,* was recently discovered and the function of its protein product is unknown (Sambuughin et al., 2010).

Mutations in the *NEB* gene are the most common cause of NM, likely accounting for more than 50% of NM cases (Pelin et al., 1999). Nebulin is a giant sarcomeric protein (~800 kDa); its C-terminus is anchored in the Z-disk and its N-terminus is located close to the thin filament pointed end. Thus, a single nebulin molecule spans nearly the entire length of the thin filament (Figure 1). Previous studies of a nebulin knockout mouse model showed that nebulin plays important roles in sarcomeric structure and contractile performance. Nebulin stabilizes the thin filament and specifies its length (Bang et al., 2006; Castillo et al., 2009; Gokhin and Bang, 2009; Pappas et al., 2010; Witt et al., 2006), and evidence suggests that it also modulates both the kinetics of actomyosin cross bridge formation (Bang et al., 2009; Chandra et al., 2009) and the calcium-sensitivity of thin filament activation (Chandra et al., 2009). Recent work from our group revealed that skeletal muscle fibers of NM patients with *NEB* mutations (*NEB*-NM) develop muscle weakness due to loss of these functions of nebulin; their myofibers contain thin filaments of shorter and non-uniform length, they show altered actomyosin cross bridge kinetics (Lawlor et al., 2011; Ottenheijm et al., 2010), and they have a lower calcium-sensitivity of force generation (Ottenheijm et al., 2009, 2010).

To date, no therapy exists that enhances force generation in *NEB*-NM. Strategies to restore thin filament length or the kinetics of actomyosin interaction currently do not exist for skeletal muscle, and, in part due to the extremely large size of the nebulin gene and protein, effective genetic strategies to combat these effects are likely far off in the future. However, the lower calcium-sensitivity of force generation in *NEB*-NM might offer a more immediate therapeutic target, as recently a fast skeletal muscle

troponin activator has been developed that amplifies the response of the thin filament to calcium in fast skeletal muscle fibers (Russell et al., 2012). The fast skeletal muscle troponin activator tirasemtiv (formerly CK-2017357) was shown to greatly increase the calcium-sensitivity of force generation in healthy rat skeletal muscle fibers (Russell et al., 2012), and is currently in Phase II clinical studies for amyotrophic lateral sclerosis (Shefner et al., 2012).

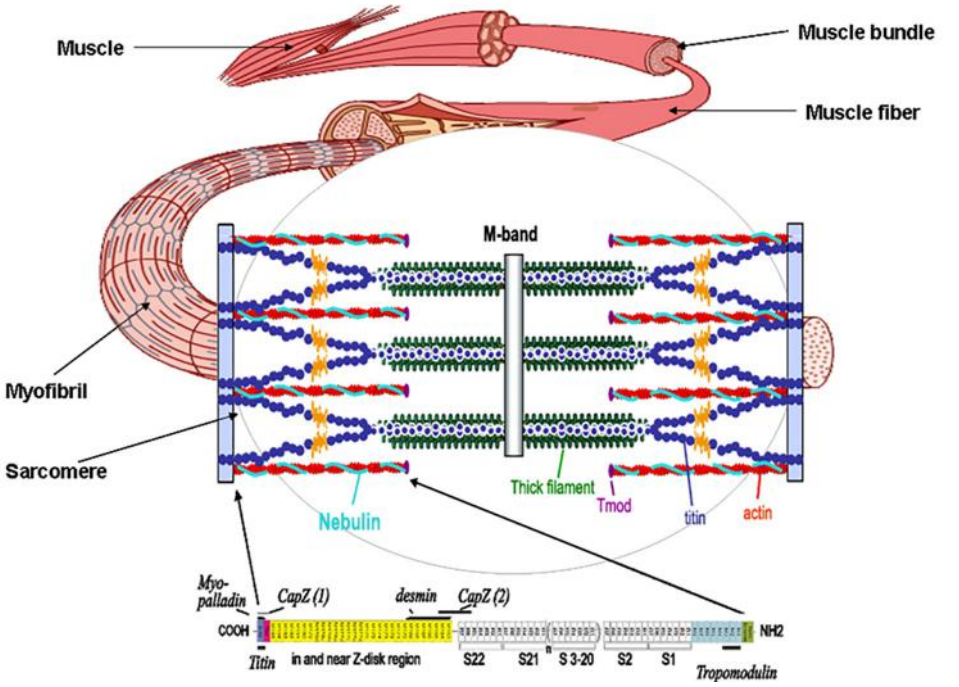

Figure 1 Schematic of nebulin's location in the skeletal muscle sarcomere
(A) single nebulin molecule spans the thin filament with its C-terminus anchored in the Z-disk and its N-terminus located close to the thin filament pointed end. The highly modular central region (M9–M162) is divided into seven modular repeats that are arranged into twenty-two super-repeats.

The goal of our study was to test the ability of the novel fast skeletal troponin activator CK-2066260 – a close structural analog of tirasemtiv - to improve muscle cell strength in patients with *NEB*-NM. Replication of tirasemtiv pharmacology with a different molecule of the same mechanistic class (CK-2066260) strengthens the argument that the described effects are not specific to a single small molecule but instead reflect an effect related to

the mechanism of action. Our findings indicate that CK-2066260 greatly increases the calcium-sensitivity of force generation in *NEB*-NM patients to levels that exceed those observed in untreated muscle cells from healthy controls. Thus, fast skeletal troponin activation is a therapeutic mechanism to augment muscle strength in NM patients with nebulin mutations and with other neuromuscular diseases.

METHODS

Muscle biopsies from NEB-NM patients

Quadriceps muscle specimens, remaining from diagnostic procedures or obtained during clinically indicated surgical procedures, were collected from four NM patients with confirmed NEB gene mutations, from four pediatric control subjects that were biopsied for other diagnostic purposes (with normal skeletal muscle histology) and from three adult control subjects with no medical history. The four biopsies from the *NEB*-NM patients and from the pediatric controls were collected following informed consent supervised by the Boston Children's Hospital IRB. The three adult control muscle biopsies were obtained under supervision of the HREC, Children's Hospital at Westmead (CHW/10/45). All biopsies were stored frozen and unfixed at −80°C until use. For details on the clinical and genetic data of the subjects, see Tables 1 and 2.

Nebulin protein levels

To assess nebulin protein levels, muscle samples were homogenized and analyzed on 1% agarose electrophoresis gels, as previously described (Warren et al., 2003). To prevent protein degradation, all buffers contained protease inhibitors (phenylmethylsulfonyl fluoride (PMSF), 0.5mM; leupeptin, 0.04mM; E64, 0.01mM). Gels were scanned and analyzed with One-D scan EX (Scanalytics Inc., Rockville, MD, USA) software. The integrated optical density of nebulin and myosin heavy chain (MHC) was determined. For Western blot analysis, one or two-color infrared western blots were scanned (Odyssey Infrared Imaging System, Li-Cor Biosciences, NE, USA) and the images analyzed with One-D scan EX.

Table 1 Clinical and pathological data of nemaline myopathy patients and characteristics of control subjects

Pt ID	Biopsy ID	Gender	Biopsy location	Age at biopsy	Fiber typing	Rod characteristics	Clinical form	Age of onset	Maximal motor ability	Clinical status
Nebulin-based NM patients										
26-2	T33	F	Quadriceps	13 mo	Extreme type 1 predominance	Numerous large rods in type 1 fibers	Inter-mediate	Birth	Sat, but never walked	nonambulant, requires vent and G-tube feedings at 13 yo
258-2	T1069	M	Quadriceps	4 mo	60-70% type 1 fibers, most smaller than type 2s	Subsarcolemmal rods in all fiber types	Typical	Birth	Ambulatory since 18 mo	Ambulatory at 5 yo, requires G-tube and bi-pap at night
974-1	T1033	M	Unspecified	2 mo	Hypotrophic type 1, no fiber type predominance	Rods predominantly in hypotrophic type 1 fibers	Inter-mediate	Birth	Rolling over	Unable to sit at 2 yo, requires G-tube, breathes independently
988-1	T887	M	Quadriceps	2.5 mo	Normal fiber type proportions with significant fiber size variation	Subsarcolemmal rods in all fiber types	Indeter-minate	Birth	n/a	Severely hypotonic. Requires G-tube and nocturnal ventilation at 5 mo
Infant control subjects										
212-1	T141	M	Quadriceps	3 y	Normal	n/a	n/a	n/a	Normal	Unaffected
213-1	T142	F	Quadriceps	2 y	Normal	n/a	n/a	n/a	Normal	Unaffected
218-1	T147	F	Quadriceps	4 y	Normal	n/a	n/a	n/a	Normal	Unaffected
219-1	T148	F	Quadriceps	5 y	Normal	n/a	n/a	n/a	Normal	Unaffected
Adult control subjects										
n/a	C1	M	Quadriceps	20	Normal	n/a	n/a	n/a	Normal	Unaffected
n/a	C2	M	Quadriceps	25	Normal	n/a	n/a	n/a	Normal	Unaffected
n/a	C3	M	Quadriceps	30	Normal	n/a	n/a	n/a	Normal	Unaffected

Table 2 Genetic data of nemaline myopathy patients

Pt ID	Biopsy ID	*NEB* mutations	Nebulin defects
26-2	T33	c.[7431+1916_7536+372del]+[7431+1916_7536+372del]	p.[Arg2478_Asp2512del]+[Arg2478_Asp2512del]
258-2	T1069	c.[3567+3_3567+7delAAGT]+[18124C>T]	exon 33 splice defect + p.Gly6041Stop
974-1	T1033	c.[7431+1916_7536+372del]+[24842_24841delAG]	p.[Arg2478_Asp2512del]+[Arg8280SerfsStop2]
988-1	T887	c.[1152+1G>A]+[17013+1G>T]	exon 13 splice defect + exon 107 splice defect

Pt 26-2 is homozygous for del exon 55
Pt 258-2 is compound heterozygous for exon 33 splice site mutation and exon 114 nonsense mutation
Pt 974-1 is compound heterozygous for del exon 55 and 2 bp deletion in exon 177
Pt 988-1 is compound heterozygous for two splice site mutations in intron 13 and 107

Reference sequences are NM_001164507 and NP_004534.2

Pathological evaluation

For electron microscopy, samples were fixed and processed per standard histological techniques for either routine histochemical staining or ultrastructural examination at the time of biopsy, and all slides and ultrastructural images were reviewed by a neuropathologist (MWL).

Muscle mechanics

From the frozen samples, muscle fiber bundles were isolated as described previously19. In brief, from the biopsies smaller sections (2x2mm) were isolated in liquid nitrogen. Subsequently, they were placed for 24h at -20°C in 4 mL 50% glycerol/relaxing solution containing high concentrations of protease inhibitors (phenylmethylsulfonyl fluoride (PMSF), 0.5mM; leupeptin, 0.04mM; E64, 0.01mM). Subsequently, the sections were placed on a 'roller band' for 24h at 4°C, followed by submersion them in skinning solution for 24h at 4°C. Finally, the skinning solution was substituted with a glycerol/ relaxing solution with lower concentrations of protease inhibitors and stored at -20°C until further use. On the day of an experiment, small strips (CSA ~0.07 mm2) were dissected from the glycerinated sections and washed thoroughly with relaxing solution. The strips were mounted using aluminum T-clips between a length motor (ASI 403A, Aurora Scientific Inc., Ontario, Canada) and a force transducer element (ASI 315C-I, Aurora Scientific Inc., Ontario, Canada) in a skinned fiber apparatus (ASI 802D, Aurora Scientific Inc., Ontario, Canada) that was mounted on an inverted microscope (Zeiss Axio Observer A1). Sarcomere length was set using a high speed VSL camera and ASI 900B software (Aurora Scientific Inc., Ontario, Canada). Mechanical experiments were performed at a sarcomere length of ~2.1 µm, a length selected to minimize force differences due to shorter thin filaments in fibers from *NEB*-NM patients (Ottenheijm et al., 2009), and at 2.6 µm to

study the effect of sarcomere length on activation. Fiber width and diameter were measured at three points along the fiber and the cross-sectional area was determined assuming an elliptical cross-section. Fiber dimensions were determined using an inverted microscope and a custom-made prism that was mounted in the bath. Using a 40x objective and a high-speed VSL camera with calibrated ASI 900B software (Aurora Scientific Inc., Ontario, Canada) the dimensions of the muscle strips were measured. Three different types of bathing solutions were used during the experimental protocols: a relaxing solution (40 mM BES; 10 mM EGTA; 6.86 mM $MgCl_2$; 5.96 mM Na-ATP; 3.28 mM K-propionate; 33 mM creatine phosphate; 1 mM DTT; 0.5 mM PMSF; 0.2 mM Leupeptin; 0.05 mM E64; 200 U/ml creatine phospokinase), a pre-activating solution with low EGTA concentration (40 mM BES; 1 mM EGTA; 6.66 mM $MgCl_2$; 5.98 mM Na-ATP; 30.44 mM K-propionate; 33 mM creatine phosphate; 1 mM DTT; 0.5 mM PMSF; 0.2 mM Leupeptin; 0.05 mM E64; 200 U/ml creatine phospokinase), and an activating solution (40 mM BES; 10 mM $CaCO_3$-EGTA; 6.64 mM $MgCl_2$; 6.23 mM Na-ATP; 2.1 mM K-propionate; 15 mM creatine phosphate; 1 mM DTT; 0.5 mM PMSF; 0.2 mM Leupeptin; 0.05 mM E64; 200 U/ml creatine phospokinase). The temperature of the bathing solutions was kept constant at 15°C using a temperature controller (ASI 825A, Aurora Scientific Inc. Ontario, Canada).

To determine a dose-response curve for the fast skeletal troponin activator CK-2066260 in muscle fibers from controls and from *NEB*-NM patients, tissue was exposed to pCa solutions of 6.0 – this pCa that yielded about 35% of maximal active tension – with increasing concentrations (1, 2, 5, 10 and 20 μM) of CK-2066260 dissolved in 1% dimethylsulfoxide DMSO as vehicle. Note that 1% DMSO did not affect muscle fiber contractility (data not shown). Figures 5B-C show that CK-2066260 enhanced submaximal force generation with a maximal effect at 5 μM, which is in accordance with previously reported dose–response curves of its analogue CK-2017357 (Russell et al., 2012). Accordingly, experiments were conducted with either CK-2066260 (5 μM) or vehicle alone (1% DMSO). To determine the force-pCa relation (pCa = -log of molar free Ca^{2+} concentration), skinned muscle fiber bundles were sequentially bathed in solutions with pCa values ranging from 4.5 to 9.0 and the steady-state force was measured (Figure 3A). Measured force values were normalized to the maximal force obtained at pCa 4.5. The obtained force-pCa data were fit to the Hill equation, providing the pCa_{50} and the Hill coefficient, nH, an index of myofilament cooperativity.

Myosin heavy chain composition of bundles used for contractility experiments

For determination of the myosin heavy chain isoform composition of the muscle fiber preparations we used specialized SDS-PAGE (Ottenheijm et al., 2009). In brief, muscles fibers were denatured by boiling for 2 min. in SDS sample buffer. The stacking gel contained a 4% acrylamide concentration (pH 6.7), and the separating gel contained 7% acrylamide (pH 8.7) with 30% glycerol (v/v). The gels were run for 24h at 15°C and a constant voltage of 275V. Finally, the gels were silver-stained, scanned, and analyzed with One-D scan EX (Scanalytics Inc., Rockville, MD, USA) software.

Statistical analyses

Data are presented as mean ± SEM. For statistical analyses, t tests and two-way ANOVA were used as appropriate. $P < 0.05$ was considered to be statistically significant.

RESULTS

Muscle fibers of NEB-NM patients have lower nebulin protein levels, while myofibrillar ultrastructure is preserved

To study the effect of mutations in *NEB* on its protein product, nebulin protein levels were determined in quadriceps muscle of pediatric *NEB*-NM patients and these were compared to those in quadriceps muscle from controls. For all muscle samples, 1% agarose gels showed a single band at the appropriate molecular weight (~800 kDa) of nebulin (Figure 2A), which was confirmed to be nebulin by Western blot studies using an antibody against nebulin's N-terminus (Figure 2B). Quantitative densitometry revealed that both the nebulin/MHC ratio and the nebulin/actin ratio in muscle from pediatric controls ($CTRL_{pediatric}$; 0.051 ± 0.007 for nebulin/MHC and 0.055 ± 0.025 for nebulin/actin, respectively) was not significantly different from the ratio found in adult controls ($CTRL_{adult}$; 0.052 ± 0.003 for nebulin/MHC and 0.040 ± 0.009 for nebulin/actin, respectively). As expected from previous studies (Lawlor et al., 2011; Ottenheijm et al., 2009, 2010), muscle from *NEB*-NM patients exhibited a significantly lower nebulin/MHC ratio (0.013 ± 0.003) and a lower nebulin/actin ratio (0.014 ± 0.004) compared to muscle from $CTRL_{pediatric}$ and $CTRL_{adult}$ (Figure 2A), indicating that the molecular basis for contractile deficits in muscle fibers from *NEB*-NM patients is related to a relative deficiency of nebulin protein.

Electron micrographs from *NEB*-NM patient muscle biopsies were used to evaluate myofibrillar structure. The organization of the contractile apparatus was normal in patients with *NEB*-NM (Figure 2C), with the exception of areas containing nemaline rods. Thus, despite the lower nebulin protein levels found in muscle from *NEB*-NM patients, their myofibrillar ultrastructure was largely preserved.

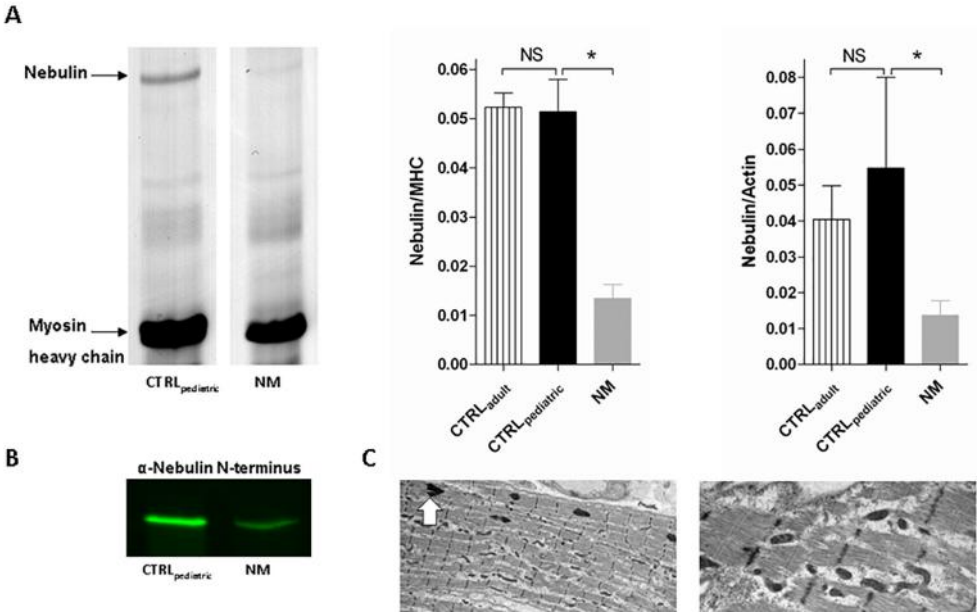

Figure 2 Nebulin protein levels and myofibrillar structure in muscle fibers from *NEB*-NM patients
(A) Protein gel example of muscle sample from $CTRL_{pediatric}$ and *NEB*-NM patients (left). Nebulin protein levels normalized over myosin heavy chain levels were not significantly different between $CTRL_{pediatric}$ and $CTRL_{adult}$, and were significantly lower in muscle from *NEB*-NM patients (middle). Nebulin protein levels normalized over actin protein levels were not significantly different between $CTRL_{pediatric}$ and $CTRL_{adult}$, and were significantly lower in muscle from *NEB*-NM patients (right). (B) Western blot studies using an antibody against nebulin's N-terminus revealed one single band at the appropriate molecular weight (~800 kDa) of nebulin; also note the lower intensity of the nebulin band in the *NEB*-NM patient, suggesting nebulin-deficiency. (C) Electron microscopy of *NEB*-NM patient revealed the presence of electron-dense nemaline rods in muscle fibers (arrows), surrounded by areas of appropriate myofibrillar organization. Bar = 2μm.

The contractile performance of skinned muscle fibers from pediatric controls resembles that of adult controls

Skeletal muscle fibers from *NEB*-NM patients exhibit shorter and non-

uniform thin filament lengths, and therefore produce maximal active tension at a sarcomere length of ~2.1 µm (Ottenheijm et al., 2009). To minimize potential force differences due to shorter thin filaments in *NEB*-NM, most of our studies were carried out at a sarcomere length of 2.1 µm in both control and *NEB*-NM fibers.

Previous work compared contractility of skeletal muscle fibers from pediatric *NEB*-NM patients to that of fibers from adult controls. In addition to adult controls, in the present study we also included a pediatric control group to evaluate the potential confounding effect of age differences on maximal active tension and calcium-sensitivity of force generation.

Figure 3A shows a typical force response of a muscle fiber to various calcium concentrations. From the force-pCa curves, the pCa_{50} – the calcium concentration that produces 50% of maximal force - was determined. The pCa_{50} of quadriceps fiber bundles from pediatric controls was not significantly different from that of slow-twitch or fast-twitch single fibers from adult controls (5.87 ± 0.02 for $CTRL_{slow}$ (n = 6), 5.87 ± 0.01 for $CTRL_{fast}$ (n = 23) and 5.88 ± 0.01 for $CTRL_{pediatric}$ (n = 15), respectively, Figure 3B). As the force-pCa curves indicate, the cooperativity of activation (nH) in slow-twitch (1.52 ± 0.16, n = 6) was lower than fast-twitch (2.50 ± 0.16, n = 23) $CTRL_{adult}$ fibers. Accordingly, the cooperativity of activation in $CTRL_{pediatric}$ bundles (nH: 2.14 ± 0.09, n = 15) was intermediate - but not significantly different from that of $CTRL_{slow}$ and $CTRL_{fast}$, reflecting the mix of slow- and fast-twitch fibers in the $CTRL_{pediatric}$ bundles.

Maximal active tension was 92.5 ± 9.6 mN/mm^2 in slow-twitch $CTRL_{adult}$ fibers (n = 6), 107.1 ± 6.4 mN/mm^2 in fast-twitch $CTRL_{adult}$ fibers (n = 23), and 91.0 ± 11.0 mN/mm^2 in $CTRL_{pediatri}$c bundles (n = 15) that contained a mix of slow- and fast-twitch muscle fibers (Figure 3C). Thus, maximal active tension of muscle fibers from pediatric controls was not significantly different from that of adult controls.

These data indicate that the maximal active tension and the calcium-sensitivity of force generation of skinned quadriceps fibers from pediatric controls are comparable to that of adult controls. As it is most ideal to compare data from pediatric *NEB*-NM patients to data obtained from pediatric controls, we limit our further comparisons to these two groups.

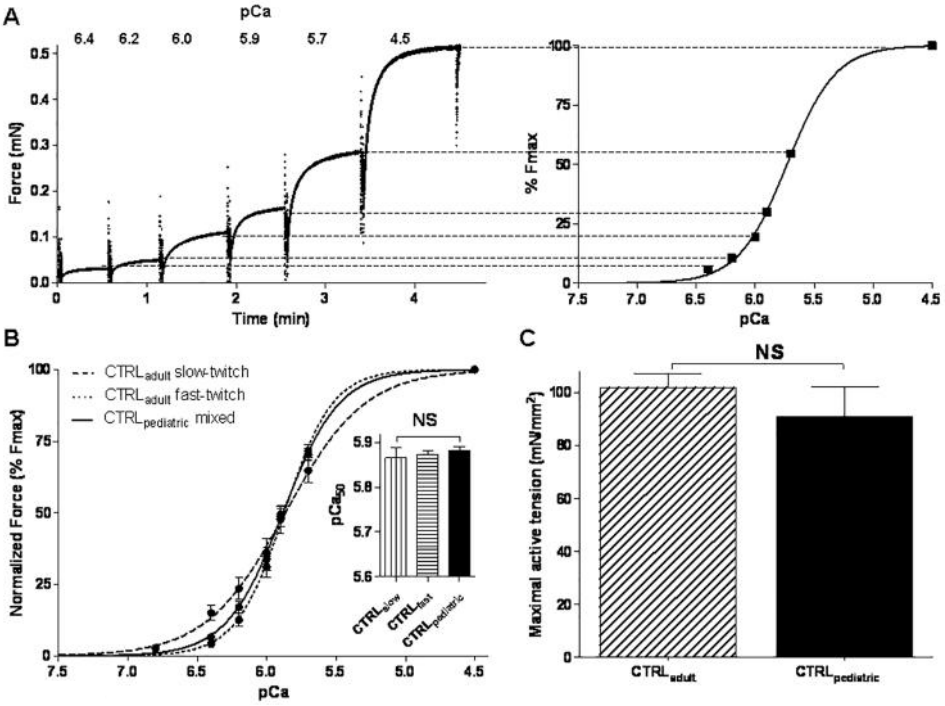

Figure 3 Maximal active tension and calcium-sensitivity of force generation in skinned muscle fibers from adult and pediatric controls

(A) Example of a force trace from a skinned muscle preparation that is sequentially exposed to incremental Ca^{2+} concentrations (here expressed as pCa: -log of molar free Ca^{2+} concentration). (B) No significant differences in calcium-sensitivity of force generation (reflected by the pCa50 value) were found between skeletal muscle bundles from $CTRL_{pediatric}$ and both slow-twitch and fast-twitch single fibers from adult controls. (C) No significant difference in maximal active tension was found between skeletal muscle fibers from adult and pediatric controls.

The calcium-sensitivity of force generation is lower in skinned muscle fibers from NEB-NM patients

The calcium-sensitivity of force generation, as reflected by the pCa_{50}, was lower in quadriceps fibers from *NEB*-NM patients (5.77 ± 0.02 , n = 20) compared to $CTRL_{pediatric}$ (5.88 ± 0.01, n = 15). As shown in Figure 4A, the slope of the force-pCa relation was less steep in *NEB*-NM patients compared to $CTRL_{pediatric}$ (nH: 1.43 ± 0.12 in *NEB*-NM (n = 20) vs. 2.14 ± 0.09 in $CTRL_{pediatric}$ (n = 15)), indicating that the cooperativity of activation was lower in nebulin-deficient muscle. Maximal active tension was also lower in

muscle fibers from *NEB*-NM patients compared to $CTRL_{pediatric}$ fibers (15.4 ± 3.5 mN/mm^2, n = 20 vs. 91.0 ± 11.0 mN/mm^2, n = 15, respectively). Thus, the calcium-sensitivity of force generation and maximal active tension were lower in muscle fibers from *NEB*-NM patients compared to those from control subjects.

Since the contractile performance of muscle bundles may be affected by its fiber type composition, we used SDS-PAGE to determine the myosin heavy chain isoforms of the bundles used for contractile measurements. $CTRL_{pediatric}$ bundles were composed of 46.4 ± 5.2% MHC 1, 24.8 ± 5.8% MHC 2A, and 30.7 ± 3.6% MHC 2X (Figure 4B). Bundles from *NEB*-NM patients had 63.7 ± 6.7% MHC 1 and 35.6 ± 7.1% MHC 2A. MHC 2X was not observed in bundles from *NEB*-NM patients. The difference in MHC 1 between $CTRL_{pediatric}$ and *NEB*-NM patients had a P-value of 0.06 suggesting that there is a trend towards a higher percentage of MHC 1. This skewing to more oxidative fiber types is not surprising, as an increased number of oxidative fibers is often noted in muscle biopsies from patients with NM (Ryan et al., 2003).

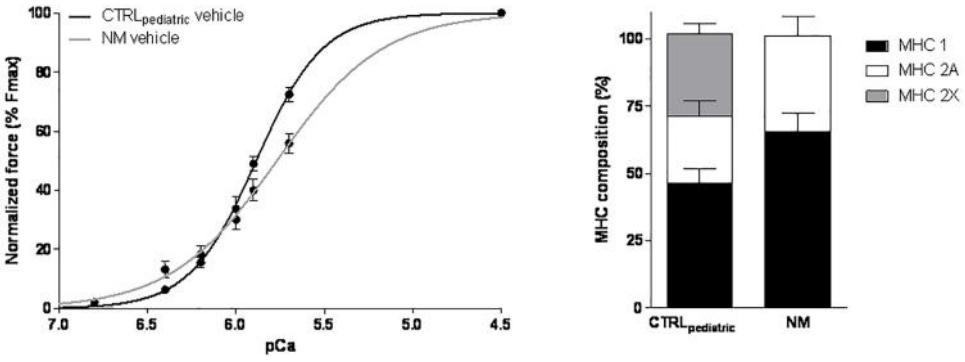

Figure 4 The calcium-sensitivity of force generation in skinned muscle fibers from *NEB*-NM patients and from pediatric controls

(A) Calcium-sensitivity of force generation was lower in *NEB*-NM bundles compared to $CTRL_{pediatric}$ bundles ($P < 0.05$). (B) Myosin heavy chain composition analyses revealed a trend to more MHC 1 in *NEB*-NM bundles compared to $CTRL_{pediatric}$ bundles ($P = 0.06$). In addition, bundles from *NEB*-NM patients lack the MHC 2X isoform.

The effect of the fast skeletal muscle troponin activator CK-2066260 on the calcium-sensitivity of force generation

Dose-response relationship Since troponin activators increase the calcium-sensitivity of force generation, we set out to determine whether the troponin activator CK-2066260 might improve the contractile properties of nebulin-deficient muscle. To determine the concentration of CK-2066260 at which it exerts its maximal effect, we first established dose-response curves for the different muscle fiber preparations relating the concentration of drugs to the percentage of maximal force (Figure 5). For this purpose, muscle fibers were activated at pCa 6.0 – this pCa was chosen because it yielded ~35% of maximal force – in the presence of incremental CK-2066260 concentrations. For a typical response of a fiber to incremental concentrations of CK-2066260, see Figure 5A.

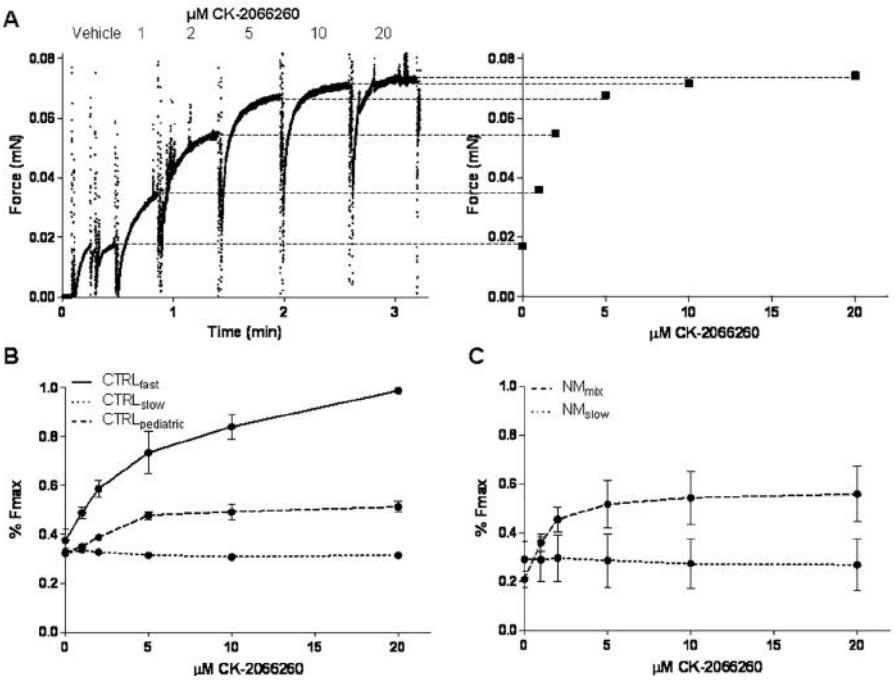

Figure 5 Dose–response relationship of CK-2066260 in skinned muscle preparations

(A) Example of a force trace from a skinned muscle bundle that is sequentially exposed to incremental CK-2066260 concentrations. (B) Dose-response relation of CK-2066260 in fast–twitch and slow-twitch CTRL$_{adult}$ single fibers and CTRL$_{pediatric}$ bundles with a mixed myosin heavy chain (MHC) composition. (C) Dose-response relationship of CK-2066260 in predominantly slow-twitch (<12% fast-twitch) and *NEB*-NMbundles with a mixed MHC composition. Vehicle (1% DMSO) was present in all experiments.

Since the bundles of both the *NEB*-NM patients and $CTRL_{pediatric}$ specimens contained a mix of both slow-twitch and fast-twitch twitch fibers, and because we were also interested in the compound's effect on pure slow-twitch and fast-twitch fibers, we also tested individual slow- and fast-twitch fibers from $CTRL_{adult}$. Slow-twitch single fibers from $CTRL_{adult}$ (n = 2) and *NEB*-NM patient bundles composed of predominantly (>90%) slow-twitch fibers (n = 2) did not respond to CK-2066260 at any of the concentrations tested (Figure 5B-C). In fast-twitch single fibers from adult $CTRL_{adult}$ (n = 2), mixed $CTRL_{pediatric}$ bundles (n = 2) and mixed *NEB*-NM patient bundles (n = 3), force enhancement was near maximal at 5 µM CK-2066260 (Figure 5B-C). Therefore, a concentration of 5 µM CK-2066260 was used to investigate the effect of the compound on contractile performance of skinned muscle fibers.

Calcium-sensitivity of force generation

The presence of 5 µM CK-2066260 induced a leftward shift in the force-pCa relation in $CTRL_{pediatric}$, as reflected by the increase of the pCa_{50} value from 5.88 ± 0.01 (n = 6) in vehicle only to 6.18 ± 0.01 (n = 6) in CK-2066260 (Figure 6A). The cooperativity of activation was lower in the presence of 5 µM CK-2066260 (nH 1.70 ± 0.11 vs. 2.47 ± 0.13 in vehicle (n = 6)). Importantly, in *NEB*-NM patient bundles a marked leftward shift in the force-pCa relation was observed in the presence of CK-2066260. The pCa_{50} increased from 5.78 ± 0.04 to 6.02 ± 0.02 (n = 19), without affecting nH (1.15 ± 0.11 vs. 1.33 ± 0.14 (n = 19) in vehicle) (Figure 6B). The magnitude of increase in pCa_{50} induced by CK-2066260 was not significantly different in $CTRL_{pediatric}$ fibers (0.26 ± 0.04 pCa units) compared to nebulin-deficient NM fibers (0.24 ± 0.05 pCa units). However, when taking into account that the fiber bundles from *NEB*-NM patients contained a higher percentage of non-responsive fibers expressing MHC 1 (Figure 4B), the effect size of the compound in fibers expressing MHC 2 might be larger in *NEB*-NM patient fibers. Indeed, a significant correlation was observed between the percentage of fast-twitch fibers in the fiber bundles from *NEB*-NM patients and the magnitude of increase in pCa_{50} upon 5 µM CK-2066260 administration (Figure 6C, Pearson r = 0.79).

Comparing skeletal muscle fibers of *NEB*-NM patients treated with 5 µM CK-2066260 to untreated $CTRL_{pediatric}$ fibers, reveals that the fast troponin activator enhances calcium-sensitivity of force generation in *NEB*-NM patients above normal control values (Figure 6D). We also investigated whether the maximal

active tension was affected by CK-2066260. $Fmax_{CK\text{-}2066260}$ expressed as percentage of $Fmax_{vehicle}$ was 96.5 ± 1.2% (n = 10) in $CTRL_{pediatric}$ and 98.3 ± 2.2% (n = 18) in *NEB*-NM patients (Figure 6E), indicating that CK-2066260 did not affect maximal active tension. Thus, the effect of CK-2066260 is that it completely restores the impaired calcium-sensitivity of force generation in skeletal muscle fibers from *NEB*-NM patients.

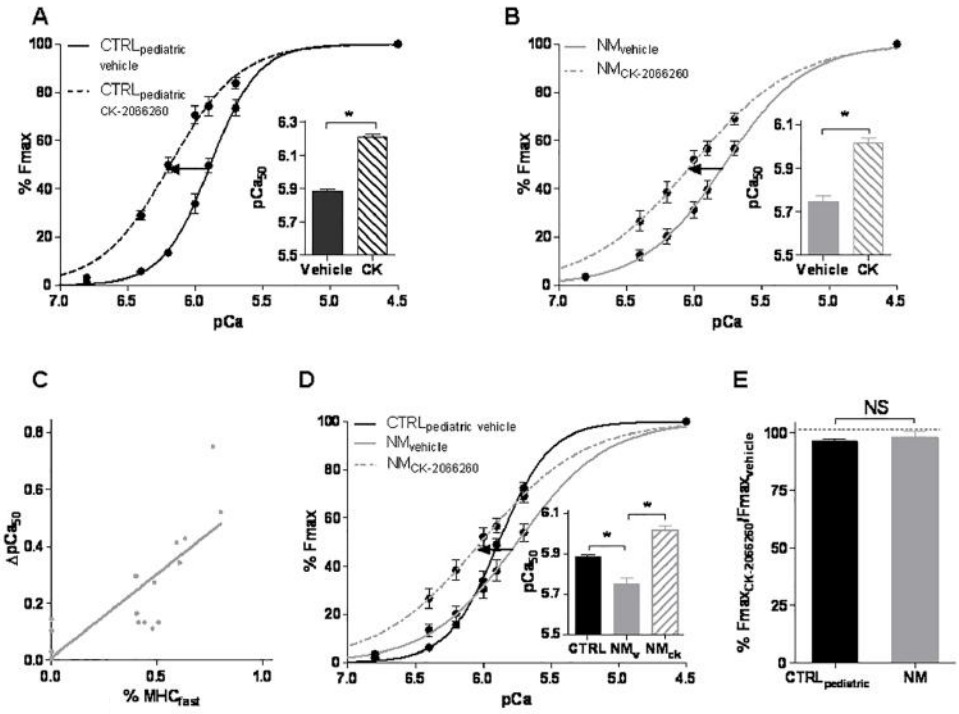

Figure 6 Effect of CK-2066260 on calcium-sensitivity of force generation in skinned muscle bundles at a sarcomere length of 2.1 µm

(A) CK-2066260 (5 µM) increased the calcium-sensitivity of force generation (reflected by the pCa_{50} value) in muscle fibers from $CTRL_{pediatric}$ ($P < 0.05$). (B) 5 µM CK-2066260 increased calcium-sensitivity of force generation in muscle fibers from *NEB*-NM patients ($P < 0.05$). (C) The CK-2066260-induced shift on the pCa_{50} value was correlated to the NM bundle's MHC_{fast} content (Pearson r = 0.79). (D) In the presence of 5 µM CK-2066260, the pCa_{50} of *NEB*-NM patients exceeded that of normal $CTRL_{pediatric}$ values. (E) No significant effect of CK-2066260 on maximal active tension in muscle fibers from $CTRL_{pediatric}$ and *NEB*-NMpatients was observed.

The experiments described above were performed at a sarcomere length of 2.1 μm. Because skeletal muscle operates at a range of sarcomere lengths, we also studied a longer sarcomere length (2.6 μm). The calcium-sensitivity of force generation increases when sarcomere length increases (Figure 7A), a well-known phenomenon called length-dependency of activation. Interestingly, this length-dependency of activation (expressed as ΔpCa50: the increase in pCa_{50} at a sarcomere length of 2.6 μm compared to that at 2.1 μm) is higher in *NEB*-NM patients (ΔpCa_{50}: 0.15 ± 0.02, n = 11) compared to $CTRL_{pediatric}$ (ΔpCa_{50}: 0.090 ± 0.01, n = 10), Figure 7A. Due to this more prominent length-dependency of activation in fibers from *NEB*-NM patients, the calcium-sensitivity of force generation in these patients (5.88 ± 0.04) was not significantly different from $CTRL_{pediatric}$ (5.97 ± 0.03) (see Figure 7B) at a sarcomere length of 2.6 μm. As shown in Figure 7B, also at a sarcomere length of 2.6 μm, CK-2066260 induced a marked increase in the calcium-sensitivity of force generation in skinned fiber bundles from both $CTRL_{pediatric}$ (pCa_{50} increased from 5.97 ± 0.03 in vehicle to 6.18 ± 0.04 in CK-2066260) and *NEB*-NM patients (pCa_{50} increased from 5.88 ± 0.04 to 6.01 ± 0.06).

For an overview of the pCa_{50} data and for a detailed description of the number of preparations used for each parameters see Table 1 of the supplemental data.

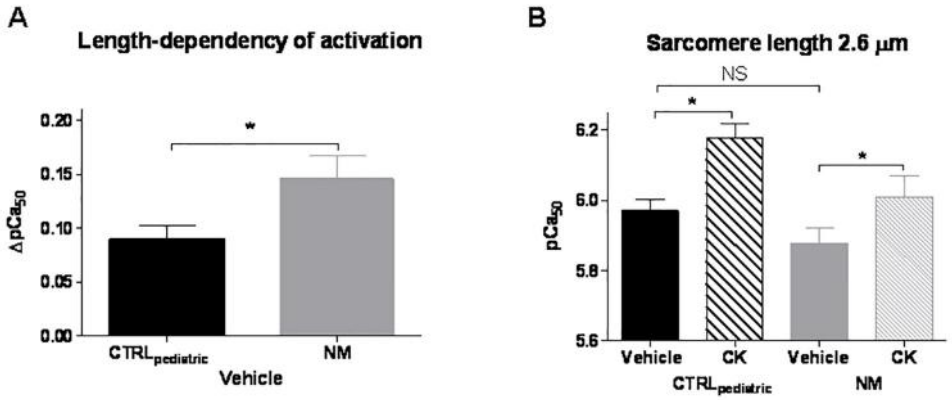

Figure 7 The calcium-sensitivity of force generation and the effect of CK-2066260 at a sarcomere length of 2.6 μm

(A) Length-dependency of activation (expressed as ΔpCa_{50}: the increase in pCa_{50} at a sarcomere length of 2.6 μm compared to that at 2.1 μm) was more prominent in *NEB*-NM patients compared to $CTRL_{pediatric}$ ($P < 0.05$). (B) At a sarcomere length of 2.6 μm, 5 μM CK-2066260 increased the pCa_{50} significantly in both muscle fibers from $CTRL_{pediatric}$ and *NEB*-NM patients ($P < 0.05$). At this longer sarcomere length, no significant difference in pCa_{50} between $CTRL_{pediatric}$ fibers and *NEB*-NM fibers was observed.

DISCUSSION

As lower calcium-sensitivity of force generation contributes to weakness of *NEB*-NM muscle, we studied the ability of the novel fast skeletal muscle troponin activator, CK-2066260, to augment force generation at submaximal levels of activation in skeletal muscle fibers from *NEB*-NM patients. CK-2066260 greatly increases the calcium-sensitivity of force generation in fast-twitch fibers at both sarcomere lengths that were studied to levels that are similar (SL 2.6 μm) or exceed (SL 2.1 μm) those observed in control subjects. Thus, fast skeletal troponin activation might be a therapeutic mechanism to augment muscle strength in *NEB*-NM patients.

Force generation is lower in muscle fibers from NEB-NM patients compared to those from controls

The severe reductions in force levels generated by fibers of NM patients are clearly due to contractile deficits caused by defects in sarcomeric proteins (Sanoudou and Beggs, 2001), rather than lower neural activation, ineffective excitation contraction coupling, or other non-contractile defects. Mechanisms that have been shown to contribute to muscle weakness in

NEB-NM include myofibrillar disarray (Ottenheijm et al., 2009; Ryan et al., 2003), shorter thin filaments (Ottenheijm et al., 2009), altered cross bridge cycling kinetics (Lawlor et al., 2011; Ottenheijm et al., 2010), and a reduced calcium-sensitivity of force generation (Ottenheijm et al., 2010).

Previous studies indicated that the calcium-sensitivity of force generation is lower in muscle fibers from pediatric *NEB*-NM patients compared to fibers from controls (Ottenheijm et al., 2010). Because control subjects in prior studies were adults, rather than age-matched pediatric control subjects (due to the lack of availability of the latter), it could not be ruled out that the age differences between groups confounded the results. Here, we overcame this limitation by including a control group of pediatric patients, with an average age that was close to that of the pediatric *NEB*-NM patients (see Table 1), and who were biopsied during investigation of diseases that turned out to be non-neuromuscular in basis and who had histologically normal muscle. Importantly, the contractile performance of muscle fibers from these pediatric controls closely resembles that of adult controls (Figure 3B-C), thereby validating our previous work in which pediatric *NEB*-NM patients were compared to adult controls. The *NEB*-NM patients that we investigated in the present study have NEB mutations that are distinct from those in our previous work (Ottenheijm et al., 2010), but their fibers exhibited similar reductions in calcium-sensitivity of force generation (Figure 4A), confirming the findings of our previous studies (Ottenheijm et al., 2010), and suggesting that lower calcium-sensitivity of force generation is a general characteristic in *NEB*-NM patients.

The mechanisms underlying the lower calcium-sensitivity of force generation in *NEB*-NM patients are unclear, but it seems likely that they are a direct consequence of the severely low nebulin protein levels that we observed here (Figure 2A) and that were also found in our previous work (Lawlor et al., 2011; Ottenheijm et al., 2010). This concept is supported by studies of a nebulin-deficient mouse model, which revealed that nebulin augments the calcium-sensitivity of force generation (Chandra et al., 2009), presumably through its interaction with other regulatory proteins such as tropomyosin and troponin or as a consequence of nebulin's effect on cross bridge cycling kinetics (Lukoyanova et al., 2002; Ogut et al., 2003; Ottenheijm and Granzier, 2010). Accordingly, a recent study of muscle fibers from a *NEB*-NM patient with only slightly reduced nebulin protein levels showed no change in calcium-

sensitivity of force generation (Ochala et al., 2011).

A novel aspect of the present study was our examination of the length-dependency of activation through determination of the calcium-sensitivity of force generation at sarcomere lengths of both 2.1 μm and 2.6 μm. Interestingly, at a sarcomere length of 2.6 μm the calcium-sensitivity of force generation in muscle fibers from *NEB*-NM patients was not significantly lower than in those from $CTRL_{pediatric}$. Hence, the reduced calcium-sensitivity of force generation contributes to weakness in *NEB*-NM patients mainly when muscles operate at short lengths. The absence of a difference in calcium-sensitivity of force generation at the longer sarcomere length is explained by the exaggerated length-dependency of activation in nebulin-deficient fibers from NM patients (as shown in Figure 7A). These findings are consistent with previous studies on nebulin-deficient mouse muscle, which also revealed a lower calcium-sensitivity of force generation compared to that of wild type muscle fibers at a sarcomere length of 2.1 μm (Chandra et al., 2009), but no difference at a longer sarcomere length (Bang et al., 2006; Witt et al., 2006). Both these findings and our results imply that nebulin plays a role in the length-dependency of activation (Ottenheijm and Granzier, 2010). This length-dependency of activation is most prominent in (nebulin-free) cardiac muscle, where it underlies the Frank-Starling law of the heart, but is much less pronounced in skeletal muscle (Konhilas et al., 2002). The presence of nebulin provides an explanation for why activation in skeletal muscle possesses less length-dependency: nebulin increases calcium-sensitivity of force generation at a short sarcomere length. Thus, nebulin-deficient muscle from NM patients lacks this feature provided by nebulin, leading to reduced calcium-sensitivity of force generation at short sarcomere lengths.

The novel fast skeletal muscle specific troponin activator CK-2066260: Clinical implications for NEB-NM patients

To date, no effective therapy is available for *NEB*-NM patients. In the present work, we studied the effect of targeting the lower calcium-sensitivity of force generation in *NEB*-NM muscle fibers by using an analogue of a recently developed compound that amplifies the response of the thin filament to calcium in fast skeletal muscle fibers (Russell et al., 2012). The compound that we used structurally and functionally resembles the fast skeletal muscle troponin activator, tirasemtiv (formerly CK-2017357) (Shefner et al., 2012). This troponin activator was shown to greatly enhance calcium-sensitivity of

force generation in healthy rat and human skeletal muscle fibers (Russell et al., 2012) and is currently being studied as therapy for amyotrophic lateral sclerosis (Shefner et al., 2012). Tirasemtiv slows the dissociation rate of calcium from the troponin complex (Russell et al., 2012), thereby stabilizing the open-conformation of the troponin/tropomyosin complex to enhance cross-bridge formation at a given calcium concentration. The analogue CK-2066260 is a close structural analog of tirasemtiv and has a similar mechanism of action. Like CK-2017357, CK-2066260 is selective for the fast skeletal troponin complex and has little effect on slow skeletal muscle (Fig. 5B and C). In the present study, we observed that CK-2066260 greatly increased the calcium-sensitivity of force generation – without affecting nH - in skeletal muscle fibers from *NEB*-NM patients to levels that exceed those observed in untreated control muscle (Figure 6D).

Other troponin activators, such as levosimendan (van Hees et al., 2009) and EMD 57033 (Ochala et al., 2008, 2012), were shown in the past to also increase the calcium-sensitivity of force generation in human skeletal muscle fibers. However, a disadvantage of these agents is that, since they are cardiac/slow skeletal-specific, they also affect cardiac function. Increasing the calcium-sensitivity of force generation in cardiac muscle might slow ventricular relaxation which compromises ventricular filling and might cause diastolic dysfunction. Thus, troponin activators that are specific for fast-twitch muscle fibers – such as CK-2066260 – are appealing compounds to ameliorate skeletal muscle weakness in skeletal muscle-specific myopathies such as NM.

Considering that the normal activation level of muscle is submaximal - between 10% and 65% of its maximal force (Jasmin and Gardiner, 1987) - during normal activity, the potential of troponin activators for the treatment of muscle weakness in NM patients is high. Our findings reveal that CK-2066260 increases force generation of muscle fibers from *NEB*-NM patients by 20-140% (Figure 6B) at the tested submaximal levels of activation. Thus, although the muscle fibers from patients have a diminished capacity to produce maximal force and CK-2066260 did not fully restore maximal muscle fiber force back to control values, the substantial increase in force at submaximal muscle activation produced by CK-2066260 may still improve quality of life in these patients. The benefit from troponin activators involves both increased force development and increased efficiency by reducing the

amount of cytosolic calcium that is required to generate a given level of force. Considering that the energy utilization of the calcium pump SERCA accounts for 30-40% of total ATP consumption during muscle contraction (Barclay et al., 2007), the use of a troponin activator has the potential to reduce the amounts of calcium that cycles each contraction, thereby reducing muscle fatigue, which is especially important for the respiratory muscles in patients with NM. Note that respiratory failure, due to diaphragm weakness, is the main cause of death in neonates and children with NM (North et al., 1997). In support of this potential role for troponin activators in attenuating respiratory failure, a recent study with a cardiac/slow-skeletal specific agent confirmed an improved neuromechanical efficiency and reduced development of fatigue of the human diaphragm during loading tasks *in vivo* (Doorduin et al., 2012).

It should be noted that the potential therapeutic value of troponin activators such as CK-2066260 is not restricted to NM patients which suffer from a lower calcium-sensitivity of force generation; Russell and coworkers (Russell et al., 2012) reported force augmentation in the face of limited neural input. In particular, patients with disorders involving defective excitation-contraction coupling such as minicore myopathy, central core myopathy or myotubular myopathy, might benefit by maximizing the effect of suboptimal calcium influx. However *NEB*-NM patients might have a larger window for improvement because they suffer from a lower calcium-sensitivity of force generation. Thus, troponin activation is a potential therapeutic mechanism to improve force in NM patients with nebulin mutations as well as potentially with other neuromuscular diseases.

REFERENCES

Bang M-L, Caremani M, Brunello E, Littlefield R, Lieber RL, Chen J, et al. Nebulin plays a direct role in promoting strong actin-myosin interactions. FASEB J. 2009; 23: 4117–4125.

Bang M-L, Li X, Littlefield R, Bremner S, Thor A, Knowlton KU, et al. Nebulin-deficient mice exhibit shorter thin filament lengths and reduced contractile function in skeletal muscle. J. Cell. Biol. 2006; 173: 905–916.

Barclay CJ, Woledge RC, Curtin N a. Energy turnover for Ca2+ cycling in skeletal muscle. J. Muscle Res. Cell. M. 2007; 28: 259–274.

Castillo A, Nowak R, Littlefield KP, Fowler VM, Littlefield RS. A nebulin ruler does not dictate thin filament lengths. Biophys. J. 2009; 96: 1856–1865.

Chandra M, Mamidi R, Ford S, Hidalgo C, Witt CC, Ottenheijm CA, et al. Nebulin alters cross-bridge cycling kinetics and increases thin filament activation: a novel mechanism for increasing tension and reducing tension cost. J. Biol. Chem. 2009; 284: 30889–30896.

Doorduin J, Sinderby C a, Beck J, Stegeman DF, van Hees HWH, van der Hoeven JG, et al. The calcium sensitizer levosimendan improves human diaphragm function. Am. J. Resp. Crit. Care 2012; 185: 90–95.

Gokhin D, Bang M. Reduced thin filament length in nebulin-knockout skeletal muscle alters isometric contractile properties. Am. J. Resp. Crit. Care 2009; 296: 1123–1132.

van Hees HWH, Dekhuijzen PNR, Heunks LM. Levosimendan enhances force generation of diaphragm muscle from patients with chronic obstructive pulmonary disease. Am. J. Resp. Crit. Care 2009; 179: 41–47.

Jasmin BJ, Gardiner PF. Patterns of EMG activity of rat plantaris muscle during swimming and other locomotor activities. J. Appl. Phys. 1987; 63: 713–718.

Konhilas JP, Irving TC, de Tombe PP. Length-dependent activation in three striated muscle types of the rat. J. Phys. 2002; 544: 225–236.

Lawlor MW, Ottenheijm CA, Lehtokari V-L, Cho K, Pelin K, Wallgren-Pettersson C, et al. Novel mutations in NEB cause abnormal nebulin expression and markedly impaired muscle force generation in severe nemaline myopathy. Skelet. Muscle. 2011; 1: 23.

Lukoyanova N, VanLoock MS, Orlova A, Galkin VE, Wang K, Egelman EH. Each actin subunit has three nebulin binding sites: implications for steric blocking. Curr. Biol. 2002; 12: 383–388.

North KN, Laing NG, Consortium I. Nemaline myopathy: current concepts. The ENMC International Consortium and Nemaline Myopathy. J. Med. Genet. 1997; 34: 705–713.

Ochala J, Gokhin DS, Pénisson-Besnier I, Quijano-Roy S, Monnier N, Lunardi J, et al. Congenital myopathy-causing tropomyosin mutations induce thin filament dysfunction via distinct physiological mechanisms. Hum. Mol. Genet. 2012: Epub ahead of print.

Ochala J, Lehtokari V-L, Iwamoto H, Li M, Feng H-Z, Jin J-P, et al. Disrupted myosin cross-bridge cycling kinetics triggers muscle weakness in nebulin-related myopathy. FASEB J. 2011; 25: 1903–1913.

Ochala J, Li M, Ohlsson M, Oldfors A, Larsson L. Defective regulation of contractile function in muscle fibres carrying an E41K beta-tropomyosin mutation. J. Phys. 2008; 586: 2993–3004.

Ogut O, Hossain MM, Jin J-P. Interactions between nebulin-like motifs and thin filament regulatory proteins. J. Biol. Chem. 2003; 278: 3089–3097.

Ottenheijm CAC, Granzier H. Lifting the nebula: novel insights into skeletal muscle contractility. Physiology 2010; 25: 304–310.

Ottenheijm CAC, Hooijman P, DeChene ET, Stienen GJ, Beggs AH, Granzier H. Altered myofilament function depresses force generation in patients with nebulin-based nemaline myopathy (NEM2). J. Struct. Biol. 2010; 170: 334–343.

Ottenheijm CAC, Witt CC, Stienen GJ, Labeit S, Beggs AH, Granzier H. Thin filament length dysregulation contributes to muscle weakness in nemaline myopathy patients with nebulin deficiency. Hum. Mol. Genet. 2009; 18: 2359–2369.

Pappas CT, Krieg PA, Gregorio CC. Nebulin regulates actin filament lengths by a stabilization mechanism. J. Cell. Biol. 2010; 189: 859–870.

Pelin K, Hilpelä P, Donner K, Sewry C, Akkari PA, Wilton SD, et al. Mutations in the nebulin gene associated with autosomal recessive nemaline myopathy. Proc. Natl. Acad. Sci. 1999; 96: 2305–2310.

Russell AJ, Hartman JJ, Hinken AC, Muci AR, Kawas R, Driscoll L, et al. Activation of fast skeletal muscle troponin as a potential therapeutic approach for treating neuromuscular diseases. Nat. Med. 2012; 18: 452–455.

Ryan MM, Ilkovski B, Strickland CD, Schnell C, Sanoudou D, Midgett C, et al. Clinical course correlates poorly with muscle pathology in nemaline myopathy. Neurology 2003; 60: 665–673.

Sambuughin N, Yau KS, Olivé M, Duff RM, Bayarsaikhan M, Lu S, et al. Dominant mutations in KBTBD13, a member of the BTB/Kelch family, cause nemaline myopathy with cores. Am. J. Hum. Genet. 2010; 87: 842–847.

Sanoudou D, Beggs AH. Clinical and genetic heterogeneity in nemaline myopathy-a disease of skeletal muscle thin filaments. Trends Mol. Med. 2001; 7: 362–368.

Shefner J, Cedarbaum JM, Cudkowicz ME, Maragakis N, Lee J, Jones D, et al. Safety, tolerability and pharmacodynamics of a skeletal muscle activator in amyotrophic lateral sclerosis. Amyotroph. Lateral. Scler. 2012; 13: 430–438.

Wallgren-Pettersson C, Laing NG. Report of the 70th ENMC International Workshop: Nemaline myopathy, 11-13 June 1999, Naarden, The Netherlands. Neuromuscul. Disord. 2000; 10: 299–306.

Warren CM, Krzesinski PR, Greaser ML. Vertical agarose gel electrophoresis and electroblotting of high-molecular-weight proteins. Electrophoresis 2003; 24: 1695–1702.

Witt CC, Burkart C, Labeit D, McNabb M, Wu Y, Granzier H, et al. Nebulin regulates thin filament length, contractility, and Z-disk structure in vivo. EMBO J. 2006; 25: 3843–3855.

Supplemental Table 1 Maximal active tension and calcium-sensitivity of force generation of nemaline myopathy patients and of control subjects

Biopsy	Maximal active tension (mN/mm^2)				Calcium-sensitivity of force generation (pCa_{50})							
	Sarcomere length 2.1 µm				Sarcomere length 2.1 µm				Sarcomere length 2.6 µm			
	Vehicle	*n*	*CK-2066260*	*n*	*Vehicle*	*n*	*CK-2066260*	*n*	*Vehicle*	*n*	*CK-2066260*	*n*
Nemaline myopathy patients with nebulin mutations												
26-2 | T33	25.6	6	24.9	6	5.80	6	5.87	6	5.93	4	5.91	4
258-2 | T1069	17.6	4	18.0	4	5.92	5	6.15	5	5.94	2	6.15	2
974-1 | T1033	9.8	4	9.3	4	5.74	5	6.17	5	-	-	-	-
988-1 | T887	22.1	5	21.6	5	5.72	5	5.91	5	5.93	5	6.09	5
Pediatric control subjects												
212-1 | T141	69.1	6	69.7	6	5.89	6	6.03	6	5.86	1	6.01	1
213-1 | T142	71.0	3	71.0	3	5.86	3	5.92	3	-	-	-	-
218-1 | T147	110.1	4	103.7	4	5.87	4	6.21	4	5.98	4	6.23	4
219-1 | T148	115.0	4	115.0	4	5.90	3	6.02	3	6.05	1	6.11	1
Adult control subjects												
$CTRL_{slow}$	85.8	4	84.9	4	5.84	4	5.86	4	-	-	-	-
$CTRL_{fast}$	103.1	17	100.0	17	5.88	20	6.33	20	5.86	4	6.34	4

N.B. Due to the experimental design, at a sarcomere length of 2.6 µm some muscle preparations had to be excluded with respect to quality criteria. Therefore, the number of experiments per group is reduced at sarcomere length 2.6 µm.

CHAPTER 9

DISCUSSION, SUMMARY AND FUTURE PERSPECTIVES

DISCUSSION AND SUMMARY

Nemaline myopathy is a debilitating muscle disease, for which currently no treatment exists as the mechanisms underlying muscle weakness are only partly understood. Therefore, the aim of this thesis was to gain more insight into the pathophysiology of muscle weakness in nemaline myopathy and to investigate genotype-functional phenotype correlations to direct targeted therapeutic interventions (Chapter 2 – 5), and to test potential therapeutic targets to restore muscle strength (Chapter 6 – 8). Here, first the outcomes of the studies are described and discussed, followed by a discussion on future directions.

Pathophysiology of nemaline myopathy

Chapter 2

Nemaline myopathy is a disease that affects the skeletal muscle thin filament. As the overlap between the thick and the thin filament determines the number of cross-bridges that can be formed, we investigated whether mutations implicated in nemaline myopathy contribute to force loss by affecting thin filament length. The force-sarcomere length dependency of force was studied in fifty-one biopsies covering the majority of genes implicated in nemaline myopathy (*NEB, ACTA1, TPM2, TPM3, TNNT1, KBTBD13, KLHL40* and *KLHL41*). This study thought us that all mutations resulted in muscle weakness at the myofilament level, but that the contribution of shorter thin filament length to muscle weakness was specific for mutations in *ACTA1* and *NEB*. Next, findings in a nebulin-deficient mouse model for nemaline myopathy revealed that skeletal muscle compensates for shorter thin filament length by adding more sarcomeres in series.

This study was designed to answer a key question in the nemaline myopathy field: are there genotype-functional phenotype correlations in nemaline myopathy? Clear correlations will guide targeted treatment of muscle weakness. The present study reveals that only specific mutations in the *NEB* and *ACTA1* gene result in changes in thin filament length. Note that from two gene cohorts - *KLHL40* and *KLHL41* – only one patient sample was studied. Both *KLHL40* and *KLHL41* are known to interact with either nebulin and leiomodin-3 and/or actin (Garg et al., 2014; Gupta et al., 2013). Mutations in leiomodin-3 have recently been reported to affect thin filament length

regulation (Yuen et al., 2014). Hence, next to *NEB, ACTA1* and *LMOD3*, mutations in *KLHL40* and *KLHL41* are potential players in thin filament length regulation.

It is presumed that mutations in *TPM2, TPM3* and *KBTBD13* do not compromise thin filament length regulation. The finding in the *TPM3* gene cohort is supported by previous structural studies on biopsies from nemaline myopathy patients with mutation in *TPM3* (Ottenheijm et al., 2011; Yuen et al., 2015). Of interest, another important parameter for force generation –the calcium-sensitivity of force generation - was affected bidirectionally in tropomyosin-based nemaline myopathy. The effect on the calcium-sensitivity of force generation was mutation-dependent: either a hypertonic or a hypotonic functional phenotype was observed (Donkervoort et al., 2015; Mokbel et al., 2013; Ottenheijm et al., 2011; Yuen et al., 2015). In line with these findings in tropomyosin-based nemaline myopathy, also in nebulin-based nemaline myopathy mutation-dependent changes in thin filament length regulation and activation are found. For example, a deletion of exon-55 compromised both thin filament length regulation and thin filament activation (lower calcium-sensitivity of force generations and lower cross-bridge cycling kinetics (Ottenheijm et al., 2009, 2010, 2013; de Winter et al., 2013), but compound heterozygous splice site mutations (in exons 3 and exon 22, respectively), revealed normal thin filament lengths and normal calcium-sensitivity of force generation but impaired cross-bridge cycling kinetics (Ochala et al., 2011). Thus, combining the present data with data that was reported previously, the concept arises that in nemaline myopathy the functional phenotype is mutation-dependent. Hence, we should revise our research question into: are there *mutation*-functional phenotype correlations in nemaline myopathy? High-throughput studies in flies or fish might aid in elucidating mutation-functional phenotype correlations in nemaline myopathy (Berger et al., 2014; Sztal et al., 2015; Telfer et al., 2012).

In part two of Chapter 2 we investigated whether muscle responds to shorter thin filament lengths by using the recently developed conditional nebulin knockout mouse. This model recapitulates nemaline myopathy: muscle fibers generate lower maximal active tension, have shorter thin filaments and as a consequence, the optimal sarcomere length for force production is shorter (Li et al., 2015). However, conditional nebulin knock-out mice increased the number of sarcomeres in series, and as a result the optimal muscle length

for force generation in intact muscle was comparable to wild-type mice. Hence, the addition of sarcomeres in series allowed the muscles to operate at a shorter sarcomere length, a length closer to their optimal sarcomere length. Adapting the number of sarcomeres in series to compensate for changes in thin filament length constitutes a novel control mechanism in muscle. Whether this control mechanism is also present in human diseased muscle is unknown. Simultaneous measurement of total fiber and sarcomere length in humans is challenging. In this respect, knowledge on the *in vivo* sarcomere length range in thin filament myopathy patients might provide valuable information: shorter sarcomeres would indicate more sarcomeres in series. The elucidation of this control mechanism might have implications for treatment strategies. In rodents, active stretching of muscle stimulates the addition of sarcomeres in series (Riley and Van Dyke, 2012). Thus, active stretching of muscles of patients with shorter thin filament lengths might be an interesting direction to explore to stimulate the addition of sarcomeres in series and alleviate muscle weakness.

Chapter 3

The aim of Chapter 3 was to investigate whether there are correlations between the ultrastructure of muscle fibers from nemaline myopathy patients with mutations in the nebulin gene and the functional phenotype and clinical phenotype of muscle fibers from these patients. We found that the clinical severity was associated with the functional phenotype and the sarcomeric ultrastructure. The latter is defined here as the alignment of myofibrils. Interestingly, related to this was the finding that the subsarcolemmal position of rods appeared to inversely correlate with the clinical and functional phenotype. Thus, when the nemaline bodies are located at the subsarcolemmal region, myofibrillar alignment is preserved which favors contractile performance. The question remains what mechanisms orchestrate the organization of nemaline bodies and whether this is correlated to nebulin protein levels. These are interesting questions for future research. Although the ultrastructure of the muscle fibers of mildly affected nemaline myopathy patients is relatively preserved, contractile weakness is observed compared to the contractile performance of control fibers. This phenomenon has been reported in literature previously (Donkervoort et al., 2015; Ottenheijm et al., 2011) de Winter et al., 2016, and suggests that intrinsic dysfunction of the contractile proteins accounts for the contractile weakness observed

at the single fiber level. An elegant way to investigate the contribution of purely contractile protein function to muscle fiber weakness is to study the contractile performance of myofibrils (Stehle et al., 2009). A muscle fiber (diameter ~ 100 μm) consists of a large collection of myofibrils (diameter ~ 1 μm), hence changes in the ultrastructure of the muscle fiber – e.g. the connectivity of adjacent myofibrils – influences the contractile performance of this interconnected collection of myofibrils. In a recent study, it was shown that the contractile deficit in myofibrils isolated from nebulin-deficient mouse muscle resembles the contractile deficit that was observed in single fibers from that muscle (Ottenheijm et al., 2013). These data suggest that dysfunctional contractile proteins are a main cause of weakness in nebulin-based nemaline myopathy.

Chapter 4

In Chapter 4 we characterized the in vivo and in vitro contractile performance of heterozygous nebulin-knockout mice, and investigated whether changes in sarcomeric gene and protein levels were correlated to the contractile phenotype of intact soleus muscle. This study revealed that heterozygous nebulin-knockout mice have normal nebulin protein levels. However, the mRNA levels encoding slow-twitch regulatory proteins troponin C, T and I and slow-twitch myosin heavy chain were 5-7 fold upregulated. In line with the upregulation of slow-twitch-myosin heavy chain mRNA, a shift in the myosin heavy chain composition was observed at the protein level: muscle of nebulin-knockout mice display a higher slow-twitch over fast-twitch myosin heavy chain ratio. The switch towards a slow-twitch proteomic phenotype was accompanied by mild muscle weakness at maximal stimulation frequencies at the in vitro intact muscle level. It's striking that the absence of one nebulin allele has no effect on nebulin protein levels, but does affect the levels of slow-twitch regulatory proteins. Also in other mouse models for nemaline myopathy (Corbett, 2001; Nguyen et al., 2011; Ravenscroft et al., 2011; Tian et al., 2015), muscle biopsies of nemaline myopathy patients and in other neuromuscular conditions (D'Antona et al., 2007) this switch is observed. An important question that remains to be addressed is what triggers this induction of a slow-twitch gene program. And why muscle responds this way: is it a preventive strategy, as a slow-twitch muscle is more fatigue resistant? These are interesting questions for future research. Especially, as a recent study on a novel nebulin-deficient mouse model revealed that the soleus

muscle – a typical example of an oxidative muscle in mice - was relatively spared compared to the glycolytic muscles (Li et al., 2015). In addition to that, nemaline myopathy patients with mutations in *KBTBD13* display mild muscle weakness and hypertrophy of slow-twitch muscle fibers (Gommans et al., 2002; Olivé et al., 2010; Sambuughin et al., 2010). Thus, when muscle possesses the potential of inducing a slow-twitch gene program, this might be a favorable strategy in nemaline myopathy.

Chapter 5

The aim of Chapter 5 was to investigate the role of KBTBD13 in the pathogenesis of muscle weakness. Contractile studies on single fibers isolated from biopsies of NEM6 patients with mutations in the *KBTBD13* gene revealed that at least part of the muscle weakness and muscle slowness is sarcomere-based. In addition, muscle characteristics of the Kbtbd13-KO mouse model partly phenocopy the muscle weakness and slowness of NEM6 patients. Hence, we developed a novel nemaline myopathy mouse model that allows us to further unravel the role of KBTBD13 in health and disease and to test therapeutic strategies for NEM6 patients. Important aspects to focus on in the near future are to elucidate the interaction partner(s) of KBTBD13 and the localization of the protein. The only identified interaction partner thus far is Cullin E3 (Sambuughin et al., 2012). For KLHL40 and KLHL41, interactions with both Cullin E3 and specific thin filament proteins are reported in literature (Cenik et al., 2015; Garg et al., 2014; Gupta et al., 2013). Therefore it is hypothesized that KBTBD13 plays a role in the turnover of (a) thin filament protein(s). Hence, kelch proteins are a very exciting new class of proteins that stabilize thin filament proteins. Therefore, they can be of interest to stabilize specific thin filament proteins that are implicated in nemaline myopathy. As *KBTBD13* is expressed in both skeletal and cardiac muscle tissue, the availability of a *Kbtbd13*-deficient mouse provided us with the possibility to investigate cardiac function under various conditions. Cardiac muscle of *Kbtbd13*-KO had a lower contractile reserve upon stress. Thus far, compromised cardiac function has not been reported in mouse models for nemaline myopathy. To date, some case studies reported cardiac complications in patients with nemaline myopathy (Finsterer and Stöllberger, 2015), but for the NEM6 phenotype this observation is new. As the lower contractile reserve was evident only during stress conditions, the possibility exists that also in other types of nemaline myopathy caused by mutations in

genes that are expressed in the heart, cardiac dysfunction develops during stress conditions. Thus, future studies should take into account the potential of cardiac involvement in nemaline myopathy.

Therapeutic targets in nemaline myopathy

Chapter 6-8

In Chapters 6-8 we investigated the potential of slow- and fast troponin activation to augment muscle strength in muscle fibers from a nebulin-deficient nemaline myopathy mouse model and from nemaline myopathy patients with mutations in the nebulin gene. Troponin activators increase the calcium-sensitivity of force generation. As we found that nebulin-deficient muscle has a lower calcium-sensitivity of force generation, these drugs could have a great potential to restore muscle strength. First, the effect of a slow troponin activator – Levosimendan – was tested. Unfortunately, no gain of function was observed in muscle fibers of controls and patients upon administration of Levosimendan. Besides Levosimendan, other slow troponin activators are available for pre-clinical and clinical use (Schlecht et al., 2016). Therefore, it would be of interest to investigate whether these slow troponin activators have the potential to augment muscle force in nemaline myopathy.

However, note that a potential drawback of slow troponin activators is that they might exert their effect on slow troponin isoforms that are present in the heart muscle. Thus, to specifically target skeletal muscle without risking potential cardiac complications, we moved our attention to a fast troponin activator – CK-2066260. First, we tested the ability of this compound to augment muscle strength in fibers from a nebulin-deficient mouse model that phenocopies nemaline myopathy. Here, a gigantic increase in muscle force was observed at submaximal calcium levels. In addition to the increase in the calcium-sensitivity of force generation, also the cross-bridge cycling kinetics were increased at submaximal calcium levels. Then, we tested the effect of the fast troponin activator on muscle fibers isolated from biopsies of nemaline myopathy patients with mutations in the nebulin gene. To our enthusiasm, also in patient fibers a great increase in muscle force at submaximal calcium levels was observed. This can be of clinical relevance, as these submaximal calcium levels reflect the physiological activity levels: i.e. activity levels that we use in daily life activities as breathing and walking. It is therefore hypothesized that administration of a fast troponin activator will lower fatigue

in daily life activities and thus contribute to the quality of life in nemaline myopathy patients with nebulin mutations. Recent studies in healthy controls reveal that a fast skeletal troponin activator could also amplify the response of the sarcomere *in vivo* (Hansen et al., 2014). In addition to that, positive effects on respiratory function are reported in patients with amyotrophic lateral sclerosis and myasthenia gravis upon administration with a fast troponin activator (Sanders et al., 2015; Shefner et al., 2012). Thus, it would be of great interest to investigate the ability of this fast troponin activator to alleviate muscle weakness in patients with nemaline myopathy. The first crucial steps that we will undertake are to study the effect of the compound on in vivo force production in various mouse models for nemaline myopathy.

FUTURE PERSPECTIVES

Besides the promising concept of fast troponin activation, also other strategies are of highly interest to further explore in the quest for directions to alleviate muscle weakness in nemaline myopathy. First, as disturbed calcium-handling can contribute to muscle weakness (Ottenheijm et al., 2008), compounds that target either the release of calcium or the re-uptake of calcium by the sarcoplasmic reticulum will aid in the alleviation of muscle weakness. In other neuromuscular conditions such as mitochondrial myopathy and duchenne muscular dystrophy, small molecules that target calcium-handling result in improved contractile performance (Cheng et al., 2015; Gineste et al., 2015; Mázala et al., 2015). Another exciting field to further explore is the role of mitochondria in nemaline myopathy. Hitherto, mitochondrial function has not been investigated in nemaline myopathic muscle. In addition to that, also the role of oxidative stress in the pathogenesis of muscle weakness in nemaline myopathy is obscure. As the primary contractile deficits caused by the gene mutations that are implicated in nemaline myopathy can put a high stress on the mitochondria, one hypothesis is that nemaline myopathic muscle can benefit from redox-modulators that reduce the overload of oxidative stress that results from disturbed mitochondrial function. Recent studies in the neuromuscular field reveal that redox-modulators can ameliorate muscle weakness in various mouse models (Cheng et al., 2016; Kang et al., 2015; Lanner et al., 2012; Paolini et al., 2015). A final interesting approach to counteract muscle weakness is to target the trophicity of skeletal muscle cells by inhibiting specific ubiquitin-proteasome pathway enzymes that target skeletal muscle proteins, such as MuRF1 (Bodine et al., 2001; Eddins et al., 2011). That way, loss of contractile proteins can be inhibited to alleviate muscle weakness.

In conclusion, this thesis focused on various mechanisms underlying the pathophysiology in nemaline myopathy, on elucidating genotype-functional phenotype correlations in nemaline myopathy and on the potential of therapeutic strategies to augment muscle force. By setting up a bank for nemaline myopathy biopsies and by the engineering of various mouse models for nemaline myopathy, unique muscle tissue was available to perform translational studies. Mechanisms that can contribute to muscle weakness are changes in (1) thin filament length regulation, (2) the calcium-sensitivity of force generation, (3) the cross-bridge cycling kinetics, (4) the

location of nemaline bodies and (4) the isoform composition of regulatory proteins. These changes revealed to be mutation-dependent. A promising therapeutic target to augment muscle strength in nemaline myopathy is fast skeletal troponin activation.

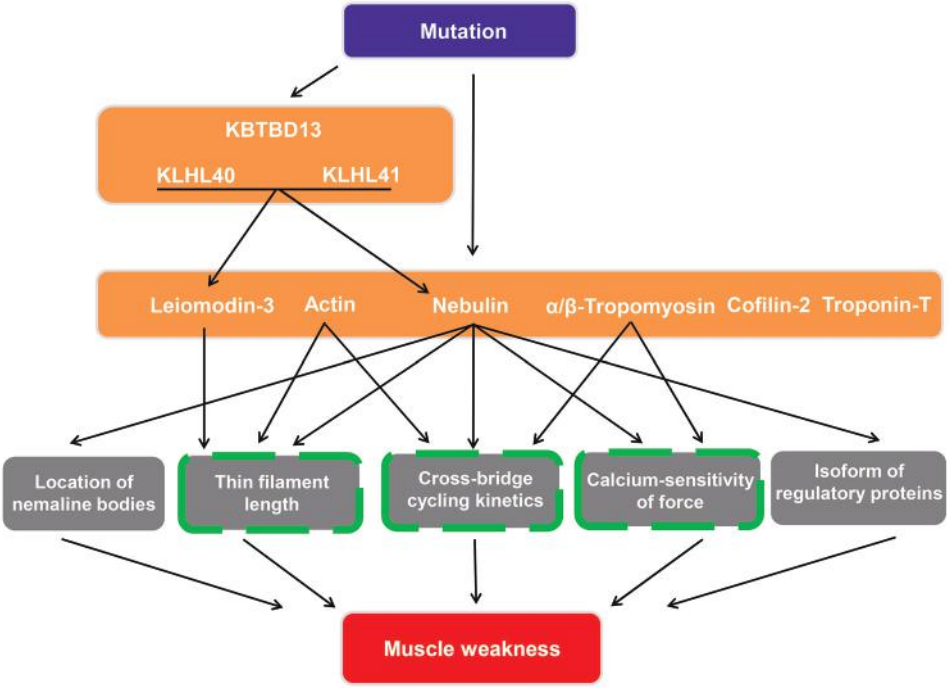

Figure 1 Thesis summary
Schematic overview of the mechanisms by which mutations in genes implicated in nemaline myopathy cause muscle weakness. Mechanisms that can contribute to muscle weakness are changes in (1) the location of nemaline bodies, (2) thin filament length regulation, (3) the cross-bridge cycling kinetics, (4) the calcium-sensitivity of force generation, and (5) the isoform composition of regulatory proteins. These changes revealed to be mutation-dependent. Green dashed lines indicate potential therapeutic targets. The addition of sarcomeres in series is an interesting approach to improve thick-thin filament overlap, and fast troponin activation is a promising target to modulate cross-bridge cycling kinetics and calcium-sensitivity of force.

REFERENCES

Berger J, Tarakci H, Berger S, Li M, Hall TE, Arner A, et al. Loss of Tropomodulin4 in the zebrafish mutant träge causes cytoplasmic rod formation and muscle weakness reminiscent of nemaline myopathy. Dis. Model. Mech. 2014; 7: 1407–15.

Bodine SC, Latres E, Baumhueter S, Lai VK, Nunez L, Clarke BA, et al. Identification of ubiquitin ligases required for skeletal muscle atrophy. Science 2001; 294: 1704–8.

Cenik BK, Garg A, McAnally JR, Shelton JM, Richardson JA, Bassel-Duby R, et al. Severe myopathy in mice lacking the MEF2/SRF-dependent gene leiomodin-3. J. Clin. Invest. 2015; 125: 1569–78.

Cheng AJ, Andersson DC, Lanner JT. Can't live with or without it: calcium and its role in Duchenne muscular dystrophy-induced muscle weakness. Focus on 'SERCA1 overexpression minimizes skeletal muscle damage in dystrophic mouse models'. Am. J. Physiol. Cell Physiol. 2015; 308: C697–8.

Cheng AJ, Yamada T, Rassier D, Andersson DC, Westerblad H, Lanner JT. ROS/RNS and contractile function in skeletal muscle during fatigue and recovery. J. Physiol. 2016

Corbett MA. A mutation in alpha-tropomyosinslow affects muscle strength, maturation and hypertrophy in a mouse model for nemaline myopathy. Hum. Mol. Genet. 2001; 10: 317–328.

D'Antona G, Brocca L, Pansarasa O, Rinaldi C, Tupler R, Bottinelli R. Structural and functional alterations of muscle fibres in the novel mouse model of facioscapulohumeral muscular dystrophy. J. Physiol. 2007; 584: 997–1009.

Donkervoort S, Papadaki M, de Winter JM, Neu MB, Kirschner J, Bolduc V, et al. TPM3 deletions cause a hypercontractile congenital muscle stiffness phenotype. Ann. Neurol. 2015; 78: 982–94.

Eddins MJ, Marblestone JG, Suresh Kumar KG, Leach CA, Sterner DE, Mattern MR, et al. Targeting the ubiquitin E3 ligase MuRF1 to inhibit muscle atrophy. Cell Biochem. Biophys. 2011; 60: 113–8.

Finsterer J, Stöllberger C. Review of Cardiac Disease in Nemaline Myopathy. Pediatr. Neurol. 2015; 53: 473–7.

Garg A, O'Rourke J, Long C, Doering J, Ravenscroft G, Bezprozvannaya S, et al. KLHL40 deficiency destabilizes thin filament proteins and promotes nemaline myopathy. J. Clin. Invest. 2014; 124: 3529–3539.

Gineste C, Hernandez A, Ivarsson N, Cheng AJ, Naess K, Wibom R, et al. Cyclophilin D, a target for counteracting skeletal muscle dysfunction in mitochondrial myopathy. Hum. Mol. Genet. 2015; 24: 6580–7.

Gommans IMP, van Engelen BGM, ter Laak HJ, Brunner HG, Kremer H, Lammens M, et al. A new phenotype of autosomal dominant nemaline myopathy. Neuromuscul. Disord. 2002; 12: 13–18.

Gupta VA, Ravenscroft G, Shaheen R, Todd EJ, Swanson LC, Shiina M, et al. Identification of KLHL41 Mutations Implicates BTB-Kelch-Mediated Ubiquitination as an Alternate Pathway to Myofibrillar Disruption in Nemaline Myopathy. Am. J. Hum. Genet. 2013; 93: 1108–17.

Hansen R, Saikali KG, Chou W, Russell AJ, Chen MM, Vijayakumar V, et al. Tirasemtiv amplifies skeletal muscle response to nerve activation in humans. Muscle Nerve 2014; 50: 925–31.

Kang C, Goodman CA, Hornberger TA, Ji LL. PGC-1α overexpression by in vivo transfection attenuates mitochondrial deterioration of skeletal muscle caused by immobilization. FASEB J. 2015; 29: 4092–106.

Lanner JT, Georgiou DK, Dagnino-Acosta A, Ainbinder A, Cheng Q, Joshi AD, et al. AICAR prevents heat-induced sudden death in RyR1 mutant mice independent of AMPK activation. Nat. Med. 2012; 18: 244–51.

Li F, Buck D, De Winter J, Kolb J, Meng H, Birch C, et al. Nebulin deficiency in adult muscle causes sarcomere defects and muscle-type dependent changes in trophicity--novel insights in nemaline myopathy. Hum. Mol. Genet. 2015

Mázala DAG, Pratt SJP, Chen D, Molkentin JD, Lovering RM, Chin ER. SERCA1 overexpression minimizes skeletal muscle damage in dystrophic mouse models. Am. J. Physiol. Cell Physiol. 2015; 308: C699–709.

Mokbel N, Ilkovski B, Kreissl M, Memo M, Jeffries CM, Marttila M, et al. K7del is a common TPM2 gene mutation associated with nemaline myopathy and raised myofibre calcium sensitivity. Brain 2013; 136: 494–507.

Nguyen M-AT, Joya JE, Kee AJ, Domazetovska A, Yang N, Hook JW, et al. Hypertrophy and dietary tyrosine ameliorate the phenotypes of a mouse model of severe nemaline myopathy. Brain 2011; 134: 3516–29.

Ochala J, Lehtokari V-L, Iwamoto H, Li M, Feng H-Z, Jin J-P, et al. Disrupted myosin cross-bridge cycling kinetics triggers muscle weakness in nebulin-related myopathy. FASEB J. 2011; 25: 1903–1913.

Olivé M, Goldfarb LG, Lee H-S, Odgerel Z, Blokhin A, Gonzalez-Mera L, et al. Nemaline myopathy type 6: clinical and myopathological features. Muscle Nerve 2010; 42: 901–7.

Ottenheijm CAC, Buck D, de Winter JM, Ferrara C, Piroddi N, Tesi C, et al. Deleting exon 55 from the nebulin gene induces severe muscle weakness in a mouse model for nemaline myopathy. Brain 2013; 136: 1718–31.

Ottenheijm CAC, Fong C, Vangheluwe P, Wuytack F, Babu GJ, Periasamy M, et al. Sarcoplasmic reticulum calcium uptake and speed of relaxation are depressed in nebulin-free skeletal muscle. FASEB J. 2008; 22: 2912–9.

Ottenheijm CAC, Hooijman P, DeChene ET, Stienen GJ, Beggs AH, Granzier H. Altered myofilament function depresses force generation in patients with nebulin-based nemaline myopathy (NEM2). J. Struct. Biol. 2010; 170: 334–343.

Ottenheijm CAC, Lawlor MW, Stienen GJM, Granzier H, Beggs AH. Changes in cross-bridge cycling underlie muscle weakness in patients with tropomyosin 3-based myopathy. Hum. Mol. Genet. 2011; 20: 2015–2025.

Ottenheijm CAC, Witt CC, Stienen GJ, Labeit S, Beggs AH, Granzier H. Thin filament length dysregulation contributes to muscle weakness in nemaline myopathy patients with nebulin deficiency. Hum. Mol. Genet. 2009; 18: 2359–2369.

Paolini C, Quarta M, Wei-LaPierre L, Michelucci A, Nori A, Reggiani C, et al. Oxidative stress, mitochondrial damage, and cores in muscle from calsequestrin-1 knockout mice. Skelet. Muscle 2015; 5: 10.

Ravenscroft G, Jackaman C, Sewry CA, McNamara E, Squire SE, Potter AC, et al. Actin nemaline myopathy mouse reproduces disease, suggests other actin disease phenotypes and provides cautionary note on muscle transgene expression. PLoS One 2011; 6: e28699.

Riley DA, Van Dyke JM. The effects of active and passive stretching on muscle length. Phys. Med. Rehabil. Clin. N. Am. 2012; 23: 51–7.

Sambuughin N, Swietnicki W, Techtmann S, Matrosova V, Wallace T, Goldfarb L, et al. KBTBD13 interacts with Cullin 3 to form a functional ubiquitin ligase. Biochem. Biophys. Res. Commun. 2012; 421: 743–9.

Sambuughin N, Yau KS, Olivé M, Duff RM, Bayarsaikhan M, Lu S, et al. Dominant mutations in KBTBD13, a member of the BTB/Kelch family, cause nemaline myopathy with cores. Am. J. Hum. Genet. 2010; 87: 842–847.

Sanders DB, Rosenfeld J, Dimachkie MM, Meng L, Malik FI. A Double-Blinded, Randomized, Placebo-Controlled Trial to Evaluate Efficacy, Safety, and Tolerability of Single Doses of Tirasemtiv in Patients with Acetylcholine Receptor-Binding Antibody-Positive Myasthenia Gravis. Neurotherapeutics 2015; 12: 455–60.

Schlecht W, Li K-L, Hu D, Dong W. Fluorescence Based Characterization of Calcium Sensitizer Action on the Troponin Complex. Chem. Biol. Drug Des. 2016; 87: 171–81.

Shefner J, Cedarbaum JM, Cudkowicz ME, Maragakis N, Lee J, Jones D, et al. Safety, tolerability and pharmacodynamics of a skeletal muscle activator in amyotrophic lateral sclerosis. Amyotroph. Lateral. Scler. 2012; 13: 430–438.

Stehle R, Solzin J, Iorga B, Poggesi C. Insights into the kinetics of Ca2+-regulated contraction and relaxation from myofibril studies. Pflügers Arch. Eur. J. Physiol. 2009; 458: 337–57.

Sztal TE, Zhao M, Williams C, Oorschot V, Parslow AC, Giousoh A, et al. Zebrafish models for nemaline myopathy reveal a spectrum of nemaline bodies contributing to reduced muscle function. Acta Neuropathol. 2015; 130: 389–406.

Telfer WR, Nelson DD, Waugh T, Brooks S V, Dowling JJ. Neb: a zebrafish model of nemaline myopathy due to nebulin mutation. Dis. Model. Mech. 2012; 5: 389–96.

Tian L, Ding S, You Y, Li T, Liu Y, Wu X, et al. Leiomodin-3-deficient mice display nemaline myopathy with fast-myofiber atrophy. Dis. Model. Mech. 2015; 8: 635–41.

de Winter JM, Buck D, Hidalgo C, Jasper JR, Malik FI, Clarke NF, et al. Troponin activator augments muscle force in nemaline myopathy patients with nebulin mutations. J. Med. Genet. 2013; 50: 383–92.

Yuen M, Cooper ST, Marston SB, Nowak KJ, McNamara E, Mokbel N, et al. Muscle weakness in TPM3-myopathy is due to reduced Ca2+-sensitivity and impaired acto-myosin cross-bridge cycling in slow fibres. Hum. Mol. Genet. 2015; 24: 6278–92.

Yuen M, Sandaradura SA, Dowling JJ, Kostyukova AS, Moroz N, Quinlan KG, et al. Leiomodin-3 dysfunction results in thin filament disorganization and nemaline myopathy. J. Clin. Invest. 2014; 124

CHAPTER 10

SAMENVATTING

SAMENVATTING

Nemaline myopathie is een ernstige spierziekte waarvoor momenteel nog geen therapie bestaat. Dit komt onder andere omdat de oorzaak van spierzwakte bij patiënten met nemaline myopathie niet volledig bekend is. Daarom was het doel van dit proefschrift om meer inzicht te krijgen in ziekteprocessen die leiden tot spierzwakte in nemaline myopathie. Daarnaast hebben we onderzocht of er een verband is tussen de verschillende genetische oorzaken van nemaline myopathie en het type spierzwakte op spiercelniveau. Hoofdstuk 2 – 5 beschijft studies die antwoord proberen te vinden op deze vragen. Met het vergrote inzicht naar mechanismen van het ziekteproces hebben we vervolgens nieuwe therapeutische benaderingen getest om kracht in spiercellen te vergroten. De uitkomsten van deze studies staan beschreven in hoofdstuk 6 – 8.

Achtergrond

De naam nemaline myopathie is gegeven door de arts die voor het eerst zogenaamde ‘nemaline bodies’ ontdekte op spierfoto’s van patiënten met spierzwakte. Deze nemaline bodies zijn donkere structuren die je kunt zien als je heel ver inzoomt op de spier. Als je goed inzoomt op deze bodies, zie je dat ze uit draadachtige structuren bestaan. De arts die dit ontdekte gaf de bodies de naam ‘nemaline bodies’, naar het Griekse woord ‘nèma’, dat ‘draad’ betekent. Normaal gesproken horen deze bodies niet voor te komen in spieren. Het klinisch beeld bij patiënten met nemaline myopathie varieert sterk: van vroegtijdige dood tot milde spierzwakte met een normale levensduur.

Toen in 1995 het eerste gen werd ontdekt dat betrokken is bij nemaline myopathie, ging het snel met de zoektocht naar oorzaken van deze spierziekte. Op moment van schrijven tellen we 11 genen die – indiend gemuteerd (dus als er een foutje zit in je genetische code) – kunnen resulteren in nemaline myopathie. Deze eiwitten coderen allemaal voor bouwstenen van de sarcomeer, de kleinste contractiele eenheid van een spier; ookwel de kleine motoren die ervoor zorgen dat de spier kan samentrekken. Deze sarcomeer bestaat uit een raderwerk van kleine eiwitten die de motor soepel laten draaien. Als een van die raderen hapert, dan loopt de machine niet optimaal, en dat is in het geval van nemaline myopathie de reden waarom de spieren niet de gewenste kracht kunnen leveren. Elke radertje heeft

weer een andere taak om de machine goed te laten lopen. Zo'n rader wordt ookwel een eiwit genoemd. Zo'n eiwit wordt door het lichaam gemaakt door het recept voor het eiwit af te lezen van de genen in je dna. In dit proefschrift hebben we onderzocht wat het effect is van foutjes in die verschillende genen – die dus coderen voor eiwitten – op de krachtsgeneratie van spiercellen. Ook hebben we getest of medicijnen die aangrijpen op een belangrijk onderdeel van het raderwerk, de spierkracht in spiercellen van patiënten met nemaline myopathie kan vergroten. Hieronder worden kort per hoofdstuk de bevindingen samengevat.

Oorzaken van spierzwakte in nemaline myopathie

Hoofdstuk 2

Nemaline myopathie is een spierziekte waarbij het dunne filament in de skeletspier is aangedaan. Het dunne filament en het dikke filament zijn beide belangrijke onderdelen van de sarcomeer, de motor van de spier. De overlap tussen het dunne en dikke filament in de spier bepaalt hoeveel dikke-dunne filament interacties gevormd kunnen worden, deze interacties worden ookwel 'cross-bridges' genoemd. Bij het vormen van een cross-bridge gaat het raderwerk in de sarcomeer draaien, en kan de spier kracht leveren. De lengte van de filamenten is dus belangrijk voor de hoeveelheid cross-bridges die gevormd kunnen worden, en dus bepalend voor de hoeveelheid kracht die geleverd kan worden. In 51 biopten van patiënten met nemaline myopathie hebben we bestudeerd of de kracht die de spiercellen leveren beinvloed wordt door veranderingen in de lengte van het dunne filament. De 51 biopten bevatten mutaties in 8 van de 11 genen die kunnen leiden tot nemaline myopathie. Van deze studie hebben we geleerd dat alle bestudeerde mutaties leiden tot spierzwakte op spiercelniveau, en dat de invloed van kortere dunne filamenten op spiercelzwakte specifiek is voor mutaties in *ACTA1* en *NEB.* Een andere interessante bevinding is dat een nebuline-deficiënt muismodel voor nemaline myopathie laat zien dat skeletspieren kunnen compenseren voor de korte dunne filamenten door meer sarcomeren in serie toe te voegen. Hierdoor kunnen de sarcomeren op een kortere lengte samentrekken, een lengte die dichter bij hun optimale lengte ligt. We weten nog niet of dit compensatoire controlemechanisme ook in patiënten aanwezig is, maar voor toekomstige studies is het interessant om te onderzoeken of het stimuleren van de aanmaak van sarcomeren in serie spierzwakte kan tegengaan.

Hoofdstuk 3

In hoofdstuk 3 hebben we onderzocht of er een verband is tussen de organisatie van sarcomeren, de krachtgeneratie op spiercelniveau en het klinisch beeld van nemaline myopathie-patiënten met mutaties in het nebuline gen. Het onderzoek liet zien dat het klinische beeld samenhangt met de krachtgeneratie op spiercelniveau en de organisatie van de sarcomeren. Met deze organisatie wordt de aaneenschakeling van myofibrillen bedoeld. Als nemaline bodies zich aan de rand van de spiervezel bevinden, dan kan de spiercel nog goed presteren en dit wordt ook teruggezien in het klinisch beeld. Echter, als nemaline bodies verspreid zijn over de gehele spiervezel en daardoor de organisatie van myofibrillen ernstig verstoord wordt, kan de spiervezel weinig kracht leveren, en vertoont de patiënt ook ernstige spierzwakte.

Hoofdstuk 4

In hoofdstuk 4 hebben het effect van de aanwezigheid van slechts één nebuline allel (in plaats van twee) bestudeerd op de mate van expressie van sarcomeergenen, de hoeveel sarcomeereiwitten en de krachtgeneratie in spieren. Deze studie liet zien dat spieren van muizen met één nebuline allel normale hoeveelheden nebuline bezitten. Wél zijn de mRNA-niveaus van genen die coderen voor sarcomeereiwitten flink verhoogd voor troponine C, T en I en myosine van langzame spiervezels. Naast de mRNA-niveaus is ook de hoeveelheid eiwit langzaam myosine verhoogd. Krachtmetingen aan geisoleerde spieren toonden milde spierzwakte in muizen met slechts één nebuline allel. Dus afwezigheid van één nebulin allel heeft geen invloed op de hoeveelheid nebuline eiwit, maar draagt wel bij aan een verhoogd niveau van langzaam troponine en myosine en milde spierzwakte.

Hoofdstuk 5

Tijdens mijn promotietraject werd er een nieuw gen ontdekt dat betrokken is bij het ontstaan van nemaline myopathie. De naam van het gen is *KBTBD13*, en patiënten met mutaties in dit gen hebben nemaline type 6, ookwel NEM6 genoemd. Kenmerken van deze groep patienten is dat ze naast spierzwakte ook spiertraagheid vertonen. We ontdekten dat spiervezels van NEM6-patiënten zwakte vertonen op sarcomeerniveau. Ook hebben we een muis gemaakt die door een genetische fout geen Kbtbd13 kan aanmaken

in de spieren. Krachtmetingen in spieren van deze muis laten zien dat de spieren zwak zijn, en ook traag. Het *KBTBD13* gen is naast skeletspieren, ook aanwezig in de hartspier. Het effect van mutaties in *KBTBD13* op hartspierfunctie in nog onbekend. Studies op het *Kbtbd13*-deficiënte muismodel laten zien dat deze muizen een lagere contractiele reserve hebben bij stress-condities. Momenteel worden NEM6 patiënten gescreend op hartfunctie, zodat we het effect van *KBTBD13* mutaties op het hart goed kunnen bestuderen, en adviezen aan de patiënten kunnen uitbrengen.

Therapeutische benaderingen in nemaline myopathie

Hoofdstuk 6 – 8

In hoofdstuk 6 – 8 hebben we de potentie van verschillende medicijnen getest om spierkracht te verhogen in spiercellen van patiënten met nemaline myopathie. We hebben specfiek gekeken naar de groep nemaline myopathie-patiënten met mutaties in het nebuline gen, dit is het meest voorkomende type nemaline myopathie. De medicijnen die we hebben getest verhogen de gevoeligheid voor calcium in de spiercellen. Spieren hebben calcium nodig om samen te trekken, en door de gevoeligheid voor calcium te vergoten, verwachten we dat bij een gelijke hoeveelheid beschikbaar calcium in de spier, de spierkracht omhoog gaat. Allereerst hebben we het effect van Levosimendan getest op spierfunctie. Levosimendan is een troponine activator die specifiek aangrijpt op de langzame spiercellen. We zagen geen toename in spierkracht bij de aanwezigheid van Levosimendan in zowel langzame spiercellen van nemaline myopathie-patiënten als in gezonde controles. Een tweede troponine activator die we hebben getest – CK-2066260 - grijpt specifiek aan op snelle spiervezels. In zowel spiercellen van nebuline-deficiënte muizen, als in spiercellen van patienten met nemaline myopathie door mutaties in nebuline verhoogt de snelle troponine activator spierkracht bij submaximale inspanningen. Dit kan juist van klinische relevantie zijn, want dit betreft het inspaningsniveau van dagelijkse activiteiten als admehalen en lopen. Juist op deze inspanningsniveaus kan de troponine activator spierkracht vergroten. Tot dusver hebben we dit alleen op geisoleerde spiercellen in het lab kunnen aantonen, maar de resultaten moedigen aan om verder uit te zoeken of dit medicijn ook daadwerkelijk spierkracht in nemaline myopathie-patiënten vergroot.

Samengevat, de focus van dit proefschrift was om te begrijpen waarom patiënten met nemaline myopathie spierzwakte hebben, en hoe we spierkracht kunnen verhogen. Door het verzamelen van een grote collectie spiermateriaal van nemaline myopathie-patiënten en het maken van diverse nemaline myopathie muismodellen hebben we toegang tot uniek weefsel om toegepaste studies uit te voeren. Oorzaken van spierzwakte bij nemaline myopathie-patiënten zijn veranderingen in (1) de lengte van het dunne filament, (2) de gevoeligheid van de spier voor calcium, (3) de snelheid waarmee cross-bridges worden gevormd, (4) de locatie van nemaline bodies in de spier en (5) de samenstelling van eiwitten die zorgen voor het samentrekken van de spier. De bijdrage van deze veranderingen aan spierzwakte bij nemaline myopathie bleek afhankelijk te zijn van de specifieke mutatie van de patiënt. Een veelbelovende invalshoek voor een toekomstige therapie is het verhogen van de gevoeligheid voor calcium in spieren van patiënten met nemaline myopathie.

QUALITY OF LIFE

Een artikel of beursaanvraag eindigt vaak met de woorden: we hopen met deze inzichten een bijdrage te leveren aan de kwaliteit van leven van de patient. Dat is het doel, en daarom kan onderzoek gelukkig nog steeds gefinancierd worden. Maar zij die zich met onderzoek bezighouden, functioneren ook het best wanneer de kwaliteit van leven goed is. Ik heb de afgelopen jaren mogen vertoeven in omgeving die enorm heeft bijgedragen aan een hoge kwaliteit van leven. Op de werkvloer, maar zeker ook daarbuiten. Ik heb zoveel leuke mensen mogen ontmoeten en ben op bijzondere plekken geweest.

Allereerst een woord van dank aan de main inspirators van mijn wetenschappelijk leven.

Coen, bedankt voor het vertrouwen dat je in mij hebt gehad vanaf dag één. Meteen mocht ik mee naar het lab van Prof. Henk Granzier in Tucson, Arizona, om de nieuwste technieken te leren. Je bent een optimist *pur sang*. Dat werkt heel aanstekelijk. Hetzelfde geldt voor het refereren aan oneliners uit *Jiskefet* of *Allo Allo* tijdens werkbesprekingen. Met name dank voor alle feedback op mijn schrijven en het pro-actief meedenken met de te nemen vervolgstappen om in de wereld van het onderzoek verder te gaan. Ik kijk uit naar het vervolg van onze samenwerking!

Beste Ger, dank voor de waardvolle feedback op de stukken die we de afgelopen jaren hebben geschreven. Ook dank voor de technische hulp wanneer apparatuur haperde. Ook onze samenwerking zet zich voort, ik kijk uit naar de eerste data die we zullen verzamelen met de nieuw ontworpen opstelling.

Dear Prof. Henk Granzier, I am very grateful for your hospitality during all three visits to your lab. I always felt like a full member of the Granzier Lab family. I won't forget the beautiful bike ride to the Biosphere. I am looking forward to a fruitful continuation of our collaboration.

Dear members of my reading committee, Prof. Carsten Bönnemann, Prof. Roberto Bottinelli, Dr. Nicol Voermans, Prof. Jan Verschuuren and Prof. Jaap Harlaar. Thank you for the time spent on reading my thesis, your valuable feedback and your presence during my defense.

Dank aan The Ottenheijm Lab door de jaren heen. Allereerst Pleuni en Emmy, wij trokken vanaf het begin samen op, ik mis jullie dan ook op de afdeling sinds jullie vertrek! Pleuni, helaas zie ik je niet meer dagelijks voor een gezonde portie grappen, wat reflectie en een Donny, maar spreken we elkaar nog wel omdat we de Sketch University zijn begonnen! Dank voor het ontwerp van de cover van mijn proefschrift! Emmy, jouw nuchterheid en gezelligheid worden gemist! Gelukkig komen we elkaar nog tegen bij werkaangelegenheden of een tochtje op de wielrenfiets. Saskia, de brug naar de kliniek, jij zit vol goeie ideeën! Sparren met jou is altijd leuk, met name omdat ik dan weer meer inzicht krijg in het klinische beeld van spierzwakte. Dank nog dat je ons in Parijs om 2.00 ’s nachts onderdak hebt geboden toen we onszelf hadden buitengesloten;) Barbara, we have worked a lot together on the nemaline myopathy studies, which resulted in nice publications. Merci beaucoup! And your cakes are the best, especially during a long train trip to Salzburg. En dan komen we bij het huidige dreamteam: Stefan, Marloes, Martijn en Sylvia. Voor iedereen geldt, gedreven en serieus, maar ook tijd voor een grapje, en daar houd ik van. We zijn een goed stel met z’n allen, op een mooie toekomst!

Many thanks to the members of the Ottenheijm and Granzier lab at the 3rd floor of the Medical Research Building at the University of Arizona in Tucson, AZ, USA. I spent many months in your lab, which resulted in very nice data, publications and above all, a lot fun. Special thanks Charles and Danielle, for hosting me during my visits.

Naast onze eigen onderzoeksgroep bestaat de fysiologie-familie uit nog veel meer mooie teams. Door de jaren heen heb ik heel veel prettige collega’s om me heen gehad, dank allen! In het bijzonder Aimee, rots in de branding en heerlijk ad-rem. Dankzij jouw hulp en geduld verloopt ons werk op rolletjes. De familie is heel groot, ik wil een aantal mensen bedanken voor de leuke discussies, waardevolle feedback en/of hulp bij experimenten: Jolanda, Diederik, Frances, Vasco, Elza, Paul, Ilse, Chris, Michiel, Aref, Ruud, Rob, Vaishali, Silvia, Denielli, Zeineb, Jurjan, Robert, Maike, Kim, Wies, Melissa, Nina, Joana, Dop, Alice, Ed, Josien, Louise, Rosalie, Charissa, Anoek, Ingrid en Max ((jij verdient de eeuwige roem! Met je hand nog in het verband hielp je ons met de verhuizing naar vier-hoog).

Collega’s van de werkplaats, en in het bijzonder Peter, dank voor jullie werk!

Naast collega's wil ik ook studenten bedanken die ik in de loop der jaren met veel plezier heb mogen begeleiden. Bijzonder dank aan Menne, Rowan, Lavanya en Senait. Jullie werk is de basis geweest voor mooie artikelen. Dank voor jullie inzet, maar vooral ook de leuke gesprekken en vragen die me aan het denken hebben gezet.

Vrienden! Wat een rijkdom om zoveel leuke en inspirerende mensen om me heen te hebben. Meiden van bewegingswetenschappen: van modulaties in een feestcafe tot een poolwind die door je botten waait, zoveel gave herinneringen, jullie zijn fantastisch! FC DubbelFrisss, het allerleukste zaalvoetbalteam van Amsterdam. En ook *het* voorbeeld dat teamspirit en inzet de basis zijn voor mooie prestaties! Let op: in het proefschrift zit een hint verstopt over de locatie van ons volgende weekendje! De Oost-Borrelgroep, fietsen langs Belgische bierbrouwerijen, wintersport en oud en nieuw op de Berlagebrug, ik heb nu al zin in de edities van komend jaar! Schaatsmeiden, op het ijs, op de fiets langs de Amstel, Gein of Vecht, en de rondjes hardlopen voor werktijd: stuk voor stuk fijne combinaties van samen sporten, lachen, filosoferen en ventileren. Op naar de volgende Wintertriathlon!

Familie en schoonfamilie: dank voor jullie gezelligheid en interesse. Het is altijd fijn om weer in het Westland te zijn, Westlanders die uitgevlogen zijn op te zoeken (of updates te ontvangen via de nichten-app!), en inmiddels praat ik ook al een woordje Drents.

Paranimfen. Lennart, lieve broer, ik vind het heel fijn dat jij naast mij staat tijdens mijn verdediging. Ik ben enorm trots op jou en Welmoet. Iris, al sinds de studietijd hebben we samen avonturen beleefd, en samen hebben we ook onze eerste stappen op het vakgebied van onderzoeker gezet: het Bachelor OnderzoeksProject. Boppie, jij bent helemaal toppie.

Lieve papa en mama, dank voor alles. Jullie staan altijd voor me klaar. Ik heb mogen opgroeien in een warm nest, waarin we veel samen hebben ondernomen. Op nog een hoop mooie activiteiten en gezelligheid samen!

Lieve Edwin, ook al lach ik snel om eigen grappen, samen lachen met jou is het allermooist. Ik ben heel blij dat ik met jou ben. Zoals Daniel Lohues zingt: Ik mag joe wel.

Proost op een mooi vervolg van onze *Grande Belezza*!

CURRICULUM VITAE

Josine de Winter was born on June 6th 1986 in Naaldwijk. She attended ISW gymnasium and was a competitive speed skater. In 2004, she graduated and decided to further explore the physiology of human movement by studying Human Movement Sciences in Amsterdam. She enjoyed her time as student, both with the exciting lectures as well as being an active member of the student association “Association In Movement’. During her Master’s program, she obtained a degree for teaching physiology and anatomy in applied sciences and attended extracurricular courses in science communication. Josine performed her internship in the lab of Prof. Roberto Bottinelli (University of Pavia, Italy) to study the role of the molecular motor myosin in disease. In 2010, she graduated in Human Movement Sciences at the VU University in Amsterdam and started her PhD in the lab of Prof. Coen Ottenheijm and Prof. Ger Stienen (VU University Medical Center, Amsterdam, The Netherlands). During her PhD, she focussed on the mechanisms underlying muscle weakness in nemaline myopathy and she tested potential therapeutic strategies. Josine performed a part of her PhD in the lab of Prof. Henk Granzier at the University of Arizona (Tucson AZ, USA). She visited many (international) conferences, won several prizes and grants and organized conferences. Josine co-founded Sketch University, a science communication company that produces animations to explain science. Currently, she works as a post-doc at the department of Physiology at VU University Medical Center in Amsterdam. Josine lives happily in Amsterdam with Edwin.

LIST OF PUBLICATIONS

De Winter JM and Ottenheijm CAC. Sarcomere dysfunction in nemaline myopathy. *Submitted.*

Joureau B, **De Winter JM**, Stam K, Granzier H, Ottenheijm CAC (2016). Muscle weakness in respiratory and peripheral skeletal muscles in a mouse model for nebulin-based nemaline myopathy. *Neuromuscular Disorders. In press.*

De Winter JM, Van Willigenburg M, Joureau B, Strom J, Van der Pijl R, Lassche S, Lawlor ML, Stienen GJM, Granzier H, Van Engelen BG, Voermans NC, Ottenheijm CAC. New kelch on the NM block: elucidating the pathophysiology of NEM6. *In preparation.*

De Winter JM*, Joureau B*, Lee EJ, Kiss B, Yuen M, Gupta VA, Pappas CT, Gregorio CC, Stienen GJM, Edvardson S, Wallgren-Pettersson C, Lehtokari VL, Pelin K, Malfatti E, Romero NB, van Engelen BG, Voermans NC, Donkervoort S, Bönnemann CG, Clarke NF‡, Beggs AH, Granzier H and Ottenheijm CAC (2016). Mutation-specific effects on thin filament length in thin filament myopathy. *Annals of Neurology* 79 (6): 959–969.

Donkervoort S, Papadaki M, **De Winter JM**, Neu MB, Kirschner J, Bolduc V, Yang ML, Gibbons MA, Hu Y, Dastgir J, Leach ME, Rutkowski A, Foley AR, Krüger M, Wartchow EP, McNamara E, Ong R, Nowak KJ, Laing NG, Clarke NF, Ottenheijm CA, Marston SB, Bönnemann CG (2016). TPM3 deletions cause a hypercontractile congenital muscle stiffness phenotype. *Annals of Neurology* 78 (6): 982-94.

Yuen M, Cooper ST, Marston SB, Nowak KJ, McNamara E, Mokbel N, Ilkovski B, Ravenscroft G, Rendu J, **De Winter JM**, Klinge L, Beggs AH, North KN, Ottenheijm CA, Clarke NF (2015). Muscle weakness in TPM3-myopathy is due to reduced Ca2+-sensitivity and impaired acto-myosin cross-bridge cycling in slow fibres. *Human Molecular Genetics* 24 (22): 6278-92.

Li F, Buck D, **De Winter JM**, Kolb J, Meng H, Birch C, Slater R, Escobar YN, Smith JE 3rd, Yang L, Konhilas J, Lawlor MW, Ottenheijm C, Granzier HL (2015). Nebulin deficiency in adult muscle causes sarcomere defects and muscle-type-dependent changes in trophicity: novel insights in nemaline myopathy. *Human Molecular Genetics* 24 (18): 5219-33.

De Winter JM, Joureau B, Sequeira V, Clarke NF, van der Velden J, Stienen GJ, Granzier H, Beggs AH, Ottenheijm CAC (2015). Effect of levosimendan on the contractility of muscle fibers from nemaline myopathy patients with mutations in the nebulin gene. *Skeletal Muscle* 5:12.

Malfatti E, Lehtokari V-L, Böhm J, **De Winter JM**, Schäffer U, Estournet B, Quijano-Roy S, Monges S, Lubieniecki F, Bellance R, Viou MT, Madelaine A, Wu B, Taratuto AL, Eymard B, Pelin K, Fardeau M, Ottenheijm CAC, Wallgren-Pettersson C, Laporte J, Romero NB (2014). Muscle histopathology in nebulin-related nemaline myopathy: ultrastrastructural findings correlated to disease severity and genotype. *Acta Neuropathologica Communications* 2 (1): 44.

De Winter JM, Buck D, Hidalgo C, Jasper JR, Malik FI, Clarke NF, Stienen GJM, Lawlor MW, Beggs AH, Granzier H & Ottenheijm CAC (2013). Troponin activator augments muscle force in nemaline myopathy patients with nebulin mutations. *Journal of Medical Genetics* 50: 383-392.

Ottenheijm CAC, Buck D, **De Winter JM**, Ferrara C, Piroddi N, Tesi C, Jasper JR, Malik FI, Meng H, Stienen GJM, Beggs AH, Labeit S, Poggesi C, Lawlor MW & Granzier H (2013). Deleting exon 55 from the nebulin gene induces severe muscle weakness in a mouse model for nemaline myopathy. *Brain* 136: 1718-1731.

Lee EJ, **De Winter JM**, Buck D, Jasper JR, Malik FI, Labeit S, Ottenheijm CAC & Granzier H (2013). Fast skeletal muscle troponin activation increases force of mouse fast skeletal muscle and ameliorates weakness due to nebulin-deficiency. *PLoS One* 8 (2):e55861.

De Winter JM*, Gineste C*, Kohl C, Witt CC, Giannesini B, Brohm K, Le Fur Y, Gretz N, Vilmen C, Pecchi E, Jubeau M, Cozzone PJ, Stienen GJ, Granzier H, Labeit S, Ottenheijm CAC, Bendahan D & Gondin J (2013). In vivo and in vitro investigations of heterozygous nebulin knock-out mice disclose a mild skeletal muscle phenotype. *Neuromuscular Disorders* 23 (4):357-369.